frontiers | Research Topics

Harnessing marine biodiversity for novel antimicrobial agents against multidrug-resistant pathogens

Edited by
Guillermin Agüero-Chapin, Dany Domínguez Pérez
and Yovani Marrero-Ponce

Published in
Frontiers in Microbiology
Frontiers in Marine Science

ISSN 1664-8714
ISBN 978-2-8325-6367-0
DOI 10.3389/978-2-8325-6367-0

About Frontiers

Frontiers is more than just an open access publisher of scholarly articles: it is a pioneering approach to the world of academia, radically improving the way scholarly research is managed. The grand vision of Frontiers is a world where all people have an equal opportunity to seek, share and generate knowledge. Frontiers provides immediate and permanent online open access to all its publications, but this alone is not enough to realize our grand goals.

Frontiers journal series

The Frontiers journal series is a multi-tier and interdisciplinary set of open-access, online journals, promising a paradigm shift from the current review, selection and dissemination processes in academic publishing. All Frontiers journals are driven by researchers for researchers; therefore, they constitute a service to the scholarly community. At the same time, the *Frontiers journal series* operates on a revolutionary invention, the tiered publishing system, initially addressing specific communities of scholars, and gradually climbing up to broader public understanding, thus serving the interests of the lay society, too.

Dedication to quality

Each Frontiers article is a landmark of the highest quality, thanks to genuinely collaborative interactions between authors and review editors, who include some of the world's best academicians. Research must be certified by peers before entering a stream of knowledge that may eventually reach the public - and shape society; therefore, Frontiers only applies the most rigorous and unbiased reviews. Frontiers revolutionizes research publishing by freely delivering the most outstanding research, evaluated with no bias from both the academic and social point of view. By applying the most advanced information technologies, Frontiers is catapulting scholarly publishing into a new generation.

What are Frontiers Research Topics?

Frontiers Research Topics are very popular trademarks of the *Frontiers journals series*: they are collections of at least ten articles, all centered on a particular subject. With their unique mix of varied contributions from Original Research to Review Articles, Frontiers Research Topics unify the most influential researchers, the latest key findings and historical advances in a hot research area.

Find out more on how to host your own Frontiers Research Topic or contribute to one as an author by contacting the Frontiers editorial office: frontiersin.org/about/contact

Harnessing marine biodiversity for novel antimicrobial agents against multidrug-resistant pathogens

Topic editors

Guillermin Agüero-Chapin — University of Porto, Portugal

Dany Domínguez Pérez — Department of Biology and Evolution of Marine Organisms, Zoological Station Anton Dohrn, Italy

Yovani Marrero-Ponce — Universidad Panamericana, Mexico

Citation

Agüero-Chapin, G., Domínguez Pérez, D., Marrero-Ponce, Y., eds. (2025). *Harnessing marine biodiversity for novel antimicrobial agents against multidrug-resistant pathogens*. Lausanne: Frontiers Media SA. doi: 10.3389/978-2-8325-6367-0

Table of contents

frontiers | Frontiers in Microbiology

TYPE Editorial
PUBLISHED 24 April 2025
DOI 10.3389/fmicb.2025.1607539

OPEN ACCESS

EDITED AND REVIEWED BY
Rustam Aminov,
University of Aberdeen, United Kingdom

*CORRESPONDENCE
Guillermin Agüero-Chapin
✉ gchapin@ciimar.up.pt

RECEIVED 07 April 2025
ACCEPTED 09 April 2025
PUBLISHED 24 April 2025

CITATION
Agüero-Chapin G, Domínguez-Pérez D and Marrero-Ponce Y (2025) Editorial: Harnessing marine biodiversity for novel antimicrobial agents against multidrug-resistant pathogens. *Front. Microbiol.* 16:1607539.
doi: 10.3389/fmicb.2025.1607539

Editorial: Harnessing marine biodiversity for novel antimicrobial agents against multidrug-resistant pathogens

Guillermin Agüero-Chapin[1]*, Dany Domínguez-Pérez[2,3] and Yovani Marrero-Ponce[4,5]

[1]CIIMAR - Centro Interdisciplinar de Investigação Marinha e Ambiental, Universidade do Porto, Porto, Portugal, [2]Department of Biology and Evolution of Marine Organisms (BEOM), Stazione Zoologica Anton Dohrn, Calabria Marine Centre (CRIMAC), Amendolara, Italy, [3]PagBiOmicS - Personalised Academic Guidance and Biodiscovery-Integrated OMICs Solutions, Porto, Portugal, [4]Universidad Panamericana, Facultad de Ingeniería, Ciudad de México, Mexico, [5]Universidad San Francisco de Quito (USFQ), Grupo de Medicina Molecular y Traslacional (MeM&T), Colegio de Ciencias de la Salud (COCSA), Escuela de Medicina, Quito, Ecuador

KEYWORDS

multidrug resistance, marine antimicrobials, bioassays, screening techniques, drug discovery

Editorial on the Research Topic
Harnessing marine biodiversity for novel antimicrobial agents against multidrug-resistant pathogens

Antimicrobial resistance (AMR) is a defining challenge of our era, responsible for an alarming number of deaths that now surpass those caused by HIV and malaria. Projections estimate that by 2050, AMR could lead to 10 million deaths annually. The COVID-19 pandemic has amplified this crisis, fueling the spread of multidrug-resistant (MDR) pathogens, particularly those associated with biofilms. In response, governments have begun adopting more agile investment models, while academia and emerging biotech initiatives play increasingly central roles in the discovery of next-generation antimicrobials.

The ocean, covering over 70% of Earth's surface, represents an extraordinary yet underexploited reservoir of chemical diversity. Marine ecosystems harbor a vast array of microorganisms and multicellular life forms adapted to extreme and varied habitats. These organisms, from actinomycetes to fish and fungi, produce structurally unique secondary metabolites as chemical defenses or communication tools—many of which exhibit promising antimicrobial activities. This Research Topic aims to showcase the potential of marine biodiversity in providing new solutions to counteract MDR pathogens.

Thematic contributions

This collection of seven peer-reviewed articles exemplifies the multidisciplinary approaches required to unlock the antimicrobial potential of the ocean.

Marine actinomycetes, long recognized as prolific producers of bioactive compounds, are at the forefront of this exploration. In their mini review, Pan et al. catalog 45 novel antibacterial compounds identified in 2024 from marine actinomycetes, such as polyketides, macrolactams, alkaloids and peptides. The review highlights

the origins, chemical structures, and biological activities of these metabolites. Their distinct structural features and potent antibacterial properties, along with detailed insights into their mechanisms of action, underscore their potential as promising leads to combat antimicrobial resistance.

De La Hoz-Romo et al. extended this work through an application-focused study investigating marine actinobacteria isolated from the sponge *Cliona varians* and the octocoral *Eunicea fusca* for their activity against acne-associated bacteria, including *Cutibacterium acnes*, *Staphylococcus epidermidis*, and methicillin-resistant *Staphylococcus aureus* (MRSA). Notably, the extract Z9.216 from *Kocuria* sp. exhibited antibacterial activity comparable to erythromycin and vancomycin, without cytotoxic effects on human keratinocytes and fibroblasts at effective concentrations. These results underscore the therapeutic promise of rare marine actinobacteria, with alkaloids and terpenoids likely contributing to the observed bioactivity.

Similarly, Pylkkö et al. employed antivirulence screening to identify metabolites from Arctic marine actinobacteria—*Kocuria* sp. and *Rhodococcus* spp.—capable of inhibiting *Escherichia coli* (EPEC) pathogenicity without affecting bacterial growth. EPEC, a major cause of infant intestinal infections in developing countries, induces epithelial lesions through actin polymerization. Using bioassay-guided fractionation and HPLC-MS dereplication, the study identified a large phospholipid and a likely antimicrobial peptide that interfered with EPEC-induced actin remodeling. These results reinforce the potential of antivirulence approaches to limit resistance by avoiding direct effects on bacterial viability.

Expanding the chemical space further, Wang et al. reviewed 337 secondary metabolites isolated from marine-derived *Aspergillus* species between 2010 and mid-2024, including 145 new compounds. Classified into terpenoids, nitrogen-containing compounds, polyketides, steroids, and others, these metabolites display notable antibacterial activities. Their structural diversity and bioactivity highlight the valuable but underexplored role of marine fungi in antimicrobial drug discovery.

Liu et al. focused on another marine-derived fungus *Trichoderma effusum*, isolating four new sesquiterpene derivatives—trichoderenes A–D—alongside six known compounds. Several of these, including compounds 1–3 and 8–10, exhibited inhibitory activity against *Agrobacterium tumefaciens*, a phytopathogen responsible for significant agricultural losses. Notably, compound 3 introduced a previously undescribed C12 nor-sesquiterpene skeleton, underscoring the structural novelty and bioactive potential accessible from marine fungal sources.

A promising example of marine-derived antimicrobial peptides (AMPs) comes from Squitieri et al., who engineered two cationic mutants—Trem-HK and Trem-HSK—based on Trematocine, a natural AMP from the Antarctic fish *Trematomus bernacchii*. These designed peptides exhibited enhanced selectivity for bacterial membranes, preserved α-helical structure, and markedly improved efficacy against ESKAPE pathogens, with MIC and MBC values reduced by up to 80% compared to the original peptide. Notably, both mutants demonstrated low cytotoxicity and hemolytic activity at effective concentrations, and showed no *in vivo* toxicity in *Galleria mellonella* larvae, supporting their potential as promising leads for antimicrobial drug development.

Finally, He et al. demonstrated the integration of nanotechnology with marine bioproducts by synthesizing silver nanoparticles (PSP-AgNPs) from a polysaccharide-protein complex of the marine mollusk *Haliotis discus*. These nanoparticles showed strong antibacterial activity against several *Vibrio* strains, including *V. fluvialis*, *V. mimicus*, *V. hollisae*, *V. vulnificus*, and *V. furnissii*, with no cytotoxic effects on human hepatocytes at effective dosages (3.125–25.0 μg/mL), underscoring their potential as biocompatible bactericides for public health.

Conclusions and future perspectives

The articles in this Topic highlight the diverse sources, strategies, and applications of marine biodiversity in antimicrobial development. While the potential is clear, challenges remain, including sustainable sourcing, low natural yields, and complex compound isolation. Overcoming these obstacles requires interdisciplinary approaches that combine omics, synthetic biology, machine learning, and cheminformatics, as well as policy support for responsible bioprospecting and resource management.

This Research Topic emphasizes that the ocean, while a vital source of life, may also hold the key to combating one of the most pressing health threats of our time. Continued investment in marine biodiscovery is not just an academic pursuit—it is critical for global public health.

Author contributions

GA-C: Writing – review & editing, Writing – original draft. DD-P: Writing – review & editing. YM-P: Writing – review & editing.

Funding

The author(s) declare that financial support was received for the research and/or publication of this article. This work was supported by the FCT—Fundação para a Ciência e a Tecnologia under UIDB/04423/2020 and UIDP/04423/2020, and to the CIIMAR Out of the Box project (UIDB-COB-31711).

Conflict of interest

The authors declare that the research was conducted in the absence of any commercial or financial relationships that could be construed as a potential conflict of interest.

Publisher's note

frontiers | Frontiers in Microbiology

TYPE Original Research
PUBLISHED 02 August 2024
DOI 10.3389/fmicb.2024.1446283

OPEN ACCESS

EDITED BY
Guillermin Agüero-Chapin,
University of Porto, Portugal

REVIEWED BY
Margherita Cacaci,
Catholic University of the Sacred Heart, Rome, Italy
Fengyu Du,
Qingdao Agricultural University, China

*CORRESPONDENCE
Na Liu
✉ lnln82@163.com
Xueli He
✉ xlh3615@126.com
Yuxing Zhang
✉ jonsonzhyx@163.com

RECEIVED 11 June 2024
ACCEPTED 23 July 2024
PUBLISHED 02 August 2024

CITATION
Liu Y, Qi L, Xu M, Li W, Liu N, He X and Zhang Y (2024) Anti-*Agrobacterium tumefactions* sesquiterpene derivatives from the marine-derived fungus *Trichoderma effusum*.
Front. Microbiol. 15:1446283.
doi: 10.3389/fmicb.2024.1446283

Anti-*Agrobacterium tumefactions* sesquiterpene derivatives from the marine-derived fungus *Trichoderma effusum*

Yunfeng Liu[1,2], Lu Qi[3], Minghui Xu[2], Wanyun Li[2], Na Liu[1]*, Xueli He[2]* and Yuxing Zhang[1]*

[1]College of Horticulture, Hebei Agricultural University, Baoding, China, [2]College of Life Sciences, Hebei University, Baoding, China, [3]College of Pharmaceutical Sciences, Hebei University, Baoding, China

Agrobacterium tumefaciens can harm various fruit trees, leading to significant economic losses in agricultural production. It is urgent to develop new pesticides to effectively treat this bacterial disease. In this study, four new sesquiterpene derivatives, trichoderenes A–D (**1**–**4**), along with six known compounds (**5**–**10**), were obtained from the marine-derived fungus *Trichoderma effusum*. The structures of **1**–**4** were elucidated by extensive spectroscopic analyses, and the calculated ECD, ORD, and NMR methods. Structurally, the hydrogen bond formed between the 1-OH group and the methoxy group enabled **1** to adopt a structure resembling that of resorcylic acid lactones, thereby producing the ECD cotton effect. Compound **3** represents the first example of C12 nor-sesquiterpene skeleton. Compounds **1**–**10** were tested for their antimicrobial activity against *A. tumefactions*. Among them, compounds **1**–**3** and **8**–**10** exhibited inhibitory activity against *A. tumefactions* with MIC values of 3.1, 12.5, 12.5, 6.2, 25.0, and 12.5μg/mL, respectively.

KEYWORDS

marine-derived fungus, *Trichoderma effusum*, sesquiterpene, *Agrobacterium tumefaciens*, bioactivity

1 Introduction

Agrobacterium tumefactions is a prevalent gram-negative bacterium found in soil, which exhibits a remarkable ability to infect the wounded sites of various fruit trees, including pear, apple, peach, kiwi, and cherry trees, under natural conditions (Yu et al., 2021; Hang et al., 2022). This infection has the propensity to induce the development of crown gall disease, a pathological condition that primarily affects the root and stem of plants (Ahmed et al., 2022). The disease is characterized by the emergence of small, round, light-yellow tumors on the infected sites, with diameters ranging from a few millimeters to several centimeters. As the disease progresses, these tumors enlarge and assume irregular shapes, ultimately leading to a substantial reduction in crop yield and, in severe cases, even plant death (Jailani et al., 2022). Currently, there is no highly effective method for treating crown gall disease, and the commonly used chemical agents for prevention can cause serious environmental pollution problems (Torres et al., 2022). It is urgent to develop new natural and green pesticides with a high degree of effectiveness and low environmental impact.

Trichoderma species are dominant fungal communities in various soil ecosystems across all climatic zones, serving as a crucial component of the soil microecological flora and possessing

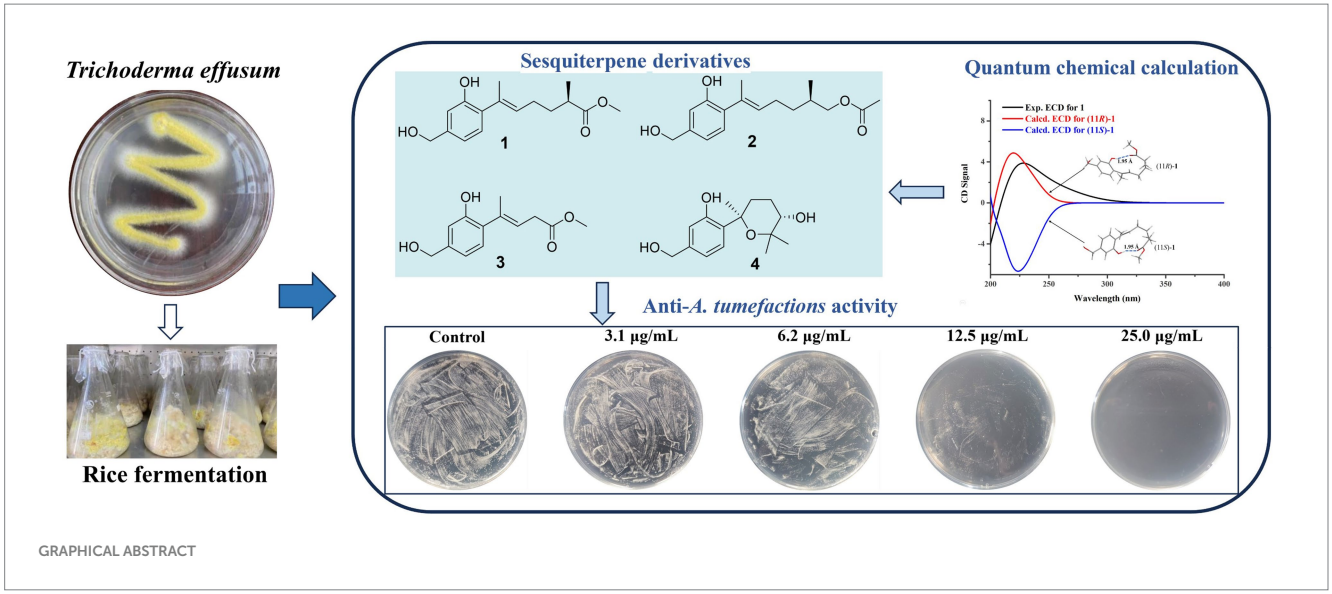

GRAPHICAL ABSTRACT

the ability to colonize plant roots (Zin and Badaluddin, 2020). Recent research has revealed that *Trichoderma* not only exhibits remarkable adaptability but also effectively controls various plant diseases and pests (Ferreira and Matías, 2021). On the one hand, its rapid growth and strong vitality enable it to swiftly occupy growth spaces, absorb necessary nutrients, and weaken and eliminate other pathogens in the same environment (Harman et al., 2012). On the other hand, *Trichoderma* inhibits the growth, reproduction, and infection of pathogenic bacteria through the production of small-molecule antibiotics, large-molecule antibacterial proteins, or cell wall-degrading enzymes (Tyśkiewicz et al., 2022). Technical measures employing *Trichoderma* in the prevention and control of fruit and vegetable diseases have garnered widespread attention in the field of biological control both domestically and internationally (Cai and Druzhinina, 2021). Currently, over 250 commercial formulations containing *Trichoderma* have been developed globally, achieving remarkable control effects in different countries and regions (Mukhopadhyay and Deepak, 2020). The research on biological control and mechanisms of *Trichoderma* is of significant importance for promoting biological control and reducing the use of chemical pesticides.

As part of our ongoing search for antibacterial natural products from marine-derived fungi (Li et al., 2022; Cao et al., 2023), the strain *Trichoderma effusum* attracted our attention because the EtOAc extract of the culture showed anti-*A. tumefactions* activity. The bioassay and HPLC guided separation of the EtOAc extract led to the isolation of four new sesquiterpene derivatives, named trichoderenes A–D (**1**–**4**), together with six known compounds (**5**–**10**) (Figure 1). Subsequently, anti-*A. tumefactions* activities of these compounds (**1**–**10**) were performed to evaluate the development value of these compounds. Herein, we report the details of the isolation, structure elucidation, and bioactivities of them.

2 Results and discussion

Trichoderene A (**1**) was obtained as pale yellow oil with the molecular formula of $C_{16}H_{22}O_4$ based on its HRESIMS (*m/z* 301.1404 $[M+Na]^+$, calcd. for $C_{16}H_{22}NaO_4^+$ 301.1410), suggesting six degrees of unsaturation. In the ^{1}H NMR spectrum (Table 1), three characteristic aromatic proton signals [7.05, d (7.2), 6.93, d (1.2), and 6.88, d (7.2, 1.2)], an olefinic methylene signal [5.51, tb (7.2, 1.2)], an oxygen-linking methylene signal [4.63, d (5.4)], and two methyl proton signals [1.96, s; 1.20, d (7.2)] revealed a bisabolene-type sesquiterpene skeleton (Shu et al., 2021) for **1**. Moreover, in the ^{13}C NMR spectrum of **1** (Table 2), 17 related carbon atoms, which could be assigned to three methyl groups including one methoxy group, three methylenes, five methines, and five quaternary carbons including a carbonyl group, were consistent with the ^{1}H NMR of **1**. Compared with the reported NMR data of anhydrowuruterpol B (**8**) isolated from the fungus *Penicillium* sp. FH-A 6260 (Henne et al., 1993), it was suggested that compound **1** shares the same bisabolene-type nucleus as compound **8**. The main difference was that the methyl ester group in **1** [δ_H 3.69, s, -OC$\underline{H}_3$; δ_C 177.3 C-12 and 51.8 -O$\underline{C}$H$_3$] was instead of primary alcohol group in **8**. This deduction was confirmed by the key HMBC correlations from H-10, H-13, and -OC$\underline{H}_3$ to C-12 (Figure 2). Based on the above analysis, the planar structure of **1** was established.

The determination of the absolute configuration of **1** posed a considerable challenge. First, due to the remote location of the chiral center C-11 from the chromophore in **1**, the ECD cotton effect may not be pronounced enough to enable the use of computed ECD methods for its absolute configuration identification. Second, the low experimental optical rotation (OR) value (−8.4) of **1** also limited the application of determining its absolute configuration through comparison of OR values. However, during the testing of compound **1**'s ECD spectrum, it was unexpectedly observed that a strong cotton absorption peak was present in its experimental ECD spectrum. Subsequently, two possible configurations of **1**, namely, (11*R*)-**1** and (11*S*)-**1**, were used to calculate their ECD spectra. The results indicated that the ECD calculated spectrum of (11*R*)-**1** agreed well with the experimental spectrum of **1** (Figure 3), suggesting that the absolute configuration of **1** was 11*R*. Further analysis revealed that the cause of the ECD cotton effect in **1** lay in the hydrogen bond formed between the 1-OH group and the methoxy group in its 3D conformation. This hydrogen bond, with a length of 1.95 Å and a strong force, enabled **1** to adopt a structure resembling that of resorcylic acid lactones (Kuttikrishnan et al., 2022) in solvents, thereby producing the ECD cotton effect. This discovery

10.3389/fmicb.2024.1446283

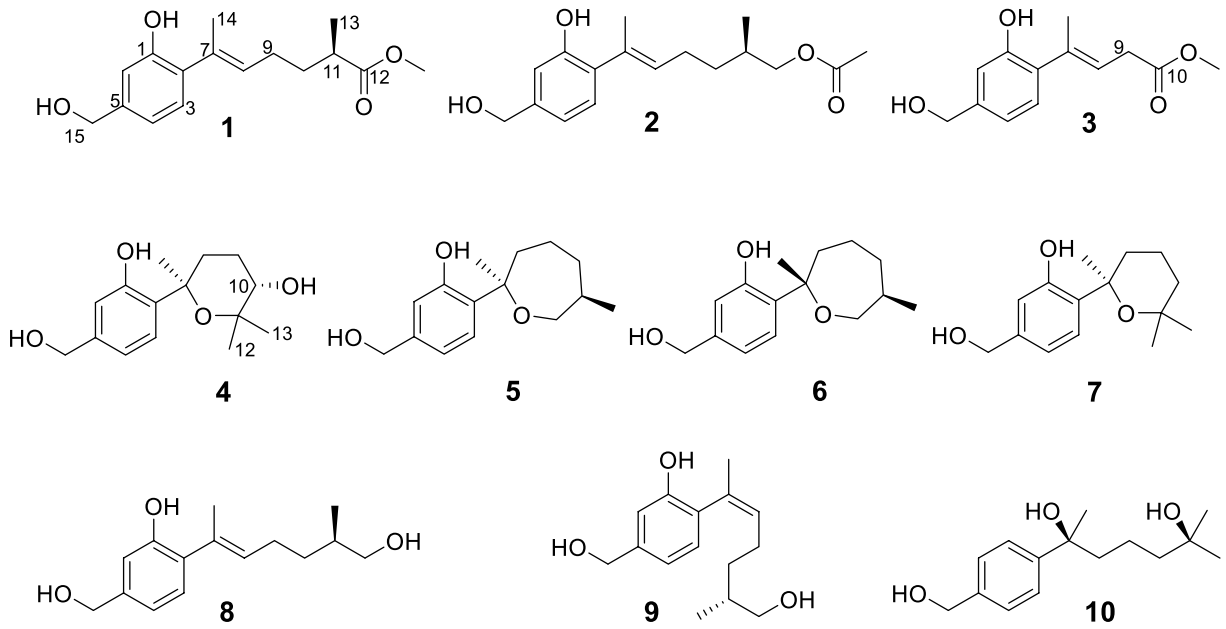

FIGURE 1
Structures of the compounds **1**–**10**.

TABLE 1 ^{1}H NMR Data (δ) of 1–4 (600 MHz, $CDCl_3$, δ in ppm, J in Hz).

Position	1	2	3	4
3	7.05, d (7.2)	7.08, d (7.8)	7.00, d (7.8)	7.03, d (7.8)
4	6.88, d (7.2, 1.2)	6.90, dd (7.8, 1.2)	6.93, dd (7.8, 1.2)	6.83, dd (7.8, 1.8)
6	6.93, d (1.2)	6.94, d (1.2)	6.95, d (1.2)	6.86, d (1.8)
8	5.51, tb (7.2, 1.2)	5.55, tb (7.2, 1.2)	5.81, tb (7.2, 1.2)	2.29, m
				2.07, m
9	2.24, m	2.29, m	2.90, d (7.2)	2.04, m
		2.22, m		1.81, m
10	1.84, m	1.56, m	-	3.48, m
	1.59, m	1.34, m		
11	2.53, m	1.86, m	-	-
12	-	4.01, dd (10.8, 6.6)	-	1.31, s
	-	3.91, dd (10.8, 6.6)		
13	1.20, d (7.2)	1.00, d (7.2)	-	1.01, s
14	1.96, s	2.00, s	2.04, s	1.53, s
15	4.63, d (5.4)	4.65, d (5.4)	4.65, s	4.63, s
-OCH3	3.69, s	-	3.68, s	-
-OAc	-	2.08, s	-	-
1-OH	5.72, s	5.60, s	5.82, s	8.96, s

reminds us that in evaluating whether a compound could produce an ECD cotton effect, it is necessary to conduct a thorough analysis of its 3D conformation, rather than relying solely on planar structural analysis.

Trichoderene B (**2**) was also obtained as colorless oil. The similar NMR spectra of **2** (Tables 1, 2) and **8** suggested that **2** should be a bisabolene-type sesquiterpene derivative. Detailed analysis of NMR differences between **2** and **8** indicated that **2** was the result of acetylation of the 12-OH in **8**, which was further verified by the key HMBC correlation from H_2-12 to -OCOCH$_3$ (Figure 2). It was also a significant challenge to determine the absolute configuration of **2**. Unlike compound **1**, the 1-OH group in **2** could not form an intramolecular hydrogen bond with the oxygen on the chain, resulting in a weak experimental ECD cotton effect that cannot be applied to its configuration identification. Fortunately, compound **2** displayed a

10.3389/fmicb.2024.1446283

relatively large OR value, which changed with the testing wavelength, forming a well-defined optical rotation dispersion (ORD) spectrum (Figure 4). Based on this characteristic, the calculated ORD spectra of the two possible configurations of **2**, (11*R*)-**2** and (11*S*)-**2**, were applied. The results indicated that the calculated ORD spectrum of (11*R*)-**2** matched well with the experimental spectrum of **2**. Therefore, the absolute configuration of **2** could be confidently determined as 11*R*.

Trichoderene C (**3**) was also isolated as colorless oil. Although 1D NMR signals (Tables 1, 2) suggested that **3** might belong to the sesquiterpene derivative, its ^{13}C NMR spectrum comprised only 13 carbons, including a methoxy carbon, which did not align with the typical 15-carbon skeleton of sesquiterpenes. This indicated that **3** was likely a nor-sesquiterpene. By carefully compared with the reported NMR data of **3** and **1**, it was found that the signals of -CH_2-$CH(CH_3)$- group between C-9 and C-12 in **1** were disappeared in **3**. The key correlations from H-8 and -O$C\underline{H}_3$ to C-10 (Figure 2) confirmed the nor-sesquiterpene skeleton of **3**. To validate the skeleton of **3**, three chemical quantitative calculation methods, namely, B3LYP/6–311 + G(d,p) (method 1), B3LYP/6–311 + G(d,p) (PCM, $CHCl_3$) (method 2), and mPW1PW91/6–311 + G(d,p) (PCM, $CHCl_3$) (method 3), were employed to compute the ^{13}C NMR data of **3**, and the computed results were compared with experimental values. The findings revealed that under all three methods, the calculated ^{13}C NMR data exhibited good fits with the experimental values, with high correlation coefficient R^2 values of 0.9972, 0.9974, and 0.9979, respectively (Figure 5A). In addition, the maximum error between the calculated and experimental ^{13}C NMR data did not exceed 4.4 ppm for any of the three methods (Figure 5B). Thus, the carbon skeleton of **3** was definitely assigned and verified.

TABLE 2 ^{13}C NMR Data (δ) of 1–4 (150 MHz, $CDCl_3$, δ in ppm).

Position	1	2	3	4
1	152.4, C	152.3, C	152.4, C	157.0, C
2	130.6, C	130.5, C	126.4, C	130.2, C
3	128.7, CH	128.7, CH	128.9, CH	124.6, CH
4	118.8, CH	118.8, CH	119.3, CH	118.2, CH
5	141.4, C	141.4, C	142.2, C	142.1, C
6	114.2, CH	114.0, CH	114.8, CH	116.2, CH
7	133.0, C	132.4, C	136.8, C	78.0, C
8	130.7, CH	131.4, CH	122.3, CH	28.1, CH_2
9	26.4, CH_2	25.9, CH_2	34.8, CH_2	24.3, CH_2
10	33.4, CH_2	33.2, CH_2	173.3, C	71.0, CH
11	39.3, CH	32.4, CH	-	77.6, C
12	177.3, C	69.2, C	-	26.4, CH_3
13	17.5, CH_3	17.0, CH_3	-	25.1, CH_3
14	18.1, CH_3	18.1, CH_3	25.5, CH_3	31.4, CH_3
15	65.2, CH_2	65.2, CH_2	65.2, CH_2	65.1, CH_2
OCH_3	51.8, CH_3	-	52.3, CH_3	
OAc	-	171.4, C	-	
	-	21.1, CH_3	-	

Trichoderene D (**4**) was also isolated and identified as sesquiterpene analogs according to its NMR data (Tables 1, 2). Its molecular formula was determined as $C_{15}H_{22}O_4$ based on its HRESIMS data, suggesting five degrees of unsaturation. In **4**, the benzene ring accounted for four degrees of unsaturation, thus requiring the side chain to form an additional ring to occupy the fifth degree of unsaturation. In fact, the structure of **4** was as analogous to the known compound **7**, with the main difference being the presence of an additional hydroxyl group at C-10 in **4**. This inference could be confirmed by the key HMBC correlations from H_2-8 and H_3-13 to C-10, and ^{1}H–^{1}H COSY correlation of H_2-8/H_2-9/H-10 (Figure 2). In the NOESY experiment, the correlations between H_3-13 and H-10, and H_3-12 and H_3-14 suggested that H-10 and H_3-14 were located on opposite sides of the molecular. To accurately determine the absolute configuration of **4**, ECD chemical quantitative calculations were performed on two possible configurations of **4**, (7*R*,10*S*)-**4** and (7*S*,10*R*)-**4**. The results indicated that the calculated ECD spectrum of (7*R*,10*S*)-**4** matched well with the experimental ECD spectrum of **4** (Figure 6), suggesting that the absolute configuration of **4** was 7*R*,10*S*.

The known compounds **5**–**10** were identified as cyclowaraterpol A (**5**) (Henne et al., 1993), cyclowaraterpol B (**6**) (Henne et al., 1993), (*S*)-(−)-5-(hydroxymethyl)-2-(2,6,6-trimethyltetrahydro-2*H*-pyran-2-yl)phenol (**7**) (Wang et al., 2016), waruterpol (**8**) (Henne et al.,

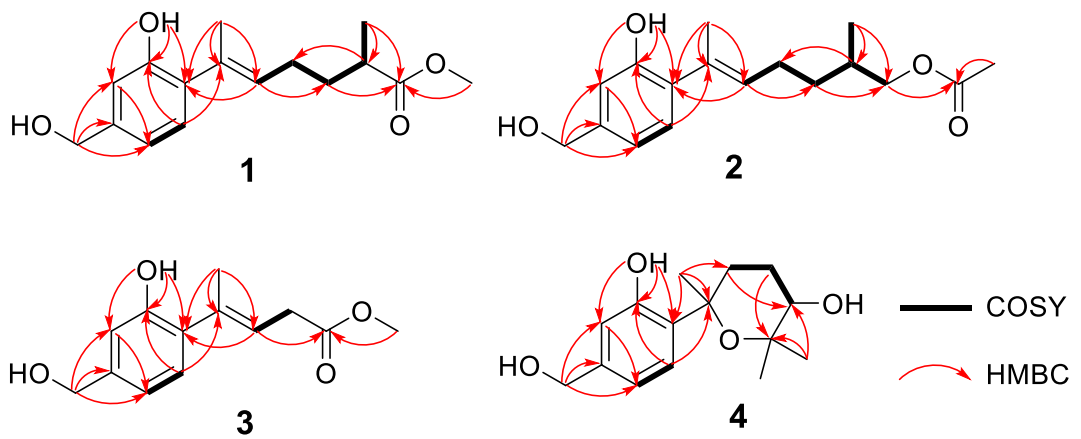

FIGURE 2
Key HMBC and COSY of compounds **1**–**4**.

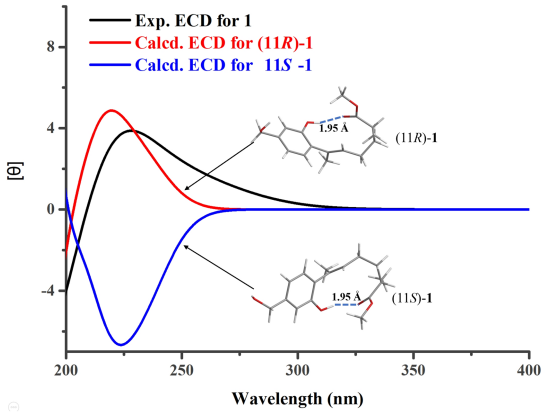

FIGURE 3
Experimental and calculated ECD curves for **1**.

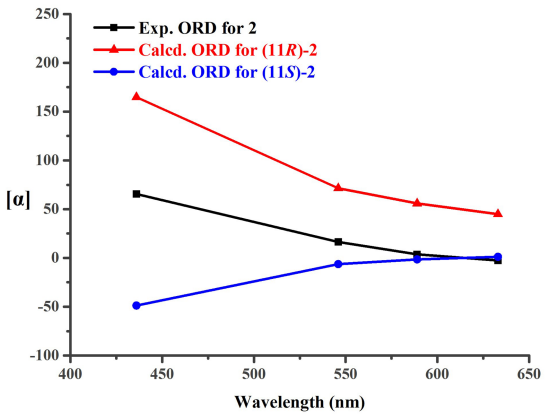

FIGURE 4
Experimental and calculated ORD curves for **2**.

1993), anhydrowuruterpol A (**9**) (Henne et al., 1993), and (7*S*,11*S*)-(+)-11-hydroxyl-sydonol (**10**) (Ye et al., 2019), by comparing their NMR data with the reference data.

Anti-*A. tumefactions* activity of the isolated compounds **1**–**10** was then determined. In the conventional 96-well broth dilution assay, compounds **1**–**3** and **8**–**10** exhibited inhibitory activity against *A. tumefactions* with MIC values of 3.1, 12.5, 12.5, 6.2, 25.0, and 12.5 μg/mL, respectively. However, compounds **4**–**7** did not inhibit *A. tumefactions* (MICs >25.0 μg/mL). This indicated that the formation of a cyclic structure in the side chain of these compounds could reduce their anti-*A. tumefactions* activity. To further confirm the antibacterial activity of these compounds, a plate spread inhibition assay was conducted on **1**. The results showed that at a concentration of 6.2 μg/mL, compound **1** inhibited the growth of *A. tumefactions* on the plate. When the concentration of **1** reached 25.0 μg/mL, the growth of *A. tumefactions* on the plate was completely inhibited (Figure 7A). Subsequently, the bactericidal time-kill curve was conducted for **1**, testing its effect at various concentrations including blank, 1/2 MIC, 2 MIC, and 8 MIC (Figure 7B). The results indicated that when the concentration of **1** reached 2 MIC and 8 MIC, bacterial killing began to manifest within 2 h. Notably, at 8 MIC concentration, nearly all bacteria were eradicated within 12 h. Furthermore, the impact of **1** on the formation of bacterial biofilm by *A. tumefaciens* was investigated (Figure 7C). It was revealed that **1** exhibited certain anti-biofilm activity. At a concentration of 5.0 μg/mL, the formation of bacterial biofilm was moderately inhibited, whereas at 10.0 μg/mL, the inhibition was highly pronounced.

3 Materials and methods

3.1 General experimental procedures

The general experimental procedures were basically consistent with our previous literature (Cao et al., 2023).

3.2 Fungal materials

The marine-derived fungal *Trichoderma effusum* HBU-2019-190, originating from the Bohai Sea, was identified and subsequently registered in the NCBI GenBank under accession number MN644788. The fungal strains have been deposited in the collection of the College of Life Sciences, Hebei University, China. *Agrobacterium tumefaciens*, originally separated from soil, was sourced from China Center of Industrial Culture Collection.

3.3 Fermentation, extraction, and isolation

In 1,000 mL Erlenmeyer flasks, the fungus HBU-2019-190 was fermented using rice solid medium, with a total of 100 flasks fermented, each containing 100 g of rice and 100 mL of water. The fermentation conditions were set at 28°C for 28 days. After fermentation, a 1:1 mixture of MeOH/CH_2Cl_2 was used to extract the fungus for six times. The extract was then dried using a rotary evaporator, resulting in 402 g of crude extract. Subsequently, the crude extract was further extracted with EtOAc and H_2O to obtain 213 g of EtOAc extract. The obtained EtOAc extract was then subjected to vacuum column chromatography using a petroleum ether (PE)/EtOAc gradient system. The gradient system was set as 90% PE, 60% PE, 30% PE, and 100% EtOAc, resulting in four fractions Fr.1–Fr.4. Among them, Fr.2 was further purified via silica gel column chromatography with a mixture of PE/EtOAc (1:1) as the mobile phase, resulting in four subfractions, Fr.2.1–Fr.2.4. Then, Fr.2.2 was further separated by reversed-phase silica gel chromatography with 80% MeOH as the mobile phase, followed by semipreparative HPLC (MeOH:H_2O = 40:60, 2.0 mL/min), ultimately yielding compounds **1** (32.0 mg), **2** (24.0 mg), **4** (16.0 mg), **5** (4.3 mg), **6** (4.6 mg), and **7** (1.5 mg). Fr.3 was separated by Sephadex LH-20 chromatography using a mixed solvent of PE, MeOH, and CH_2Cl_2 in a ratio of 2:1:1 as the mobile phase, resulting in five subfractions, Fr.3.1–Fr.3.5. Among them, Fr.3.3 was further purified through silica gel column chromatography and HPLC preparation, leading to the isolation of compounds **3** (12.0 mg), **8** (9.5 mg), **9** (2.2 mg), and **10** (3.7 mg).

Trichoderene A (**1**): Pale yellow oil; [α]25 D = −8.4 (*c* 1.00, MeOH); UV (MeOH), λmax (log ε) 246 (4.20), 305 (2.83) nm; ECD (5.2 μM, MeOH), λmax ($\Delta\varepsilon$) 228 (3.87) nm; ^{1}H and ^{13}C NMR data (see Tables 1, 2); HRESIMS *m/z* 301.1404 [M + Na]$^+$ (calcd. for $C_{16}H_{22}NaO_4^+$ 301.1410).

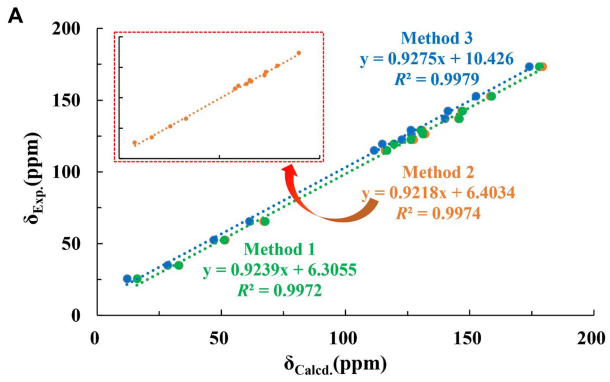

FIGURE 5
Regression analysis and individual deviations of experimental vs. calculated 13C NMR chemical shifts of **3**.

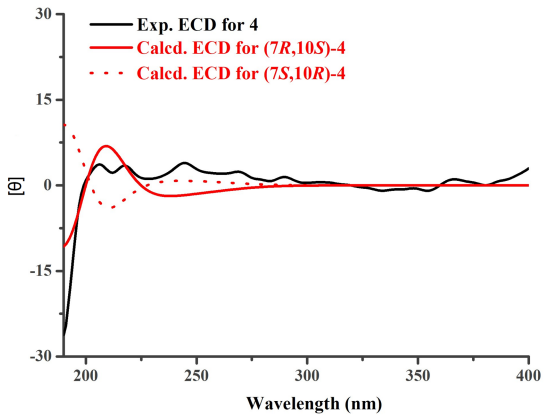

FIGURE 6
Experimental and calculated ECD curves for **4**.

Trichoderene B (**2**): Pale yellow oil; [α]25 D = −70.9 (*c* 1.00, MeOH); UV (MeOH), λmax (log ε) 245 (4.25), 304 (2.81) nm; ^{1}H and ^{13}C NMR data (see Tables 1, 2); HRESIMS *m/z* 315.1563 [M + Na]$^{+}$ (calcd. for $C_{17}H_{24}NaO_4^{+}$ 315.1567).

Trichoderene C (**3**): Pale yellow oil; UV (MeOH), λmax (log ε) 244 (4.61), 307 (2.86) nm; ^{1}H and ^{13}C NMR data (see Tables 1, 2); HRESIMS *m/z* 259.0938 [M + Na]$^{+}$ (calcd. for $C_{13}H_{16}NaO_4^{+}$ 259.0941).

Trichoderene D (**4**): Pale yellow oil; [α]25 D = −10.7 (*c* 1.00, MeOH); UV (MeOH), λmax (log ε) 242 (4.39), 302 (2.74) nm; ECD (5.0 μM, MeOH), λmax ($\Delta\varepsilon$) 206 (3.68), 218 (3.44) nm; ^{1}H and ^{13}C NMR data (see Tables 1, 2); HRESIMS *m/z* 289.1401 [M + Na]$^{+}$ (calcd. for $C_{15}H_{22}NaO_4^{+}$ 289.1410).

3.4 Computational section

The different configurational molecules of **1**–**4**, including (11*R*)-**1**, (11*S*)-**1**, (11*R*)-**2**, (11*S*)-**2**, **3**, (7*R*,10*S*)-**4**, and (7*S*,10*R*)-**4**, seven molecules in total, were used for quantitative chemical calculations. Initially, minimum energy conformation search for these molecules was conducted using the Compute VOA software, with relative energy within a 10.0 kcal/mol energy window and the MMFF94 force field applied. This resulted in 47 stable conformers for (11*R*)-**1**, 36 stable conformers for (11*S*)-**1**, 30 stable conformers for (11*R*)-**2**, 36 stable conformers for (11*S*)-**2**, 53 stable conformers for **3**, 12 stable conformers for (7*R*,10*S*)-**4**, and 12 stable conformers for (7*S*,10*R*)-**4**, respectively. Subsequently, these minimum energy conformations were optimized for the first time using Gaussian software at the B3LYP/6-31G(d) level (gas phase). Following the initial optimization, the conformations were ranked based on their energies, and those with an energy difference within 2.5 kcal/mol were selected for a second round of optimization at the B3LYP/6–311 + G(d) level (gas phase). After the second optimization, ECD or NMR calculations were performed on the optimized conformations. Finally, based on Boltzmann statistics, the final ECD and NMR spectra for each configurational molecule were computed.

3.5 Anti-*Agrobacterium tumefactions* activity assay

Using 96-well broth dilution assay method (Schug et al., 2020), the anti-*A. tumefactions* activity of compounds **1**–**10** was determined, with ampicillin serving as the positive control, having a MIC value of 0.3 μg/mL. Subsequently, the inhibitory effect of **1** against *A. tumefactions* was evaluated using the plate spreading method (Lewis and Fleming, 1995). Specifically, 20 mL of LB medium containing various concentrations of **1** was poured into a 9 cm-diameter petri dish. The bacteria of *A. tumefactions*, cultured 1 day prior, were then uniformly spread on the plate. Following this, the plate was inverted and incubated at 28°C for 12 h. Finally, photographs were taken to record the growth of colonies. The design of the bactericidal time-kill curve test experiment and bacterial biofilm experiment for **1** was based on previous literature. For time kill assays, tubes were prepared containing freshly prepared LB broth supplemented with compound **1** at various concentrations, including a blank control, 1/2 MIC, 2 MIC, and 8 MIC, along with *A. tumefactions* isolates at a concentration of 10^4 CFU/mL. The tubes were incubated at 28°C in a shaking incubator (200 rpm). Then, 100 μL aliquots were obtained from each tube at 0, 2, 4, 8, and 12 h of incubation and serially diluted in saline for the determination of viable counts. Diluted samples (10 μL) were plated on LB plates and incubated at 28°C for 12 h, and then, the number of colonies was counted. The lower limit

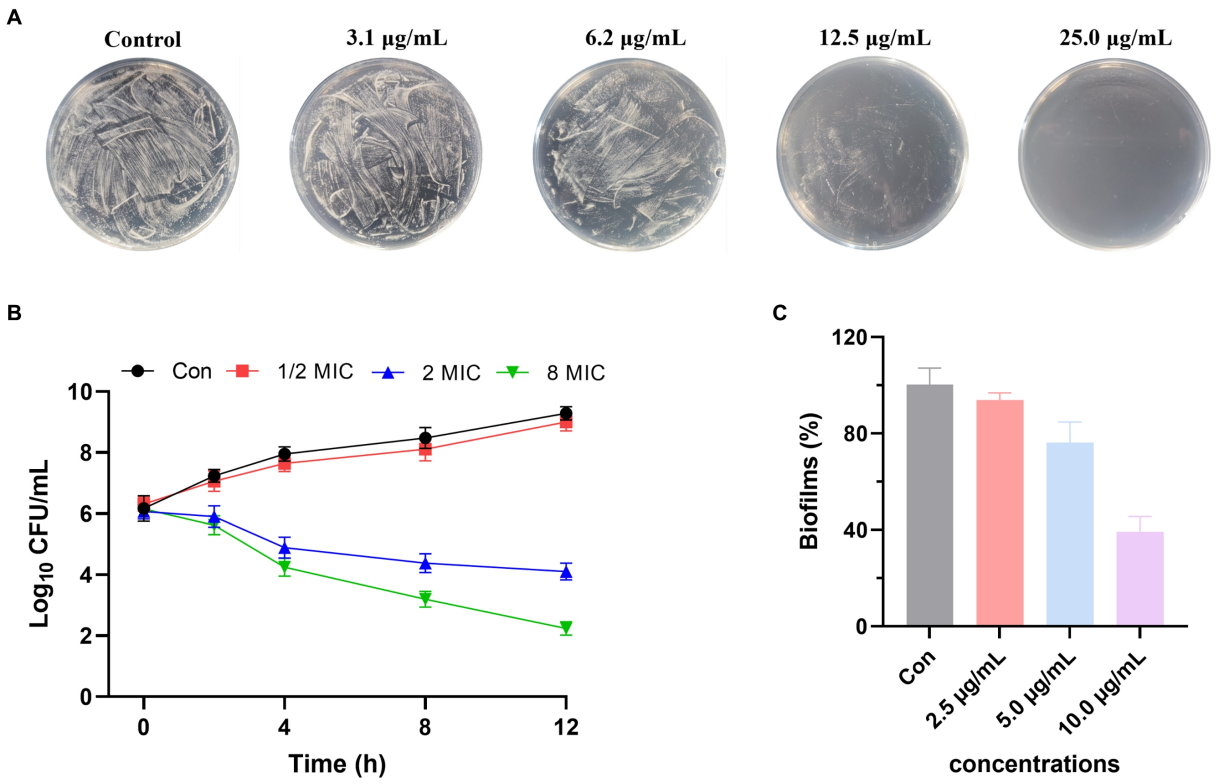

FIGURE 7
(A) Anti-*Agrobacterium tumefactions* activity of **1** using plate spread inhibition assay. **(B)** Time-kill curves of **1** against *A. tumefactions*. **(C)** Biofilm inhibition activity of **1** against *A. tumefactions*.

of detection for the colony counts was 2 $\log_{10}$ CFU/mL (Foerster et al., 2016). For bacterial biofilm experiment, after overnight cultivation, 100 μL/well of the bacterial culture, diluted in LB broth with 0.5% glucose, was aliquoted into 96-well microplates with 1 μL of different concentrations of **1** and incubated at 37°C for 24 h. After incubation, each well was rinsed with 1 × PBS to remove non-adherent cells and then dried at 37°C. CV staining was used to determine the remaining total biofilm biomass, and the absorbance was measured at 550 nm (Song et al., 2021).

4 Conclusion

In conclusion, 10 sesquiterpene derivatives (**1**–**10**), including four new compounds (**1**–**4**), were obtained from the marine-derived fungal strain *Trichoderma effusum* HBU-2019-190 by using bioassay and HPLC guided methods. The chemical structures of these compounds were determined and confirmed through extensive spectroscopic methods and chemical calculations. Notably, some of these compounds exhibited strong inhibitory activity against *Agrobacterium tumefaciens*, providing significant value for the development of novel anti-*A. tumefactions* pesticides.

Data availability statement

The original contributions presented in the study are included in the article/supplementary material; further inquiries can be directed to the corresponding authors.

Author contributions

YL: Methodology, Writing – original draft. LQ: Data curation, Formal analysis, Writing – original draft. MX: Formal analysis, Investigation, Writing – original draft. WL: Data curation, Methodology, Writing – original draft. NL: Supervision, Writing – review & editing. XH: Funding acquisition, Supervision, Writing – review & editing. YZ: Funding acquisition, Supervision, Writing – review & editing.

Funding

The author(s) declare that financial support was received for the research, authorship, and/or publication of this article. This study was supported by the Natural Science Foundation of Hebei Province of China (No. H2022201056).

Acknowledgments

We thank the High Performance Computer Center of Hebei University.

Conflict of interest

The authors declare that the research was conducted in the absence of any commercial or financial relationships that could be construed as a potential conflict of interest.

Publisher's note

References

Ahmed, B., Jailani, A., Lee, J. H., and Lee, J. (2022). Effect of halogenated indoles on biofilm formation, virulence, and root surface colonization by *Agrobacterium tumefaciens*. *Chemosphere* 293:133603. doi: 10.1016/j.chemosphere.2022.133603

Cai, F., and Druzhinina, I. S. (2021). In honor of John Bissett: authoritative guidelines on molecular identification of *Trichoderma*. *Fungal Divers.* 107, 1–69. doi: 10.1007/s13225-020-00464-4

Cao, F., Liu, X.-M., Wang, X., Zhang, Y.-H., Yang, J., Lou, D.-Q., et al. (2023). Structural diversity and biological activities of indole-diterpenoids from *Penicillium janthinellum* by co-culture with *Paecilomyces formosus*. *Bioorg. Chem.* 141:106863. doi: 10.1016/j.bioorg.2023.106863

Ferreira, F. V., and Matías, A.-M. (2021). *Trichoderma* as biological control agent: scope and prospects to improve efficacy. *World J. Microbiol. Biotechnol.* 37:90. doi: 10.1007/s11274-021-03058-7

Foerster, S., Unemo, M., Hathaway, L. J., Low, N., and Althaus, C. L. (2016). Time-kill curve analysis and pharmacodynamic modelling for in vitro evaluation of antimicrobials against *Neisseria gonorrhoeae*. *BMC Microbiol.* 16, 1–11. doi: 10.1186/s12866-016-0838-9

Hang, P., Yang, X., Xie, A.-L., Zhu, L., Ding, H.-X., Yuan, X.-J., et al. (2022). The antibacterial mechanism of phenylacetic acid isolated from *Bacillus megaterium* L2 against *Agrobacterium tumefaciens*. *Peer J.* 10:e14304. doi: 10.7717/peerj.14304

Harman, G. E., Herrera-Estrella, A. H., Horwitz, B. A., and Lorito, M. (2012). *Trichoderma*–from basic biology to biotechnology. *Microbiology* 158, 1–2. doi: 10.1099/mic.0.056424-0

Henne, P., Thiericke, R., Grabley, S., Hutter, K., Wink, J., Jurkiewicz, E., et al. (1993). Secondary metabolites by chemical screening, 23. Waraterpols, new *Penicillium* metabolites and their derivatives. *Eur. J. Org. Chem.* 1993, 565–571. doi: 10.1002/jlac.199319930192

Jailani, A., Ahmed, B., Lee, J. H., and Lee, J. (2022). Inhibition of *Agrobacterium tumefaciens* growth and biofilm formation by tannic acid. *Biomedicine* 10:1619. doi: 10.3390/biomedicines10071619

Kuttikrishnan, S., Prabhu, K. S., Al Sharie, A. H., Al Zu'bi, Y. O., Alali, F. Q., Oberlies, N. H., et al. (2022). Natural resorcylic acid lactones: a chemical biology approach for anticancer activity. *Drug Discov. Today* 27, 547–557. doi: 10.1016/j.drudis.2021.10.001

Lewis, J. A., and Fleming, J. T. (1995). Basic culture methods. *Method. Cell Biol.* 48, 3–29. doi: 10.1016/S0091-679X(08)61381-3

Li, L., Chang, Q.-H., Zhang, S.-S., Yang, K., Chen, F.-L., Zhu, H.-J., et al. (2022). (±)-Brevianamides Z and Z1, new diketopiperazine alkaloids from the marine-derived fungus *aspergillus versicolor*. *J. Mol. Struct.* 1261:132904. doi: 10.1016/j.molstruc.2022.132904

Mukhopadhyay, R., and Deepak, K. (2020). *Trichoderma*: a beneficial antifungal agent and insights into its mechanism of biocontrol potential. *Egypt J. Biol. Pest. Control* 30, 1–8. doi: 10.1186/s41938-020-00333-x

Schug, A. R., Bartel, A., Scholtzek, A. D., Meurer, M., Brombach, J., Hensel, V., et al. (2020). Biocide susceptibility testing of bacteria: development of a broth microdilution method. *Vet. Microbiol.* 248:108791. doi: 10.1016/j.vetmic.2020.108791

Shu, H.-Z., Peng, C., Bu, L., Guo, L., Liu, F., and Xiong, L. (2021). Bisabolane-type *sesquiterpenoids*: structural diversity and biological activity. *Phytochemistry* 192:112927. doi: 10.1016/j.phytochem.2021.112927

Song, Z. M., Zhang, J. L., Zhou, K., Yue, L. M., Zhang, Y., Wang, C. Y., et al. (2021). Anthraquinones as potential antibiofilm agents against methicillin-resistant *Staphylococcus aureus*. *Front. Microbiol.* 12:709826. doi: 10.3389/fmicb.2021.709826

Torres, M., Jiquel, A., Jeanne, E., Naquin, D., Dessaux, Y., and Faure, D. (2022). *Agrobacterium tumefaciens* fitness genes involved in the colonization of plant tumors and roots. *New Phytol.* 233, 905–918. doi: 10.1111/nph.17810

Tyśkiewicz, R., Nowak, A., Ozimek, E., and Jaroszuk-Ściseł, J. (2022). *Trichoderma*: the current status of its application in agriculture for the biocontrol of fungal phytopathogens and stimulation of plant growth. *Int. J. Mol. Sci.* 23:2329. doi: 10.3390/ijms23042329

Wang, C.-Y., Liu, Y.-F., Cao, F., and Wang, C.-Y. (2016). Bisabolane-type *Sesquiterpenoids* from a gorgonian-derived *aspergillus* sp. fungus induced by DNA methyltransferase inhibitor. *Chem. Nat. Compd.* 52, 1129–1132. doi: 10.1007/s10600-016-1885-z

Ye, F., Liu, M., Cao, Y., and Lu, C. (2019). Two new bisabolane-type sesquiterpenes isolated from the endophytic fungal strain CM112 in *Xishuangbanna*. *Chin. J. Antibiot.* 44, 674–678. doi: 10.13461/j.cnki.cja.006414

Yu, M., Wang, Y.-C., Huang, C.-J., Ma, L.-S., and Lai, E.-M. (2021). *Agrobacterium tumefaciens* deploys a versatile antibacterial strategy to increase its competitiveness. *J. Bacteriol.* 203, e00490–e00520. doi: 10.1128/JB.00490-20

Zin, N. A., and Badaluddin, N. A. (2020). Biological functions of *Trichoderma* spp. for agriculture applications. *Ann. Agric. Sci.* 65, 168–178. doi: 10.1016/j.aoas.2020.09.003

frontiers | Frontiers in Microbiology

TYPE Original Research
PUBLISHED 07 August 2024
DOI 10.3389/fmicb.2024.1447301

OPEN ACCESS

EDITED BY
Yovani Marrero-Ponce,
University of Valencia, Spain

REVIEWED BY
Dexi Li,
Henan Agricultural University, China
Ruoyu Mao,
Chinese Academy of Agricultural Sciences, China

*CORRESPONDENCE
Francesco Buonocore
✉ fbuono@unitus.it
Francesca Bugli
✉ francesca.bugli@unicatt.it

†These authors have contributed equally to this work and share first authorship

‡These authors share last authorship

RECEIVED 11 June 2024
ACCEPTED 18 July 2024
PUBLISHED 07 August 2024

CITATION
Squitieri D, Massaro F, Graziano MM, Borocci S, Cacaci M, Di Vito M, Porcelli F, Rosato R, Ceccacci F, Sanguinetti M, Buonocore F and Bugli F (2024) Trematocine-derived antimicrobial peptides from the Antarctic fish *Trematomus bernacchaii*: potent antibacterial agents against ESKAPE pathogens. *Front. Microbiol.* 15:1447301. doi: 10.3389/fmicb.2024.1447301

Trematocine-derived antimicrobial peptides from the Antarctic fish *Trematomus bernacchaii*: potent antibacterial agents against ESKAPE pathogens

Damiano Squitieri[1†], Federica Massaro[2†], Monica Mollica Graziano[2], Stefano Borocci[2,3], Margherita Cacaci[1,4], Maura Di Vito[1], Fernando Porcelli[2], Roberto Rosato[1], Francesca Ceccacci[3], Maurizio Sanguinetti[1,4‡], Francesco Buonocore[2*‡] and Francesca Bugli[1,4*‡]

[1]Department of Basic Biotechnological Sciences, Intensive and Perioperative Clinics, Catholic University of the Sacred Heart, Rome, Italy, [2]Department for Innovation in Biological, Agro-Food and Forest Systems (DIBAF), University of Tuscia, Viterbo, Italy, [3]Institute for Biological Systems of Italian National Research Council (ISB-CNR), Secondary Office of Rome-Reaction Mechanisms c/o Department of Chemistry, La Sapienza University of Rome, Rome, Italy, [4]Department of Laboratory Sciences and Infectious Diseases, A. Gemelli University Hospital Foundation IRCCS, Rome, Italy

Introduction: This study investigated the interaction with membrane mimetic systems (LUVs), bacterial membranes, the CD spectra, and the bactericidal activity of two designed trematocine mutants, named Trem-HK and Trem-HSK. Mutants were constructed from the scaffold of Trematocine (Trem), a natural 22-amino acid AMP from the Antarctic fish *Trematomus bernacchii*, aiming to increase their positive charge.

Methods: The selectivity of the designed AMPs towards bacterial membranes was improved compared to Trematocine, verified by their interaction with different LUVs and their membranolytic activity. Additionally, their α-helical conformation was not influenced by the amino acid substitutions. Our findings revealed a significant enhancement in antibacterial efficacy against ESKAPE (*Enterococcus faecium, Staphylococcus aureus, Klebsiella pneumoniae, Acinetobacter baumannii, Pseudomonas aeruginosa*, and *Enterobacteriaceae* family) pathogens for both Trem-HK and Trem-HSK.

Results: Firstly, we showed that the selectivity of the two new designed AMPs towards bacterial membranes was greatly improved compared to Trematocine, verifying their interaction with different LUVs and their membranolytic activity. We determined that their α-helical conformation was not influenced by the amino acid substitutions. We characterized the tested bacterial collection for resistance traits to different classes of antibiotics. The minimum inhibitory and bactericidal concentration (MIC and MBC) values of the ESKAPE collection were reduced by up to 80% compared to Trematocine. The bactericidal concentrations of Trematocine mutants showed important membranolytic action, evident by scanning electron microscopy, on all tested species. We further evaluated the cytotoxicity and hemolytic activity of the mutants. At 2.5μM concentration, both mutants demonstrated low cytotoxicity and hemolysis, indicating selectivity towards bacterial cells. However, these effects increased at higher concentrations.

Discussion: Assessment of *in vivo* toxicity using the *Galleria mellonella* model revealed no adverse effects in larvae treated with both mutants, even

at concentrations up to 20 times higher than the lowest MIC observed for *Acinetobacter baumannii*, suggesting a high potential safety profile for the mutants. This study highlights the significant improvement in antibacterial efficacy achieved by increasing the positive charge of Trem-HK and Trem-HSK. This improvement was reached at the cost of reduced biocompatibility. Further research is necessary to optimize the balance between efficacy and safety for these promising AMPs.

KEYWORDS

antimicrobial peptides, antimicrobial resistance, ESKAPE pathogens, membranolytic agents, multi-drug resistant bacteria

1 Introduction

One of the most severe threats to modern public health is related to the antimicrobial resistance (AMR) establishment, with particular regard on bacterial opportunistic pathogens (O'Neill, 2016; Mba et al., 2022). This phenomenon occurs when genetic and phenotypic changes in bacteria cause the antibiotics to become less effective when used to treat infections. Recently, it was estimated that in 2019, on the basis of predictive models, there were 4.95 million (3.62–6.57) deaths globally associated with bacterial AMR (Murray et al., 2022). In 2017 (and in 2024 update), the World Health Organization (WHO) published a list of pathogens for which urgent action was needed: it includes pathogens of the ESKAPE group (Browne et al., 2020; WHO, 2024). These bacteria have garnered the acronym "ESKAPE" due to their remarkable ability to escape the antimicrobial actions of conventional antibiotics, making them responsible for a significant portion of healthcare-associated infections worldwide (Ayobami et al., 2022). Among all the different classes of antibiotics currently in use, β-lactams stand out as some of the most frequently prescribed (Kapoor et al., 2017). Regrettably, many strains of bacteria have developed β-lactamases, enzymes that deactivate β-lactam antibiotics by breaking down the characteristic 4-atom β-lactam ring by hydrolysis. These versatile enzymes have a broad range of substrates and are known as Extended Spectrum β-lactamases (ESBLs). According to Ambler's classification, which categorizes β-lactamases based on structural similarities, there are four classes: three of them feature a serine residue in their active site, while the fourth class consists of metallo-β-lactamases (MBLs) that incorporate a Zinc ion in their active site (referred to as Group B β-lactamases) (Pandey et al., 2023). The majority of these MBLs are encoded by genes such as *bla*VIM, *bla*IMP, and *bla*NDM-1. Horizontal gene transfer is a key mechanism by which ESKAPE pathogens acquire and spread antibiotic resistance genes. The rise of pathogens that are resistant to existing antibiotics, making infections more difficult to treat and increasing the risk of deadly outbreaks, coincides with a declining pipeline of new antibiotic development (Hussain et al., 2021). Therefore, the design and development of new antimicrobial drugs to fight resistant infections is increasingly urgent for public health. Antimicrobial peptides (AMP) are possible candidates to help in solving this problem (Magana et al., 2020). These peptides are widely distributed in all organisms, from plants to bacteria, invertebrates, and vertebrates, as part of the innate immune responses (Koo and Seo, 2019; Cardoso et al., 2021; Li et al., 2022). Classification is often based on their structure, such as α-helices, β-sheets, or extended and loop structures, with α-helix AMPs typically displaying an amphipathic nature (Buonocore et al., 2019). These peptides primarily target the bacteria plasmatic membrane, and their selectivity, with respect to mammalian cell membrane, depends on primary and secondary structure and membrane charge density, considering the negative charge commonly found in bacterial cell walls. Their ability to target a broad spectrum of pathogens (bacteria, viruses, fungi, and parasites), including ESKAPE group, united with their relatively low likelihood of inducing resistance, makes them attractive candidates for developing novel antimicrobial treatments (Luo et al., 2023). In this paper, we investigate the biological activity of two mutants of trematocine (Della Pelle et al., 2020), an AMP identified from the red-blooded Antarctic fish *Trematomus bernacchii*. Antarctic species are an excellent source for novel biomolecules due to the peculiar environment where they live and to the specific adaptations that they have evolved. Some specific site mutations were designed to improve the bactericidal activity of the natural peptide. Firstly, we determined the interactions between these new AMPs and phospholipid vesicles of different composition designed to mimic both bacterial and mammalian cell membranes. Subsequently, we analyzed their structural characteristics and assessed their bactericidal efficacy against a large spectrum of clinical isolates ($n = 50$) belonging to the ESKAPE group. The different bacterial strains were firstly genotypically and phenotypically characterized for resistance traits to different classes of antibiotic drugs commonly used in clinical practice. Successively, we evaluated the *in vitro* toxicity of these AMPs on both mammalian cell lines and human erythrocytes. Finally, we conducted *in vivo* toxicity experiments using *Galleria mellonella* larvae model to preliminary evaluate the potential pharmacological applications of these peptides. This multifaceted approach not only enhances our understanding on the peptides' properties but also provides valuable information for their future possible applications as new antibacterial drugs.

2 Materials and methods

2.1 Chemicals and peptides

All chemicals and solvents were purchased from Sigma-Aldrich. The lipids 1-palmitoyl-2-oleoyl-*sn*-glycero-3-phosphocholine (POPC) and 1-palmitoyl-2-oleoyl-*sn*-glycero-3-phospho-(1′-rac-glycerol) (POPG) were purchased from Avanti Polar Lipids (Alabaster, AL, USA).

Peptides Trem (FFGHLLRGIVSVGKHIHGLITG), Trem-HSK (WFFGKLLRGIVKVGKKIKGLIT) and Trem-HK (WFFGKLLRGIVSVGKKIKGLIT) were purchased from CASLO ApS, c/o Scion Technical University of Denmark with a purity >98%. Peptide concentrations were determined by absorption spectroscopy at 280 nm before each analysis.

2.2 Lipid vesicles preparation

The large unilamellar vesicles (LUVs) were composed of 100% POPC and a 70/30% (w/w) combination of POPC/POPG at a final concentration of 10 mM. The LUVs were prepared as previously described (Della Pelle et al., 2020). Briefly, specific amounts of lipids were dissolved in chloroform/methanol 9:1 (v/v). The solvent was then removed by rotary evaporation, and the samples were placed overnight under high vacuum. The lipid film was subsequently hydrated by adding 1 mL of buffer solution (10 mM phosphate buffer pH 7.4 with 150 mM NaCl and 0.8 mM EDTA) to obtain 10 mM lipid dispersion and subjected to 5 freeze–thaw cycles. The lipid suspensions were finally extruded through a polycarbonate membrane with pore of 100 nm using an Avanti Polar mini extruder. The LUVs obtained were used within 48 h from their preparation.

2.3 Partition constant determination

Peptide partitioning between a polar and apolar environment was studied by fluorescence spectroscopy, monitoring the increase of fluorescence of tryptophan (contained in the sequence of the two mutant peptides) upon increasing concentration of LUVs in the range between 0 to 1.1 mM.

Precisely, 1.0 μM solution of the peptide was titrated with LUVs of different compositions (POPC 100% and (70/30%) (w/w) POPC/POPG), and the fluorescence emission spectra were recorded between 315 and 400 nm with $\lambda_{exc} = 290$ nm. The measurements were performed with a scan speed of 200 nm/min, bandwidth for excitation and emission of 5 and 10 nm, respectively, and with a cross-oriented configuration of the polarizers ($pol_{em} = 0°$ and $pol_{exc} = 90°$) to reduce scattering from vesicles. The background buffer emission was subtracted from each spectrum. Mole fraction partition coefficients (K_x) were calculated from the fraction of the partitioned peptide (f_p) as previously described according to the Wimley equation (Wimley, 2010):

$$f_p = \frac{K_x [L]}{W + K_x [L]}$$

Finally, the free energy of partition was calculated using the relationship:

$$\Delta G^{\circ} = -RTln\, K_x$$

A Perkin Elmer LS 55 fluorometer was used for steady-state fluorescence measurements. The experiments were carried out at 25°C.

2.4 Quenching experiments

For all peptides, the fluorescence quenching was evaluated both in buffer solution, and in the presence of liposomes, by measuring the change of tryptophan emission fluorescence upon the addition of acrylamide as a quencher in the range between 0 and 170 mM. For the quenching experiments a 3 μM concentration of peptides was used. Measurements in the presence of liposomes were carried out using a peptide-lipid ratio of 1:1,000 (w/w). Before titration, each peptide was incubated with lipid vesicles for 30 min. Fluorescence spectra were recorded using an excitation wavelength of 295 nm and a scan speed of 200 nm/min. The obtained data were fitted using the Stern–Volmer equations:

$$\frac{F_0}{F} = 1 + K_{sv}[Q]$$

where F_0 and F are the fluorescence in the absence and in the presence of the acrylamide (Q), respectively, and K_{sv} is the Stern–Volmer constant.

Also, the Net Accessibility Factor (NAF) was calculated using the equation:

$$\mathrm{NAF} = \frac{K_{sv(\mathrm{LUV})}}{K_{sv(\mathrm{buffer})}}$$

2.5 Membrane permeabilization assay

The uptake of fluorescent probe 1-aminonaphtalene-8-sulfonic acid (ANS) was used for cell permeabilization studies. Specifically, the bacteria used as a model for a Gram− and a Gram+ strain (*Escherichia coli* ATCC 25922, and *Bacillus cereus* ATCC 10876) were grown in Luria Bertani (LB) medium. Subsequently, the cell suspensions were centrifuged at 3600 rpm and 4°C, washed, and resuspended in PBS buffer to achieve an OD_{600} of ~0.6.

Increasing amounts of peptide (ranging from 0 to 20 μM) were added to 700 μL of cell suspension in presence of 25.0 μM of ANS. Fluorescence spectra were recorded from 400 nm to 600 nm, using an excitation wavelength of 360 nm and excitation and emission band-pass of 5 nm and 2.5 nm, respectively. The disruption of cell membrane integrity was quantified by the increase of intensity of fluorescence using the following equation (Della Pelle et al., 2020):

$$\%\mathrm{Uptake\ ANS} = \frac{(F - F_0)}{F}\%$$

where F is the fluorescence of ANS observed at a given peptide concentration and F_0 is the fluorescence of ANS in the absence of peptides.

2.6 Circular dichroism spectroscopy

The secondary structures of the two peptides in a buffer solution (phosphate buffer 10 mM, pH 7.4 and 0.1 mM EDTA) and in presence of the membrane's mimicking system of POPC and (70/30%) (w/w) POPC/POPG were evaluated by Circular Dichroism (CD) spectroscopy using a J715 JASCO spectropolarimeter.

Briefly, a solution containing 30 μM of peptide was titrated with increasing amounts (ranging between 0 and 2.3 mM) of LUVs. CD spectra were recorded from 190 to 260 nm. The reported spectra are the average of 8 scans with a scanning speed of 100 nm/min, a response time of 2 s, and a bandwidth of 1.0 nm.

The CD signals in millidegrees were converted into mean residue molar ellipticities, $[\theta]_{mr}$ (deg cm^2 dmol^{-1}), using the equation:

$$[\theta]_{mr} = \frac{\theta_{Obs}}{10 \times C \times l \times (N-1)}$$

here θ_{Obs} is the observed ellipticity in millidegrees, C is the molar concentration of the peptide, l is the path length of the cell in cm, and N is the number of amino acids in the peptide.

2.7 Bacterial strains

A collection of 50 bacterial strains was used for AMPs susceptibility testing. Those strains are clinical isolates derived from positive blood cultures and each ten strains belong to the following ESKAPE bacterial species: *K. pneumoniae*, *A. baumannii*, *P. aeruginosa*, *E. faecium* and *S. aureus*. Each strain was firstly characterized for genotypic and phenotypic antibiotic-resistance determinants. The genotypic analysis, that also include the species identification, was performed using the FilmArray Blood Culture Identification 2 panel (Bio-Mérieux, Marcy l'Etoile, France). The phenotypic antimicrobial susceptibility testing was performed using VITEK® 2 system with n379 or n397 and xn24 cards (Bio-Mérieux). The susceptibility categorization was performed using EUCAST breakpoint tables version 13.1 (EUCAST, 2014).

2.8 Minimum inhibitory concentration (MIC)

To determine the minimum inhibitory concentrations (MIC) of the three antimicrobial peptides, a broth microdilution assay was performed. Bacterial suspensions equal to 0.5 McFarland standard of the individual selected isolates was prepared in saline solution (Fresenius Kabi, Bad Homburg vor der Höhe, Germany) using Densicheck (bio-Mérieux). These suspensions were then diluted in a 1:100 ratio in cation-adjusted Muller Hinton broth (Sigma-Aldrich; St. Louis, Missouri, United States). The final concentration of the peptides ranged from 2 to 128 μg/mL, while the microorganism concentrations were maintained at approximately 5×10^5 CFU/mL, in compliance with the EUCAST guidelines for the broth microdilution method v5.0 (EUCAST, 2024). In each assay, which was conducted in duplicate, we included both growth controls (microorganism without peptides) and negative controls (peptides without microorganisms). The plates were then incubated overnight at 37°C in an atmosphere of 5% CO_2 using the New Brunswick™ Excella® E24 Series (New Brunswick Scientific; Edison, New Jersey, United States). The MICs were visually determined as the outcome of this assay. MIC_{50} and MIC_{90} were calculated as previously described (Schwarz et al., 2010).

2.9 Minimum bactericidal concentration (MBC)

To determine the Minimum Bactericidal Concentrations (MBC) of the three AMPs, a new broth microdilution assay was conducted, following the same protocol as that employed for MIC determination. After an overnight incubation, for MBC determination, we plated a 3 μL aliquot of each condition present in the 96-well plate onto Mueller Hinton agar plates (Sigma-Aldrich, St. Louis, Missouri, United States). Following an overnight incubation period, we assigned the MBC values to conditions where no visible bacterial growth was observed on the Mueller Hinton agar plates. MBC_{50} and MBC_{90} were calculated as previously described for MIC_{50} and MIC_{90} (Schwarz et al., 2010).

2.10 Growth curves

A sensible and resistant representant strain of each species has been randomly selected to perform an optic-based kinetic growth curve obtained using the Cytation5 multimode reader from Biotek (Winooski, Vermont, United States). This reader performed a kinetic protocol spanning 21 h, during which absorbance readings were taken every 30 min in a 96-well plate with a flat bottom (Falcon Corning Incorporated, New York, United States). The experimental setup reflects the broth microdilution assay parameters. The kinetic protocol included plate incubation at 37°C with a 5% CO_2 atmosphere, accompanied by continuous orbital shaking. The absorbance readings were conducted at a wavelength of 630 nm. The acquired data were subsequently processed and visualized using GraphPad Prism software version 9.3.1 (La Jolla, CA, United States).

2.11 Scanning electron microscopy

To evaluate morphological changes (due to the membranolytic activity of the AMPs) on different species tested, a resistant representant strain of each species has been randomly selected. Around 5×10^5 CFU/mL inoculum of each strain has been treated, or not (growth control), for 4 h with peptide concentrations equal to 0.75× MIC_{90} values in cation-adjusted Muller Hinton broth (Sigma-Aldrich). After the treatment, bacterial cells were collected by centrifugation, concentrated in saline solution, and 20 microliters were spread on a sterile Thermanox plastic coverslip (Thermofischer Scientific, Waltham, Massachusetts, United States) and let dry under laminar flow hood.

Afterwards, samples were fixated with 2.5% Glutaraldehyde solution (Sigma-Aldrich) and dehydrated via immersion in crescent gradient of ethanol concentration, from 30 to 100%, with a multi-step procedure of 10 min each. Successively samples were metallized with gold using a High-Resolution Sputter Coater AGB7234 (Agar Scientific, Stansted, United Kingdom). Morphology of cells onto surfaces were observed with Supra25 SEM microscope (Zeiss, Oberkochen, Germany). Representative micrographs were acquired in secondary electrons mode at an acceleration voltage of 8 kV. For each sample at least four randomly selected fields were acquired at magnification of 8,000×.

2.12 Hemolytic activity

The peptide's hemolytic activity was evaluated by testing different concentrations of peptides (from 1.25 to 20 μM, so from 3 to 50 μg/mL) against rabbit erythrocytes (Rockland) previously purified and maintained in Alsever's solution. After removing Alsever's solution by centrifugation, the erythrocytes were washed and resuspended in PBS to the appropriate dilution. Following, for each concentration tested, 100 μL of erythrocytes solution (at density of 2.5×10^6 cells/well) were incubated with peptides for 2 h at 37°C. After this time, intact erythrocytes were removed by centrifugation, and the absorbance (A) of the supernatant was measured at 492 nm. Erythrocytes were incubated only with PBS buffer as the negative control and in the presence of Triton X-100 at 2% (v/v) for the positive control. The Hemolysis percentage was calculated as follows (Chen et al., 2023):

$$\%\text{Hemolysis} = \frac{\left(A_{\text{Test group}} - A_{\text{Negative control}}\right)}{\left(A_{\text{Positive control}} - A_{\text{Negative control}}\right)}\%$$

2.13 *In vitro* cytotoxicity

The cytotoxicity of the two peptides was determined with the ATPLite Luminescence Assay against a primary human fibroblast cell line (FB789) (Bugli et al., 2022). The cells were grown in Dulbecco's Modified Eagle Medium (DMEM) containing 10% fetal calf serum (FCS), penicillin, and streptomycin antibiotics at 37°C and in a humidified atmosphere with 5% CO_2. Briefly, the cells were seeded at a density of 3,000 cells per well in 100 µL of culture medium and were allowed to adhere for 24 h. Subsequently 100 µL of culture medium was removed and replaced with a new culture medium containing the peptide to be tested diluted to the appropriate concentration (from 1.25 to 20 µM, so from 3 to 50 µg/mL). After 3 and 6 h of treatment the cells were lysed and incubated with substrate solution (Luciferase/Luciferin) for 10 min in the dark. The luminescence was measured using a microplate luminometer (Victor II PerkinElmer). As a negative control the cells were grown in medium without the peptides, and for a positive control the cells were grown in medium with 2% v/v NaN_3. The percentage of cell viability was determined as follows:

$$\%\text{Cells viability} = \frac{\text{RLU}_{\text{Test group}}}{\text{RLU}_{\text{Negative control}}}\%$$

where RLU is the unit of relative light measured by the instrument.

2.14 *In vivo* toxicity testing on *Galleria mellonella* larvae

The *in vivo* toxicity testing of the peptides was performed using the *Galleria mellonella* larvae as described before (Garcia Maset et al., 2022; Di Vito et al., 2023). The treatments administration was performed with a 0.5 mL syringe into the haemocoel through the last right pro-leg in aseptic conditions. Before injections the pro-leg area was decontaminated with 70% (v/v) Ethanol solution (Carlo Erba, Milan, Italy). Each treatment and control group were composed of 10 larvae. The treatments administered volumes was equal to 10 µL with peptides concentration of 62.5 µg/mL, that is twice the biggest MIC_{90} obtained value (except for Trem-HK and *P. aeruginosa*), 32 µg/mL. The control group was administered with 0.9% NaCl injectable solution (Fresenius Kabi, Bad Homburg vor der Höhe, Germany). After the treatment, larvae were incubated at 33°C in aerobic conditions. The viability of larvae was visually evaluated every 24 h for 72 h; lack of motility after stimulation, and melanization were considered as death indicators according to Loh et al. (2013) criteria. Cocoon formation was excluded as criteria because the phenomenon was not observed in the 3-day observational period.

2.15 Statistical analysis

All experiments were repeated at least in triplicate, to ensure reproducibility. Gaussian distribution data were analyzed using mean and standard deviation parameters. *In vivo* toxicity testing on *Galleria mellonella* larvae was performed with 10 replicates per group. Significant difference was defined as p-value < 0.05. Numerical data are normally presented in the text as means + SD. Homogeneity of variances was tested before data processing. Data from ATPlite assay were analysed by one-way ANOVA, followed by Bonferroni's test. Statistical analysis and graphics were performed and obtained using GraphPad Prism software version 9.3.1 (La Jolla, CA, United States).

3 Results

3.1 Peptide design

Two new peptides, named Trem-HK and Trem-HSK, were designed starting from the sequence of Trematocine, a 22 amino acids AMP identified from the Antarctic fish *Trematomus bernacchii*. This peptide was not cytotoxic and hemolytic and had shown antimicrobial activity against some model bacteria, including *Escherichia coli* and *Bacillus pumilus* (Della Pelle et al., 2020). Since the positive charge is significant for the interaction with the negatively charged bacterial membrane, the sequence of this natural peptide was modified by enhancing the number of positively charged residues. In this way, the peptides affinity for anionic membranes should be improved and, therefore, also their antibacterial activity.

Figure 1 shows an alignment between the peptide sequences of the Trematocine and the two mutants carried out by "Clustal Omega".[1]

In the Trem-HK peptide, three His residues have been substituted with a Lys, whereas in the Trem-HSK peptide, in addition, a Ser residue has also been changed with a Lys. Moreover, a tryptophan amino acid residue was added at the N-terminus to allow physico-chemical investigations on the peptides by fluorescence spectroscopy,

1 https://www.ebi.ac.uk/Tools/msa/clustalo

```
Trematocine     -FFGHLLRGIVSVGKHIHGLITG   22
Trem-HK         WFFGKLLRGIVSVGKKIKGLIT-   22
Trem-HSK        WFFGKLLRGIVKVGKKIKGLIT-   22
                ***:******.***:*:****
```

FIGURE 1
Alignment between Trematocine (Trem), Trem-HK and Trem-HSK peptide sequences. Asterisks (*) indicate amino acid residues that are conserved in all peptides. Colon (:) and dot (.) correspond to positions in which amino acids have been substituted with others showing similar physico-chemical characteristics.

and the final Gly residue was removed to maintain constant the total number of amino acids.

The net charge, molecular weight, isoelectric point and hydrophobic moment of the peptides are reported in Table 1.

3.2 Partition constant determination

Tryptophan fluorescence is sensitive to the environment polarity (Lakowicz, 2006). Thus, tryptophan can be used as probe to study the interaction between peptides and membranes since when tryptophan is in contact with a lipid bilayer, an increase in fluorescence and a blue shift is observed (Freire et al., 2011).

The change of Trp fluorescence was used to evaluate the interaction of Trematocine mutants with two membrane mimetic systems (LUVs), composed of 100% 1-Palmitoyl-2-oleoyl-*sn*-glycero-3-phosphocholine (POPC), that mimic the mammalian cell membranes, and (70/30)% w/w POPC/POPG (1-Palmitoyl-2-oleoyl-*sn*-glycero-3-[phospho-*rac*-(1-glycerol)]), mimicking the bacterial membrane. Supplementary Figure S1 shows the binding isotherms for the peptides upon addition of increasing amount of lipid vesicles.

Table 2 reports the mole fraction partition constant K_x, the free energy of partition, and the selectivity ratio defined as the ratio between the value of the partition constant measured in the presence of POPC/POPG vesicles and the value measured in the presence of POPC vesicles.

The high values of the partition constants indicate that both peptides strongly interact with lipid vesicles partitioning from the water environment. However, the close to 1 value of the selectivity ratio for both peptides indicate a very low selectivity toward one of the two tested membrane models.

TABLE 1 Physico-chemical properties of the trematocine and the two mutant peptides.

Peptide	Net charge	Molecular weight (Da)	pI	
Trematocine	+2	2358.82	11.00	0.550
Trem-HSK	+6	2502.17	11.39	0.488
Trem-HK	+5	2461.08	11.33	0.533

3.3 Quenching experiments

Fluorescence quenching studies with acrylamide for Trem-HK and Trem-HSK peptides were conducted to further elucidate their interactions with model membranes. We used acrylamide since it is a neutral collisional quencher for Trp and it is a small molecule that can easily diffuse in solution. The obtained quenching values depend on the tryptophan accessibility to the quencher itself (Phillips et al., 1986).

Figure 2 shows the classical Stern-Volmer plots obtained for Trem-HSK and Trem-HK peptides in buffer and in the presence of LUVs of different composition.

Table 3 shows the values of the Stern-Volmer constants (K_{SV}), obtained by the Stern-Volmer equation, and the NAF (Net Accessibility Factor). The reciprocal of K_{SV} is the quencher concentration capable of decreasing the initial fluorescence by 50%. Therefore, the value of the Stern-Volmer constant is indicative of the exposure of the fluorophore (Trp) to the quencher and to the solvent. The lower values obtained in the presence of liposomes, compared to the value measured in buffer, indicate a decrease in quenching efficiency resulting from a lower exposure of tryptophan to the solvent. The results obtained from the partition measurements and the quenching experiments show that both peptides interact with the liposomes formed by POPC and POPC/POPG.

The NAF value, lower in the presence of POPC/POPG than in the presence of POPC for both peptides, indicates a more robust interaction with anionic membrane models, making the Trp less accessible to the quencher.

TABLE 2 Partition constant, selectivity ratio, and free energy change of partition for the peptides Trem-HK and Trem-HSK in presence of POPC and POPC/POPG LUVs.

Peptide	LUVs	K_x	Selectivity ratio	ΔG (kJ/mol)
Trem-HSK	POPC	$(4.53 \pm 1.02) \times 10^5$	1.28	−31.73
	POPC/POPG	$(5.80 \pm 1.19) \times 10^5$		−32.33
Trem-HK	POPC	$(5.43 \pm 1.12) \times 10^5$	1.10	−32.17
	POPC/POPG	$(5.98 \pm 1.32) \times 10^5$		−32.40

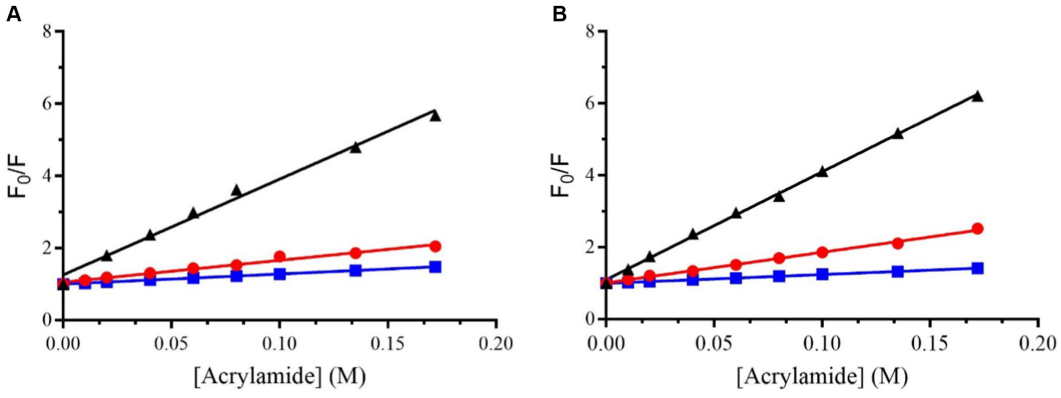

FIGURE 2
Stern–Volmer plots for the quenching of Trp (the first amino acid of the sequence) in Trem-HSK **(A)** and Trem-HK **(B)** measured in buffer (black), in the presence of POPC (red) and in the presence of (70/30)% w/w POPC/POPG (blue).

3.4 ANS membrane permeabilization assay

To determine the ability of Trem-HK and Trem-HSK peptides to disrupt and permeabilize the outer membrane of a model Gram-negative bacteria (*Escherichia coli* ATCC 25922) and the plasmatic membrane of a model Gram-positive bacteria (*Bacillus cereus* ATCC 10876) we carried out the permeabilization assay using the fluorescent probe (ANS).

The fluorescence of ANS is relatively weak in an aqueous solution and strong in hydrophobic environment. ANS is not able to pass the bacterial membrane. Still, upon addition of peptides capable of interfering with the cell membrane integrity, it can be incorporated into the lipid bilayer and, therefore, its fluorescence intensity increases drastically (Schäfer and Wenzel, 2020).

Figure 3 shows the percentage of ANS uptake at the different tested concentrations of peptides.

From these data it is possible to highlight that the peptides have a great ability to alter both the plasmatic membrane of *Bacillus cereus* and the outer membrane of *Escherichia coli*. In fact, the percentage of uptake is already very high at low concentration values.

3.5 Circular dichroism spectroscopy

Most antimicrobial peptides are unstructured in aqueous solutions, but when they interact with membranes a total or partial transition into an α-helical structure can be observed. CD studies were performed to investigate the structural changes of the two peptides in the presence of the tested model membrane. CD spectra are reported in Figure 4. A strong negative band at ~200 nm (red line) characteristics of random coil conformation was highlighted in buffer. Upon addition of lipid vesicles, a positive band at ~195 nm and two minima at ~208 nm and ~222 nm show up, suggesting that the peptides were assuming an α-helical conformation.

The percentage of α-helical content of Trem-HK and Trem-HSK in presence of POPC and POPC-POPG vesicles was calculated from experimental CD data by using the K2D3 algorithm (Louis-Jeune et al., 2012) (Supplementary Figure S2). The percentage of α-helical content, for both peptides, increases with the increase of lipid-peptide ([L]/[P]) ratio passing from zero (random coil, [L]/[P] = 0) to ~75% in the presence of POPC-POPG vesicles and 30–40% in presence of POPC vesicles for a [L]/[P] ratio above of 16.7. Moreover, Trem-HK and Trem-HSK show a higher α-helix content, for each [L]/[P] ratio, in the presence of anionic membrane (POPC-POPG) with respect to zwitterionic membrane (POPC) (Louis-Jeune et al., 2012).

TABLE 3 Stern-Volmer constants and NAF values for the two peptides for the different tested conditions.

Peptide	System	K_{sv} (M^{-1})	NAF
Trem-HSK	Buffer	27.0 ± 0.7	1.00
	POPC	6.0 ± 0.1	0.22
	POPC-POPG	3.00 ± 0.02	0.11
Trem-HK	Buffer	27.0 ± 0.9	1.00
	POPC	9.0 ± 0.3	0.33
	POPC-POPG	2.40 ± 0.03	0.09

3.6 Clinical isolates characterization

The bacterial collection consists of clinical strains isolated from monomicrobic positive blood cultures, and successively tested genotypically and phenotypically for species identification and AMR characterization. The search for AMR traits included qPCR-based detection of some important resistance-associated genes from primary sample and antimicrobial susceptibility testing from sub-cultured plates.

As shown in Table 4, the collection divided each species in five Resistant (R) and five Susceptible (S) strains based on the upcoming criteria. *K. pneumoniae* and *P. aeruginosa* resistant isolates involved in this study must be intended as MDR strains alongside with ESBL genotype and phenotype involving carbapenem resistance (CRE and CRPA, respectively). *A. baumannii* resistant strains, are carbapenem-resistant *A. baumannii* (CRAB) with an additional Colistin resistance to discriminate them from the sensible clinical isolate, this classification was made on AST phenotypic base (bla_{OXA-23} is not a target in the used syndromic panel). Gram-positive bacteria *S. aureus* and *E. faecium* are indicated as resistant strains to Methicillin (MRSA) and Vancomycin (VRE) respectively, based on genetic presence of resistance genes, but also confirmed by Oxacillin and Vancomycin MIC values.

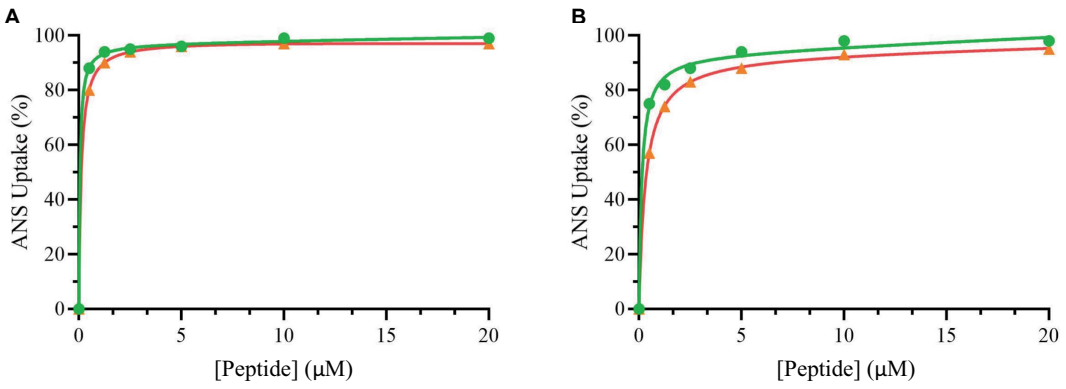

FIGURE 3
Percentage of ANS uptake of *Bacillus cereus* (orange), *Escherichia coli* (green) as a function of peptide Trem-HSK **(A)** and Trem-HK **(B)** concentration.

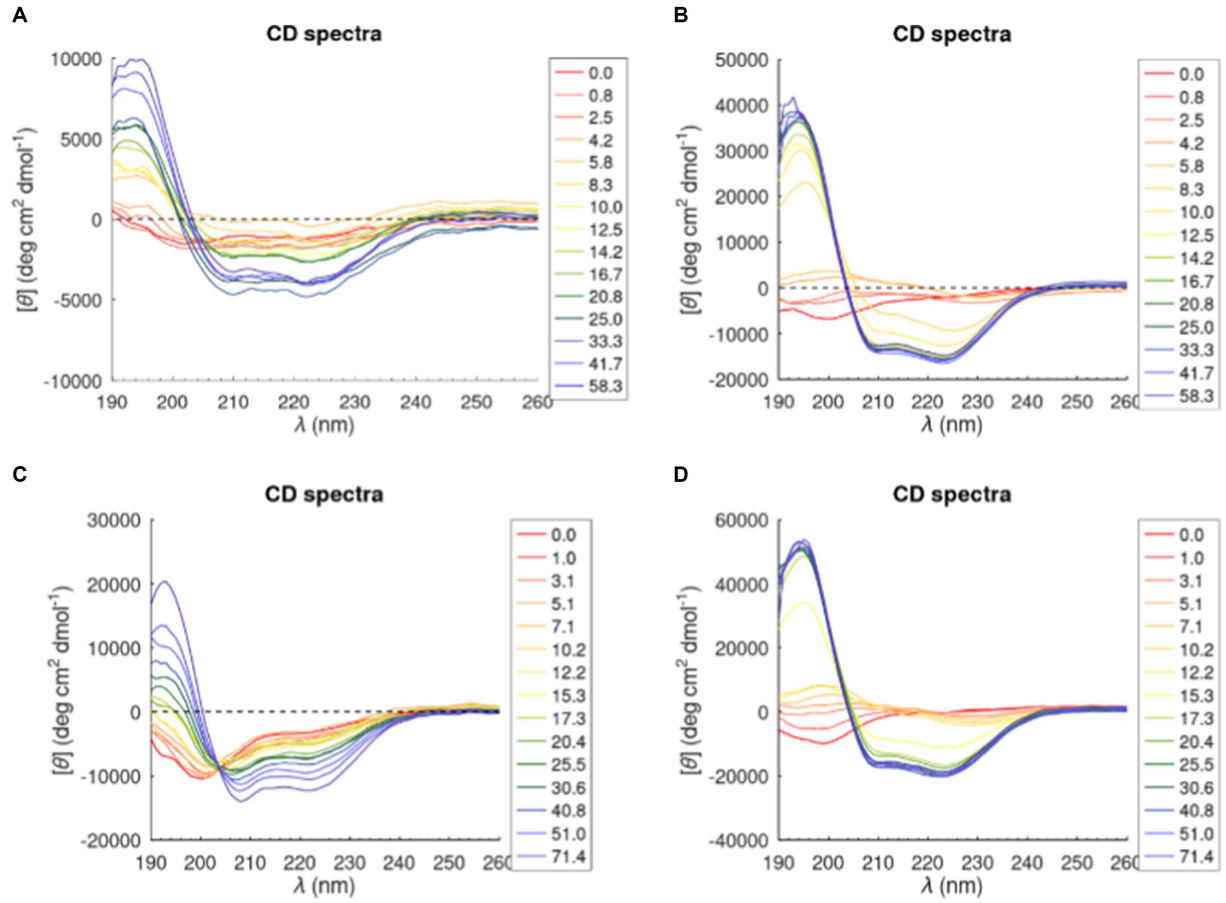

FIGURE 4
CD spectra of Trem-HK and Trem-HSK peptides in POPC **(A)** and **(C)** and (70/30)% w/w POPC—POPG **(B)** and **(D)**. The legend shows the lipid/peptide ratio value in each graph.

TABLE 4 Summarizing table of the bacterial collection used in this study.

Species	Strain number (R/S)	Antimicrobial resistance genes detected
Enterococcus faecium	10 (5/5)	van_A (4), van_B (1)
Staphylococcus aureus	10 (5/5)	mec_A (3), mec_C (2)
Klebsiella pneumoniae	10 (5/5)	bla_{KPC} (3*), bla_{KPC} & bla_{OXA-48} (1), bla_{NDM} & bla_{CTX-M} (1)
Acinetobacter baumannii	10 (5/5)	–
Pseudomonas aeruginosa	10 (5/5)	bla_{VIM} (2), bla_{IMP} (2), bla_{GES} (1)

The table stratifies the bacterial features regarding species, strain number and categorization (R/S), and antimicrobial resistance genes detected. *One of the bla_{KPC} positive *K. pneumoniae* results as sensible to carbapenem drugs and resistant to the β-Lactam-β-Lactamase inhibitor combination Ceftazidime-avibactam (CAZ-AVI). This behavior is often observed in mutated bla_{KPC-14} or bla_{KPC-3} strains, reflecting amino acid deletions or substitutions that affect both carbapenem and CAZ-AVI susceptibility (Shields et al., 2017; Niu et al., 2020).

3.7 Minimum inhibitory and bactericidal concentrations

The two peptides were strategically designed to increase their positive charges to enhance their interaction with bacterial membranes, thereby boosting their antibacterial efficacy. The obtained results do not demonstrate any difference in susceptibility between the resistant and susceptible subgroups of each species. Notably, as evidenced in Table 5, the Minimum Inhibitory Concentration values for three of five bacterial species have at least halved compared to those observed with the wild-type peptide. Particularly noteworthy is the significant reduction for *Acinetobacter baumannii* mean MIC, which shows a substantial drop from a value bigger than 32 μg/mL (13.57 μM) to just 8 and 7.6 μg/mL (3.39 and 3.22 μM) for both Trem-HK and Trem-HSK. In general, the results consistently demonstrate a reduction in MIC values or, at most, the maintenance of similar values. Moreover, regarding the MBC results, it is possible to highlight an improvement of bactericidal activity due to the peptide mutations. As an example, mean MBC values related to *A. baumannii* decreased from a value bigger than 32 μg/mL (13.57 μM) to 8.8 μg/mL (3.73 μM) for both mutants. The mutant peptides' MIC and MBC were significantly decreased for the 20 isolates of the gram-positive bacteria: *Enterococcus faecalis* seems to be the most effected by the charge-positivization mutations of the Trematocine.

Moreover, in most cases the two mutants show similar values of both MIC and MBC for the tested strains: the inhibitory and bactericidal activity of the peptides seem to be strictly related. The antimicrobial susceptibility testing data for both common antibiotic and antimicrobial peptides studied is available as a database (Supplementary material S1).

TABLE 5 Minimum Inhibitory (MIC) and Bactericidal (MBC) mean concentrations of the tested ESKAPE bacteria ($n = 50$) divided by species (10 strains each).

	MIC ± SD (μg/mL)			MIC_{50} (μg/mL)			MIC_{90} (μg/mL)		
	Trem WT	Trem HK	Trem HSK	Trem WT	Trem HK	Trem HSK	Trem WT	Trem HK	Trem HSK
E. faecium (n = 10)	23.2 ± 9.6	6.8 ± 1.9	6.4 ± 2.1	32	8	8	32	8	8
S. aureus (n = 10)	15.2 ± 2.5	7.6 ± 1.3	8.0 ± 0.0	16	8	8	16	8	8
K. pneumoniae (n = 10)	>32	32.0 ± 0.0	30.4 ± 5.1	>32	32	32	>32	32	32
A. baumannii (n = 10)	>32	8.0 ± 0.0	7.6 ± 1.3	>32	8	8	>32	8	8
P. aeruginosa (n = 10)	>32	>32	28.8 ± 6.7	>32	>32	32	>32	>32	32

	MBC ± SD (μg/mL)			MBC_{50} (μg/mL)			MBC_{90} (μg/mL)		
	Trem WT	Trem HK	Trem HSK	Trem WT	Trem HK	Trem HSK	Trem WT	Trem HK	Trem HSK
E. faecium (n = 10)	30.4 ± 5.1	8.8 ± 2.5	7.6 ± 1.3	32	8	8	32	8	8
S. aureus (n = 10)	23.2 ± 9.6	9.2 ± 3.8	8.8 ± 2.5	32	8	8	32	8	8
K. pneumoniae (n = 10)	>32	>32	32.0 ± 0.0	>32	>32	32	>32	>32	32
A. baumannii (n = 10)	>32	8.8 ± 2.5	8.8 ± 2.5	>32	8	8	>32	8	8
P. aeruginosa (n = 10)	>32	>32	>32	>32	>32	>32	>32	>32	>32

The table also comprehend MIC_{50}, MBC_{50}, MIC_{90} and MBC_{90} values. The concentrations are expressed in μg/mL unit.

3.8 Bacterial growth curves

To thoroughly investigate the antimicrobial properties of mutant peptides, our study explored their effects on microbial growth within a kinetic setting. As a result, we produced growth curves for a sensible and resistant representants, randomly chosen, of each ESKAPE species exposed to concentrations of the two mutated peptides at 0.5 × MIC_{90}, MIC_{90}, and 2 × MIC_{90}. For MIC_{90} values above 32 μg/mL, the tested concentrations are 128, 64 and 32 μg/mL (indicated in Figure 5 as 2 × MIC, MIC and 0.5 × MIC respectively). During a 21-h period, we followed changes in optical density (O.D.) to gain valuable insights into growth kinetics. In all kinetics experiments, when using twice the MIC_{90} concentrations of both peptides, microbial growth is completely inhibited. However, when using the MIC_{90} concentration, we observe a delay in the rise of the growth curves, along with lower absorbance readings during the plateau phase. The growth curves consistently illustrate a dose-dependent inhibition of microbial growth. In comparison, the untreated growth control for various bacterial isolates, whether susceptible or resistant, exhibits the highest optical density (OD) values and enters the exponential growth phase earlier than the samples treated with different concentrations of antimicrobial peptides. These comparative growth curves (Figures 5A,B) provide strong evidence of the rapid and effective cytocidal action of the two peptides.

3.9 Scanning electron microscopy

The obtained data from biochemical and antimicrobial characterizations suggest that Trematocine mutants have an enhanced membranolytic activity against most of the ESKAPE species. Gram-positive species seems to be the more effected by Trematocine itself, while aminoacidic mutations in addition to ameliorate bactericidal potency, broaden the antibacterial activity at low concentrations for *A. baumannii*. To better investigate the improved membranolytic action of mutans, a high magnification microscopy has been performed. Scanning electron imaging was utilized after a short-term treatment of 4 h with 0.75× MIC_{90} concentrations of Trematocine and mutants, with a gram-negative and a gram-positive representant of ESKAPE opportunistic pathogens: Colistin-resistant *A. baumannii* and Methicillin-resistant *S. aureus, respectively.* For MIC_{90} values above than 32 μg/mL, the tested concentration (compared with 0.75 × MIC) is 32 μg/mL. The magnification used (Figures 6, 7) to assess the presence of membranolytic activity on *A. baumannii* and *S. aureus* is 20,000×, while micrographs of *K. pneumoniae*, *P. aeruginosa*, and *E. faecium* were acquired at 8,000× to 20,000× magnification (Supplementary Figures S3–S5 respectively).

As shown in Figure 6, *A. baumannii* growth control cells have an approximal length of 1.5 μm, some evident bacterial division secta and a swollen appearance. In contrast Trem-HK and Trem-HSK seems to produce a cell wall and membrane alteration of the gram-negative bacteria, evident from the shrunken appearance and for the reduced perpendicular extension to the main axis of the bacillus. Trem-WT, differently from the double and triple mutants of Trematocine, have a less extent impact on the bacterial morphology and membrane integrity: the majority of cells in the micrograph has a morphological integrity similar to growth control, and only one cell exhibits deflated and potentially symptom of an enhanced bactericidal activity.

Figure 7 display the SEM imaging session for a Methicillin-resistant *S. aureus* strain involved in the study. Staphylococcal cells in the growth control appeared grouped and isotonic, while the Trematocine-treated one seems suffering and undersized. Trematocine and both mutants, HK and HSK, provoke an extended morphological alteration to cell wall and membrane with and evident shrinking and elongation of cocci.

10.3389/fmicb.2024.1447301

3.10 Hemolytic activity

To get more information of the Trem-HK and Trem-HSK peptides selectivity toward bacterial cells, their hemolytic activity against rabbit red blood cells was investigated. Overall, the peptides displayed little to no hemolysis of erythrocytes until 2.5 μM (6.1 μg/mL), with values of about 35% at 5 μM (12.2 μg/mL) as shown in Figure 8. At higher concentrations, the peptides caused up to 80–100% hemolysis.

3.11 Cytotoxic activity

To investigate the effect of the peptides on the viability of mammalian cell lines, an ATP-lite assay was performed using the primary fibroblast cell line FB-789. Cell vitality was evaluated after 3 and 6 h of treatment with different concentrations of the peptides. As shown in Figures 9A,B, the peptides were little or no cytotoxic until 2.5 μM (6.1 μg/mL) at the two considered time points. However, already at a

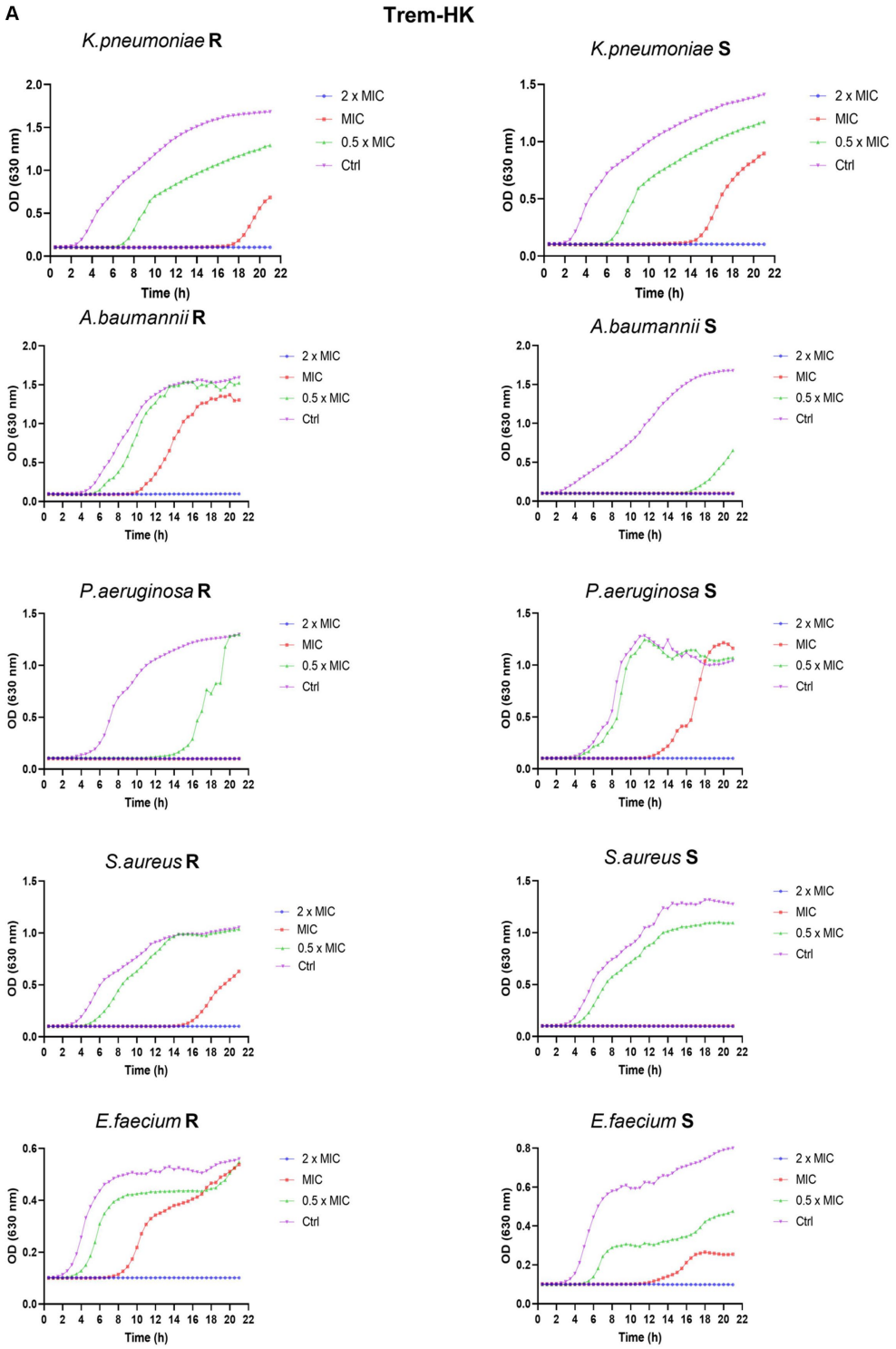

FIGURE 5 (Continued)

10.3389/fmicb.2024.1447301

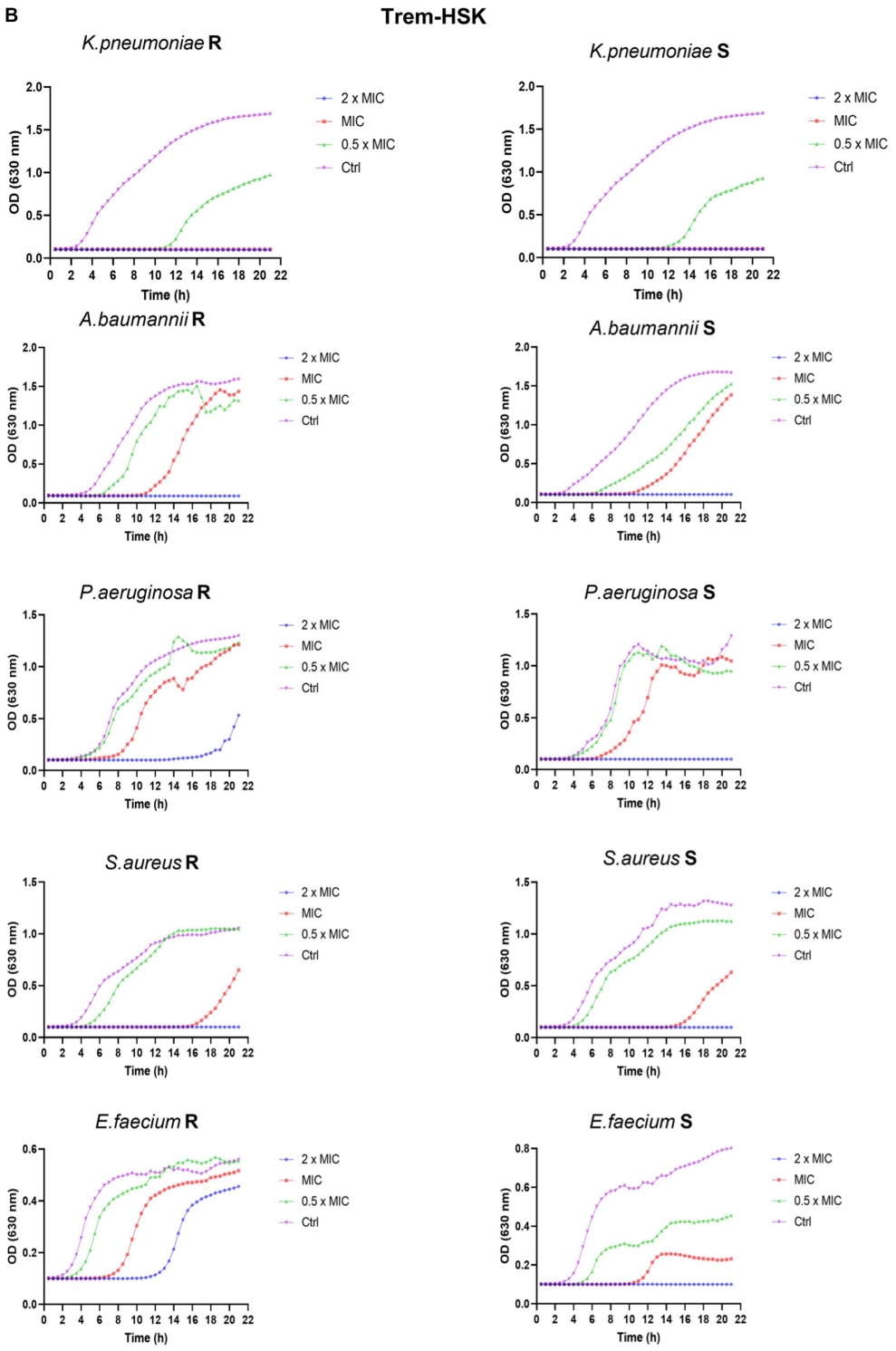

FIGURE 5
Panel **(A,B)** reports the growth curves of Trem-HK and Trem-HSK for the different tested bacterial strains. R = resistant. S = susceptible (following categorization stated in Section 3.6).

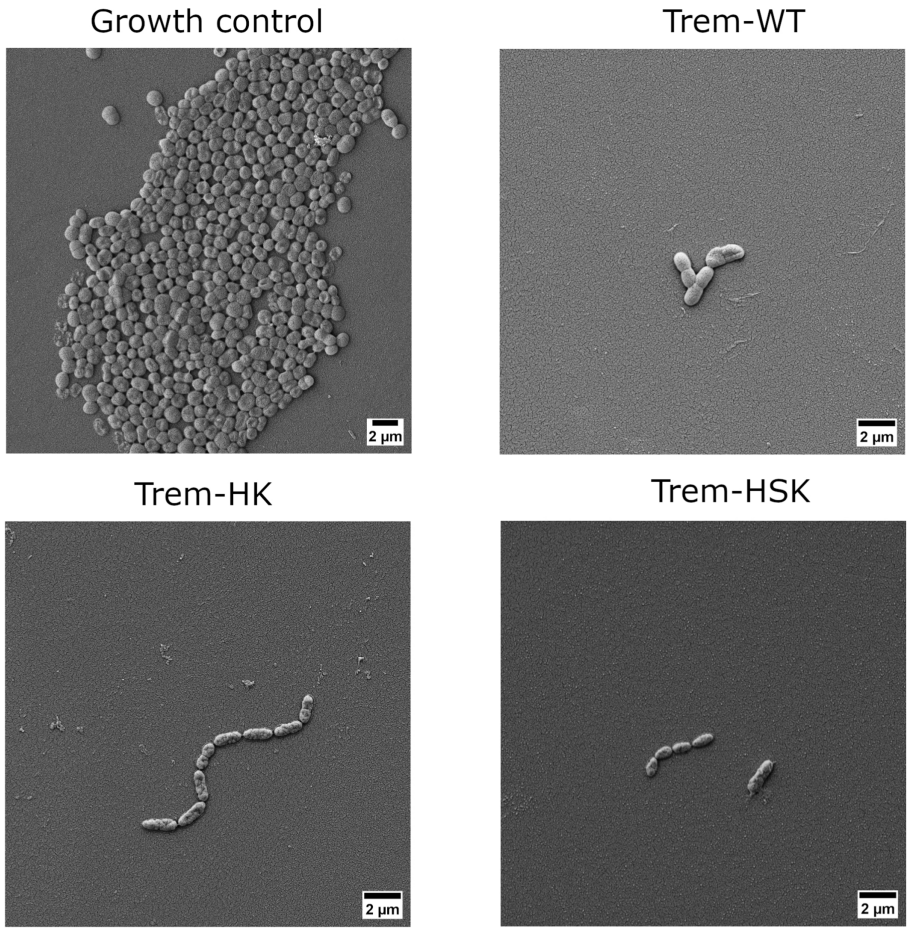

FIGURE 6
Scanning electron micrographs of a colistin-resistant *A. baumannii* cells untreated or treated with 0.75 × MIC of Trem-WT, Trem-HK and Trem-HSK for 4 h. Magnification is 8,000× and scale bar is equal to 2 µm.

concentration of 5 µM (12.2 µg/mL) a significant reduction in the cell viability can be observed in comparison to the negative control (100% of viability). Trem-HK seems less cytotoxic than Trem-HSK.

3.12 Assessment of *in vivo* toxicity of Trem-HK and Trem-HSK using a *Galleria mellonella* larvae model

To assess the toxicity of Trem-HK and Trem-HSK, we conducted *in vivo* experiments using *Galleria mellonella* larvae as a model organism. A single concentration of 62.5 µg/mL (25.5 µM) was selected for the toxicity test on the larvae. It's worth noting that this concentration, for example, is about eight times higher than the lowest MIC_{90} value obtained for *A. baumanni*. Following the administration of both peptides, we monitored the larvae for a period of 72 h, looking for any signs of toxicity such as melanization or reduced motility. Remarkably, as shown in Figure 10, no signs of toxicity were observed in any of the treated larvae when compared to the control group, and all larvae maintained 100% viability throughout the experiment. These results demonstrate an outstanding biocompatibility profile for both mutant peptides, suggesting their good potential for application in clinical settings. The discrepancy between *in vitro* and *in vivo* toxicity evaluations can be reflected by intrinsic differences in study models and pharmacokinetic variables.

4 Discussion

Antimicrobial resistance (AMR) stands as a grave public health concern, particularly in the context of bacterial infections. The escalating impact of antibiotic-resistant strains has led to a significant global health crisis. The WHO has identified the ESKAPE group—*Enterococcus faecium*, *Staphylococcus aureus*, *Klebsiella pneumoniae*, *Acinetobacter baumannii*, *Pseudomonas aeruginosa*, and *Enterobacteriaceae* family.—as urgent targets due to their exceptional ability to evade conventional antibiotics (De Oliveira et al., 2020; Abebe and Birhanu, 2023). Addressing the critical need for novel strategies against resistant infections and the development of new antimicrobials is, therefore, fundamental. AMPs emerge as promising candidates, offering a potential breakthrough in facing AMR challenges. With their ability to target a broad spectrum of pathogens, including the ESKAPE group, through interactions with cell membranes, AMPs present an attractive alternative for innovative antimicrobial treatments (Bugli et al., 2022; Ji et al., 2024; Straus, 2024). Their potential to minimize the appearance of resistance

10.3389/fmicb.2024.1447301

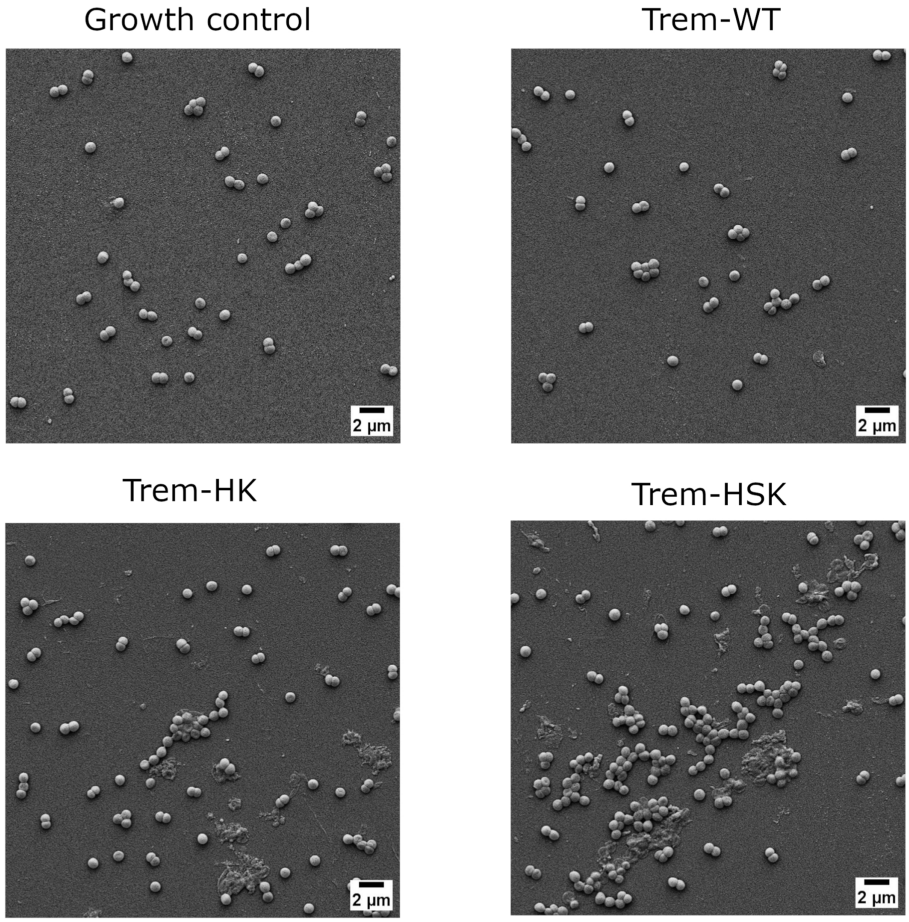

FIGURE 7
Scanning electron micrographs of Methicillin-resistant *S. aureus* strain cells untreated or treated with 0.75 × MIC of Trem-WT, Trem-HK and Trem-HSK for 4 h. Magnification is 8,000× and scale bar is equal to 2 µm.

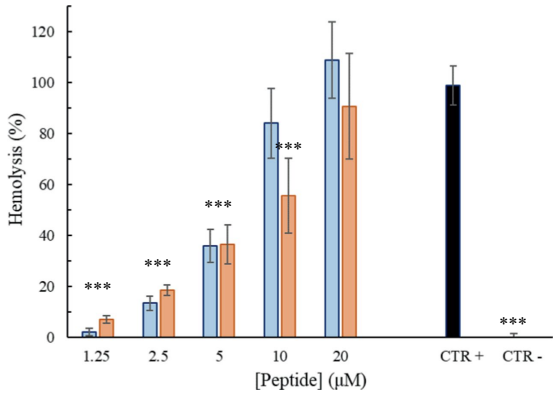

FIGURE 8
Percentage of hemolysis as a function of peptide Trem-HSK (orange) and Trem-HK (blue) concentration. The asterisks indicate the significance level respect to positive control (black): ***$p < 0.001$.

further enhances their appeal. In this research, we explored the biological activity of two mutants derived from the scaffold of trematocine, an AMP identified in the red-blooded Antarctic fish *Trematomus bernacchii* (Della Pelle et al., 2020). The site-specific mutations were strategically designed to enhance the bactericidal activity of the native peptide, primarily achieved by augmenting the positive charge and facilitating a greater affinity of the peptides for the bacterial cellular membranes (Dathe et al., 2001). Different papers have emphasized the important impact of positive charges in the electrostatic interactions between AMPs and membranes, studying their mode of insertion and ability to alter bilayer properties (Alfred et al., 2024). Therefore, Trem-HK and Trem-HSK have been designed to have a net positive charge increase, compared to the natural peptide, from +2 to +5 and + 2 to +6, respectively. We studied the effects of these mutations, evaluating the ability of peptides to interact with different membrane-mimicking systems. Partition constant values for LUVs mimicking mammalian and bacterial membranes are 10 time higher compared to trematocine (Della Pelle et al., 2020) for the two mutants, but there is no indication of a selectivity for a specific cell wall. Stern-Volmer constants indicates, for both mutant peptides, that the Trp at the N-terminus get inserted in the interfacial region of the lipid bilayer in presence of LUVs, whereas the NAF values are lower for POPC-POPG membranes, indicating a lower accessibility of Trp-1 to the quencher in this case. The ability of Trem-HK and Trem-HSK peptides to permeabilize the outer membrane of *E. coli* was greatly improved compared to the

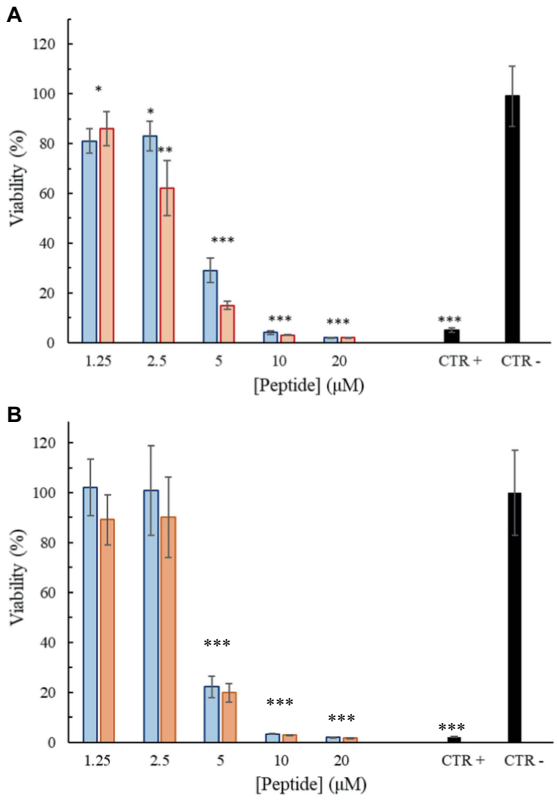

FIGURE 9
Percentage of viability as a function of peptide Trem-HSK (red) and Trem-HK (blue) concentration after 3 **(A)** and 6 **(B)** hours of treatment. The asterisks indicate the significance level respect to negative control (black): *$p < 0.05$; **$p < 0.01$; ***$p < 0.001$.

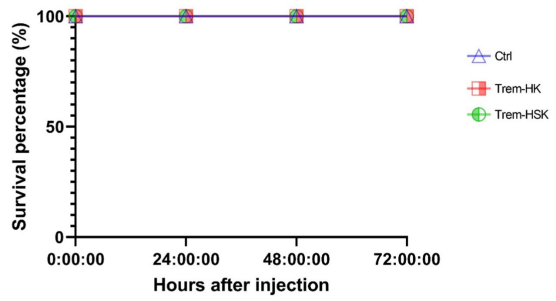

FIGURE 10
Toxicity of trematocine mutants on an insect larvae model.

trematocine and, therefore, an effect due to the increase of the net positive charge was highlighted. Finally, both peptides assume an α-helical conformation in the presence of LUVs, with a higher percentage of secondary structure evidenced in the presence of increasing concentrations of anionic membrane.

Trem-HK and Trem-HSK, moreover, present compelling evidence of their enhanced antibacterial efficacy at the expense of a slightly lower biocompatibility profile. The antimicrobial evaluation was performed on an important collection of MDR and susceptible strains of the WHO's prioritized list of bacterial pathogens, the ESKAPE group. As described in Table A2.1 of the WHO Bacterial Priority Pathogens List (WHO, 2024), the ESKAPE bacteria selected in this study are all included in medium–high (21–30%) or high (> 30%) mortality rate list. To better summarize the intrinsic heterogeneity of these resistant bacteria, each species has at least two different AMR associated genes variants detected. The bacterial collection presents the most represented genotypes detected in recent surveillance studies and systematic analyses published on antibiotic-resistant bacterial threats in public health (Jean et al., 2022; Mestrovic et al., 2022; WHO, 2024).

The observed reduction in MIC values across various bacterial species, especially the substantial drop for *A. baumannii* and *E. faecium,* is a noteworthy achievement. The designed positive charge strategy appears effective, considering this parameter, in enhancing the peptides' interaction with bacterial membranes. The consistency in the reduction or maintenance of MIC values implies a broad-spectrum antibacterial potential. Additionally, the improvements in MBC values, particularly for *A. baumannii* and *E. faecium*, underscore the peptides' enhanced bactericidal activity, supporting their potential therapeutic utility. The growth curve experiments provide valuable insights into the kinetics of peptides microbial inhibition. The dose-dependent inhibition of microbial growth, illustrated by delayed rise and lower absorbance readings, is a strong indicator of the peptides' effectiveness. The complete inhibition at $2 \times MIC_{90}$ emphasizes their potency. The comparison with untreated controls further supports the peptides' antimicrobial efficacy, as evidenced by the rapid and effective cytocidal action highlighted by growth-rate differences in the curves.

The morphological characterization of the bactericidal effect of the tested peptides on ESKAPE representants was conducted with a slightly reduced peptide concentration ($0.75 \times$MIC) to avoid extended bacterial lysis during the 4-h treatment and to focus on cell wall and membrane physiology alterations. The scanning electron microscopy was performed till 20,000× magnification to have enough resolution to investigate superficial alterations of bacterial cells when compared to control samples, and to include more than one cell per micrograph, when applicable. Both CRAB and VRE isolates, included as critical and high priority AMR pathogens by WHO (2024), show an enhanced cell wall and membrane alterations when treated with Trematocine mutants, compared to wild-type peptide. The differences are even more evident for Trem-WT, when bacterial integrity and numerosity is compared to control samples. The membranolytic activity of Trematocine and its mutants, already demonstrated for reference model of bacterial strains, is also confirmed by high-magnification microscopy on clinical multi-drug resistant bacteria. Cell wall and membrane differences between gram-negative and gram-positive bacteria seem to have no impact on Trem-HK and Trem-HSK peptides, while *Pseudomonas aeruginosa* isolates show a better resilience to those treatments.

The investigation of hemolytic activity against rabbit red blood cells indicates low hemolysis until 2.5 μM (6.1 μg/mL), suggesting a favorable selectivity toward bacterial cells. However, the increase in hemolysis at higher concentrations raises concerns about potential toxicity. Optimizing antimicrobial peptides requires a delicate balance between maximizing antimicrobial efficacy and ensuring a favorable safety profile. While enhancing binding affinity with biological membranes may result in a modest increase in cytotoxicity, our study observed only a marginal increment in this regard.

Overall, further exploration and optimization of peptide concentrations may be necessary to minimize adverse effects while maintaining antibacterial efficacy. The cytotoxicity assessment on mammalian cell lines reveals a non-cytotoxic effect until 2.5 μM (6.1 μg/mL), aligning with the favorable selectivity observed in hemolytic activity. As discussed for peptides hemolytic activity, the significant reduction in cell viability at 5 μM (12.2 μg/mL) opens questions about the peptides' potential cytotoxicity at higher concentrations. The cytotoxicity assessment on mammalian cell lines reveals a non-cytotoxic effect until 2.5 μM (6.1 μg/mL), aligning with the favorable selectivity observed in hemolytic activity. As discussed for peptides hemolytic activity, the significant reduction in cell viability at 5 μM (12.2 μg/mL) opens questions about the peptides' potential cytotoxicity at higher concentrations. The use of the *Galleria mellonella* model to assess *in vivo* toxicity is a valuable step towards understanding the peptides' safety profile. The absence of toxicity signs in treated larvae, even at a concentration eight times higher than the lowest MIC for *A. baumannii*, is promising. The 100% viability throughout the experiment suggests a high level of biocompatibility, supporting the peptides' potential for clinical applications. This result underscores the superiority of *in vivo* testing in providing a more reliable understanding of the peptides' safety profile and it validates the peptides' viability for practical medical applications emphasizing the importance of filling the gap between *in vitro* and *in vivo* assessments for a more robust evaluation of safeness.

In conclusion, the rationale design of these mutants has added new insight on the impact of adding charge residue on the biological activity of a natural AMP, evidencing that the increase improves antimicrobial properties of peptides but also collide with their safety profile.

Data availability statement

The original contributions presented in the study are included in the article/Supplementary material, further inquiries can be directed to the corresponding author.

Ethics statement

Ethical approval was not required for the studies on animals in accordance with the local legislation and institutional requirements because only commercially available established cell lines were used. Directive 2010/63/EU of the European Parliament and Council of 22 September 2010 on the protection of animals used for scientific purposes does not include invertebrates as an object of ethical regulation.

Author contributions

DS: Conceptualization, Data curation, Formal analysis, Funding acquisition, Investigation, Methodology, Project administration, Resources, Software, Supervision, Validation, Visualization, Writing – review & editing. FM: Conceptualization, Data curation, Formal analysis, Funding acquisition, Investigation, Methodology, Project administration, Resources, Software, Supervision, Validation, Visualization, Writing – review & editing. MG: Conceptualization, Data curation, Formal analysis, Funding acquisition, Investigation, Methodology, Project administration, Resources, Software, Supervision, Validation, Visualization, Writing – review & editing. SB: Conceptualization, Data curation, Formal analysis, Funding acquisition, Investigation, Methodology, Project administration, Resources, Software, Supervision, Validation, Visualization, Writing – review & editing. MC: Writing – original draft, Writing – review & editing. MV: Writing – original draft, Writing – review & editing. FP: Conceptualization, Data curation, Formal analysis, Funding acquisition, Investigation, Methodology, Project administration, Resources, Software, Supervision, Validation, Visualization, Writing – review & editing. RR: Conceptualization, Data curation, Formal analysis, Funding acquisition, Investigation, Methodology, Project administration, Resources, Software, Supervision, Validation, Visualization, Writing – review & editing. FC: Conceptualization, Data curation, Formal analysis, Funding acquisition, Investigation, Methodology, Project administration, Resources, Software, Supervision, Validation, Visualization, Writing – review & editing. MS: Writing – original draft, Writing – review & editing. FBuo: Conceptualization, Data curation, Formal analysis, Funding acquisition, Investigation, Methodology, Project administration, Resources, Software, Supervision, Validation, Visualization, Writing – original draft, Writing – review & editing. FBug: Conceptualization, Data curation, Formal analysis, Funding acquisition, Investigation, Methodology, Project administration, Resources, Software, Supervision, Validation, Visualization, Writing – original draft, Writing – review & editing.

Funding

The author(s) declare financial support was received for the research, authorship, and/or publication of this article. We acknowledge financial support under the National Recovery and Resilience Plan (NRRP), Mission 4, Component 2, Investment 1.1, Call for tender No. 104 published on February 2, 2022 by the Italian Ministry of University and Research (MUR), funded by the European Union – NextGenerationEU—Project Title: Fish-inspired antimicrobial peptide delivered by specific nanosystems to fight ESKAPE bacteria: a powerful weapon against antibiotic resistance (code 2022FKLKSY)—CUP J53D23001090006. FBug and MS acknowledge EU funding within the MUR PNRR Extended Partnership initiative on Emerging Infectious Diseases (Project no. PE00000007, INF-ACT).One Health Basic and Translational Research Actions Addressing Unmet Needs on Emerging Infectious Diseases (INF-ACT), PE00000007. National Recovery and Resilience Plan (NRRP), Mission 4 Education and research – Component 2 From research to business – Investment 1.3 "Extended Partnerships", theme "13. Emerging infectious diseases", funded by the European Union – NextGenerationEU. CUP: B83C22004770006. The physico-chemical characterizations of peptides were supported by Progetto ECS 0000024 Rome Technopole, – CUP B83C22002820006, PNRR Missione 4 Componente 2 Investimento 1.5, finanziato dall'Unione europea – NextGenerationEU.

Conflict of interest

The authors declare that the research was conducted in the absence of any commercial or financial relationships that could be construed as a potential conflict of interest.

Publisher's note

All claims expressed in this article are solely those of the authors and do not necessarily represent those of their affiliated organizations, or those of the publisher, the editors and the reviewers. Any product that may be evaluated in this article, or claim that may be made by its manufacturer, is not guaranteed or endorsed by the publisher.

Supplementary material

The Supplementary material for this article can be found online at: https://www.frontiersin.org/articles/10.3389/fmicb.2024.1447301/full#supplementary-material

References

Abebe, A. A., and Birhanu, A. G. (2023). Methicillin resistant *Staphylococcus aureus*: molecular mechanisms underlying drug resistance development and novel strategies to combat. *Infect. Drug Resist.* 16, 7641–7662. doi: 10.2147/IDR.S428103

Alfred, R., Bryant, G., Mata, J. P., Bhave, M., and Shah, R. M. (2024). Unraveling the effects of cationic peptides on vesicle structures: insights into peptide-membrane interactions. *ACS Appl. Bio Mater.* 7, 220–229. doi: 10.1021/acsabm.3c00824

Ayobami, O., Brinkwirth, S., Eckmanns, T., and Markwart, R. (2022). Antibiotic resistance in hospital-acquired ESKAPE-E infections in low- and lower-middle-income countries: a systematic review and meta-analysis. *Emerg. Microbes Infect.* 11, 443–451. doi: 10.1080/22221751.2022.2030196

Browne, K., Chakraborty, S., Chen, R., Willcox, M. D. P., Black, D. S., Walsh, W. R., et al. (2020). A new era of antibiotics: the clinical potential of antimicrobial peptides. *Int. J. Mol. Sci.* 21, 1–23. doi: 10.3390/ijms21197047

Bugli, F., Martini, C., Di Vito, M., Cacaci, M., Catalucci, D., Gori, A., et al. (2022). Antimicrobial peptides for tackling cystic fibrosis related bacterial infections: a review. *Microbiol. Res.* 263:127152. doi: 10.1016/j.micres.2022.127152

Buonocore, F., Picchietti, S., Porcelli, F., Della Pelle, G., Olivieri, C., Poerio, E., et al. (2019). Fish-derived antimicrobial peptides: activity of a chionodracine mutant against bacterial models and human bacterial pathogens. *Dev. Comp. Immunol.* 96, 9–17. doi: 10.1016/j.dci.2019.02.012

Cardoso, P., Glossop, H., Meikle, T. G., Aburto-Medina, A., Conn, C. E., Sarojini, V., et al. (2021). Molecular engineering of antimicrobial peptides: microbial targets, peptide motifs and translation opportunities. *Biophys. Rev.* 13, 35–69. doi: 10.1007/s12551-021-00784-y

Chen, M., Lin, N., Liu, X., Tang, X., Wang, Z., and Zhang, D. (2023). A novel antimicrobial peptide screened by a *Bacillus subtilis* expression system, derived from *Larimichthys crocea* ferritin H, exerting bactericidal and parasiticidal activities. *Front. Immunol.* 14:14. doi: 10.3389/fimmu.2023.1168517

Dathe, M., Nikolenko, H., Meyer, J., Beyermann, M., and Bienert, M. (2001). Optimization of the antimicrobial activity of magainin peptides by modification of charge. *FEBS Lett.* 501, 146–150. doi: 10.1016/S0014-5793(01)02648-5

De Oliveira, D. M. P., Forde, B. M., Kidd, T. J., Harris, P. N. A., Schembri, M. A., Beatson, S. A., et al. (2020). Antimicrobial resistance in ESKAPE pathogens. *Clin. Microbiol. Rev.* 33:e00181-19. doi: 10.1128/CMR.00181-19

Della Pelle, G., Perà, G., Belardinelli, M. C., Gerdol, M., Felli, M., Crognale, S., et al. (2020). Trematocine, a novel antimicrobial peptide from the Antarctic fish *Trematomus bernacchii*: identification and biological activity. *Antibiotics (Basel).* 9:66. doi: 10.3390/antibiotics9020066

Di Vito, M., Garzoli, S., Rosato, R., Mariotti, M., Gervasoni, J., Santucci, L., et al. (2023). A new potential resource in the fight against Candida auris: the *Cinnamomum zeylanicum* essential oil in synergy with antifungal drug. *Microbiol. Spectr.* 11:e0438522. doi: 10.1128/spectrum.04385-22

EUCAST (2024). EUCAST reading guide for broth microdilution [Internet]. Available at: www.eucast.org

EUCAST (2014) Breakpoint Tables [Internet]. Available at: http://www.eucast.org

Freire, J. M., Domingues, M. M., Matos, J., Melo, M. N., Veiga, A. S., Santos, N. C., et al. (2011). Using zeta-potential measurements to quantify peptide partition to lipid membranes. *Eur. Biophys. J.* 40, 481–487. doi: 10.1007/s00249-010-0661-4

Garcia Maset, R., Hapeshi, A., Hall, S., Dalgliesh, R. M., Harrison, F., and Perrier, S. (2022). Evaluation of the antimicrobial activity in host-mimicking media and in vivo toxicity of antimicrobial polymers as functional mimics of AMPs. *ACS Appl. Mater. Interfaces* 14, 32855–32868. doi: 10.1021/acsami.2c05979

Hussain, H. I., Aqib, A. I., Seleem, M. N., Shabbir, M. A., Hao, H., Iqbal, Z., et al. (2021). Genetic basis of molecular mechanisms in β-lactam resistant gram-negative bacteria. *Microb. Pathog.* 158:105040. doi: 10.1016/j.micpath.2021.105040

Jean, S. S., Harnod, D., and Hsueh, P. R. (2022). Global threat of Carbapenem-resistant gram-negative bacteria. *Front. Cell Infect. Microbiol.* 12:12. doi: 10.3389/fcimb.2022.823684

Ji, S., An, F., Zhang, T., Lou, M., Guo, J., Liu, K., et al. (2024). Antimicrobial peptides: An alternative to traditional antibiotics. *Eur. J. Med. Chem.* 265:116072. doi: 10.1016/j.ejmech.2023.116072

Kapoor, G., Saigal, S., and Elongavan, A. (2017). Action and resistance mechanisms of antibiotics: a guide for clinicians. *J. Anaesthesiol. Clin. Pharmacol.* 33, 300–305. doi: 10.4103/joacp.JOACP_349_15

Koo, H. B., and Seo, J. (2019). Antimicrobial peptides under clinical investigation. *Peptide Sci.* 111:e24122. doi: 10.1002/pep2.24122

Lakowicz, J. R. (2006). Principles of fluorescence spectroscopy. 3rd Edn. (New York, NY: Springer). 1–954.

Li, X., Zuo, S., Wang, B., Zhang, K., and Wang, Y. (2022). Antimicrobial mechanisms and clinical application prospects of antimicrobial peptides. *Molecules* 27:2675. doi: 10.3390/molecules27092675

Loh, J. M. S., Adenwalla, N., Wiles, S., and Proft, T. (2013). *Galleria mellonella* larvae as an infection model for group a streptococcus. *Virulence* 4, 419–428. doi: 10.4161/viru.24930

Louis-Jeune, C., Andrade-Navarro, M. A., and Perez-Iratxeta, C. (2012). Prediction of protein secondary structure from circular dichroism using theoretically derived spectra. *Proteins* 80, 374–381. doi: 10.1002/prot.23188

Luo, X., Chen, H., Song, Y., Qin, Z., Xu, L., He, N., et al. (2023). Advancements, challenges and future perspectives on peptide-based drugs: focus on antimicrobial peptides. *Eur. J. Pharm. Sci.* 181:106363. doi: 10.1016/j.ejps.2022.106363

Magana, M., Pushpanathan, M., Santos, A. L., Leanse, L., Fernandez, M., Ioannidis, A., et al. (2020). The value of antimicrobial peptides in the age of resistance. *Lancet Infect. Dis.* 20, e216–e230. doi: 10.1016/S1473-3099(20)30327-3

Mba, I. E., Okeke, O. P., Sharndama, H. C., Osondu-chuka, G. O., Ukuomadu, J., and Ugwu, C. (2022). Antimicrobial resistance: revisiting the mechanisms of resistance. *Access Microbiol.* 4. doi: 10.1099/acmi.ac2021.po0053

Mestrovic, T., Robles Aguilar, G., Swetschinski, L. R., Ikuta, K. S., Gray, A. P., Davis Weaver, N., et al. (2022). The burden of bacterial antimicrobial resistance in the WHO European region in 2019: a cross-country systematic analysis. *Lancet Public Health* 7, e897–e913. doi: 10.1016/S2468-2667(22)00225-0

Murray, C. J., Ikuta, K. S., Sharara, F., Swetschinski, L., Robles Aguilar, G., Gray, A., et al. (2022). Global burden of bacterial antimicrobial resistance in 2019: a systematic analysis. *Lancet* 399, 629–655. doi: 10.1016/S0140-6736(21)02724-0

Niu, S., Chavda, K. D., Wei, J., Zou, C., Marshall, S. H., Dhawan, P., et al. (2020). A ceftazidime-avibactam-resistant and Carbapenem-susceptible *Klebsiella pneumoniae* strain harboring blaKPC-14 isolated in New York City. *mSphere* 5:e00775-20. doi: 10.1128/mSphere.00775-20

O'Neill, J. Tackling drug-resistant infections globally: Final report and recommendations the review on antimicrobial resistance chaired; (2016)

Pandey, D., Singhal, N., and Kumar, M. (2023). β-LacFamPred: An online tool for prediction and classification of β-lactamase class, subclass, and family. *Front. Microbiol.* 13:13. doi: 10.3389/fmicb.2022.1039687

Phillips, S. R., Wilson, L. J., and Borkman, R. F. (1986). Acrylamide and iodide fluorescence quenching as a structural probe of tryptophan microenvironment in bovine lens crystallins. *Curr. Eye Res.* 5, 611–620. doi: 10.3109/02713688609015126

Schäfer, A. B., and Wenzel, M. (2020). A how-to guide for mode of action analysis of antimicrobial peptides. *Front. Cell Infect. Microbiol.* 10:10. doi: 10.3389/fcimb.2020.540898

Schwarz, S., Silley, P., Simjee, S., Woodford, N., van Duijkeren, E., Johnson, A. P., et al. (2010). Editorial: assessing the antimicrobial susceptibility of bacteria obtained from animals. *J. Antimicrob. Chemother.* 65, 601–604. doi: 10.1093/jac/dkq037

Shields, R. K., Chen, L., Cheng, S., Chavda, K. D., Press, E. G., Snyder, A., et al. (2017). Emergence of ceftazidime-avibactam resistance due to plasmid-borne blaKPC-3 mutations during treatment of Carbapenem-resistant *Klebsiella pneumoniae* infections. *Antimicrob. Agents Chemother.* 61:e02097-16. doi: 10.1128/AAC.02097-16

Straus, S. K. (2024). Tryptophan-and arginine-rich antimicrobial peptides: anti-infectives with great potential. *Biochim. Biophys. Acta Biomembr.* 1866:184260. doi: 10.1016/j.bbamem.2023.184260

WHO (2024). WHO Bacterial Priority Pathogens List, 2024: Bacterial pathogens of public health importance to guide research, development and strategies to prevent and control antimicrobial resistance [Internet]. Geneva: WHO.

Wimley, W. C. (2010). Energetics of peptide and protein binding to lipid membranes. *Adv. Exp. Med. Biol.* 677, 14–23. doi: 10.1007/978-1-4419-6327-7_2

frontiers | Frontiers in Microbiology

TYPE Original Research
PUBLISHED 30 August 2024
DOI 10.3389/fmicb.2024.1432475

OPEN ACCESS

EDITED BY
Dany Domínguez Pérez,
Zoological Station Anton Dohrn, Italy

REVIEWED BY
Sabrina Mühlen,
Ruhr University Bochum, Germany
Mohamad Hamad,
University of Sharjah, United Arab Emirates

*CORRESPONDENCE
Päivi Tammela
✉ paivi.tammela@helsinki.fi

RECEIVED 14 May 2024
ACCEPTED 28 June 2024
PUBLISHED 30 August 2024

CITATION
Pylkkö T, Schneider YK-H, Rämä T, Andersen JH and Tammela P (2024) Bioprospecting of inhibitors of EPEC virulence from metabolites of marine actinobacteria from the Arctic Sea.
Front. Microbiol. 15:1432475.
doi: 10.3389/fmicb.2024.1432475

Bioprospecting of inhibitors of EPEC virulence from metabolites of marine actinobacteria from the Arctic Sea

Tuomas Pylkkö[1], Yannik Karl-Heinz Schneider[2], Teppo Rämä[2], Jeanette Hammer Andersen[2] and Päivi Tammela[1]*

[1]Drug Research Program, Faculty of Pharmacy, University of Helsinki, Helsinki, Finland, [2]Marbio, Faculty for Fisheries, Biosciences and Economy, UiT—The Arctic University of Norway, Tromsø, Norway

A considerable number of antibacterial agents are derived from bacterial metabolites. Similarly, numerous known compounds that impede bacterial virulence stem from bacterial metabolites. Enteropathogenic *Escherichia coli* (EPEC) is a notable human pathogen causing intestinal infections, particularly affecting infant mortality in developing regions. These infections are characterized by microvilli effacement and intestinal epithelial lesions linked with aberrant actin polymerization. This study aimed to identify potential antivirulence compounds for EPEC infections among bacterial metabolites harvested from marine actinobacteria (*Kocuria* sp. and *Rhodococcus* spp.) from the Arctic Sea by the application of virulence-based screening assays. Moreover, we demonstrate the suitability of these antivirulence assays to screen actinobacteria extract fractions for the bioassay-guided identification of metabolites. We discovered a compound in the fifth fraction of a *Kocuria* strain that interferes with EPEC-induced actin polymerization without affecting growth. Furthermore, a growth-inhibiting compound was identified in the fifth fraction of a *Rhodococcus* strain. Our findings include the bioassay-guided identification, HPLC-MS-based dereplication, and isolation of a large phospholipid and a likely antimicrobial peptide, demonstrating the usefulness of this approach in screening for compounds capable of inhibiting EPEC virulence.

KEYWORDS

antivirulence, EPEC, arctic marine microorganisms, bioprospecting, actinobacteria

1 Introduction

The antimicrobial crisis is the result of the convergence of two phenomena. To begin with, there have been few pharmaceutical antibiotic breakthroughs in recent decades (World Health Organization, 2022). Second, there are reports of increasingly troublesome cases of antibiotic resistance, globally already contributing to millions of deaths annually (Murray et al., 2022). Historically, researchers have sought antibacterial compounds in natural products, particularly in other microbes (Schneider, 2021). And this has had a high success rate; in fact, soil actinobacteria have produced 80% of all currently licensed antibiotics. However, marine actinobacteria found in the sea, on the seafloor or within the microbiome of marine organisms have received far less attention as possible sources of antibiotics, even more so with respect to virulence-modifying compounds.

Inhibiting bacterial virulence is a well-studied alternative method to the more traditional killing of microorganisms or inhibiting their growth (Zambelloni et al., 2015; Defoirdt, 2016; Buroni and Chiarelli, 2020). In essence, the idea is to inhibit the action of virulence causing molecules using pharmaceutical interventions. In the best-case scenario, the treated pathogens would then remain incapable of causing symptoms, but nevertheless alive, and thus selection pressure for resistance would not form so easily. Furthermore, due to their specificity, such drugs would most likely have fewer adverse effects on normal flora, which are affected adversely by drugs inhibiting bacterial growth or viability in general. Many compounds that to date have been described to be able to prevent bacterial virulence have been discovered from natural sources using phenotypic screening assays (Kimura et al., 2011; Duncan et al., 2014; Wu et al., 2019; Mühlen et al., 2021). These include inhibitors of the expression of virulence molecules, inhibitors of the translocation of effectors, pilicides, and adhesion blockers.

Enteropathogenic *Escherichia coli* (EPEC) is a gram-negative bacterium responsible for a significant portion of diarrheal illnesses and mortality in children under five worldwide (Ochoa and Contreras, 2011). EPEC isolates also display many different forms of antimicrobial resistance, including fluoroquinolone-resistance (Eltai et al., 2020), plasmid-mediated carbapenem and colistin resistance, and extended spectrum betalactamases (Karami et al., 2017; Mahmud et al., 2020). EPEC virulence is caused by it adhering to enterocytes and causing lesions in the intestinal epithelium characterized by the destruction of microvilli, a phenomen called attaching and effacing (A/E) lesions (Kaper et al., 2004). Once adhered to the cell, EPEC employs a type III secretion system (T3SS) to deliver various virulence factors into host cells that use the cell's own actin nucleation machinery to induce pathological changes in the cell (Campellone et al., 2002). Among the secreted factors is the translocated intimin receptor (Tir), which is critical for A/E lesion formation (Cleary, 2004). The receptor's ligand is a protein autotransported by the bacterium to its outer membrane, facilitating intimate attachment to the host cell. Once in place, the phosphorylation of the receptor initiates the recruitment of NCK, N-WASP and the Arp2/3 complex leading to abnormal actin polymerization and actin-rich protrusions on the plasma membrane (pedestals) beneath adherent EPEC (Deborah Chen and Frankel, 2005). Consequently, targeting this process holds promise for the development of antivirulence therapies, and it could be inhibited at various different stages of the pathway, for example, by preventing the contact of Tir and its ligand, intimin by orthostatic inhibition of the receptor, via down regulation of the virulence factors, or inhibition of transport via the T3SS.

As a first step toward discovering antivirulence compounds for EPEC infections, we studied the effects of extracts and fractions from four marine actinobacteria for the ability to decrease Tir-mediated virulence and the following abnormal actin condensation within the cells. Additionally, we sought to evaluate the suitability of these assays for screening bacterial extract fractions with a complex mixture of compounds, including potential pan-assay interference compounds (PAINS). The actinobacteria were isolated from sampling sites near Svalbard in the Arctic Sea and identified as using 16S marker gene sequencing. Next, they were cultured in artificial media, extracted for secondary metabolites, and the extracts fractionated for studying their effects against EPEC caused virulence *in vitro*. Three bioactivity screening methodologies were used for each extract. These included (1) testing for their capacity to inhibit the translocation of Tir, (2) their capacity to prevent actin pedestals, and (3) their capacity to inhibit the growth of EPEC in liquid culture. The recognized active fractions were then studied further to narrow down their possible mechanism of action and to elucidate the chemical structure of the active compounds.

Our aim was to design and validate an isolation and automated screening workflow for use with fractions from microbial cultures and explore the presence of virulence-inhibitory compounds within marine bacterial fractions and their potential application for drug development as the complex nature of extracts and extract fractions may interfere with screens that have been developed and validated using pure chemical compounds only. First due to the complex mixtures potentially containing a high number of "promiscuous binders" or pan assay interfering compounds (PAINS), but also due to the high concentration (10–100 μg extract/fraction per mL) commonly tested in initial screens. This requires (1) assaying methodology suitable for high-throughput screening (2) that can be used with complex fractions, not only pure compounds and (3) methodology to isolate and recognize which constituents are the active ones. We show that this workflow can indeed recognize bioactive compounds in these microbial fractions. In addition, the specific inhibition of enteropathogenic *Escherichia coli* (EPEC) virulence could offer an alternative to conventional antibiotic-based approaches, helping to mitigate the issue of antimicrobial resistance over the long term.

2 Materials and methods

2.1 Chemicals and reagents

pH_2O was produced by the in house MilliQ system (Merk, Millipore), methanol (HiperSolv, VWR) and acetone (HiperSolv, VWR), dimethyl sulfoxide (DMSO, VWR) were used if not otherwise indicated.

Modified marine ISP2 medium was produced using 4.0 g glucose (Sigma Aldrich) 4.0 g yeast extract (Sigma), 10.0 g malt extract (Sigma), 300 mL filtered seawater, 700 mL dH_2O, and a trace element solution 0.2% (v/v). Filtered seawater was produced by the seawater supply of the Norwegian college of fishery science in Tromsø, Norway, by filtration through a 0.22 μm Millidisk® 40 filter-cartridge (Millipore). The trace element solution was prepared by dissolving 10% $MgSO_4$ 7 × H_2O, 0.01% $FeSO_4$ 7 × H_2O, 0.01% $ZnSO_4$ 7 × H_2O, 0.01% $CuSO_4$ 5 × H_2O, and 0.01% CoCl2 6 × H_2O, in pH_2O, (w/v). The media was autoclaved at 121°C for 30 min using an autoclave (MLS-3781L, Panasonic).

2.2 Bacterial strains, culture, and extraction

For the infection model, the EPEC E2348/69 from Bacteriology reference department (BRD) (UK), was used. The strain was transformed using the plasmid pON.mCherry, Addgene #84821

deposited by Howard Schuman, constitutively expressing mCherry, a fluorescent protein, and grown on LB agar plates or LB broth supplemented with 30 μg mL^{-1} chloramphenicol at 37°C and 200 rpm. For more details (see Pylkkö et al., 2021).

For Tir translocation assays, an EPEC E2348/69 strain containing a beta-lactamase chromosomal fusion in LEE5 (for Tir) under the control of the native promotor, was used (CX2135) (Mills et al., 2008). This strain was kindly provided to us by Ilan Rosenshine from the Hebrew University of Jerusalem. This was cultured on LB agar plates or LB broth supplemented with 50 μg mL^{-1} tetracycline at 37°C and 200 rpm.

The actinobacteria strains were isolated from animals collected in the Arctic Sea in August 2020 (Schneider et al., 2022) (listed in Table 1). For the screening of bioactivity, 2 × 500 mL of the strains were cultivated and extracted as described below. For the isolation of compounds, the strains T091 and T160-02 were cultured in 6 × 500 mL modified marine ISP2 medium for 14 days at 20°C and 140 rpm using a shaking-incubator (Multitron Pro, INFORS HT). For extraction, 40 g of Diaion® HP20 Resin (Merck) was used. The resin was activated by incubation in methanol for 30 min and washed with pH_2O, for 20 min before the resin was added to the cultures and incubated for 3 days. The resin was separated from the cultures using vacuum filtration and cheese cloth filter (1057, Dansk Hjemmeproduktion). The pooled resin for each strain was extracted two times using 2 × 300 mL of methanol for 45 min of extraction. The extract was separated from the resin using Whatman No.3 filter paper and vacuum filtration. The extract was dried *in vacuo* at 40°C.

The exact contents of the used growth media are listed in Supplementary Table S1.

2.3 Preparation of fractions

Crude extracts were fractionated using flash liquid chromatography. The extracts were loaded onto resin (Diaion® HP-20ss, Supelco) by dissolving them in 90% methanol aq. (v/v) and adding resin in a ratio of 1:1.5 (resin/dry extract, w/w). Subsequently, the solution was dried under reduced pressure at 40°C. Flash columns (Biotage® SNAP Ultra, Biotage) were prepared by activating the resin by incubation in methanol for 20 min, washing with ddH_2O, and loading it into the column ensuring the resin being always covered with water. 6.0 g HP-20ss resin was loaded on one column. The fractionation was performed using a Biotage SP4™ system and a water: methanol gradient from 5–100% methanol over 36 min (6 min 5% B, 6 min 25% B, 6 min 50% B, 6 min 75% B, 12 min 100% B) followed by a methanol: acetone step-gradient (4 min methanol, 12 min acetone). The flow rate was set to 12 mL/min. Twenty-seven eluent fractions of 24 mL each were collected in glass tubes and pooled into six flash fractions in total (1–3 were pooled to fraction 1; 4–6 to fraction 2; 7–9 to fraction 3; 10–12 to fraction 4; 13–15 to fraction 5; 16–27 to fraction 6). An appropriate amount of extract-resin mixture was loaded onto the column after equilibration to 5% methanol aq. (v/v). The flash fractions were dried under reduced pressure at 40°C.

2.4 Analysis of fractions using HPLC-HR-MS2

For HPLC-HR-MS2 analysis an Acquity I-class UPLC (Waters) was used coupled to a PDA detector and a Vion IMS QToF (Waters). The HPLC was equipped with a Acquity C-18 UPLC column (1.7 μm, 2.1 × 100 mm) (Waters). The mobile phases consisted of acetonitrile (HiPerSolv, VWR) for mobile phase A and pH_2O as mobile phase B, both containing 0.1% formic acid (v/v) (33015, Sigma). The gradient was run from 10 to 100% B over 13 min at a flow rate of 0.45 mL/min. Samples were run in ESI+ and ESI- ionization mode. The data was processed and analyzed using UNIFI 1.9.4 (Waters). Exact masses were calculated using ChemCalc (Patiny and Borel, 2013). For dereplication an extract of modified marine ISP2-medium and flash fractions of the extract were prepared and analyzed using the same HPLC-MS2 method in order to exclude media components from consideration. (i) PubChem (Kim et al., 2023) and (ii) Chemspider (Pence and Williams, 2010) where used to identify potential compounds during dereplication by elemental composition search (i + ii) and MS-fragment search (ii, implemented in UNIFI).

2.5 Isolation of compounds using RP-HPLC-MS via mass triggered fractionation

For the isolation of compounds from flash fractions preparative reversed phase HPLC was used. Fractionation was triggered by the recorded mass signal throughout the chromatographic separation. The HPLC system consisted of a Waters 600 HPLC-pump with a degasser and flow-splitter, a Waters 515 HPLC-pump as a "make-up" pump, a Waters 3100 Mass detector, a Waters 2996 photo array detector and a Waters 2767 sample manager (all Waters). The system was controlled using MassLynx V4.1 (Waters) software A Sunfire RP-18 preparative column (10 μm, 10 × 250 mm) and XSelect CSH preparative Fluoro-Phenyl column (5 μm, 10 × 250mm) (both Waters) were used as solid phases for the first and second round of purification, respectively. The mobile phases for the gradients were A [pH_2O with 0.1% (v/v) formic acid] and B [acetonitrile with 0.1% (v/v) formic acid]. The flow rate was set to 6 mL/min. Acetonitrile (Prepsolv®, Merck) and formic acid (33015, Sigma) were purchased in appropriate quality, ddH_2O was produced with the in-house Milli-Q® system. For the MS-detection of the eluting compounds one percent of the flow was split and blended with 80% MeOH in pH_2O (v/v) acidified with 0.2% formic acid (Sigma) and directed to the ESI-quadrupole-MS. The fractions were collected by mass triggered fraction collection and the respective fractions were reduced to dryness under reduced pressure and by vacuum centrifugation, both at 40°C.

2.6 Fluorescent actin stain assay

Screening was performed using a modification of the widely used FAS assay published earlier at various concentrations (Pylkkö et al., 2021). In short, this is an imaging-based infection assay. A

10.3389/fmicb.2024.1432475

TABLE 1 Actinobacteria isolates investigated.

Strain ID:	T091	T289	T060	T160-2
Animal/origin	*Caulophacus arcticus* (*Porifera*)	*Chlamys islandica* (*Mollusca*)	*Dendrobeania sp.* (*Bryozoa*)	*Tricellaria ternata* (*Bryozoa*)
Actinobacterium	*Kocuria* sp.	*Rhodococcus* sp.	*Rhodococcus* sp.	*Rhodococcus* sp.
Location/depth	77.37491402 °N, 8.268010617 °E/1,400 m	74.78804448 °N, 8.57096443 °E/285 m	75.16057145 °N, 13.71765962 °E/1,500 m	75.16057145 °N, 13.71765962 °E/1,500 m
GenBank accession no.	OP537112.1	OP537141.1	OP537103.1	OP537122.1

More detail on the field sites and methodology used to isolate and culture the strains can be found in Schneider et al. (2022).

cell monolayer of 2 × 10^5 Caco-2 cells mL^{-1} (ATCC CCL-23) is infected with EPEC E2348/69 emitting fluorescence (mCherry) at a MOI of 1:15. This MOI has been determined to be appropriate for clearly distinquizable EPEC-mCherry microcolonies to form during the infection. Following this, actin is stained with phalloidin and nuclei with Hoechst 33342. For each well five fields of view are collected, and all well-level data are mean aggregates of the data from five fields of view. The data is processed using a custom data reduction pipeline which produces as a readout the proportion of all bacterial microcolonies with actin pedestals. This is achieved by segmentation algorithms and a colocalization analysis, each image is segmented into the microcolonies and features are extracted from the channels of both the bacteria and cells within these segments. The main readout produced by this is the proportion of segmented microcolonies that is associated with actin condensation, although other readouts are collected, such as the number and size of microcolonies. The images were analyzed using the custom scripts on a high-performance computing cluster, Puhti, provided by CSC—IT Center for Science, Finland. The code used for analysis is available at https://github.com/tpylkko/FAS-HCS.

To screen the samples, minimum essential media (MEM) preincubated (1:50, 3 h) mCherry-EPEC suspension at 2 × concentration was added to 96-well source plates (NUNC) using a dispenser (Mantis, Formulatrix), and the fractions dissolved in 2.5% DMSO-MQ were added in 2 × concentrations so that the correct concentration of the samples and bacterial suspension with a multiplicity of infection of 1:15 was achieved in the source plate. A volume of 60 µL of this mixture was transferred to the screening plates (Phenoplate 384, PerkinElmer) and the plates were centrifuged at 1,000 × g for 4 min to allow the bacteria to come into contact with the cells. The plates were subsequently incubated for 2 h at 37°C, 95%, humidity 5% CO_2 (Biospa, Biotek). After this, a staining solution was applied to the plate using a dispenser (Mantis, Formulatrix) and incubated at RT for 20 min. The plate was then washed three times (100 µL) with Hanks buffered saline solution (HBSS) with an automated liquid handling workstation (Biomek i7, Beckman Coulter) and imaged using a protocol in the imaging plate reader Cytation 5 (Biotek). The contents of this solution are in the Supplementary Table S2. More details about image capture techniques are in Pylkkö et al. (2021).

2.7 Tir translocation assay

For translocation assays, 2 × 10^5 Caco-2 cells mL^{-1} (ATCC CCL-23) were seeded into black 384-well plates with transparent bottom (Phenoplate, PerkinElmer, Germany). Bacterial overnight cultures, grown in 50 µg mL^{-1} tetracycline, were diluted 1:50 into MEM with GlutaMAX (Gibco, Germany) and incubated for 2 h at 37°C 5% CO_2 in a filter capped 50 mL Falcon tube. Hundred microliter of the bacterial suspension was subsequently added to a source plate (96-well, NUNC) to which samples were serially diluted. These plates were incubated for an additional 1 h. Caco-2 cells were washed once with HBSS. The bacteria-sample suspension (60 µL per well) was then added to the cells, the plates were centrifuged at 1,000 × g for 4 min (Eppendorf Centrifuge 5810R) and incubated for 1.5 h (37°C, 5% CO_2). Media was then removed, and infected cells were washed twice with 60 µL HBSS. MEM with 100 µgmL^{-1} gentamicin was added to the cells and mixed with LifeBLAzer CCF4-AM staining solution (Invitrogen). The plates were then incubated for 1 h at room temperature. Subsequently, the fluorescence was determined in a Cytation 5 (Biotek, Germany) using an excitation wavelength of 405 nm (10 nm bandwidth). Emission was detected with 460 and 530 nm. Effector translocation was determined by calculating the ratio of blue to green fluorescence (Em520 nm/Em460 nm) following the manufacturer's instructions.

2.8 Red blood cell hemolysis assay

EPEC overnight cultures were diluted 1:25 in DMEM high glucose without phenol red (Gibco) and grown for 3 h at 37°C, 5% CO_2 in the presence or absence of decreasing concentrations of the fractions. Red blood cells (RBC) were purified from Defibrinated Oxoid Sheep Blood (Thermo Fisher Scientific) by three rounds of centrifugation in 1.5 mL eppendorf tubes using a table top centrifuge at 2,000 × g and washing with PBS, then resuspended to 5% (v/v) in DMEM high glucose without phenol red. Bacterial cultures were equalized to 10^8 in 100 µL and added to 100 µL sheep RBCs (5% v/v) in a 96-well plate. Uninfected RBCs in DMEM were used as a negative control. Total lysis was achieved by adding 0.5% Triton-X to the culture medium. To synchronize infection and mediate bacterial-cell contact, tubes were centrifuged 1 min at 3,220 × g before incubation at 37°C, 5% CO_2. After 2 h, cells were gently resuspended, followed by centrifugation at 3,220 × g for 1 min. Fifty microliter of each supernatant was transferred to a 96-well plate, and the amount of hemoglobin released was assessed at 543 nm in Cytation 5 (Biotek) plate reader. Hemolysis was calculated as the percentage of hemoglobin released by the DMSO-treated wild-type-infected RBCs.

2.9 Analysis of the inhibition of growth of EPEC

Wild-type EPEC E2348/69 was grown overnight in LB broth at 37°C, 200 rpm and resuspended to 2×10^6 cells mL^{-1}. For the assay, 100 μL were added to each well of a 384-well plate containing appropriate amounts of sample or gentamicin 4 μg mL^{-1} as a control. Plates were incubated at 37°C, 95% humidity without shaking (Biospa, Biotek) and the OD_{600} was determined every hour for 24 h using Cytation 5 (Biotek).

3 Results

The actinobacteria strains investigated in this study were obtained during a research expedition aboard the Norwegian research vessel Kronprins Haakon in the Arctic Sea. These strains were isolated from samples of invertebrates (Schneider et al., 2022) (see Table 1, Section 2.2) Bacterial strains, cultures and extraction). After collection, the isolates were cultured in marine modified ISP2 media. Subsequently, they were subjected to solid-phase extraction using HP20-resin, followed by fractionation into six fractions via FLASH liquid reversed-phase chromatography. These fractions were then screened using various EPEC virulence related *in vitro* assays and further investigation was conducted on the bioactive fractions to identify the active compounds responsible for these effects (see Figure 1 for overview of workflow).

3.1 Fractions 5 from a *Kocuria* sp. and a *Rhodococcus* sp. reduce actin pedestals

To evaluate if the bacterial extract fractions suppress the establishment of actin pedestals, a hallmark of EPEC infections, we employed a high-content screening format of the commonly used fluorescent actin staining (FAS-HCS) assay (Knutton et al., 1989; Pylkkö et al., 2021). When EPEC infects host cells it causes actin-rich pedestals in the vicinity of the microbial microcolonies adhered to the host cells (Campellone et al., 2002). These structures—often called pedestals in the literature—can be visualized using actin staining in cell culture monolayers by phalloidin conjugated fluorophores. This assay additionally quantifies the counts and size of EPEC microcolonies. Previous research in our labs has indicated that these readouts can be used to recognize known antibiotics, as microcolony counts and size tend to show dramatic decrease with these treatments (Pylkkö et al., 2023). Bacteria are typically not entirely killed (and washed away) by short-term treatment with antibiotics, particularly at lower concentrations.

Fractions originating from two of the bacteria (fractions 5 of T091 *Kocuria* sp. and T160-2/*Rhodococcus* sp.) reduced actin pedestals (Figure 2A). The subsequent fraction (fr.6) also had a similar, but weaker effect, likely due to the fact that they contain the same compounds in lower quantities. The other fractions did not display such activity (Supplementary Figure S1). A reduction in the assay readout can occur due to mechanisms relating to bacterial virulence, such as the constituents inhibiting the adhesion of EPEC to the cells, or down regulating virulence related proteins. However, it can also occur due to other indirect mechanisms such as the compounds being toxic to the organisms, or somehow obscuring the image processing pipeline. Therefore, further studies were conducted.

3.2 Fractions 5 from a *Kocuria* sp. and a *Rhodococcus* sp. also reduce Tir translocation

In order to cause pathological changes, such as A/E lesions and associated actin pedestals, EPEC injects virulence factors (e.g., Tir) into the host using a molecular syringe-like device called the type three secretion system. The efficiency of virulence molecule translocation has been studied using beta-lactamase reporter fusions. In this high-throughput method, one C-terminally tags the effector of interest (Tir in this study) with the TEM-1 β-lactamase and infects cells loaded with a FRET signal capable molecule (CCF2-AM) (Mills et al., 2008). CCF2-AM is a molecule in which the donor and acceptor fluorophores are linked together with a beta-lactam. Therefore, the signal emitted by the cells correlates with the degree to which the reporter fusion enzyme (beta beta-lactamase) has cleaved the intracellular molecule, and thus, indirectly with the efficiency of translocation. Beta-lactamase enzymes will not normally be present in unmodified cultured human cell lines. The marine bacterial fractions previously recognized as inhibiting actin pedestals (T091-5 and T160-2-5) also reduced the translocation efficiency of Tir to the infected cells in a concentration dependent manner in this assay (Figure 2B).

3.3 Fractions from a *Rhodococcus* sp. T160-2 prevent red blood cell hemolysis

EPEC infection causes rapid red blood cell hemolysis, and this is likely caused by the injection of EspB and EspD proteins that form a pore on the plasma membrane, which is then used by the type three secretion needle complex to inject molecules into the host cell (Luo and Donnenberg, 2006). Some compounds, such as aurodox for example, can prevent hemolysis efficiently even if they may only modestly prevent actin pedestals (Kimura et al., 2011; Pylkkö et al., 2021). Nevertheless, in *in vivo* murine infection experiments with *Citrobacter rodentium*—a murine specific A/E-pathogen—aurodox protected the entire treatment cohort from death, while all individuals were lost in the no treatment condition and antibiotic treated condition by day 13 (Kimura et al., 2011) suggesting that such compounds may nevertheless be useful. Fractions 4 and 5 from T091 neither showed decrease in hemolysis activity in a dose-dependent manner ($\beta_{fraction4} = 0.00$, $p = 0.46$, $\beta_{fraction5} = 0.00$, $p = 0.35$) but fractions 4 and 5 from T160-2 did ($\beta_{fraction4} = -0.013$, $p = 0.17$, $\beta_{fraction5} = -0.011$, $p = 0.003$) (Figure 3).

10.3389/fmicb.2024.1432475

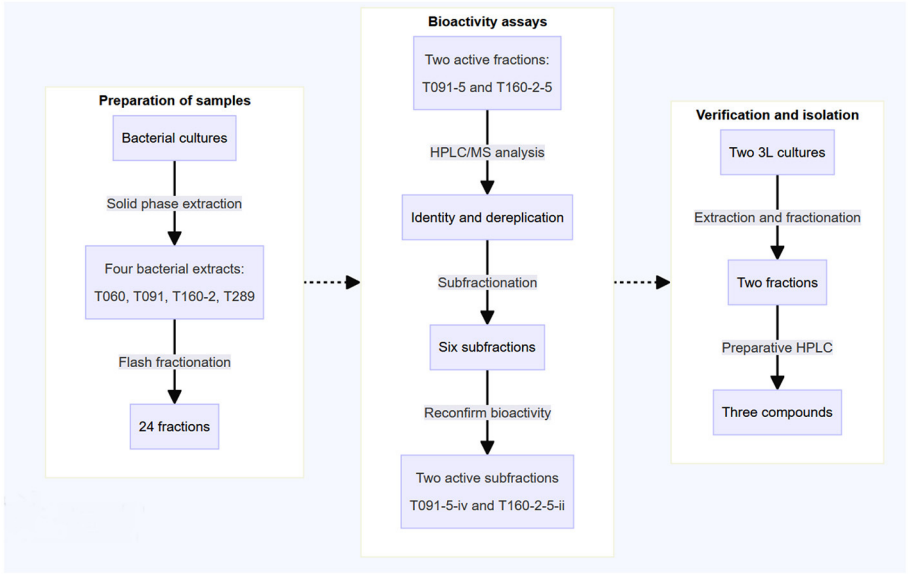

FIGURE 1
The schematic representation outlines the workflow employed in this study. Previously collected marine actinobacteria were cultured in 500 mL flasks in marine modified ISP2 media. Subsequently, the extracts underwent solid-phase extraction and fractionation using reversed-phase liquid chromatography, resulting in the generation of six fractions per sample (24 in total). The crude fractions were then screened for bioactivity in virulence-related *in vitro* assays, monitoring both the translocation of Tir and actin pedestal formation. The active fractions were also checked for their capacity to induce red blood cell hemolysis. Following this, the two active fractions were further fractionated and the activity of these subfractions was reconfirmed. Finally, the isolation and analysis of the active compounds was performed using RP-HPLC-MS via mass triggered fractionation.

3.4 Fraction 5 from the *Rhodococcus* sp. T160-2 prevents formation of microcolonies and the growth of EPEC

Bacterial virulence can also be inhibited, via non-specific mechanisms, i.e., generalized toxicity, such as that caused by growth inhibiting antibiotics. Inspection of the images revealed normal looking microcolonies when treated with fraction 5 from T091, suggesting that this was not the case (Figure 4A). Antibiotics typically cause the abolishment of microcolonies in the FAS-HCS assay and then very few adherent bacteria are visible on the cells as individual bacteria (no microcolonies), so this can be used as an indirect measure of toxicity. Fraction 5 from T160-2, in contrast, did decrease the size of microcolonies severely (Figure 4A; Supplementary Figure S2). These images also suggest that fraction T091-5 is not preventing adhesion entirely either, as there are clearly bacteria and microcolonies in the images (Figure 4A). Therefore, all fractions showing activity were also assessed for growth inhibition of EPEC in broth microdilution assays. Fraction 5 from T091 did not inhibit growth in this assay at concentrations up to 100 μg mL^{-1}, whereas fraction 5 from T-160-2 did (Figure 4B).

3.5 Individual subfractions of the crude FLASH fractions explain the bioactivities

Because the flash fractions contain a several compounds, further subfractionation (refractionation) of these primary fractions was performed using HPLC in order to reconfirm the activities and to get an improved understanding of the specific compounds involved. These subfractions were retested in the assays and then subjected to mass spectrometry to investigate their individual constituents. Following this, the individual molecules of the fractions were purified and tested again in the assays to reconfirm the active ones.

From T091-5, four subfractions, supposedly representing the major constituents (i, ii, iii, iv) were isolated using MS-coupled preparative HPLC equipped with a RP18 column, and then re-examined in the FAS-assay by dissolving into 2.5% DMSO with MQ, and applied to the cells dissolved in 35 μL of MEM. From these one (iv) decreased the average proportion of colonies with pedestals (0.63) compared to the no treatment (0.84) condition of the entire fraction, whilst the rest seemed to have lesser or no effect. Aurodox had a slightly lower mean effect of 0.56. Inspection of the images indicated similar decreases in actin condensates underneath the colonies between iv and aurodox (Figure 5A). Similarly, fraction T160-2-5 was subfractionated into two subfractions (i and ii), of which one (ii) showed similar growth inhibitory activity, whereas the other one (i) did not show any kind of growth inhibition (Figure 5B).

3.6 Isolation of compounds

Two subfractions were therefore considered bioactive. From strain T091 two compounds were isolated. The 3 L culture of T091 yielded 3.68 g of extract that was fractionated into six fractions.

10.3389/fmicb.2024.1432475

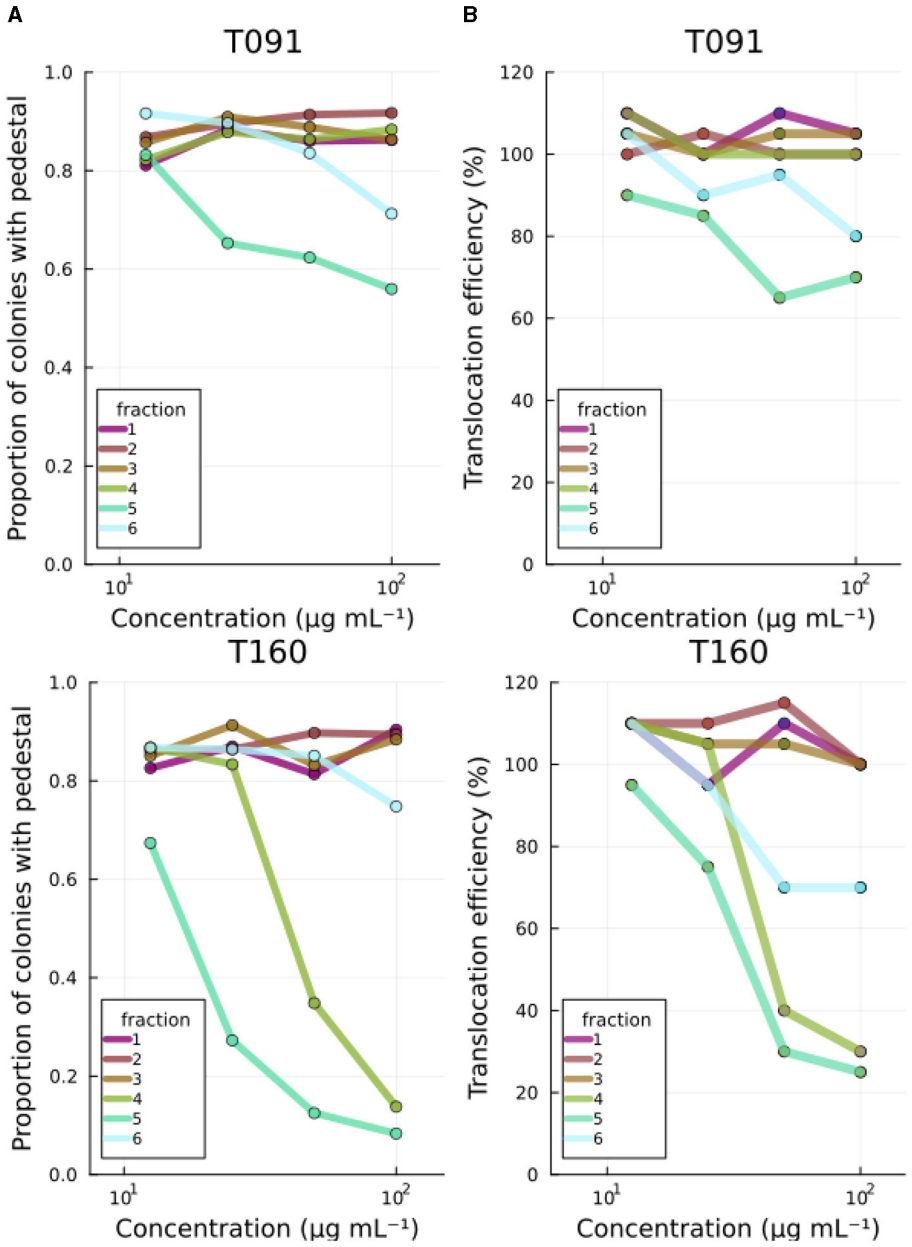

FIGURE 2
Primary screening results. **(A)** Fractions 5 from T091 and T160-2 decrease both the number of EPEC colonies with actin pedestals and **(B)** the translocation efficiency of the translocated intimin receptor in a concentration-dependent manner. The images are segmented by microcolonies, and the actin condensation under these is analyzed from the equivalent area in the phalloidin channel from the cells by segmenting inside of the first segments from the bacterial signal, thus creating a readout of proportion of microcolonies with detectable actin condensation beneath. For translocation assays, the readout is based on the FRET signal from the LifeBLAzer CCF4-AM dye and normalized to No treatment. The primary screening was performed at four concentrations (100, 50, 25, and 12.5 µg mL^{-1}). Fractions from the other strains had no effect (see Supplementary Figure S1).

Fraction 5 (321 mg) and 6 (108 mg) contained compounds **1** and **2**. In the first round of purification using the setup described under Section 2.5, the two molecules were isolated using a Sunfire RP18 column and a gradient from 25 to 100% (v/v) B in 15 min, the quadrupole was recording m/z from 200 to 800 in ESI+ and the signals m/z 782.5 and m/z 769.5 (low resolution MS) were set to trigger the collection of the eluents. The retention times were 8.36 min for **1** (yielding 2.4 mg) and 8.74 min for **2** (yielding 5.3 mg). In a second round of purification **1** was further purified using a Fluoro-Phenyl column and a gradient from 25 to 100%B (v/v) in 15 min, the retention time of 1 within that condition was 7.19 min. **2** was purified in a second purification step using a Fluoro-Phenyl column and a gradient from 25 to 75% (v/v) B in 14 min, the fraction from the first purification still contained traces of **1**. Compounds **1** and **2** were therefore collected at retention times of 7.87 and 8.25 min, respectively. The isolations

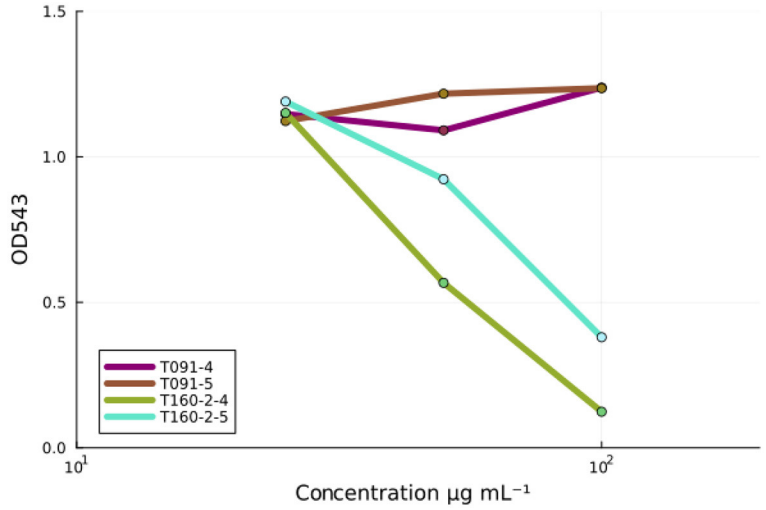

FIGURE 3
The inhibition of EPEC-induced red blood cell hemolysis by fractions. Fractions (4 and 5) from the strain T091 do not prevent EPEC induced hemolysis of sheep red blood cells at any concentrations, whereas fractions (4 and 5) from the strain T160-2 inhibit red blood cell hemolysis in a concentration dependent manner (100, 50, and 25 µg mL^{-1}). Linear models fit to the data: T091 $\beta_{fraction4} = -0.013$, $p = 0.17$, $\beta_{fraction5} = -0.011$, $p = 0.003$ and T160-2 ($\beta_{fraction4} = 0.00$, $p = 0.46$, $\beta_{fraction5} = 0.00$, $p = 0.35$). These results suggest that the observed activity in the screening assays is not due to the inhibition of T3SS-based injection, as compounds, such as aurodox, that do inhibit the expression of the T3SS injection needle, are known to inhibit hemolysis.

were executed by multiple injections and pooling of the respective fractions. The final yields after pooling and drying were **1**: 1.2 mg of red-brown wax-like compound and **2**: 0.9 mg of pale-brown wax-like compound. However, upon attempting to isolate more of the compound, isolation of **3** from 3 L culture of T160, yielding 2.01 g of crude extract was not successful, no visible or weighable amount of compound could be collected.

3.7 Identification and de-replication of compounds

As the individual compounds causing the bioactivities were recognized, we succeeded to analyze their structure and perform dereplication. The compound (from T091-5) that appeared to be changing the properties of the microculture and adherence of the bacteria was demonstrated to be a phospholipid. HPLC-HR-IMS-MS analysis revealed two potentially bioactive compounds in the active subfraction of T091, which are potential phospholipid-like compounds according to their elemental composition, and one potentially bioactive compound from the subfraction of T160-2-5 (see Table 2).

4 Discussion

Natural product mixtures derived from sources such as plants, bacteria, or animals, comprise a diverse collection of major and minor compounds, and therefore the analysis of them is a more challenging endeavor than the evaluation of individual pure compounds. The complex composition of these extracts requires prefractionation techniques to reduce complexity (Appleton et al., 2007; Tu et al., 2010) and certain constituents within these extracts, such as fluorophores, chromophores, or compounds harboring pan assay interference (PAINS), can directly influence assay outcomes (Bisson et al., 2016; Bolz et al., 2021). The reduced complexity of flash fractions compared to crude extracts and the possibility to compare active with "neighboring" inactive fractions eases the de-replication of active fractions significantly. In our experience, fractionation increases the relative concentration of potentially active compounds (e.g., in relation to media components or inactive metabolites), which then enables their detection using *in vitro* screening. Additionally, employing multiple distinct assays alongside quantitative and qualitative assessment based on raw images enables us to address these complexities effectively. Imaging and other high-content methods are notably less susceptible to interference on detection signals, as the artifacts can typically be directly recognized from the images by the operator or well-designed quality control in the analysis pipeline. For example, surfactants, particularly rhamnolipids, have recurrently exhibited bioactivity when screening extract fractions from marine bacteria, demonstrating efficacy in both antibacterial and anticancer screenings within our laboratory (Schneider et al., 2019; Kristoffersen et al., 2021). In this study, we noticed very little, if any, interference in the measurements based on optical density, despite some of the fractions being somewhat dark in appearance. It is worth noting that the widely used optical density measuring hemolysis assay has been modified into an imaging-based method, wherein problematic fractions could be reevaluated in case of uncertainty (Knutton et al., 2002). Nonetheless, to our knowledge, this study marks the first utilization of the Tir-translocation and FAS-assays for bioassay-guided discovery from

10.3389/fmicb.2024.1432475

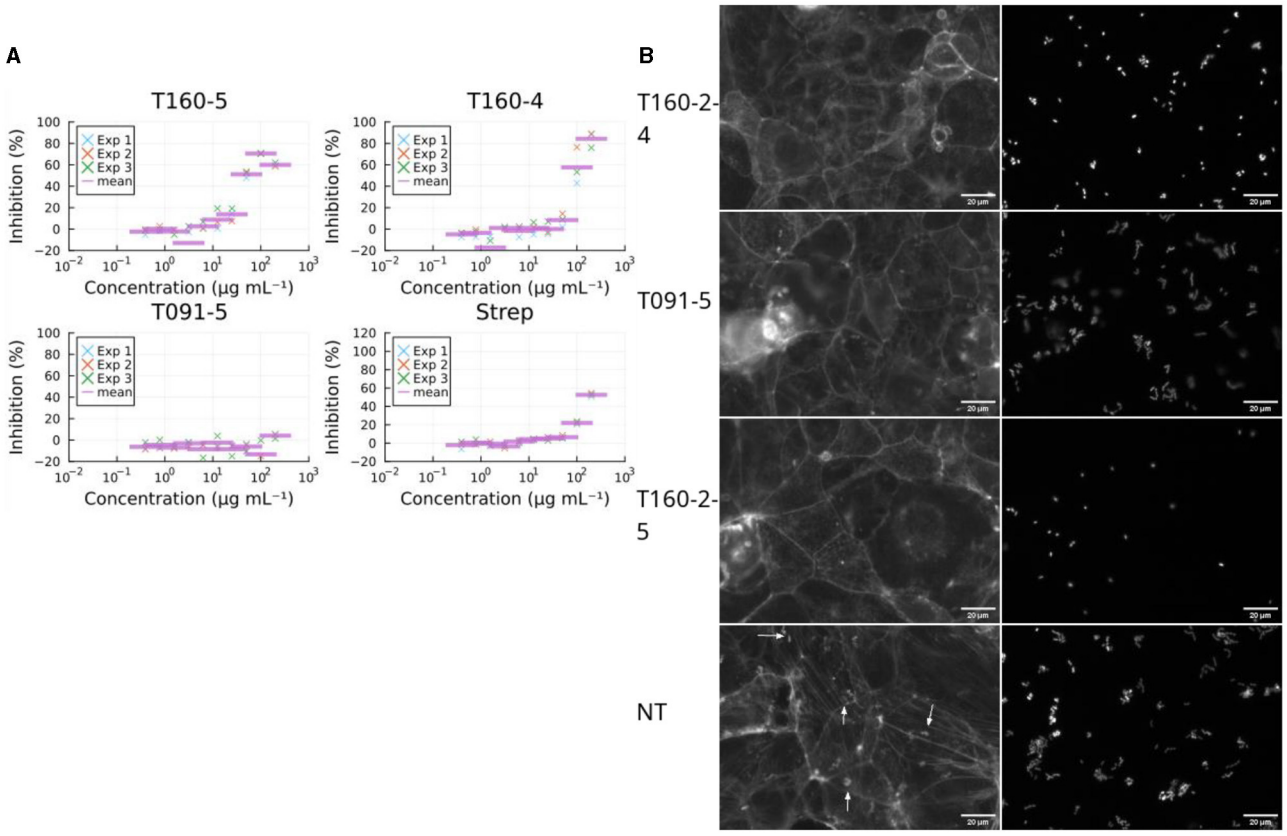

FIGURE 4
Effects on growth. **(A)** Fraction T091-5 did not inhibit growth in the broth microdilution assay (at 6 h post infection, three biological replicates marked by "×" and their arithmetic mean with a purple bar). This supports the view that the decrease in virulence caused by the compounds in fraction 5 of T091 do not achieve this via a bactericidal or growth inhibiting mechanism of action, whereas the compounds of fractions 4 and 5 from T160-2 are likely growth inhibitory. Streptomycin is shown for comparison, the strain (E2348/69) carries resistance genes for streptomycin (*strA* and *strB*), in contrast T091-5 does not show inhibition at any concentration. The results are normalized to the no treatment condition and 4 μg mL^{-1} gentamicin. **(B)** Fractions also change microcolony morphology in the coinfection model. In the no treatment condition (Size mean = 102) the bacteria form normal microcolonies, where multiple bacteria adhere in a pattern called "localized adherence", whereas in the growth inhibiting conditions smaller colonies or even individual bacteria are only present. Mean sizes at 100 μg ml^{-1} T160-2 f4 = 54.7, T160-2 f5 = 59.7 and T091 f5 = 137. Arrows indicate actin condensation foci, the scale bar is 20 μm in size.

TABLE 2 **Elemental compositions calculated from ESI-HR-MS2 data.**

Compound	Observed *m/z* and observed RT	Calcd. *m/z*	Mass error:	Observed CCS	Formula:	Final yield
1	782.46051 $[M+H]^+$ 7.01 min	782.46082	0.396186 ppm	279.99 Å^2	$C_{41}H_{68}NO_{11}P$	1.2 mg
2	796.47660 $[M+H]^+$ 7.39 min	796.47647	0.163219 ppm	281.52 Å^2	$C_{42}H_{70}NO_{11}P$	0.9 mg
3	316.10369 $[M+H]^+$ 3.7 min	316.10458	2.815524 ppm	160.04 Å^2	$C_{14}H_{13}N_5O_4$	–

bacterial extract fractions, providing evidence for the applicability of these assays as valuable tools for the bioprospecting of specific inhibitors of virulence.

Many antimicrobial and virulence inhibiting compounds have previously been discovered in natural products of especially microbial origin. For example, one of the first type three secretion system inhibitors ever discovered was the glycolipid caminoside A isolated from extracts of the marine sponge *Caminus sphaeroconia* (Linington et al., 2002). The compound was discovered using an ELISA-based high-throughput assay to screen a large (20,000 compounds) library monitoring virulence protein secretion via the pore forming EPEC secreted translocator EspB (Gauthier et al., 2005). Caminoside A decreased the secretion of the EspB from EPEC culture into the supernatant without effect on the secretion of other proteins nor bacterial growth. Guadinomines, the most potent known T3SS inhibitors, were similarly discovered using EPEC-mediated red blood cell hemolysis to screen natural product extracts (of *Streptomyces* sp. K01-0509) (Iwatsuki et al., 2008). In another study, this same screening assay methodology was used to discover polyketides generated by *Streptomycetes* that appear to particularly inhibit virulence molecule expression in EPEC (Kimura et al., 2011). It was later demonstrated that the most potent of these, aurodox, down-regulates virulence genes on a pathogenicity island (Locus of enterocyte effacement) by affecting

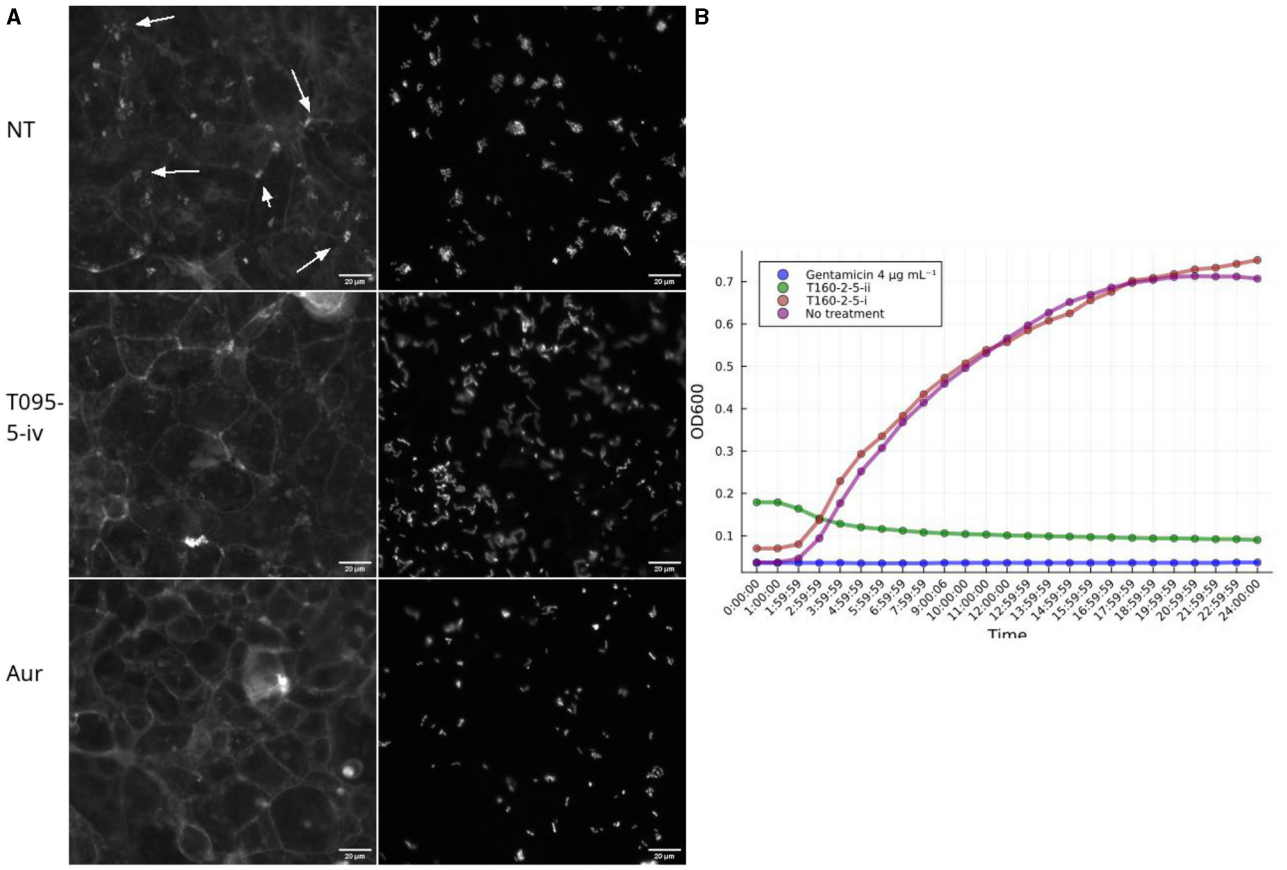

FIGURE 5
Subfractions demonstrate a similar biological activity as the full fractions in the screening assays. **(A)** Example images of pedestal inhibition. Each picture depicts a Caco-2 cell monolayer that is stained using phalloidin-Alexafluor488 and on the right EPEC-mCherry. Subfraction iv from T091-5 shows decrease in actin condensations, whereas in the no treatment (NT) condition there are multiple pedestals apparent as bright colony-sized spots. Aurodox (aur), a T3SS inhibitor that prevents actin pedestals in EPEC infections. **(B)** The two subfractions (i and ii) isolated from the fifth flash fraction of T160-2 had opposite effects on growth kinetics of EPEC, so that T160-2-5-ii is inhibitory similar to 4 μg mL^{-1} gentamicin, whereas T160-2-i is similar to no treatment.

an upstream regulator, Ler (McHugh et al., 2018). Recently, EPEC Tir translocation inhibitors were discovered from bacterial metabolite collections utilizing a high-throughput translocation screening assay (Mühlen et al., 2021). The active compounds appear to not affect the expression of EPEC virulence genes, but nevertheless decrease the translocation of effectors into the host cell by as of yet unknown means.

We studied the effects of the marine actinobacterial extracts on EPEC virulence and growth. Fraction 5 from the strain T091 inhibited EPEC caused actin condensation and the translation of the translocated intimin receptor. Analysis of the images and data reduced from them on bacterial counts suggests that subfraction T091-5-iv is not eradicating the bacteria, and the fact that this fraction does not show inhibition of growth suggest that it does not have antibiotic activity. Interestingly, the subfraction neither prevented red blood hemolysis, a phenomenon believed to be caused by the pore forming capacity of translocators such as EspB/EspD which are a part of the T3SS injection needle. Antibiotic compounds typically prevent EPEC-induced hemolysis, as do compounds that down-regulate the genes from the Locus of enterocyte effacement pathogenicity island of EPEC. Such down-regulation could otherwise explain the decreased translocation and subsequent actin condensation. However, the compounds (**1**, **2**) in the subfraction (T091-5-iv) responsible for the activity are large (molecular weight around 700) phospholipids by composition and are unlikely to access intercellular compartments of the bacterial cells. Additionally, it is known that EPEC uses multiple pili and attachment molecules both to adhere to cells and to autoaggregate into microcolonies. Because it is known that adherence of typical EPEC strains—such as the EPEC E2348/69 used here—to cells and other EPEC individuals is largely mediated by a type 4 pilus, called the bundle forming pilus, and that one target of this pilus is cell wall phospholipids (Barnett Foster et al., 1999; Wu et al., 2004), it is possible that the compound acts by competing with the membrane-based ligand, thus decreasing the adherence of the pathogen to the cells. For example, naturally occurring EPEC strains that do not express the bundle forming pilus (BFP), for example due to not carrying the pEAF plasmid, do not display localized adherence, but typically adhere in a diffuse pattern (Rocha et al., 2011). The main target of BFP is believed to be phosphatidylethanolamine,

which is the second most abundant phospholipid present in the plasma membrane of eukaryotes (Barnett Foster et al., 1999). On the other hand, one would expect to see smaller microcolonies if this were the case. Further investigation is needed to uncover the exact mechanism of action in more detail.

In addition, we discovered that compound **3** from the subfraction T160-2-5-ii from the *Rhodococcus* T160-2 was able to decrease actin condensation and Tir translocation. This, however, showed clear signs of growth inhibition in EPEC both in the images from the infection models, but also in broth microdilution assays. Therefore, these effects are clearly caused by a decrease in viable organisms and not specific virulence related mechanisms. This compound was tentatively identified to be the cause of this EPEC growth inhibiting effect and is under further investigation.

Data availability statement

The original contributions presented in the study are included in the article/Supplementary material, further inquiries can be directed to the corresponding author.

Ethics statement

Ethical approval was not required for the studies on humans in accordance with the local legislation and institutional requirements because only commercially available established cell lines were used. Ethical approval was not required for the studies on animals in accordance with the local legislation and institutional requirements because only commercially available established cell lines were used.

Author contributions

TP: Conceptualization, Data curation, Investigation, Methodology, Software, Validation, Visualization, Writing – original draft, Writing – review & editing. YS: Investigation, Methodology, Writing – review & editing. TR: Conceptualization, Writing – review & editing. JA: Conceptualization, Writing – review & editing. PT: Conceptualization, Funding acquisition, Supervision, Writing – review & editing.

Funding

The author(s) declare financial support was received for the research, authorship, and/or publication of this article. TP acknowledges mobility funding from EU-OPENSCREEN ERIC and NordForsk for the Nordic University Hub project #85352 (Nordic POP, Patient Oriented Products), which allowed onsite visit to MARBIO/UiT-The Arctic University of Norway. The work on compound identification and isolation was supported by UiT-The Arctic University of Norway and Tromsø Forskningstiftelse (grant 2520855, Center for New Antibacterial Strategies).

Acknowledgments

The authors wish to acknowledge CSC—IT Center for Science, Finland, for computational resources. The facilities and expertise of the DDCB unit at the Faculty of Pharmacy, University of Helsinki, supported by HiLIFE and Biocenter Finland, are gratefully acknowledged. We would like to thank Ilan Rosenshine for providing the reporter strain for the Tir translocation assays and Kirsti Helland for technical help organizing lab visit and training.

Conflict of interest

The authors declare that the research was conducted in the absence of any commercial or financial relationships that could be construed as a potential conflict of interest.

Publisher's note

Supplementary material

The Supplementary Material for this article can be found online at: https://www.frontiersin.org/articles/10.3389/fmicb.2024.1432475/full#supplementary-material

References

Appleton, D. R., Buss, A. D., and Butler, M. S. A. (2007). Simple method for high-throughput extract prefractionation for biological screening. *Chimia* 61:327. doi: 10.2533/chimia.2007.327

Barnett Foster, D., Philpott, D., Abul-Milh, M., Huesca, M., Sherman, P. M., Lingwood, C. A., et al. (1999). Phosphatidylethanolamine recognition promotes enteropathogenic *E. coli* and enterohemorrhagic *E. coli* host cell attachment. *Microb. Pathog.* 27, 289–301. doi: 10.1006/mpat.1999.0305

Bisson, J., McAlpine, J. B., Friesen, J. B., Chen, S. N., Graham, J., Pauli, G. F., et al. (2016). Can invalid bioactives undermine natural product-based drug discovery? *J. Med. Chem.* 59, 1671–1690. doi: 10.1021/acs.jmedchem.5b01009

Bolz, S. N., Adasme, M. F., and Schroeder, M. (2021). Toward an understanding of pan-assay interference compounds and promiscuity: a structural perspective on binding modes. *J. Chem. Inf. Model.* 61, 2248–2262. doi: 10.1021/acs.jcim.0c01227

Buroni, S., and Chiarelli, L. R. (2020). Antivirulence compounds: a future direction to overcome antibiotic resistance? *Fut. Microbiol.* 15, 299–301. doi: 10.2217/fmb-2019-0294

Campellone, K. G., Giese, N., Tipper, O. J., and Leong, J. M. A. (2002). tyrosine-phosphorylated 12-amino-acid sequence of enteropathogenic *Escherichia coli* Tir binds the host adaptor protein Nck and is required for Nck localization to actin pedestals: Nck binding by EPEC Tir. *Mol. Microbiol.* 43, 1227–1241. doi: 10.1046/j.1365-2958.2002.02817.x

Cleary, J. (2004). Enteropathogenic *Escherichia coli* (EPEC) adhesion to intestinal epithelial cells: role of bundle-forming pili (BFP), EspA filaments and intimin. *Microbiology* 150, 527–538. doi: 10.1099/mic.0.26740-0

Deborah Chen, H., and Frankel, G. (2005). Enteropathogenic *Escherichia coli*: unravelling pathogenesis. *FEMS Microbiol. Rev.* 29, 83–98. doi: 10.1016/j.femsre.2004.07.002

Defoirdt, T. (2016). Specific antivirulence activity, a new concept for reliable screening of virulence inhibitors. *Trends Biotechnol.* 34, 527–529. doi: 10.1016/j.tibtech.2016.01.009

Duncan, M. C., Wong, W. R., Dupzyk, A. J., Bray, W. M., Linington, R. G., Auerbuch, V., et al. (2014). An NF-κB-based high-throughput screen identifies piericidins as inhibitors of the *Yersinia pseudotuberculosis* type III secretion system. *Antimicrob. Agents Chemother.* 58, 1118–1126. doi: 10.1128/AAC.02025-13

Eltai, N. O., Al Thani, A. A., Al Hadidi, S. H., Al Ansari, K., and Yassine, H. M. (2020). Antibiotic resistance and virulence patterns of pathogenic *Escherichia coli* strains associated with acute gastroenteritis among children in Qatar. *BMC Microbiol.* 20:54. doi: 10.1186/s12866-020-01732-8

Gauthier, A., Robertson, M. L., Lowden, M., Ibarra, J. A., Puente, J. L., Finlay, B. B., et al. (2005). Transcriptional inhibitor of virulence factors in enteropathogenic *Escherichia coli*. *Antimicrob. Agents Chemother.* 49, 4101–4109. doi: 10.1128/AAC.49.10.4101-4109.2005

Iwatsuki, M., Uchida, R., Yoshijima, H., Ui, H., Shiomi, K., Matsumoto, A., et al. (2008). Guadinomines, type III secretion system inhibitors, produced by *Streptomyces* sp. K01-0509: I. taxonomy, fermentation, isolation and biological properties. *J. Antibiot.* 61, 222–229. doi: 10.1038/ja.2008.32

Kaper, J. B., Nataro, J. P., and Mobley, H. L. T. (2004). Pathogenic *Escherichia coli*. *Nat. Rev. Microbiol.* 2, 123–140. doi: 10.1038/nrmicro818

Karami, P., Bazmamoun, H., Sedighi, I., Mozaffari Nejad, A. S., Aslani, M. M., Alikhani, M. Y., et al. (2017). Antibacterial resistance patterns of extended spectrum β-lactamase -producing enteropathogenic *Escherichia coli* strains isolated from children. *Arab. J. Gastroenterol.* 18, 206–209. doi: 10.1016/j.ajg.2017.11.004

Kim, S., Chen, J., Cheng, T., Gindulyte, A., He, J., He, S., et al. (2023). PubChem 2023 update. *Nucleic Acids Res.* 51, D1373–D1380. doi: 10.1093/nar/gkac956

Kimura, K., Iwatsuki, M., Nagai, T., Matsumoto, A., Takahashi, Y., Shiomi, K., et al. (2011). A small-molecule inhibitor of the bacterial type III secretion system protects against *in vivo* infection with *Citrobacter rodentium*. *J. Antibiot.* 64, 197–203. doi: 10.1038/ja.2010.155

Knutton, S., Baldwin, T., Williams, P. H., and McNeish, A. S. (1989). Actin accumulation at sites of bacterial adhesion to tissue culture cells: basis of a new diagnostic test for enteropathogenic and enterohemorrhagic *Escherichia coli*. *Infect. Immun.* 57, 1290–1298. doi: 10.1128/iai.57.4.1290-1298.1989

Knutton, S., Shaw, R., and Frankel, G. (2002). Interaction of enteropathogenic *Escherichia coli* with red blood cell monolayers. *Meth. Enzymol.* 358, 350–355. doi: 10.1016/S0076-6879(02)58101-5

Kristoffersen, V., Jenssen, M., Jawad, H. R., Isaksson, J., Hansen, E. H., Räm,ä, T., et al. (2021). Two novel lyso-ornithine lipids isolated from an arctic marine *Lacinutrix* sp. Bacterium. *Molecules* 26:5295. doi: 10.3390/molecules26175295

Linington, R. G., Robertson, M., Gauthier, A., Finlay, B. B., van Soest, R., Andersen, R. J., et al. (2002). Caminoside A, an antimicrobial glycolipid isolated from the marine sponge *Caminus sphaeroconia*. *Org. Lett.* 4, 4089–4092. doi: 10.1021/ol0268337

Luo, W., and Donnenberg, M. S. (2006). Analysis of the function of enteropathogenic *Escherichia coli* EspB by random mutagenesis. *Infect. Immun.* 74, 810–820. doi: 10.1128/IAI.74.2.810-820.2006

Mahmud, Z. H., Kabir, M. H., Ali, S., Moniruzzaman, M., Imran, K. M., Nafiz, T. N., et al. (2020). Extended-spectrum beta-lactamase-producing *Escherichia coli* in drinking water samples from a forcibly displaced, densely populated community setting in Bangladesh. *Front. Public Health* 8:228. doi: 10.3389/fpubh.2020.00228

McHugh, R. E., O'Boyle, N., Connolly, J. P. R., Hoskisson, P. A., and Roe, A. J. (2018). Characterization of the mode of action of aurodox, a type III secretion system inhibitor from *Streptomyces* goldiniensis. *Infect. Immun.* 87:e00595-18. doi: 10.1128/IAI.00595-18

Mills, E., Baruch, K., Charpentier, X., Kobi, S., and Rosenshine, I. (2008). Real-time analysis of effector translocation by the type III secretion system of enteropathogenic *Escherichia coli*. *Cell Host Microbe* 3, 104–113. doi: 10.1016/j.chom.2007.11.007

Mühlen, S., Zapol'skii, V. A., Bilitewski, U., and Dersch, P. (2021). Identification of translocation inhibitors targeting the type III secretion system of enteropathogenic *Escherichia coli*. *Antimicrob. Agents Chemother.* 65, e00958–e00921. doi: 10.1128/AAC.00958-21

Murray, C. J., Ikuta, K. S., Sharara, F., Swetschinski, L., Robles Aguilar, G., Gray, A., et al. (2022). Global burden of bacterial antimicrobial resistance in 2019: a systematic analysis. *Lancet* 399, 629–655. doi: 10.1016/S0140-6736(21)02724-0

Ochoa, T. J., and Contreras, C. A. (2011). Enteropathogenic *Escherichia coli* infection in children. *Curr. Opin. Infect. Dis.* 24, 478–483. doi: 10.1097/QCO.0b013e32834a8b8b

Patiny, L., and Borel, A. (2013). ChemCalc: a building block for tomorrow's chemical infrastructure. *J. Chem. Inf. Model.* 53, 1223–1228. doi: 10.1021/ci300563h

Pence, H. E., and Williams, A. (2010). ChemSpider: an online chemical information resource. *J. Chem. Educ.* 87, 1123–1124. doi: 10.1021/ed100697w

Pylkkö, T., Ilina, P., and Tammela, P. (2021). Development and validation of a high-content screening assay for inhibitors of enteropathogenic *E. coli* adhesion. *J. Microbiol. Methods.* 184:106201. doi: 10.1016/j.mimet.2021.106201

Pylkkö, T., Tomašič, T., Poso, A., and Tammela, P. (2023). Virtual screening assisted search for inhibitors of the translocated intimin receptor of enteropathogenic *Escherichia coli*. *Chembiochem Eur. J. Chem. Biol.* 25:e202300638. doi: 10.1002/cbic.202300638

Rocha, S. P. D., Abe, C. M., Sperandio, V., Bando, S. Y., and Elias, W. P. (2011). Atypical enteropathogenic *Escherichia coli* that contains functional locus of enterocyte effacement genes can be attaching-and-effacing negative in cultured epithelial cells. *Infect. Immun.* 79, 1833–1841. doi: 10.1128/IAI.00693-10

Schneider, Y. K. (2021). Bacterial natural product drug discovery for new antibiotics: strategies for tackling the problem of antibiotic resistance by efficient bioprospecting. *Antibiotics* 10:842. doi: 10.3390/antibiotics10070842

Schneider, Y. K., Hagestad, O. C., Li, C., Hansen, E. H., and Andersen, J. H. (2022). Selective isolation of Arctic marine actinobacteria and a down-scaled fermentation and extraction strategy for identifying bioactive compounds. *Front. Microbiol.* 13:1005625. doi: 10.3389/fmicb.2022.1005625

Schneider, Y. K. H., Hansen, Ø. K., Isaksson, J., Ullsten, S. H., Hansen, E., Hammer Andersen, J., et al. (2019). Anti-bacterial effect and cytotoxicity assessment of lipid isolated from *Algibacter* sp. *Molecules* 24:3991. doi: 10.3390/molecules24213991

Tu, Y., Jeffries, C., Ruan, H., Nelson, C., Smithson, D., Shelat, A. A., et al. (2010). Automated high-throughput system to fractionate plant natural products for drug discovery. *J. Nat. Prod.* 73, 751–754. doi: 10.1021/np9007359

World Health Organization (2022). *2021 Antibacterial Agents in Clinical and Preclinical Development: An Overview and Analysis*. Geneva: WHO.

Wu, S. C., Liu, F., Zhu, K., and Shen, J. Z. (2019). Natural products that target virulence factors in antibiotic-resistant *Staphylococcus aureus*. *J. Agric. Food Chem.* 67, 13195–13211. doi: 10.1021/acs.jafc.9b05595

Wu, Y., Lau, B., Smith, S., Troyan, K., and Barnett Foster, D. E. (2004). Enteropathogenic *Escherichia coli* infection triggers host phospholipid metabolism perturbations. *Infect. Immun.* 72, 6764–6772. doi: 10.1128/IAI.72.12.6764-6772.2004

Zambelloni, R., Marquez, R., and Roe, A. J. (2015). Development of antivirulence compounds: a biochemical review. *Chem. Biol. Drug Des.* 85, 43–55. doi: 10.1111/cbdd.12430

frontiers | Frontiers in Microbiology

TYPE Review
PUBLISHED 19 September 2024
DOI 10.3389/fmicb.2024.1464135

OPEN ACCESS

EDITED BY
Dany Domínguez Pérez,
Zoological Station Anton Dohrn, Italy

REVIEWED BY
Fei Cao,
Hebei University, China
Joko Tri Wibowo,
National Research and Innovation Agency (BRIN), Indonesia
Muaaz Alajlani,
Al-Sham Private University, Syria

*CORRESPONDENCE
Guolei Huang
huangguolei1982@163.com
Caijuan Zheng
caijuan2002@163.com

†These authors have contributed equally to this work

RECEIVED 13 July 2024
ACCEPTED 16 August 2024
PUBLISHED 19 September 2024

CITATION
Wang B, Cai J, Huang L, Chen Y, Wang R, Luo M, Yang M, Zhang M, Nasihat, Chen G, Huang G and Zheng C (2024) Significance of research on natural products from marine-derived *Aspergillus* species as a source against pathogenic bacteria. *Front. Microbiol.* 15:1464135. doi: 10.3389/fmicb.2024.1464135

Significance of research on natural products from marine-derived *Aspergillus* species as a source against pathogenic bacteria

Bin Wang[1,2†], Jin Cai[1,2†], Longtao Huang[1,2], Yonghao Chen[1,2], Ruoxi Wang[1,2], Mengyao Luo[1,2], Meng Yang[1,2], Mohan Zhang[1,2], Nasihat[1,2], Guangying Chen[1,2], Guolei Huang[1,2*] and Caijuan Zheng[1,2*]

[1]Key Laboratory of Tropical Medicinal Resource Chemistry of Ministry of Education, College of Chemistry and Chemical Engineering, Hainan Normal University, Haikou, China, [2]Key Laboratory of Tropical Medicinal Plant Chemistry of Hainan Province, Haikou, China

Bacterial infections pose a significant clinical burden on global health. The growing incidence of drug-resistant pathogens highlights the critical necessity to identify and isolate bioactive compounds from marine resources. Marine-derived fungi could provide novel lead compounds against pathogenic bacteria. Due to the particularity of the marine environment, *Aspergillus* species derived from marine sources have proven to be potent producers of bioactive secondary metabolites and have played a considerable role in advancing drug development. This study reviews the structural diversity and activities against pathogenic bacteria of secondary metabolites isolated from marine-derived *Aspergillus* species over the past 14 years (January 2010–June 2024), and 337 natural products (including 145 new compounds) were described. The structures were divided into five major categories—terpenoids, nitrogen-containing compounds, polyketides, steroids, and other classes. These antimicrobial metabolites will offer lead compounds to the development and innovation of antimicrobial agents.

KEYWORDS

marine-derived, *Aspergillus* sp., secondary metabolites, antibacterial activity, antimicrobial resistance

1 Introduction

Bacterial infections pose a significant clinical burden on global health (Xuan et al., 2023; Wallis et al., 2023). An estimated 7.7 million deaths are attributed to bacterial infections each year (Okeke et al., 2024; Ikuta et al., 2022). For example, *Staphylococcus aureus*, a frequent colonizer of the human population and one of the foremost opportunistic bacterial pathogens of humans, was associated with more than 1 million deaths in 2019. *Staphylococcus aureus* caused significant morbidity and mortality globally (Howden et al., 2023). Additionally, four additional pathogens (*Escherichia coli*, *Streptococcus pneumoniae*, *Klebsiella pneumoniae*, and *Pseudomonas aeruginosa*) were also associated with more than 0.5 million deaths each in 2019

(Ikuta et al., 2022). Deaths related to bacteria would rank as the second leading cause of death globally. Furthermore, antimicrobial resistance (AMR) remains a global threat. AMR posed a significant global public health threat owing to the rapid global acceleration of resistance in microorganisms. This trend limited the effectiveness of preventing and treating infections caused by viruses, bacteria, and parasites (Charani et al., 2023; Haenni et al., 2022; de Alcântara Rodrigues et al., 2020). A global surveillance report by the World Health Organization (WHO) identified the severe economic effects of AMR (de Alcântara Rodrigues et al., 2020). For instance, the estimated annual expense for the US healthcare system alone ranges from $21 to $34 billion. Beyond the health sector, AMR was projected to cause a decline in actual gross domestic product (GDP) of 0.4 to 1.6% (Gow et al., 2022; Jin et al., 2023). Consequently, the lack of new antimicrobial drugs to replace those that become ineffective underscored the urgent need to preserve the efficacy of existing drugs (Prestinaci et al., 2015). The increasing challenge of AMR highlighted the importance of marine microbial resources as crucial assets in developing new antimicrobial drugs (Alahmari et al., 2022; Carroll et al., 2024). Marine microorganisms, through long-term adaptation to extreme environments, have evolved unique metabolic pathways capable of synthesizing various structurally diverse antimicrobial compounds (Pinedo-Rivilla et al., 2022; Hai et al., 2021), such as marine sponge-derived terpenoid 13-(*E*)-geoditin A (Chen B. et al., 2022), marine coral-derived steroid lobocaloid B (Zhu et al., 2024), ascidian lactone prunolide C (Holland et al., 2022), mangrove sediments polyketone stemphone C (Cai et al., 2023). Thus, marine microorganism resources emerged as an essential source of structurally novel and antimicrobial natural products (Jeewon et al., 2023; Yurchenko et al., 2021; Han et al., 2023; Xu et al., 2022).

Genus *Aspergillus* has been considered one of the most significant general fungi, and representatives have been found in almost all aerobic environments, such as plants, soil, marine life, and submarine sediments (Ibrahim et al., 2023; Sun et al., 2022). Several metabolites of *Aspergillus* have been proven to possess valuable activities, such as aspergillomarasmine A from *Aspergillus versicolor* surmount metallo-*β*-lactamase antibiotic resistance, and Simvastatin, from *Aspergillus terreus* with a critical blood-lipid-lowering medicine, as a potential drug against *S. aureus* biofilm (King et al., 2014; Graziano et al., 2015). Furthermore, marine-derived *Aspergillus* fungi, which lived the diverse and hostile environments, produced a variety of structurally novel and antibacterial chemical compounds, and a significant proportion of these compounds were secondary metabolites with antimicrobial activity (Orfali et al., 2021; Li H. H. et al., 2023; Wang and Ding, 2018; Lee et al., 2013), such as marine-derived fungus *Aspergillus ustus* polyketone stromemycin B (Xue et al., 2024), marine gorgonian-derived fungus *Aspergillus sclerotiorum* alkaloid sclerotiamide L (Meng et al., 2022), marine coral-derived fungus *Aspergillus hiratsukae* terpene chevalone H (Chen X. Y. et al., 2022), marine sediment-derived fungus *A. terreus* lactone butyrolactone I (Bao et al., 2021). Moreover, a series of outstanding reviews on marine-derived *Aspergillus* fungi has been published. In 2013, Lee et al. reviewed the bioactive secondary metabolites of *Aspergillus* derived from marine sources. In 2018, Wang et al. conducted a review of 232 new bioactive metabolites of *Aspergillus* in the marine environment from 2006 to 2016 and categorized their bioactivity and chemical structures (Wang and Ding, 2018). In 2020, Xu et al. summarized the structural diversity and biological activity of 130 heterocyclic alkaloids produced by *Aspergillus* of marine origin from 2014 to 2018 (Xu K. et al., 2020). In 2021, Orfali et al. highlight secondary metabolites from various marine-derived *Aspergillus* species reported between 2015 and 2020 along with their biological potential and structural aspects whenever applicable (Orfali et al., 2021). In 2023, Li et al. summarized the antimicrobial compounds from marine *Aspergillus* from January 2021 to March 2023 (Li H. H. et al., 2023). However, no studies have been carried out on the antimicrobial compounds from marine *Aspergillus* from 2010 to 2024. It is believed that the study of *Aspergillus* living in marine environments will facilitate the discovery of drug lead compounds. Consequently, this review discussed the antibacterial substances derived from *Aspergillus* species in the marine environment from January 2010 to June 2024. A total of 117 cited references were presented in the review. It comprehensively covered the chemical diversity and antimicrobial properties of 337 reported compounds, including 145 new compounds isolated from marine-derived *Aspergillus* fungi. These compounds were structurally categorized into terpenoids (32 compounds), nitrogen-containing compounds (98 compounds), polyketides (139 compounds), steroids (18 compounds), and other compounds (50 compounds). Some potential compounds' relevant biological and pharmacological activities are also highlighted, which will benefit future drug development and innovation. Notably, some antimicrobial compounds against human pathogenic bacteria produced by *Aspergillus* fungi also showed activities against agriculture and fish pathogenic bacteria and so on (Zhang et al., 2024; Xue et al., 2024), which might be suggested as one of the probable candidate drugs for "One Health" in the utilization in healthcare, agriculture, and fishery.

2 Structural and antibacterial activity studies

2.1 Terpenoids

Terpenoids were generally composed of structural units derived from isoprene or isopentane. A total of 32 antibacterial terpenoids (including 13 new compounds) were found in the marine-derived fungal genus *Aspergillus* sp., comprising 18 sesquiterpenes, four diterpenes, and 10 triterpenoids. The structures and the absolute configurations of the new compounds and novel skeleton compounds were elucidated by a detailed spectroscopic analysis of nuclear magnetic resonance (NMR) spectroscopy and mass spectrometry (MS) data, electronic circular dichroism (ECD) calculations, and single-crystal X-ray diffraction.

2.1.1 Sesquiterpenes

One new ophiobolin sesterterpenoid, (5*S*,6*S*)-16,17-dihydroophiobolin H (**1**), together with two known analogs, (6*α*)-21,21-*O*-dihydroophiobolin G (**2**) and 6-epi-ophiobolin G (**3**), were isolated from the cold-seep-derived fungus *A. insuetus* SD-512 (Chi et al., 2020). Compound **1**–**3** exhibited broad-spectrum antibacterial efficacy against eight tested bacterial strains (*Escherichia coli*, *P. aeruginosa*, *Aeromonas hydrophilia*, *Edwardsiella tarda*, *Vibrio alginolyticus*, *Vibrio anguillarum*, *Vibrio Parahemolyticus*, and *Vibrio vulnificus*) with the minimum inhibitory concentration (MIC) values from 4.0 to 32.0 μg/mL. A novel ophiobolin sesterterpenoid ophiobolin U (**4**) and a known analog (5*α*,6*α*)-ophiobolin H (**5**) were

obtained from alga-derived fungus *A. ustus cf*-42 (Liu et al., 2013). Compounds **4**–**5** showed inhibitory effects against *E. coli*, demonstrating inhibition zones of 15.0 and 10.0 mm at a concentration of 30 μg/disk, respectively. Asperophiobolin E (**6**) was obtained from the coral-derived fungus *A. hiratsukae* SCSIO 5Bn$_1$003 (Zeng et al., 2022a). Compound **6** demonstrated strong antibacterial efficacy against *Bacillus subtilis* (MIC, 17.0 μg/mL), which exhibited weak activity against *S. aureus*, with the MIC value of 102.86 μg/mL. One new sesterterpenoid, asperbrunneo acid (**7**), was obtained from the marine-derived fungus *Aspergillus brunneoviolaceus* MF180246 (Xu et al., 2024). Compound **7** showed weak antibacterial efficacy against *S. aureus* with the MIC value of 200 μg/mL. Aspergilol C (**8**) was obtained from the marine-derived fungus *Aspergillus* sp. ZZ1861 (Ha et al., 2024). Compound **8** exhibited potent antibacterial activity against *E. coli*, with the MIC value of 6.25 μg/mL. Punctaporonins B (**9**), D (**10**), and G (**11**), were obtained from the fungus *A. terreus* SCSIO 41202 (Zhang et al., 2024). Compounds **9**–**11** showed a strong antibacterial effect against *Xanthomonas citri* subsp. *citri* with the MIC values of 0.625, 0.625, and 0.3125 mg/mL, respectively. One novel bisabolene-type sesquiterpenoid, 12-hydroxysydowic acid (**12**), along with two known analogs, aspergoterpenin C (**13**) and engyodontiumone I (**14**), were extracted from the fungus *A. versicolor* SD-330 (Li et al., 2021). Compounds **12**–**14** exhibited selective inhibitory activity against *A. hydrophilia*, *E. coli*, *E. tarda*, and *Vibrio harveyi*, with the MIC values ranging 1.0–8.0 μg/mL. Aspergillusene B (**15**), (7*S*,11*S*)-(+)-12-hydroxysydonic acid (**16**), expansol G (**17**), and (*S*)-sydonic acid (**18**), were isolated from the fungus *Aspergillus. sydowii* LW09 (Yang et al., 2023). Compounds **15**, **17**, and **18** demonstrated weak antibacterial efficacy against *Ralstonia solanacarum* (the same MIC, 32.0 μg/mL). Compound **16** demonstrated weak antibacterial activity against *P. syringae*, exhibiting the MIC value of 32.0 μg/mL (Figure 1).

2.1.2 Diterpenoids

A new tetranorlabdane diterpenoid asperolide D (**19**), along with one known analog asperolide A (**20**), was isolated from the fungus *Aspergillus wentii* SD-310 (Li et al., 2016). Compounds **19** and **20** exhibited antibacterial activity against *E. tarda*, with the same MIC value of 16.0 μg/mL. Two pimarane diterpenes, sphaeropsidin A (**21**) and aspergiloid E (**22**), were obtained from the algal-derived fungus *Aspergillus porosus* G23 (Neuhaus et al., 2019). Compounds **21** and **22** showed activity against *S. aureus* ATCC 25923 and ATCC BAA-41, with the MIC values ranging 32.6–77.8 μM (Figure 2).

2.1.3 Meroterpenoids

A new 3,5-dimethylor-sellinic acid-based meroterpenoid, aspergillactone (**23**), from the marine-derived fungus *Aspergillus* sp. CSYZ-1 (Cen et al., 2021), exhibited potent antimicrobial activity against *Helicobacter pylori* (ATCC 43504, G27, Hp159, and BY583) and *S. aureus* (ATCC 25923, USA300, BKS231, BKS233) with the MIC values of 1.0–4.0 and 2.0–16.0 μg/mL. A new meroterpenoid, chevalone B (**24**), was obtained from the marine-derived fungus *Aspergillus* sp. H30 (Hu et al., 2019). Compound **24** showed weak antimicrobial activity against *S. aureus* with the MIC value of 50 μg/mL. Five new α-pyrone meroterpenoids, chevalones H–L (**25**–**29**), isolated from the gorgonian-derived fungus *A. hiratsukae* SCSIO 7S2001 (Chen X. Y. et al., 2022), showed antibacterial activities against *Micrococcus lutea*, *K. pneumoniae*, methicillin-resistant *Staphylococcus aureus* (MRSA) and *Streptococcus faecalis*, with the MIC values of 6.25–100 μg/mL. A new meroterpenoid, austalide R (**30**), and two known compounds, austalides M (**31**) and N (**32**), were isolated from the sponge-derived fungus *Aspergillus* sp. (Zhou et al., 2014). Compounds **30** and **31** displayed broad-spectrum inhibitory activity against eight tested strains (*Halomonas aquamarine*, *Pseudoalteromonas elyakovii*, *V. harveyi*, *Roseobacter litoralis*, *Polaribacter irgensii*, and *Shewanella putrefaciens*) with the MIC values range from 0.01 to 0.1 μg/mL, whereas **32** displayed inhibitory activity against *V. natriegens* and *R. litoralis* with the same MIC value of 0.01 μg/mL (Figure 3).

2.2 Nitrogen-containing compounds

Nitrogenous secondary metabolites were ubiquitous in nature with a wide range of biological activities. A total of 98 nitrogen-containing antimicrobial compounds (including 53 new compounds) were discovered from the genus *Aspergillus* sp., including 39 indole alkaloids, 11 quinazolinone alkaloids, four cytochalasan alkaloids, 13 peptides, and 31 other nitrogen-containing metabolites. The structures and the absolute configurations of the new compounds and novel skeleton compounds were elucidated by a detailed spectroscopic analysis of NMR and MS data, ECD calculations, and single-crystal X-ray diffraction. The absolute configurations of the amino acid residues of the peptides were determined by Marfey's method.

2.2.1 Indole alkaloids

Griseofamine A (**33**), isolated from the deep-sea derived fungus *Aspergillus* sp. SCSIO 41024 (Chen et al., 2020), exhibited weak antibacterial activity against *E. coli* with the MIC value of 64.0 μg/mL. Four new indole alkaloids brevianamides S–V (**34**–**37**), together with two known analogs brevianamide K (**38**) and deoxybrevianamide E (**39**), were isolated from the fungus *A. versicolor* MF030 (Song F. H. et al., 2021). Compounds **34**–**39** displayed antibacterial effects against *Bacille Calmette-Guérin* (BCG), with the MIC values of 6.25, 50, 25, 100, 50, and 100 μg/mL, respectively. Compound **39** also showed antibacterial effects against *S. aureus* and *B. subtilis* with the MIC values of 100 and 50 μg/mL, respectively. A new alkaloid, 9ξ-*O*-2(2,3-dimethylbut-3-enyl)brevianamide Q (**40**), was isolated from the alga-derived fungus *A versicolor* pt20 (Miao et al., 2012). Compound **40** exhibited a weak inhibitory effect on *E. coli* and *S. aureus*, with the same inhibition zone of 7.0 mm at a disk concentration of 30 μg/mL, respectively. 12,13-Dihydroxy-fumitremorgin C (**41**), separated from the fungus *Aspergillus* sp. SCSIO Ind09F01 demonstrated potent inhibitory activity against *Mycobacterium tuberculosis*, with the MIC value of 2.41 μM (Luo et al., 2017). (−)-stephacidin A (**42**) was separated from a gorgonian-derived fungus *Aspergillus* sp. XS-20090066 revealed a selective antibacterial effect against *Staphylococcus epidermidis* (MIC, 14.5 μM) (Chen et al., 2013). Notoamide *F* (**43**) was obtained from the fungus *A. sclerotiorum* GDST-2013-0501 (Wang C. Y. et al., 2022). Compound **43** exhibited a moderate antibacterial effect against *S. epidermidis*, with the MIC value of 12.5 μM. Two new indole alkaloids, asperthrins A (**44**) and E (**45**), were obtained from the fungus *Aspergillus* sp. YJ191021 (Yang et al., 2021). Compound **44** displayed antibacterial effects against *E. tarda*, *V. anguillarum*, *A. hydrophilia* and *Vibrio parahaemolyticus* (MIC, 16, 8, 32, and 16 μg/mL, respectively). Compound **45** displayed

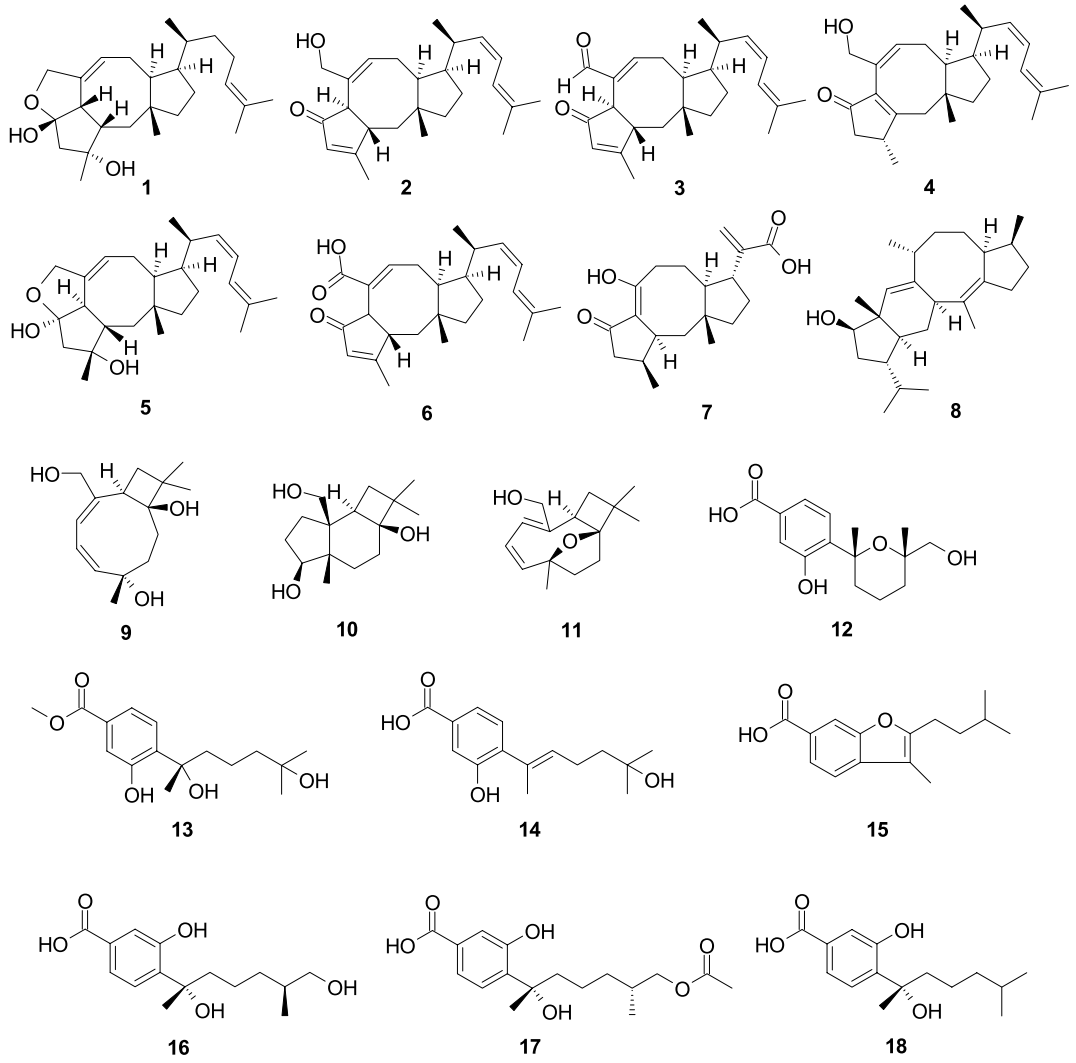

FIGURE 1
Chemical structures of antibacterial sesquiterpenes **1**–**18** from *Aspergillus* spp.

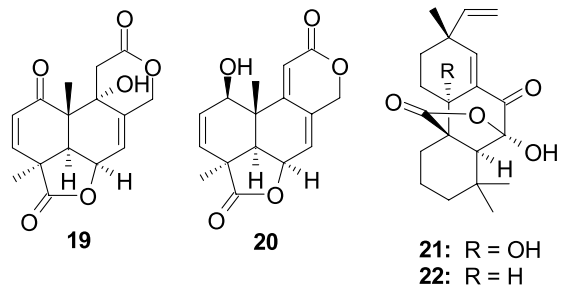

FIGURE 2
Chemical structures of antibacterial diterpenoids **19**–**22** from *Aspergillus* spp.

an inhibitory effect against *Rhizoctonia solani* with the MIC value of 25 μg/mL. Five new indole alkaloids, 24,25-dihydroxyvariecolorin G (**46**), 25-hydroxy-rubrumazine B (**47**), 22-chloro-25-hydroxyrubrumazine B (**48**), 25-hydroxy-variecolorin *F* (**49**), and 27-epi-aspechinulin D (**50**), along with the known analog neoechinulin B (**51**) were isolated from the fungus *Aspergillus Chevalieri* CS-122 (Yan et al., 2023). Compound **46** displayed significant inhibitory activity against *E. coli* (MIC, 4.0 μg/mL), while compound **48** displayed an inhibitory effect against *Vibrio harveyi* (MIC, 8.0 μg/mL). Moreover, compounds **47** and **50** exhibited broad-spectrum antibacterial effects against five evaluated bacterial strains (*V. harveyi*, *E. tarda*, *Aeromonas hydrophila*, *E. coli*, and *Micrococcus luteus*) with the MIC values ranging 16.0–32.0 μg/mL. Compound **51** showed significant activities against *A. hydrophila* (MIC, 4.0 μg/mL) and *E. coli* (MIC, 8.0 μg/mL). A known compound, neoechinulin A (**52**), was separated from the coral-derived fungus *A. hiratsukae* SCSIO 7S2001 (Chen X. Y. et al., 2022). Compound **52** showed weak antibacterial activities against *K. pneumoniae* and *S. faecalis* with MIC values of 50.0 and 12.5 μg/mL, respectively. Compound **52** also had an antibacterial effect against *H. pylori* Hp159 with the MIC value of 16 μg/mL (Yu et al., 2022). Asperfumigatin (**53**), 12,13-dihydroxyfumitremorgin C (**41**), fumitremorgin B (**54**), 13-oxofumitremorgin B (**55**), spirotryprostatin C (**56**), (−)-chaetominine (**57**), and fumigaclavine C (**58**) were isolated from the fungus *Aspergillus fumigatus* H22 (Zhang R. et al., 2022).

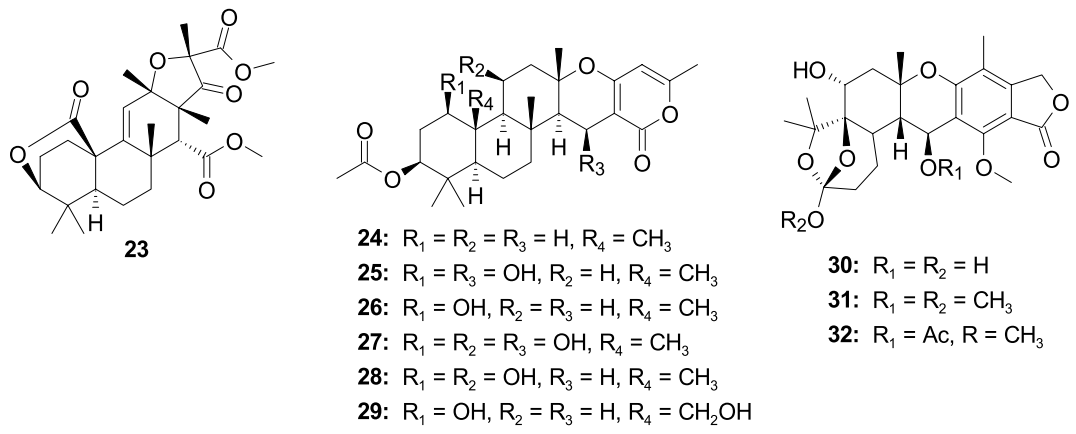

FIGURE 3
Chemical structures of antibacterial meroterpenoids **23**–**32** from *Aspergillus* spp.

Compounds **41** and **53**–**58** showed antibacterial activity against MRSA, with the MIC values from 1.25 to 25.0 μM. Epi-aszonalenin A (**59**) were isolated from the fungus *A. fumigatus* SCSIO 41012 (Limbadri et al., 2018). Compound **59** displayed antibacterial effect against *A. baumanii* ATCC19606 (MIC, 50 μg/mL) and ATCC 15122 (MIC, 6.25 μg/mL). A new tryptophan-derived alkaloid, 3-((1-hydroxy-3-(2-methylbut-3-en-2-yl)-2-oxoindolin-3-yl)methyl)-1-methyl-3,4-dihydrobenzo[e]-[1,4]-diazepine-2,5-dione (**60**), was separated from the sponge-associated fungus *Aspergillus* sp. (Zhou et al., 2014). Compound **60** selectively inhibited *V. harveyi* and *Vibrio natriegens*, with the same MIC value of 1.0 μg/mL. Gliotoxin (**61**), separated from the fungus *Aspergillus* sp. SCSIO Ind09F01, strongly inhibited *M. tuberculosis* (MIC, 0.03 μM) (Luo et al., 2017). *β*-Cyclopiazonic acid (**62**), isolated from sponge-derived fungus *Aspergillus felis* FM324, showed antibacterial effects on *S. aureus*, MRSA, and *B. subtilis*—all exhibiting the same MIC value of 59.2 μM (Wang et al., 2021). One new indole-diterpenoid, (2*R*,4b*R*,6a*S*,12b*S*,12c*S*,14a*S*)-4b-deoxy-*β*-aflatrem (**63**), was isolated from the marine-derived fungus *Aspergillus flavus* OUCMDZ-2205 (Sun et al., 2014). Compound **63** exhibited antibacterial activity against *S. aureus* with the MIC value of 20.5 μM. Eight new notoamide-type alkaloids, sclerotiamides K–R (**64**–**71**), were isolated from a marine gorgonian-derived fungus *A. sclerotiorum* LZDX-33-4 (Meng et al., 2022). Compounds **64**–**71** showed antibacterial activity against *S. aureus* ATCC29213 with MIC values ranging 4–64 μM (Figure 4).

2.2.2 Quinazolinone alkaloids

Two novel alkaloids fumigatosides E–F (**72**–**73**), along with a known alkaloid fumiquinazoline G (**74**), were isolated from *A. fumigatus* SCSIO 41012 (Limbadri et al., 2018). Compound **72** showed activities against *Acinetobacter baumanii* ATCC 19606, *A. baumanii* ATCC 15122, *S. aureus* ATCC 16339, and *K. pneumonia* ATCC 14578 with the MIC values of 12.5, 6.25, 6.25, and 12.5 μg/mL, respectively. Compound **73** exhibited activity against *A. baumanii* ATCC 19606 with the MIC value of 6.25 μg/mL. Compound **73** exhibited significant activity against *S. aureus* ATCC16339 and 29,213, (MIC, 1.56 and 0.78 μg/mL). Compound **74** showed activities against *A. baumanii* ATCC 15122, *S. aureus* ATCC 16339, *S. aureus* ATCC29213, and *K. pneumonia* ATCC 14578 with the MIC values of 6.25, 12.5, 12.5, and 25 μg/mL, respectively. One new alkaloid cottoquinazoline H (**75**) and a known analog cottoquinazoline A (**76**) were separated from the coral-associated fungus *A. versicolor* AS-212 (Dong et al., 2023a). Compound **75** showed potent inhibitory effects against the aquatic pathogenic bacterium *Vibrio harvryi* (MIC, 18.1 μM) and *V. parahemolyticus* (MIC, 9.0 μM). Compound **76** exhibited moderate activity against *A. hydrophila* with an MIC value of 18.6 μM. Compound **76** also showed strong antibacterial effect against *E. coli* with the MIC value of 5.0 μM (Zhang L. et al., 2020; Zhang Y. H. et al., 2020). A new alkaloid, aspergicin (**77**), was separated from the mixed cultivation of two mangrove-associated mangrove fungi *Aspergillus* sp. (Zhu et al., 2011). Compound **77** exhibited a moderate antibacterial effect against *B. subtilis* and *B. dysenteriae*, with consistent MIC values of 15.6 μg/mL. Brevianamide M (**70**) was separated from the alga-associated fungus *A. versicolor* pt20 (Miao et al., 2012). Compound **78** exhibited antibacterial activity against *E. coli* and *S. aureus*, with inhibition zones of 11.0 and 10.0 mm observed at a concentration of 30 μg/disk, respectively. Fumiquinazolines D (**79**) and C (**80**), were separated from the sea cucumber-associated fungus *A. fumigatus* M580 (Tuan et al., 2022). Compounds **79** and **80** exhibited antibacterial activity against Gram-positive *Enterococcus faecalis* with the same MIC value of 32.0 μg/mL. 3-Hydroxy-6-methoxy-4-phenylquinolin-2(1*H*)-one (**81**) and 3-methoxy-6-hydroxy-4-phenylquinolin-2(1*H*)-one (**82**) were separated from a coral-derived fungus *A. versicolor* AS-212 (Dong et al., 2023b). Compounds **81** and **82** demonstrated an antibacterial effect against aquatic pathogenic bacteria *V. harveyi* and *V. alginolyticus*, with the MIC values from 8 to 32 μg/mL (Figure 5).

2.2.3 Cytochalasan alkaloids

Cytochalasin Z17 (**83**) was isolated from the sponge-derived fungus *Aspergillus* sp., and it showed selective and pronounced activity effect *R. litoralis* with the MIC value of 0.0001 μg/mL (Zhou et al., 2014). Aspochalasins I (**84**), D (**85**), and PZ (**86**), were separated from the coral-associated fungus *Aspergillus elegans* (Zheng et al., 2013). Compound **84** showed moderate antibacterial activity against *S. epidermidis* (MIC, 20 μM) and *S. aureus* (MIC, 10 μM). Compound **85** exhibited extensive antibacterial effects against four pathogenic bacteria (*S. albus*, *S. aureus*, *E. coli*, and *Bacillus cereus*) with a consistent

MIC value of 10 μM. Compound **86** displayed an antibacterial effect against *S. epidermidis* with the same MIC value of 20 μM (Figure 6).

2.2.4 Peptides

One novel thiodiketopiperazine, emestrin M (**87**), and a known monomer compound, emethacin C (**88**), were separated from the fungus *A. terreus* RA2905 (Wu et al., 2020a). Compounds **87** and **88** displayed antibacterial activity against *P. aeruginosa* ATCC 27853 with the MIC values of 64 and 32 μg/mL, respectively. One novel phenylalanine derivative 4′-OMe-asperphenamate (**89**) and another known phenylalanine derivative asperphenamate (**90**) were separated from the coral-associated fungus *A. elegans* ZJ-2008010 (Zheng et al.,

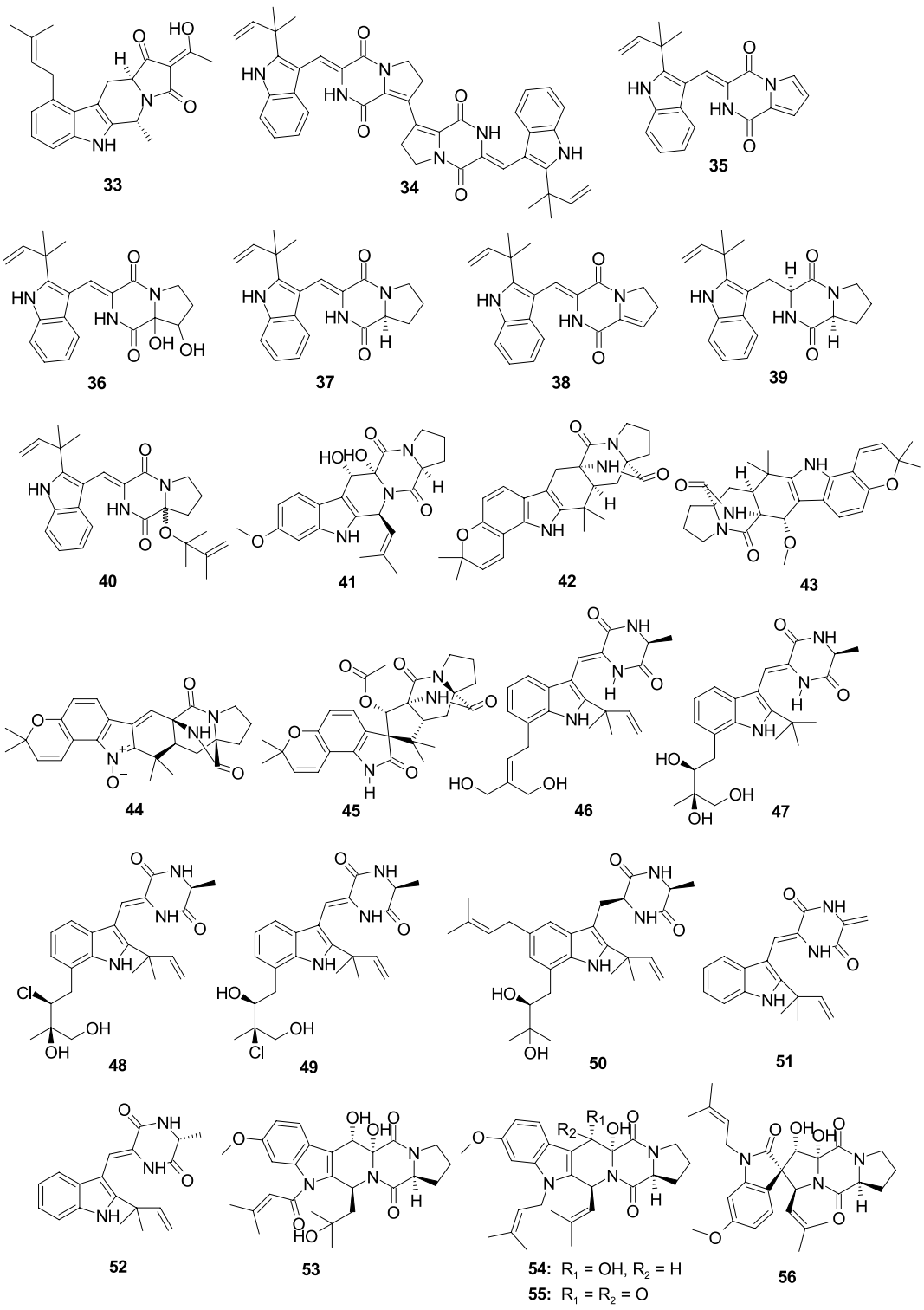

FIGURE 4 (Continued)

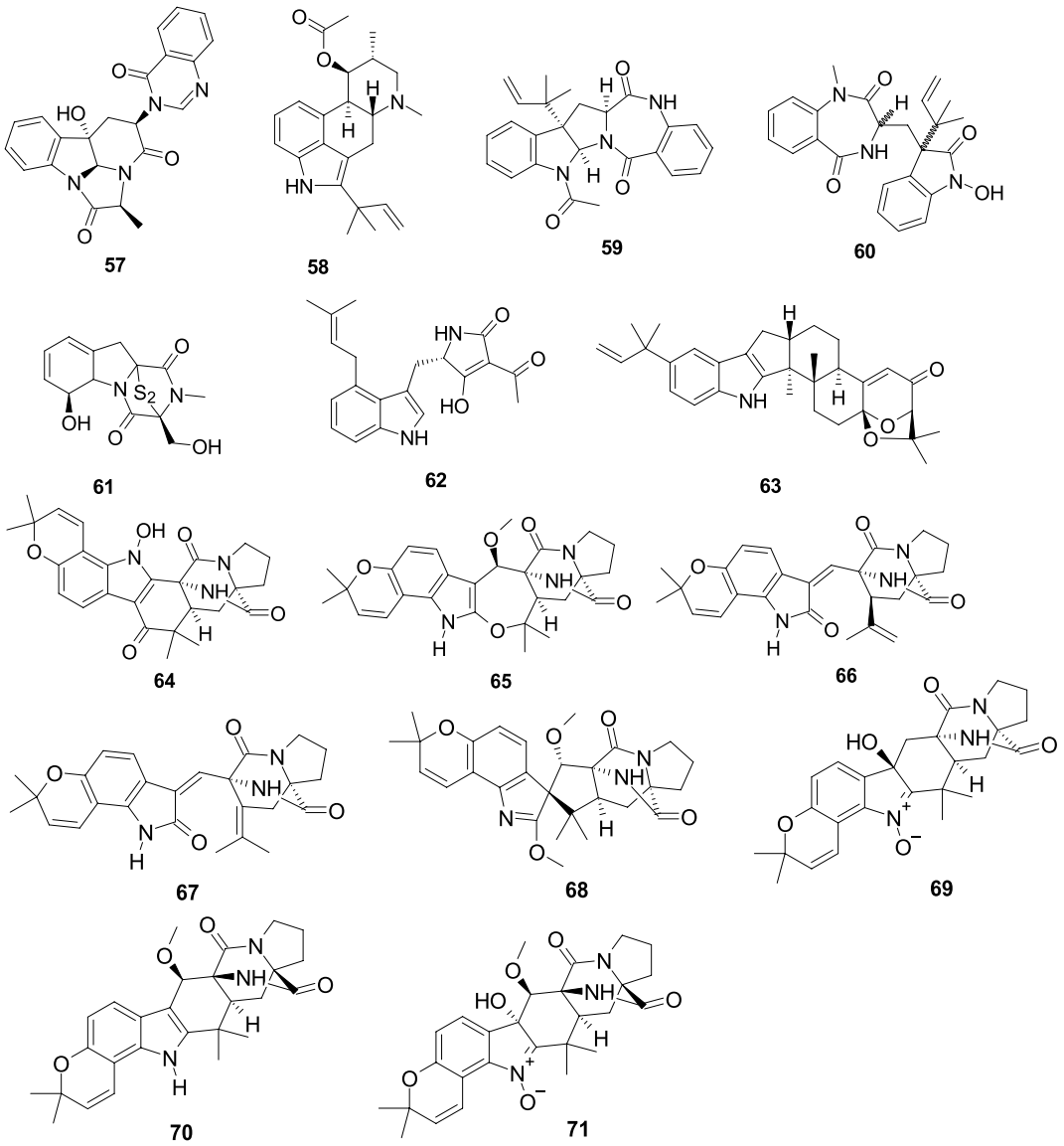

FIGURE 4
Chemical structures of antibacterial indole alkaloids **33**–**71** from *Aspergillus* spp.

2013). Compounds **89** and **90** showed an antibacterial effect against *S. epidermidis* with the same MIC value of 10.0 μM. Three novel aspochracin-type cyclic tripeptides, sclerotiotides M–O (**91**–**93**), together with two previously identified analogs, sclerotiotides L (**94**) and *F* (**95**), were originated from the fungus *Aspergillu insulicola* HDN151418 (Sun et al., 2020). Compounds **91** and **92** dispalyed a broad antibacterial effect on eight pathogenic strains (*B. cereus*, *Proteus*species, *Mycobacterium phlei*, *B. subtilis*, *V. parahemolyticus*, *E. tarda*, MRCNS, and MRSA) with the MIC values ranging 1.56–25.0 μM. Compound **93** showed an antibacterial effect on *E. tarda* and *V. parahemolyticus* with consistent MIC values of 25 μM. Compounds **94** and **95** showed antibacterial activity effects on four bacterial strains (*B. cereus*, *Proteus* species, *E. tarda*, and *V. parahemolyticus*) with consistent MIC values of 25 μM. Two new pentadepsipeptides, aspertides D (**96**) and E (**97**), were originated from the multistrain fermentation of two marine-associated fungi *Aspergillus tamarii* MA-21 and *Aspergillus insuetus* SD-512 (Chi et al., 2023). Compound **96** exhibited an antibacterial effect on four aquatic bacterial pathogens (*E. tarda*, *V. alginolyticus*, *V. anguillarum*, and *V. vulnificus*) with the MIC values of 8.0–32.0 μg/mL. Compound **97** had an antibacterial effect on *E. tarda* and *S. aureus* with the MIC values of 16.0 and 8.0 μg/mL, respectively (Figure 7). Unguisins A (**98**) and B (**99**) were isolated from marine sponge-derived fungus *Aspergillus nidulans* M256, displayed antibacterial activity against *E. faecalis* with the MIC values of 32 and 128, respectively.

2.2.5 Other nitrogen-containing metabolites

Ochratoxin A methyl ester (**100**) was separated from the fungus *A. elegans* KUFA0015 (Kumla et al., 2021). Compound **100** showed a broad spectrum of antibacterial effect against *E. faecalis* ATCC29212, *E. faecalis* B3/101, *S. aureus* ATCC29213, and MRSA *S. aureus* 66/1 with the MIC values of 16, 16, 8, and 16 μg/mL, respectively. A new chlorinated amino acid derivative, aspergamide A (**101**), was obtained from the sponge-associated fungus *Aspergillus* sp. LS53 (Zhang

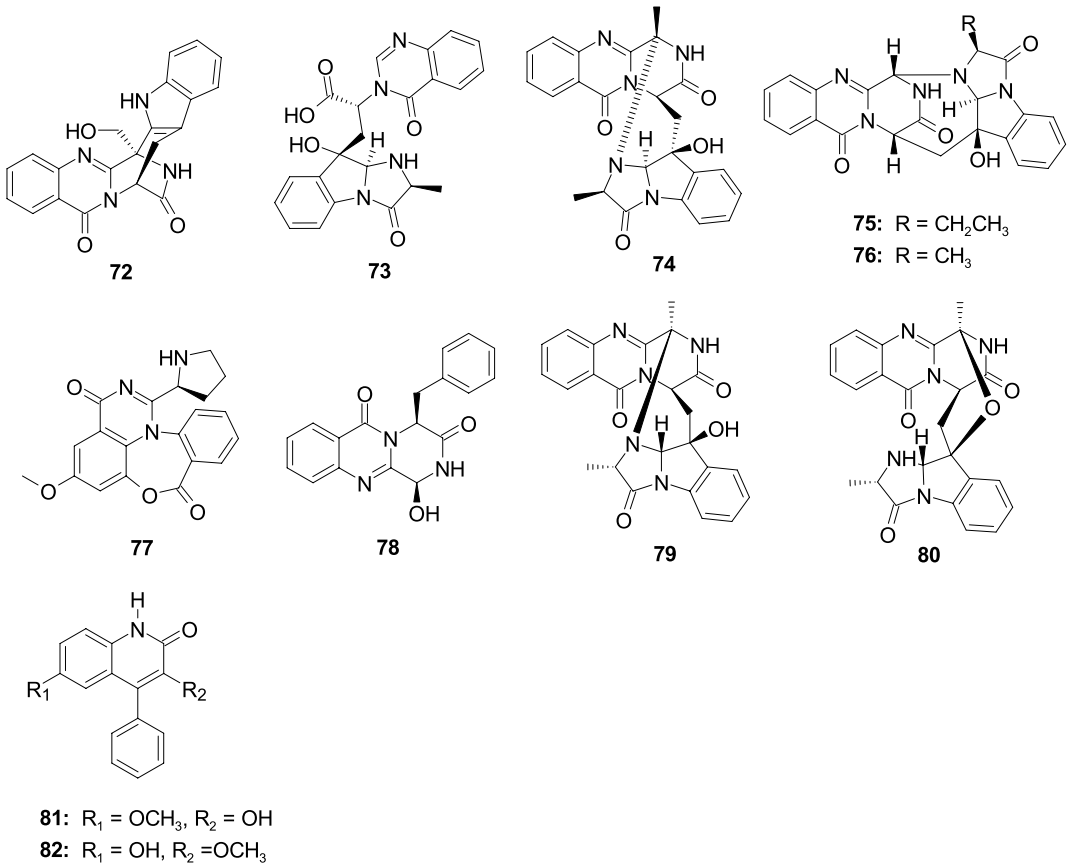

FIGURE 5
Chemical structures of antibacterial quinazolinone alkaloids **72**–**82** from *Aspergillus* spp.

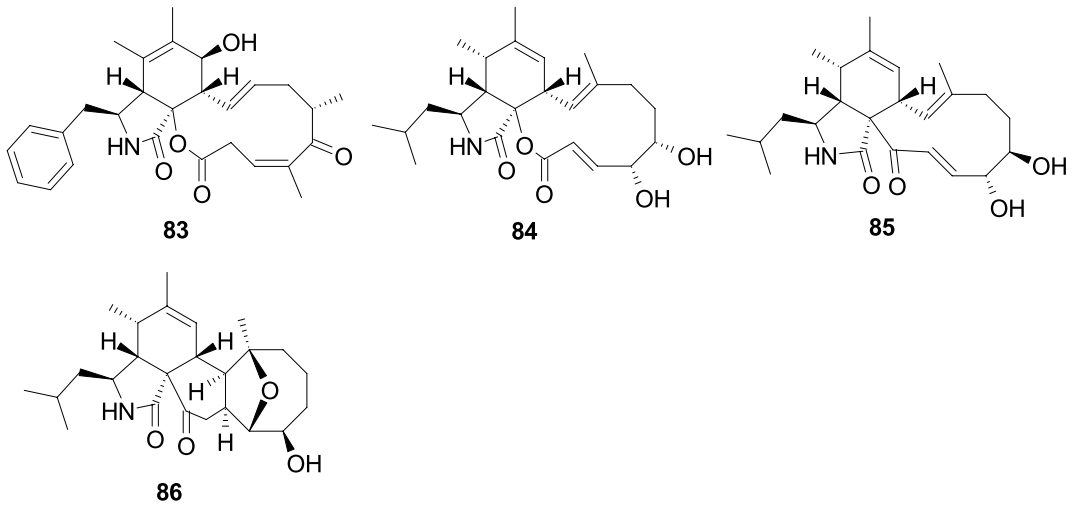

FIGURE 6
Chemical structures of antibacterial cytochalasan alkaloids **83**–**86** from *Aspergillus* spp.

L. et al., 2020; Zhang Y. H. et al., 2020). Compound **101** had a weak antibacterial effect on *V. harveyi*, with the MIC value of 16 μg/mL. 11-*O*-methylpseurotin A (**102**), azaspirofurans B (**103**), and A (**104**) were separated from the marine-associated fungus *A. fumigatus* H22 (Zhang R. et al., 2022). Compounds **102**–**104** showed a strong antibacterial effect against MRSA (MIC, 10.0, 5.0, and 5.0 μM, respectively). A new benzofuran derivative, dibetanide (**105**), was separated from the sponge-derived fungus *Aspergillus* sp. LS57 (Li W. H. et al., 2023). Compound **105** displayed inhibitory activity against *Botrytis cinerea* with the MIC value of 256 μg/mL. Ochratoxin

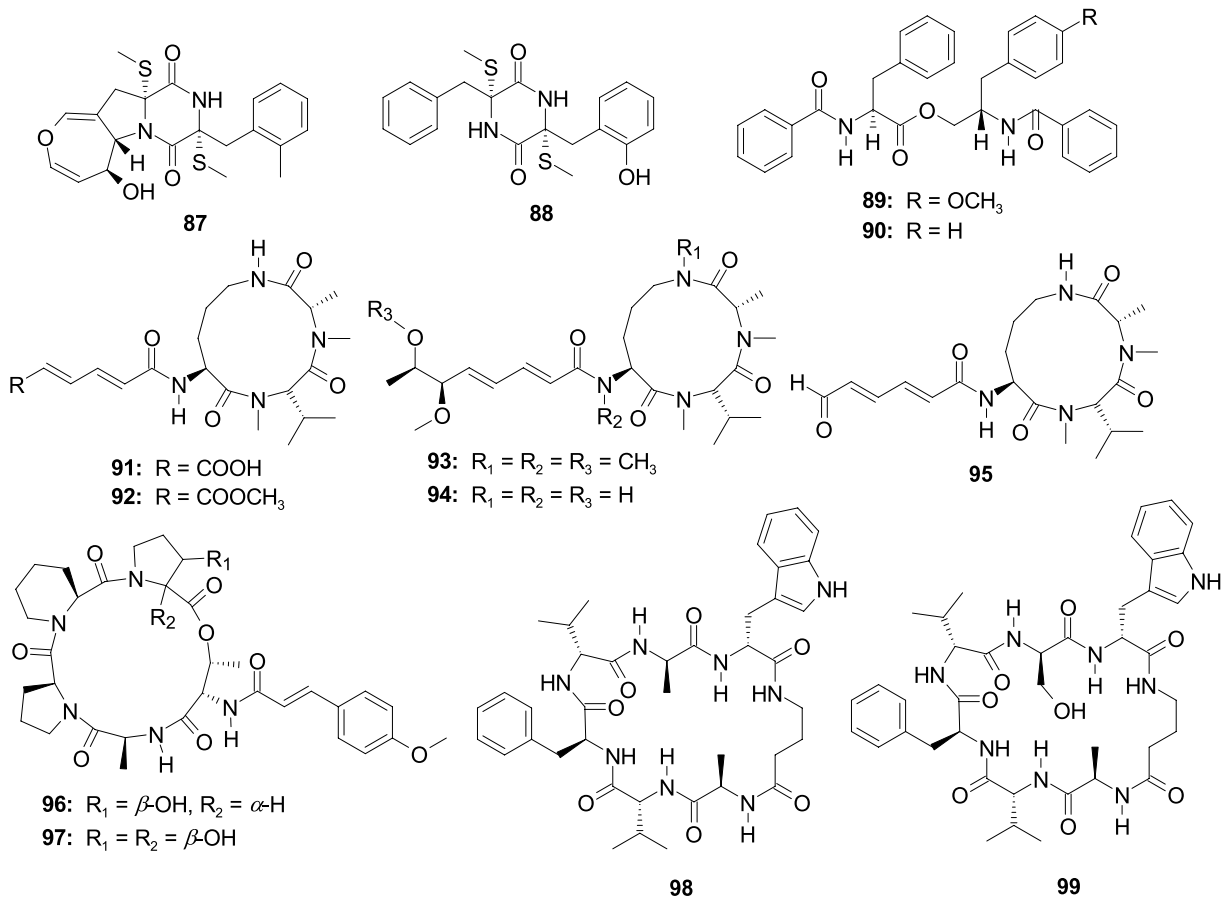

FIGURE 7
Chemical structures of antibacterial cytochalasan alkaloids **87**–**99** from *Aspergillus* spp.

B (**106**) was separated from the sponge-associated fungus *A. elegans* KUFA0015 (Duraes et al., 2021). Compound **106** had a weak antibacterial effect against *S. aureus* 272,123 with the MIC value of 50.0 μM. Dihydroisoflavipucine (**107**) was separated from the sponge-associated fungus *Aspergillus* sp. and showed strong activity against *R. litoralis* with the MIC value of 0.0001 μg/mL (Zhou et al., 2014). A racemate of benzyl furanone, (+)-asperfuranone (**108**) and (−)-asperfuranone (**109**), were separated from coral-associated fungus *A. terreus* RA2905 (Wu et al., 2020b). Compounds **108**–**109** displayed an antibacterial effect against *P. aeruginosa* ATCC 27853 with the MIC values of 32 and 128 μg/mL, respectively. A novel compound, carneusin B (**110**), was separated from the fungus *Aspergillus carneus* GXIMD00519 (Lu et al., 2023). Compound **110** displayed weak antibacterial activities against *Vibrio rotiferianus* and *Alteromonas macleodii* with the consistent MIC value of 64.0 μg/mL. Seven novel benzoic acid-containing alkaloids, asperalins A–F (**111**–**116**) and *N*-(3-acetamidopropyl)-3,4-dihydroxybenzamide (**117**), were separated from a seagrass-associated fungus *Aspergillus alabamensis* SYSU-6778 (Hu et al., 2023). Compounds **111**–**116** revealed moderate-to-potent activities against *Streptococcu iniae* and *Streptococcus parauberis* with the MIC values ranging 2.2–87.3 μM, respectively. Compound **117** showed weak antibacterial effect on *Edwardsiella ictaluri* with MIC value of 79.3 μM. Two new compounds, sclerotiamides I (**118**) and J (**119**), were isolated from a marine gorgonian-derived fungus *A. sclerotiorum* LZDX-33-4 (Meng et al., 2022). Compounds **118** and **119** displayed antibacterial activity against *S. aureus* ATCC29213 with the same MIC value of 16 μM. Two novel nucleoside derivatives, kipukasins H (**120**) and I (**121**), together with two known analogs, kipukasins E (**122**) and D (**123**), originated from the fungus *A. versicolor* (Chen et al., 2014). Compounds **120**–**123** exhibited antibacterial effects on *S. epidermidis* with the MIC values of 12.5, 12.5, 50.0, and 50.0 μM, respectively. Two rare tetracyclic skeleton alkaloids, perinadines B (**124**) and C (**125**), were originated from the fungus *Aspergillus* sp. LS116 (Liu Y. et al., 2022). Compounds **124**–**125** exhibited moderate antibacterial effects on *B. subtilis* (MIC, 32.0 and 64.0 μg/mL, respectively). Neoaspergillic (**126**), isolated from coral-associated fungus *Aspergillus* sp. CF07002 showed a weak antibacterial effect on three tested bacterial strains (*B. cereus*, *K. pneumoniae*, and *E. coli*) with MIC values ranging 30.0–40.0 μg/mL (Cardoso-Martinez et al., 2015). A novel dimer of a zinc complex, dizinchydroxyneoaspergillin (**128**), and a known compound hydroxyneoaspergillic acid (**127**), originated from the fungus *Aspergillus ochraceopetaliformis* SCSIO 41018 (Guo et al., 2021). Compound **127** exhibited potent inhibitory effects against *A. baumannii* with the MIC value of 0.45 μg/mL. Compound **128** showed significant bactericide effects against MRSA, *S. aureus*, *E. faecalis*, *A. baumannii*, and *K. pneumonia* with the MIC values from 0.45 to 7.8 μg/mL. A racemic mixture alkaloid, (±)-puniceusine N (**129**), was isolated from the fungus *Aspergillus puniceus* SCSIO z021 (Liu C. M. et al., 2022). Compound (±)-**129** had medium antibacterial

activities against *S. aureus*, MRSA, and *E. coli* with a consistent MIC value of 100 μg/mL. Preussin (**130**), separated from the fungus *Aspergillus candidus* KUFA0062, displayed inhibitory activity against *S. aureus* ATCC 29213, *E. faecalis* ATCC 29212, MRSA, and vancomycin-resistant *enterococci* with consistent MIC value of 32.0 μg/mL (Buttachon et al., 2018) (Figure 8).

2.3 Polyketides

Polyketides were a group of compounds recognized for their wide range of structures and biological activities. These compounds were produced through a series of Claisen condensation reactions, usually utilizing acetyl-coenzyme A (acetyl-CoA), malonyl-coenzyme A (malonyl-CoA), and other substrates. A total of 139 antibacterial polyketides (including 54 new compounds) were separated from the genus of *Aspergillus* sp., including 20 anthraquinones, 31 xanthones, 59 lactones, and 29 other polyketide metabolites. The structures and the absolute configurations of the new compounds were elucidated by a detailed spectroscopic analysis of NMR and MS data, ECD calculations, as well as single-crystal X-ray diffraction.

2.3.1 Anthraquinones

Two new anthraquinone dimers, 6,6′-oxybis(1,3,8-trihydroxy-2-((*S*)-1-methoxyhexyl)anthracene-9,10-dione) (**131**) and 6,6′-oxybis(1,3,8-trihydroxy-2-((*S*)-1-hydroxyhexyl)anthracene-9,10-dione) (**132**) were originated from the fungus *A. versicolor* INF16-17 (Li et al., 2019). Compounds **131**–**132** demonstrated a selective antibacterial effect on *S. aureus* at a concentration of 30.0 μg/well. Xanthomegnin (**133**) and viomellein (**134**) were separated from the sponge-associated fungus *A. elegans* KUFA0015 (Kumla et al., 2021). Compounds **133**–**134** had a moderate antibacterial effect on *E. faecalis* ATCC29212, *S. aureus* ATCC29213, and *S. aureus* 66/1 (MRSA), with the MIC values ranging 2.0–32.0 μg/mL. One new anthraquinone versiconol B (**135**) and a known compound versiconol (**136**) were originated from the fungus *Aspergillus* sp. F40 (Tian et al., 2018). Compounds **135**–**136** exhibited weak antibacterial activity against *S. aureus* and *V. parahaemolyticus* with the MIC values of 12–48 μg/mL. One novel anthraquinone derivative, 2-(dimethoxymethyl)-1-hydroxyanthracene-9,10-dione (**137**), along with two previously reported analogs, damnacanthal (**138**) and xanthopurpurin (**139**), were separated from the fungus *A. versicolor* 3A00029 (Wang et al., 2018). Compound **137** displayed a potent inhibitory effect on MRSA (ATCC 43300 and CGMCC 1.12409), with the MIC values of 3.9 and 7.8 μg/mL, respectively. Compound **138**–**139** showed a weak antibacterial effect on *V. vulnificus* MCCC E1758, *V. rotiferianus* MCCC E385, and *Vibrio campbellii* MCCC E333, with the MIC values ranging 62.5–125 μg/mL. One novel anthraquinone isoversicolorin C (**140**) and one known anthraquinone derivative versicolorin C (**141**) were separated from the fungus *A. nidulans* MA-143 (Yang et al., 2018a). Compound **140** demonstrated a remarkable antibacterial effect on *V. alginolyticus* (MIC, 1.0 μg/mL) and *E. ictaluri* (MIC, 4.0 μg/mL). Compound **141** exhibited an antibacterial effect against five tested bacterial strains (*E. coli*, *M. luteus*, *V. alginolyticus*, *V. parahaemolyticus*, and *E. ictaluri*), with the MIC values ranging 1.0–8.0 μg/mL. Emodin (**142**) was separated from the fungus *A. fumigatus* MF029 (Song Z. J. et al., 2021). Compound **142** showed potent activity against BCG with the MIC value of 1.25 μg/mL, along with **142** demonstrated moderate antibacterial activities effect on MRSA and *S. aureus* with the same MIC value of 50.0 μg/mL. 6,8-Di-*O*-methylaverufin (**143**) and 6-*O*-methylaverufin (**144**) were separated from the alga-associated fungus *A. versicolor* pt20 (Miao et al., 2012). Compounds **143**–**144** displayed an antibacterial effect against *E. coli* and *S. aureus*, showing the same inhibition zone of 10.0 mm at 30 μg/disk. The new anthraquinone, 6,8-di-*O*-methylaverantin (**145**), together with one known congener 6,8-di-*O*-methylversiconol (**146**), was separated from the fungus *A. versicolor* EN-7 (Zhang et al., 2012). Compounds **145** and **146** showed weak inhibition against *E. coli*, with the inhibition zones 7.0 and 6.5 mm at 20 μg/disk, respectively. Averantin (**147**), averufin (**148**), and nidurufin (**149**) were originated from the fungus *A. versicolor* PF10M (Lee et al., 2010). Compounds **147**–**149** showed a better antibacterial effect on *Streptococcus pyogenes* and *S. aureus* with the MIC values from 0.78 to 6.25 μg/mL. 6,8-Di-*O*-methylversicolorin A (**150**) was originated from the fungus *Aspergillus* sp. WHUF05236 (Lv et al., 2022). Compound **150** displayed an antibacterial effect against *H. pylori*, with the MIC values from 20.00 to 43.47 μM (Figure 9).

2.3.2 Xanthones

Asperpyrone A (**151**), aurasperones A (**152**), *F* (**153**), and B (**154**), were separated from the mangrove-associated fungus *Aspergillus* sp. DM94 (Gou et al., 2020). Compound **151**–**154** displayed an obvious antibacterial effect on *H. pylori* with the MIC values ranging 4.0–32.0 μg/mL. Fonsecinone A (**155**) and asperpyrone C (**156**) were separated from the fungus *A. welwitschiae* CUGBMF180262 (Han et al., 2022). Compounds **155** and **156** showed moderate antibacterial activities against *H. pylori* with the same MIC value of 16 μg/mL. Three novel prenylxanthone derivatives, aspergixanthones I–K (**157**–**159**), and four known analogss aspergixanthone A (**160**), 15-acetyl tajixanthone hydrate (**161**), tajixanthone hydrate (**162**), and 16-chlorotajixanthone (**163**), were originated from the fungus *Aspergillus* sp. ZA-01 (Zhu et al., 2018). Compounds **157**–**163** displayed anti-*Vibrio* activities to three pathogenic *Vibrio* spp. (*V. parahemolyticus*, *V. anguillarum*, and *V. alginolyticus*), with the MIC values between 1.56 and 25.0 μM. Among them, **157** exhibited significant anti-*Vibrio* activity, suggesting that the propenyl group at C-20 with α-stereoconfiguration might be crucial for the anti-*Vibrio* activity. Homodimeric tetrahydroxanthone secalonic acid D (**164**) was isolated from *A. aculeatinus* WHUF0198 and **164** performed activities against *H. pylori* G27, *H. pylori* 26,695, *H. pylori* 129, *H. pylori* 159, *S. aureus* USA300, and *B. subtilis* 168 with MIC values of 4.0, 4.0, 2.0, 2.0, 2.0, and 1.0 μg/mL, respectively (Wu et al., 2023). A new tetrahydroxanthone dimer, 5-epi-asperdichrome (**165**), was originated from the mangrove-associated fungus *A. versicolor* HDN1009 (Yu et al., 2018). Compound **165** exhibited weak activity against four tested bacterial strains (*V. parahemolyticus*, *B. subtilis*, *M. phlei*, and *P. aeruginosa*), with the MIC values ranging 100.0–200.0 μg/mL. Two new heterodimeric tetrahydroxanthones, aflaxanthones A (**166**) and B (**167**), were separated from mangrove-associated fungus *A. flavus* QQYZ (Zang et al., 2022). Compound **166** possessed a moderate inhibitory effect on MRSA (MIC, 12.5 μM), and compounds **166** and **167** showed a weak inhibitory effect on *B. subtilis* with the same MIC value of 25 μM. A new sterigmatocystin, 5-methoxydihydrosterigmatocystin (**168**), was originated from the sponge-associated fungus *A. versicolor* MF359 (Song et al., 2014). Compound **168** exhibited a significant antibacterial effect against *B. subtilis* (MIC, 3.125 μg/mL) and *S. aureus* (MIC, 12.5 μg/mL). Oxisterigmatocystin C (**169**) was separated from the fungus *Aspergillus* sp. F40 (Tian et al., 2018). Compound **169** displayed

weak antibacterial activity against *S. aureus* (MIC, 48.0 μg/mL). Sterigmatocystin (**170**) originated from a sponge-derived fungus *A. sydowii* DC08 (Handayani et al., 2022). Compound **170** showed activities against MRSA, Multidrug-resistant *P. aeruginosa* (MDRPA), *E. coli*, *S. aureus*, and *P. aeruginosa* with the MIC values of 64.0, 128.0, 16.0, 32.0, and 32.0 μg/mL, respectively. Two new anthrone derivatives, 2-hydroxy-6-formyl-vertixanthone (**171**) and 12-*O*-acetyl-sydowinin A (**172**), together with two known analogs aspergillusone A (**173**) and AGI-B4 (**174**), were originated from the fungus *A. sydowii* C1-S01-A7 (Wang et al., 2019). Compounds **171**–**174** showed weak activities to MRSA with the MIC values ranging 15.0–32.0 μg/mL. A new xanthone, isosecosterigmatocystin (**175**) was separated from the fungus *A. nidulans* MA-143 (Yang et al., 2018a). Compound **175** showed weak activity against *E. ictaluri* (MIC, 16.0 μg/mL). A new citrinin dimer, *seco*-penicitrinol A (**176**), was separated from the algal-associated fungal *A. sydowii* EN-534 (Yang et al., 2018b). Compound **176** showed weak

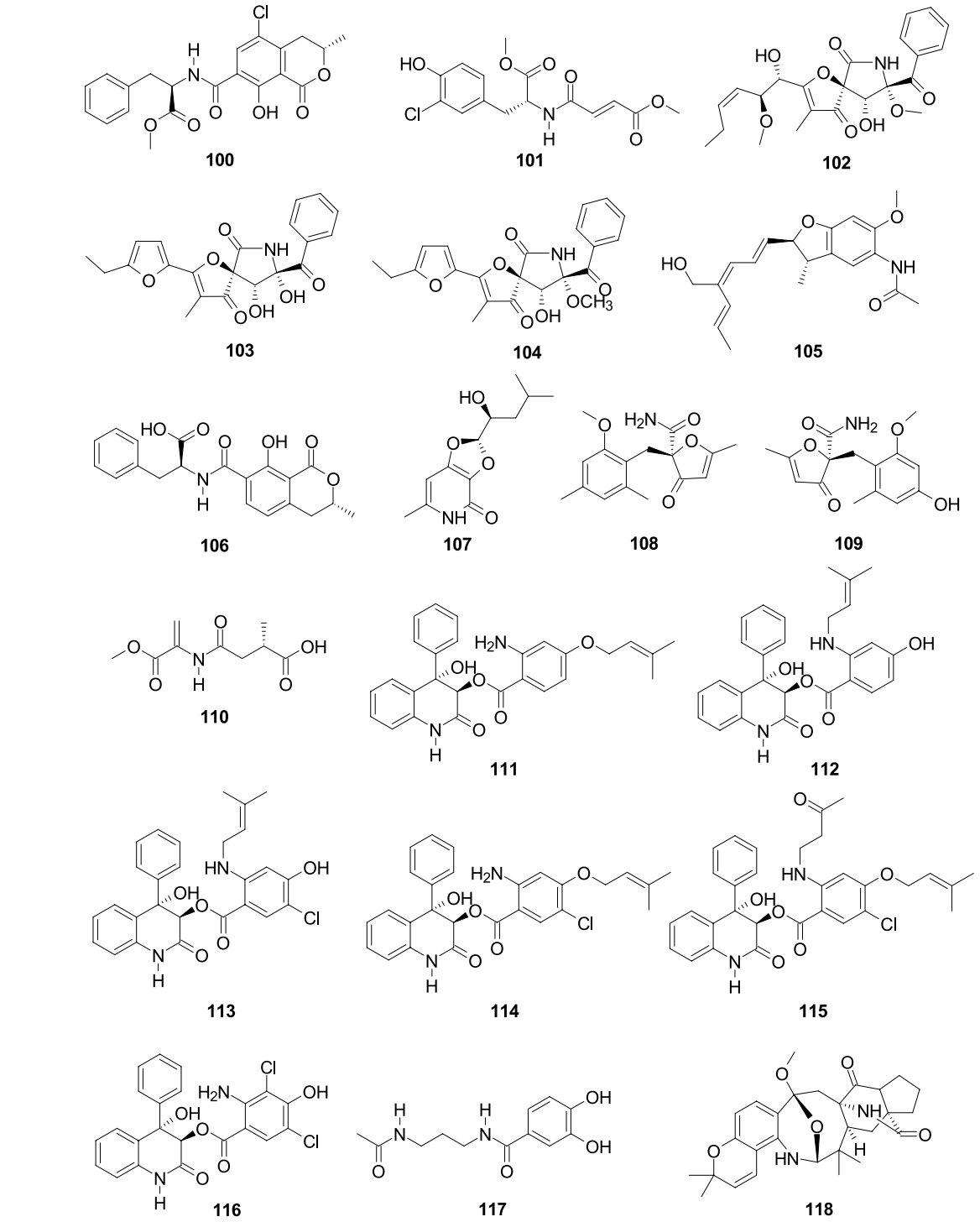

FIGURE 8 (Continued)

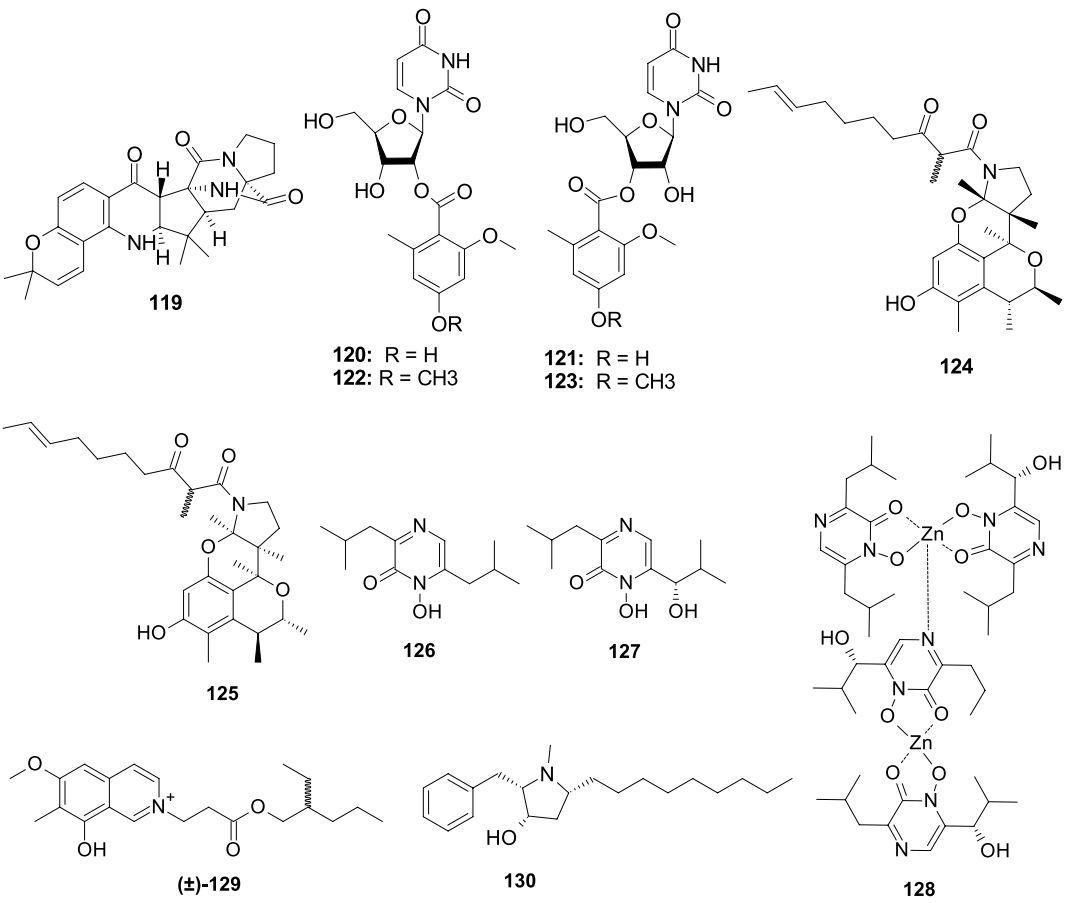

FIGURE 8
Chemical structures of other nitrogen-containing antibacterial metabolites **100**–**130** from *Aspergillus* spp.

inhibitory activity against four bacterial strains (*M. luteus*, *E. ictaluri*, *V. alginolyticus*, and *V. c*), with the MIC values ranging 16.0–32.0 μg/mL. Secalonic acid F1 (**177**), secalonic acid H (**178**), penicillixanthone A (**179**), and chrysoxanthone C (**180**) showed weak antibacterial activity against *S. aureus* with the MIC values 25.0, 50.0, 6.25, and 50.0 μg/mL, respectively, which were separated from the fungus *A. brunneoviolaceus* MF180246 (Xu et al., 2024). A new chlorinated biphenyl, aspergetherin A (**181**), displayed weak activity against MRSA 05–72 and MRSA USA300, with the same MIC value of 128.0 μg/mL, which was separated from the sponge-associated fungus *A. terreus* 164,018 (Li J. X. et al., 2023) (Figure 10).

2.3.3 Lactones

Vioxanthin (**182**) showed significant antibacterial effect on *E. faecalis* ATCC29212, *E. faecalis* (VRE) B3/101, *S. aureus* ATCC29213, and *S. aureus* (MRSA) 66/1 with the MIC values 2.0, 1.0, 2.0 and 0.5, respectively, which was separated from the sponge-associated fungus *A. elegans* KUFA0015 (Kumla et al., 2021). Two new prenylated phenylbutyrolactones, aspulvinones R–S (**185**–**186**), together with two known compounds aspulvinones B′ (**183**) and H (**184**) were separated from the fungus *Aspergillus flavipes* KUFA1152 (Machado et al., 2021). Compounds **183**–**186** displayed strong activities against *E. faecalis* and *S. aureus* with the MIC values ranging 8.0–16.0 μg/mL. Asperteretal E (**187**) and aspernolide A (**188**) were originated from the fungus *A. terreus* SCSIO FZQ028 (Zeng et al., 2020b), and they showed moderate antimicrobial activities against *S. aureus* ATCC 29213 and *Bacillus thuringiensis* ATCC 10792, with inhibitory diameters from 7.49 to 8.94 mm at 30 μg/disk, respectively. Butyrolactone I (**189**) displayed significant antibacterial against *S. aureus* with the MIC value of 0.78 μg/mL, which was collected from the fungus *Aspergillus* sp. SCSIO 41029 (Chen et al., 2021). A new aromatic butanolide, asperbutenolide D (**190**), along with two known analogs (+)-3′,3′-di-(dimethylallyl)-butyrolactone II (**191**) and aspernolide E (**192**), displayed moderate antibacterial against *S. aureus* with the MIC values of 21.3, 17.4, and 26.1 μM, respectively, which were separated from sediment-associated fungus *A. terreus* SCAU011 (Bao et al., 2021). A novel butyrolactone derivative, flavipesin A (**193**), demonstrated obvious antibacterial activities against *S. aureus* (MIC, 8.0 μg/mL) and *B. subtillis* (MIC, 0.25 μg/mL), and the fungus was separated from the mangrove-associated fungus *A. flavipes* AIL8 (Bai et al., 2014). Versicolactone B (**194**) and butyrolactone VI (**195**) were separated from the coral-derived fungus *A. terreus* SCSIO41404 (Peng et al., 2022). Compound **194** demonstrated weak antibacterial against *E. faecalis* (MIC, 5 μg/mL). Compound **195** demonstrated weak antibacterial against *K. pneumoniae* (MIC, 50 μg/mL). A novel aromatic butanolide, asperbutenolide A (**196**), with strong inhibition activity against *S. aureus* (MIC, 1.30 μg/mL) and *V. splendidus* (MIC, 3.70 μg/mL), was separated from the mangrove sediment-derived fungus *A. terreus* SCAU011 (Bao et al., 2020). 5*R*-(+)-9-hydroxymicroperfuranone (**197**) and 5*R*-(+)-microperfuranone

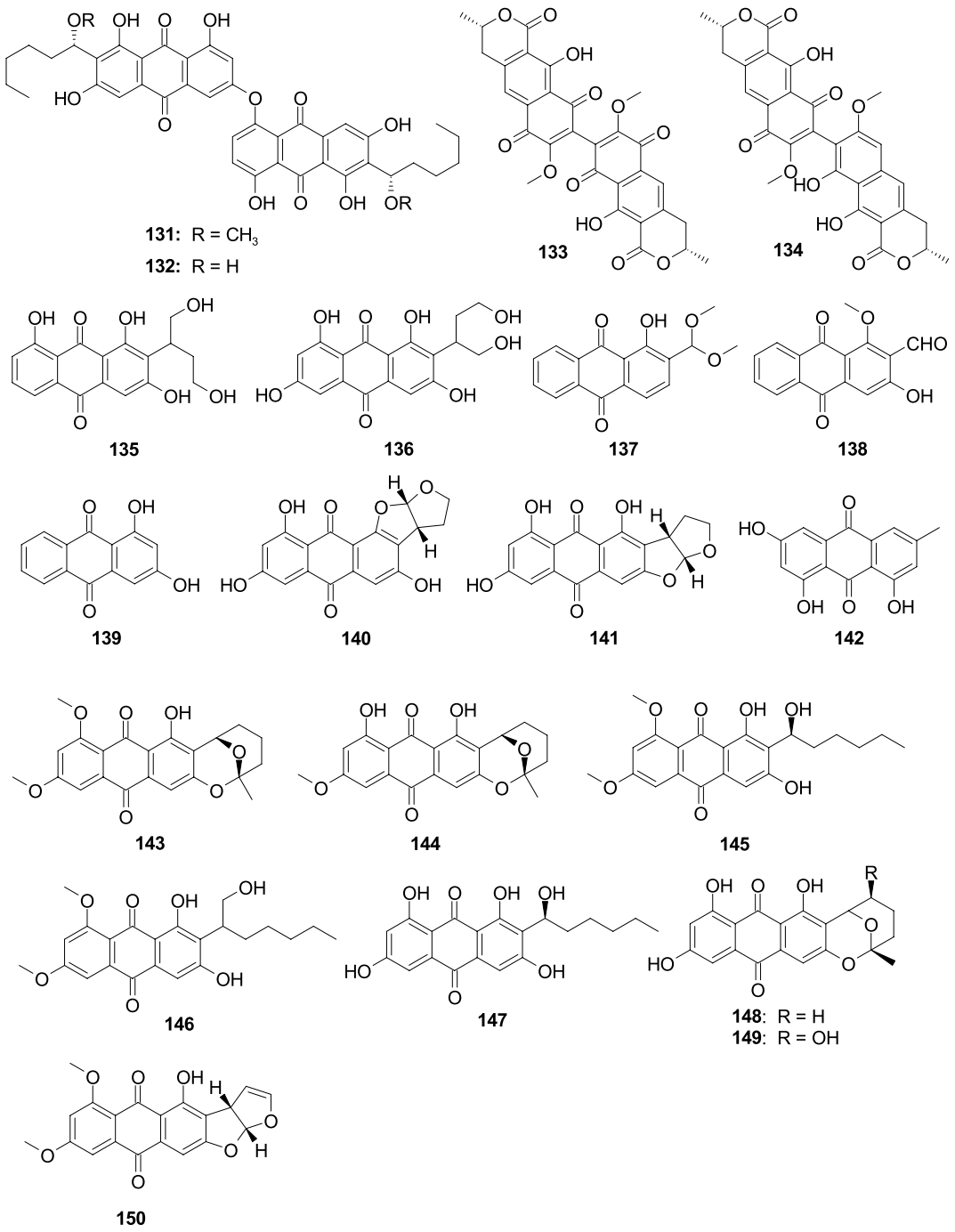

FIGURE 9
Chemical structures of antibacterial anthraquinones **131**–**150** from *Aspergillus* spp.

(**198**), with weak inhibition activity against *E. coli* with the MIC values of 50 and 25 μg/mL, respectively, which were separated the fungus *Aspergillus* sp. ZZ1861 (Ha et al., 2024). Two new benzyl pyrones, asperpyranones A–B (**199**–**200**), exhibited weak antibacterial against *P. aeruginosa* ATCC 27853 with the MIC values of 32 and 128 μg/mL, respectively, which were separated from a marine-derived fungus *A. terreus* RA2905 (Wu et al., 2020b). Nectriapyrone (**201**) and asperisocoumarin A (**202**), displayed a weak antibacterial effect on *V. harveyi* with MIC values of 64.0 and 32.0 μg/mL, respectively, which were separated from the fungus *Aspergillus* sp. LS53 (Zhang L. et al., 2020; Zhang Y. H. et al., 2020). Unguinol (**203**), 2-chlorounguinol (**204**), and nidulin (**205**) showed strong antibacterial activity against *E. coli*, *P. aeruginosa*, *S. aureus*, *E. faecalis*, *B. subtilis*, *Salmonella. typosa*, *Vibrio cholera* Inaba, and *M. luteus*, with MIC values ranging 0.78–3.12 μg/disk, which were separated from the fungus *Aspergillus unguis* WR8 (Handayani et al., 2020). One novel depsidone derivative, aspergillusidone H (**206**), together with three known compounds nornidulin (**207**), aspergillusidones B (**208**), and C (**209**), were separated from the fungus *A. unguis* GXIMD02505 (Zhang Y. T. et al., 2022). Compounds **207** and **209** had antibacterial activity against

MRSA, *Mylabris variabilis*, and *Methanocaldococcus jannaschii*, with MIC values from 2 to 32 μg/mL. Compound **208** displayed antibacterial activity against *M. variabilis* (MIC, 128 μg/mL). One new depsidone 7-dechloronidulin (**210**), together with two known compounds 2,4-dichlorounguinol (**211**) and emeguisin B (**212**) were separated from the fungus *A. unguis* GXIMD02505 (Thi et al., 2023).

Compound **210** was selectively bioactive on three Gram-positive bacteria (*B. cereus*, *E. faecalis*, *S. aureus*) (MICs: 2–4 μg/mL). Compound **211** had broad-spectrum antimicrobial activity against six bacteria (*B. cereus*, *E. faecalis*, *S. aureus*, *E. coli*, *P. aeruginosa*, and *S. enterica*), with the MIC values ranging 16–64 μg/mL. Compound **212** showed weak activity against *E. faecalis* with the MIC value of

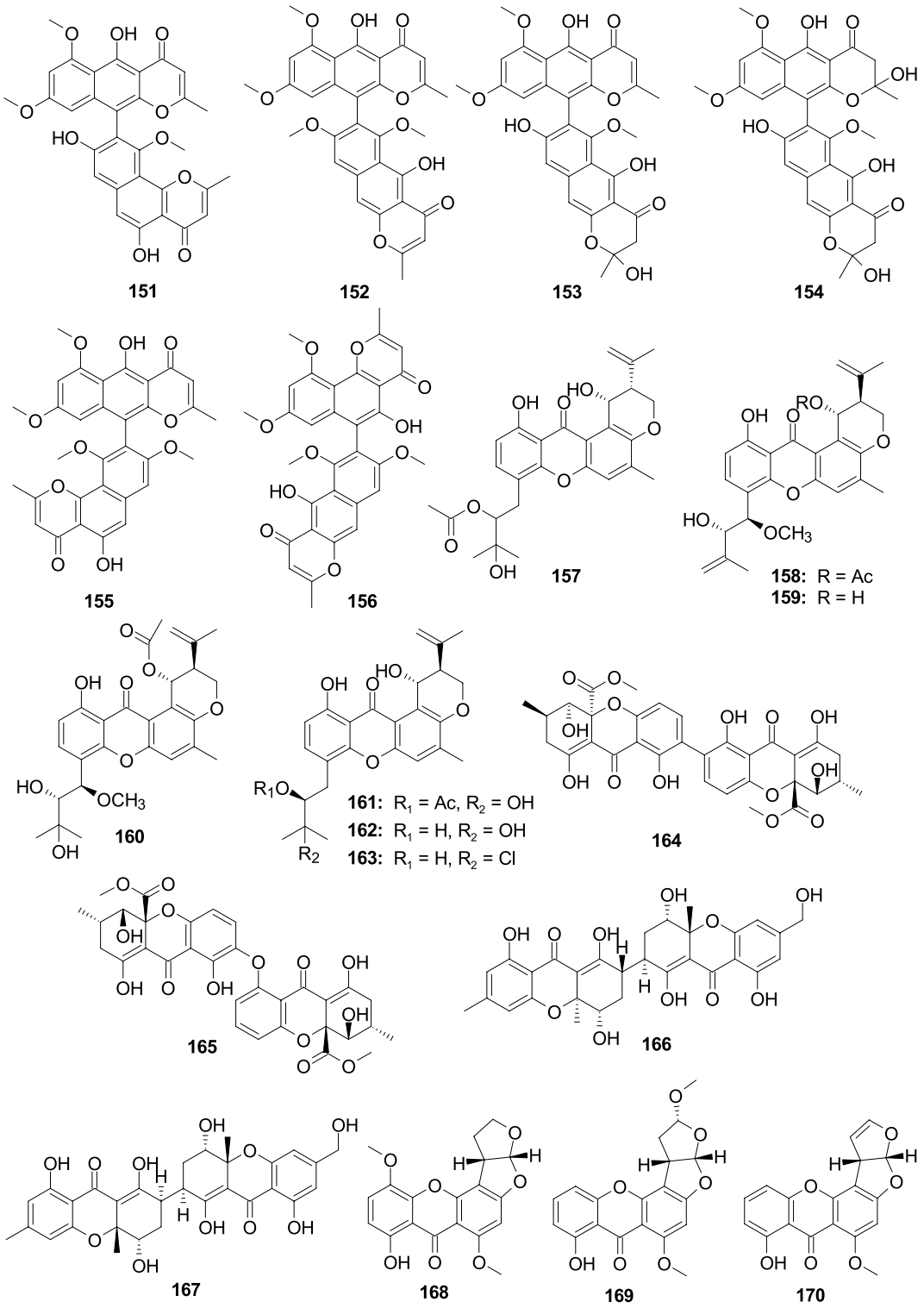

FIGURE 10 (Continued)

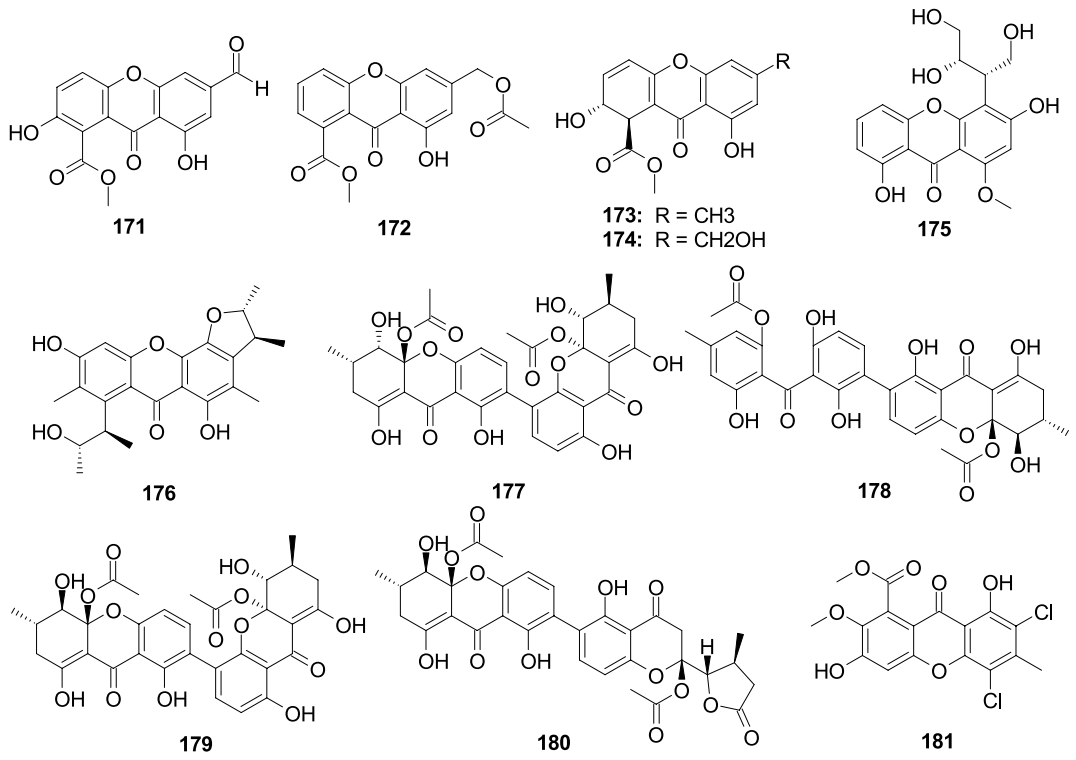

FIGURE 10
Chemical structures of antibacterial xanthones **151**–**181** from *Aspergillus* spp.

256 μg/mL. One new depsidone asperunguissidone A (**213**), one new phthalide asperunguislide A (**214**), and six known compounds asperlide (**215**), aspergiside C (**216**), (3*S*)-3-ethyl-5,7-dihydroxy-3,6-dimethylphthalide (**217**), aspergisidone (**218**), folipastatin (**219**), emeguisins A (**220**), were separated from the fungus *A. unguis* PSU-MF16 (Saetang et al., 2021). Compounds **213**–**220** showed activity against *S. aureus* and MRSA with the MIC values from 1.0 to 200.0 μg/mL. 8-Demethoxy-10-methoxy-wentiquinone C (**221**) was separated from the fungus *A. sydowii* C1-S01-A7, and showed a weak antibacterial activity against MRSA with an MIC value of 32.4 μg/mL (Wang et al., 2019). Three new farnesylated phthalide derivatives farnesylemefuranones D–F (**222**–**224**) were isolated from the cold-seep-derived fungus *A. insuetus* SD-512, and they exhibited inhibitory effects against *V. vulnificus* with the same MIC value of 4.0 μg/mL, while **221** and **223** also inhibited *V. alginolyticus* with the same MIC value of 4.0 μg/mL (Chi et al., 2020). Silvaticol (**225**) was separated from the fungus *Aspergillus* sp. ZZ1861, and **225** displayed inhibitory activity against *E. coli* with the MIC value of 12.5 μg/mL (Ha et al., 2024). Two novel dihydroisocoumarin derivatives, aspergillumarins A (**226**) and B (**227**), were separated from the marine-associated fungus *Aspergillus* sp. (Li et al., 2012). Compounds **226** and **227** demonstrated weak antibacterial against *S. aureus* and *B. subtilis* at a concentration of 50 μg/mL. A new dihydroisocoumarin, aspergimarin G (**228**), was separated from the sponge-associated fungus *Aspergillus* sp. NBUF87 (Lin S. X. et al., 2023), and showed a moderate activity against *S. aureus* and *S. enteritidis* with MIC values from 16.0 to 64.0 μg/mL. (*R*)-3-Hydroxymellein (**229**) and (3*R*,4*S*)-trans-4-hydroxymellein (**230**) were separated from the fungus *Aspergillus* sp. SCSCIO41405 (Peng et al., 2021). Compound **229** demonstrated a weak antibacterial effect on MRSA (MIC, 100.0 μg/mL). Compound **230** displayed a weak antibacterial effect on *E. faecalis* (MIC, 100.0 μg/mL). Three new 4-hydroxy-α-pyrones nipyrones A–C (**231**–**233**) and one known analog germicidin C (**234**) were separated from the sponge-associated fungus *A. niger* LS24 (Ding et al., 2019). Compound **233** demonstrated a significant inhibitory effect on *S. aureus* and *B. subtilis* with the MIC values of 8.0 and 16.0 μg/mL, respectively. Sartorypyrone A (**235**) was separated from the fungus *Aspergillus* sp. WHUF03110 and displayed a strong inhibitory activity against *B. subtilis*, *S. aureus* ATCC25923, *S. aureus* NEWMAN, *S. aureus* USA300, and *S. aureus* NRS 271 with MIC values ranging 1.0–2.0 μg/mL (Lv et al., 2021). Asperochrin A (**236**), chlorohydroaspyrones A (**237**) and B (**238**), were separated from the mangrove-associated fungus *spergillus ochraceus* MA-15 (Liu et al., 2015). Compound **236** showed an inhibitory activity against *A. hydrophila*, *V. anguillarum*, and *V. harveyi* with the MIC values of 8.0, 16.0, and 8.0 μg/mL, respectively. **237** and **238** showed weak inhibitory activity against the above three pathogenic bacterial (MIC, 16–32 μg/mL). One novel penicillide analog, $\Delta^{2'}$-1′-dehydropenicillide (**239**) and a known analog dehydropenicillide (**240**), were separated from the fungus *Aspergillus* sp. IMCASMFI80035 (Song F. H. et al., 2021), which demonstrated significant antibacterial activities against *H. pylori* (MIC, 21.73 and 21.61 μM, respectively) (Figure 11).

2.3.4 Other polyketide metabolites

The novel compound aspergiloxathene A (**241**), separated from the marine-associated fungus *Aspergillus* sp. IMCASMF180035, exhibited significant antibacterial activities against *S. aureus* (MIC, 5.60 μM) and MRSA (MIC, 22.40 μM) (Song F. H. et al., 2021). A new

compound, cowabenzophenone A (**242**), was separated from the mangrove-associated fungus *A. terreus* (Ukwatta et al., 2020). Compound **242** showed strong antibacterial activity against *B. subtilis* (MIC, 1.0 μg/mL) and *S. aureus* (MIC, 2.0 μg/mL). Penicitrinone A (**243**), penicitrinone *F* (**244**), and citrinin (**245**) showed weak activity against *E. ictaluri* and *V. alginolyticus* with the MIC values from 16.0 to 32.0 μg/mL, were separated from the fungal *A. sydowii* EN-534 (Yang et al., 2018b). Two new compounds 25*S*-*O*-methylarugosin A (**246**), 25*R*-*O*-methylarugosin A (**247**) were separated from the fungus *Aspergillus* sp. ZZ1861 (Ha et al., 2024). Compound **247** showed weak activities against MRSA (MIC, 50.0 μg/mL). The new compound 12*S*-aspertetranone D (**248**), separated from sea

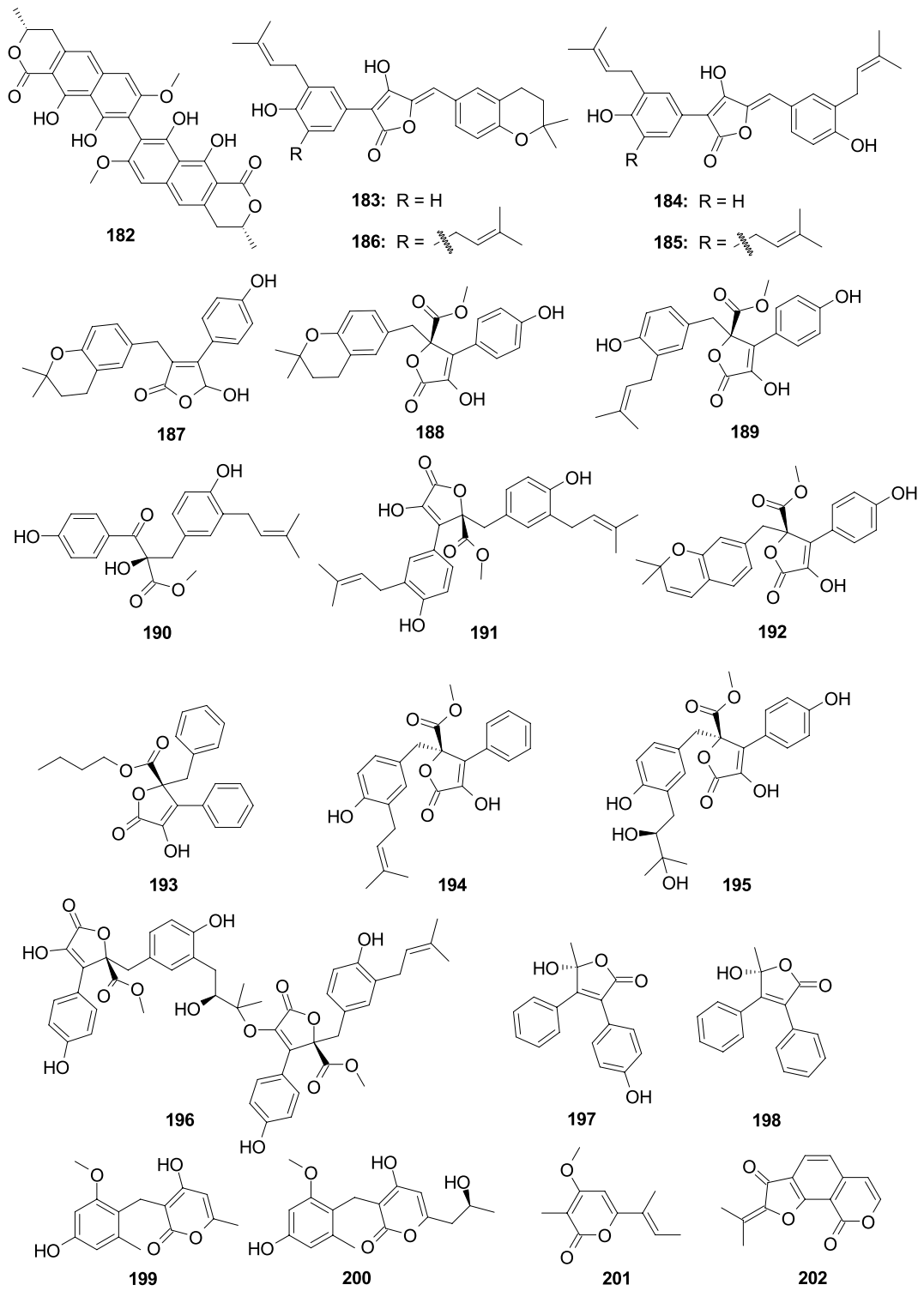

FIGURE 11 (Continued)

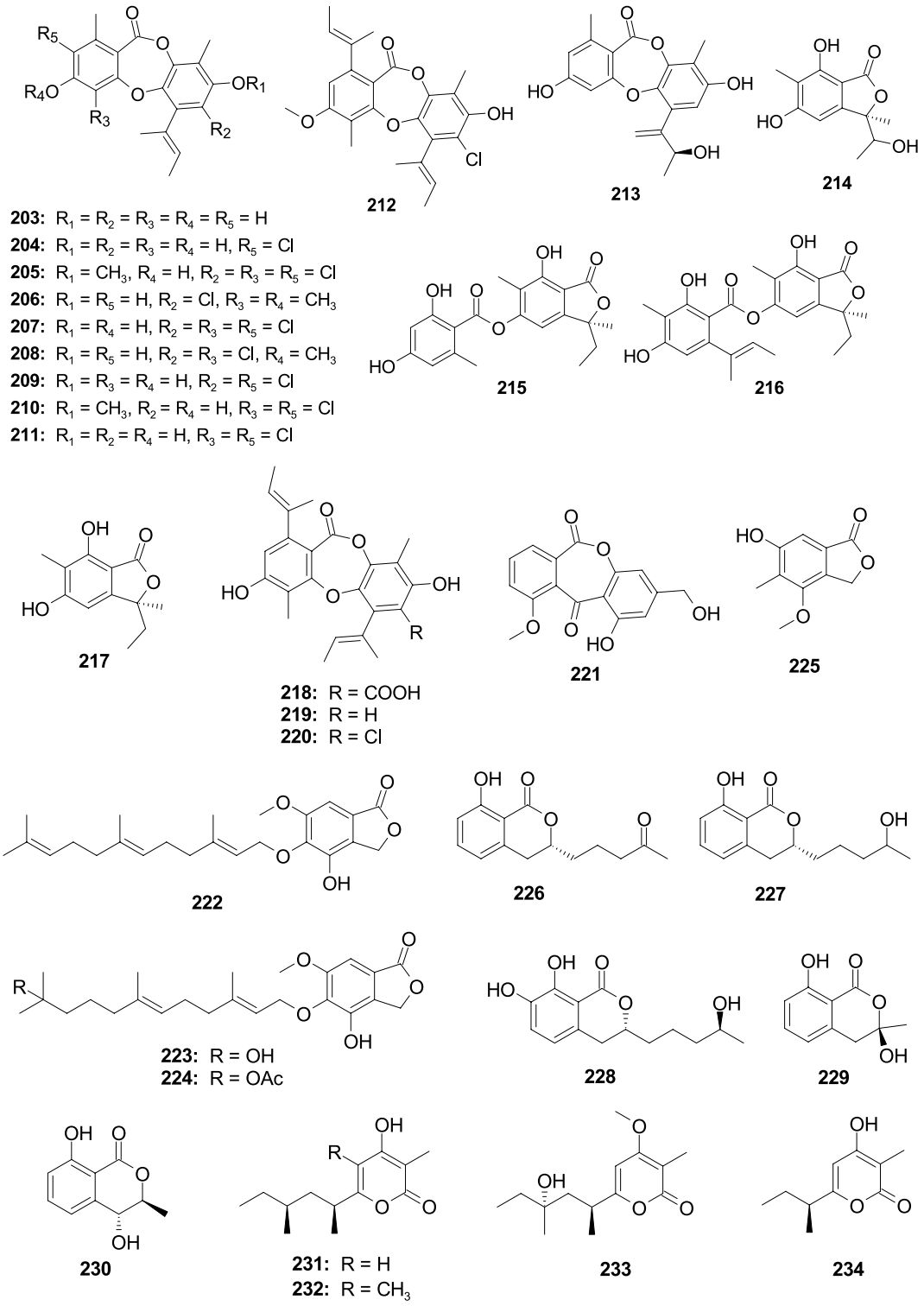

FIGURE 11 (Continued)

trench-derived fungus *Aspergillus* sp. SY2601 (Sun et al., 2024), exhibited antibacterial effects on MRSA and *E. coli* with the MIC values of 3.75 and 5.0 μg/mL, respectively. Four new anthraquinone derivatives, (10*S*,12*S*)-chevalierone, (10*S*,12*R*)-chevalierone, (10*R*,12*S*)-chevalierone, and (10*R*,12*R*)-chevalierone (**249**–**252**), were isolated from the fungus *A. chevalieri* HP-5 (Wang Q. Y. et al., 2022). Compounds **250**–**252** showed significant inhibition against the opportunistic pathogenic bacterium *P. aeruginosa* (inhibition rate: 81.0–91.5%) and MRSA (inhibition rate: 74.0–88.5%) at the concentration of 200 μM, while the structural congener compound **249** only showed weak inhibition (inhibition rate: 38.2%) against the *P. aeruginosa* at 200 μM. Two novel phenome compounds,

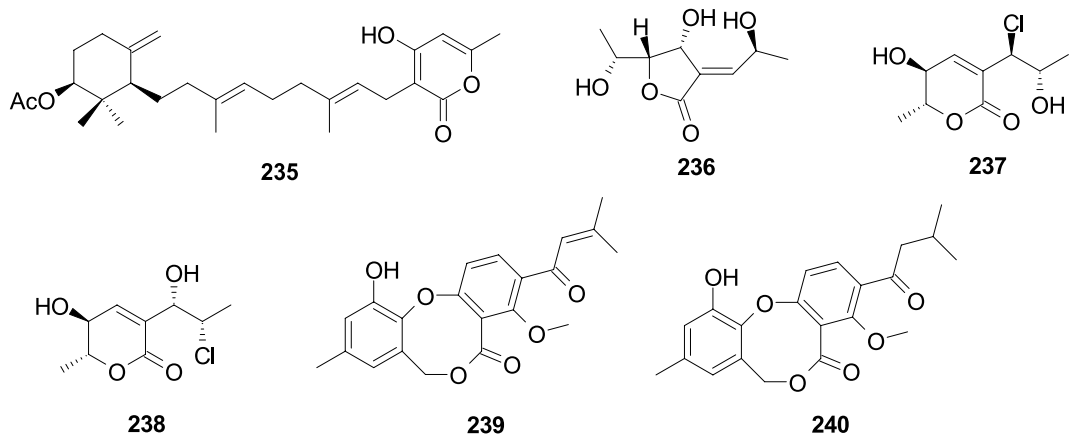

FIGURE 11
Chemical structures of antibacterial lactones **182**–**240** from *Aspergillus* spp.

asperphenones A (**253**) and B (**254**), were separated from the mangrove-derived fungus *Aspergillus* sp. YHZ-1 (Guo et al., 2018). Compounds **253** and **254** demonstrated weak antibacterial effects on four Gram-positive bacteria, *S. aureus*, *S. pyogenes*, *B. subtilis*, and *M. luteus*, with the MIC values from 32.0 to 64.0 μg/mL. One new compound penibenzophenone E (**255**) and a known compound sulochrin (**256**) were originated from the fungus *A. fumigatus* H22 (Zhang R. et al., 2022). Compounds **255** and **256** demonstrated activity against MRSA with the same MIC value of 1.25 μM. Aspergisides A–B (**257**–**258**), together with agonodepsides A–B (**259**–**260**), were separated from sponge-derived fungus *A. unguis* PSU-MF16 (Saetang et al., 2021). Compounds **257**, **259**, and **260** had strong antibacterial activity against *S. aureus* and MRSA with the MIC values from 2.0 to 16.0 μg/mL. Compound **258** displayed a weak activity against *S. aureus* and MRSA with the same MIC value of 200.0 μg/mL. Guisinol (**261**) was separated from the fungus *A. unguis* GXIMD 02505 (Zhang Y. T. et al., 2022). Compound **261** showed antibacterial activities against MRSA (MIC, 16.0 μg/mL) and *M. var**iabilis* (MIC, 64.0 μg/mL). Two new phenolic polyketides, unguidepside C (**262**) and agonodepside C (**263**), were isolated from two marine-associated fungal strains of *A. unguis* (Anh et al., 2022). Compounds **262** and **263** demonstrated inhibitory effects against *S. aureus*, *M. luteus*, and *B. subtilis*, with the MIC values from 8.0 to 22.1 μM. One new chromone, aspergilluone A (**264**), was separated from the fungus *Aspergillus* sp. LS57, which displayed an antibacterial effect on *M. tuberculosis* (MIC, 32.0 μg/mL) and *S. aureus* (MIC, 64.0 μg/mL) (Liu et al., 2021). Phomaligol A (**265**), separated from the fungus *A. flavus* MFA500, displayed a weak activity against *S. aureus* with MIC value of 31.2 μg/mL (Yang et al., 2011). Trypacidin (**266**) showed significant antitubercular activity with the MIC value of 1.25 μg/mL, which was separated from the fungus *A. fumigatus* MF029 (Song Z. J. et al., 2021). (+)-Geodin (**267**) and chlorotrypacidin (**268**) showed a weak antibacterial effect on *Staphylococcus albus*, *S. aureus*, and *V. anguillarum* with the same MIC value of 25.0 μM, and they were separated from the fungi of *A. versicolor* TA01-14 (Zhang et al., 2019). Eugenitol (**269**) demonstrated weak inhibitory activity against MRSA with the MIC value of 485.4 μM, which was separated from the mangrove sediment-associated fungus *Aspergillus* sp. SCSIO41407 (Cai et al., 2021) (Figure 12).

2.4 Steroids

Steroids were biosynthesized through complex cyclization reactions involving squalene and mevalonate pathways. A total of 18 antibacterial steroids (including 11 new compounds) were identified from marine-derived *Aspergillus* species. The steroid structures and the absolute configurations of the new compounds were elucidated by a detailed spectroscopic analysis of NMR and MS data, optical rotatory dispersion, ECD calculations, and single-crystal X-ray diffraction.

A new steroid 7*β*,8*β*-Epoxy-(22*E*,24*R*)-24-methylcholesta-4,22-diene-3,6-dione (**270**) and a known steroid ergosta-4,6,8(14),22-tetraene-3-one (**271**) were separated from the fungus *Aspergillus penicillioides* SD-311 (Chi et al., 2021b). Compound **270** showed antibacterial activity against *V. anguillarum* with the MIC value of 32.0 μg/mL, while **271** displayed inhibitory activity against *E. tarda* and *M. luteus* with the same MIC value of 16.0 μg/mL. One new ergosterol derivative, isocyathisterol (**272**), exhibited a weak antibacterial activity against *E. coli* and *S. aureus*, with inhibitory diameters of 6.7 and 5.7 mm at 30 μg/disk, respectively, was originated from the alga-derived fungus *A. ustus cf*-42 (Liu et al., 2014). One new oxygenated steroid, aspersteroid A (**273**), was isolated from the marine-derived fungus *A. flavus* YJ07-1 (Yang M. Y. et al., 2018). Compound **273** showed antibacterial activities against *V. anguillarum*, *V. parahemolyticus*, and *V. alginolyticus* with the same MIC value of 12.5 μM. One new oxygenated ergostane-type steroid, 3*β*-hydroxy-5*α*,6*β*-methoxyergosta-7,22-dien-15-one (**274**), was isolated from the marine sponge-derived fungus *Aspergillus* sp. NR151817 (Wen et al., 2024). Compound **274** showed weak inhibitory activity against *S. aureus* with an MIC value of 64 μg/mL. A known steroid C-21 acid helvolic acid (**275**) was isolated from the fungus *Aspergillus* sp. SCS-KFD66 (An et al., 2018). Compound **275** exhibited strong activity against *S. aureus* ATCC 6538 with an MIC value of 2.0 μg/mL. Three new helvolic acid derivatives, 16-*O*-propionyl-16-*O*-deacetylhelvolic acid (**276**), 6-*O*-propionyl-6-*O*-deacetylhelvolic acid (**277**), and 24-epi-6*β*,16*β*-diacetoxy-25-hydroxy-3,7-dioxo-29-nordammara-1,17(20)-diene-21,24-lactone (**278**), were isolated from the marine-derived fungus *A. fumigatus* HNMF0047 (Kong et al., 2018). Compounds **276**–**278** showed antibacterial activities against

10.3389/fmicb.2024.1464135

Streptococcus agalactiae and *S. aureus* with MIC values ranging 2.0–64.0 μg/mL. A new steroid 3,7-diketo-cephalosporin P_1 (**279**), along with a known analog 22-*O*-acetylisocyclocitrinol A (**280**), were isolated from deep sea-derived fungus *A. fumigatus* SCSIO 41012 (Limbadri et al., 2018). Compound **279** showed weak activity against *A. baumanii* 19,606 with the MIC value of 50.0 μg/mL. Compound **280** exhibited high antibacterial activity with *A. baumanii* ATCC15122 and *K. pneumonia* ATCC14578 with the MIC values of 12.5 and 3.12 μg/mL, respectively. Fusidic acid (**281**) and neocyclocitrinol D (**282**) were obtained from the marine-derived fungus *A. flavus* JK07-1

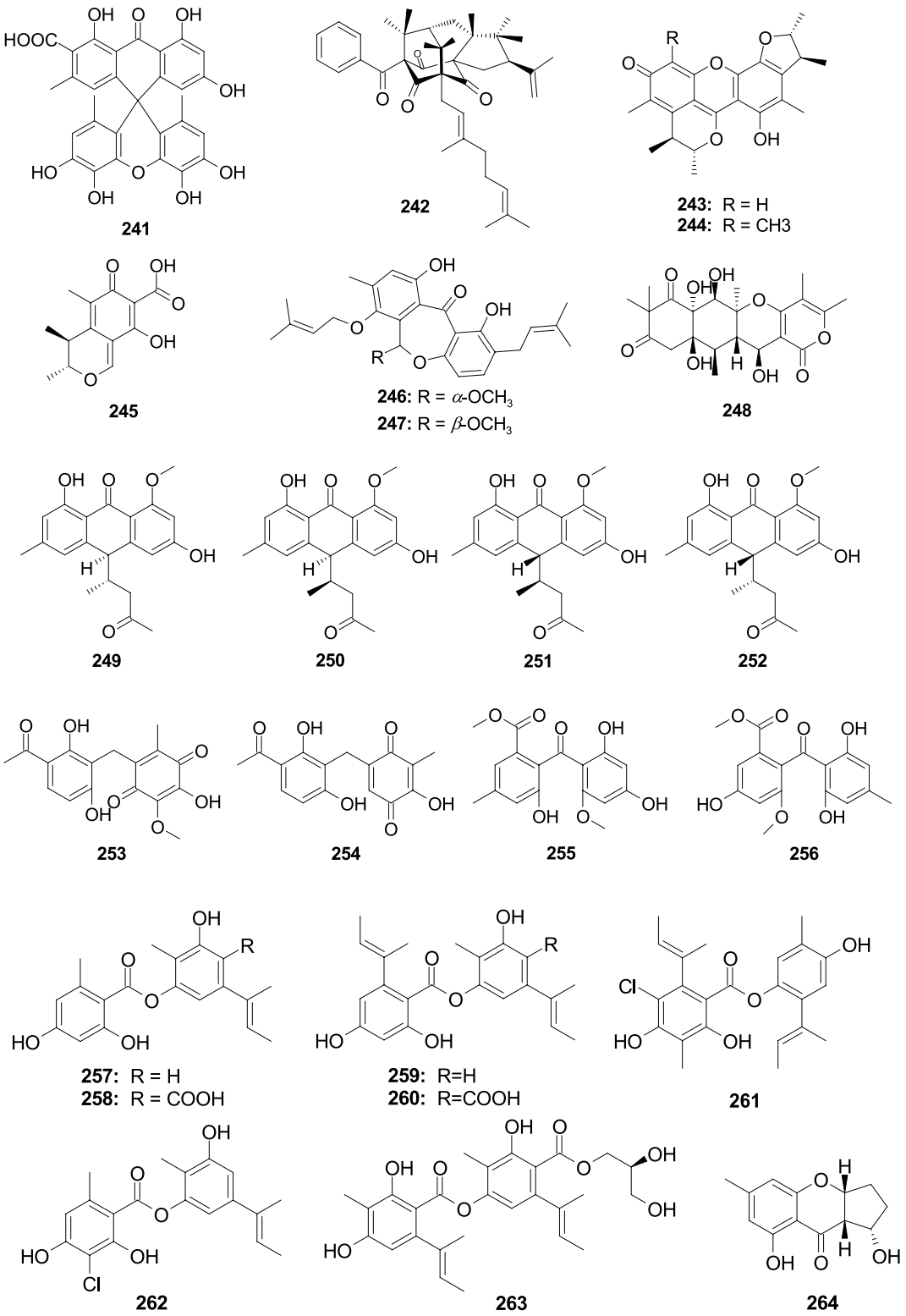

FIGURE 12 (Continued)

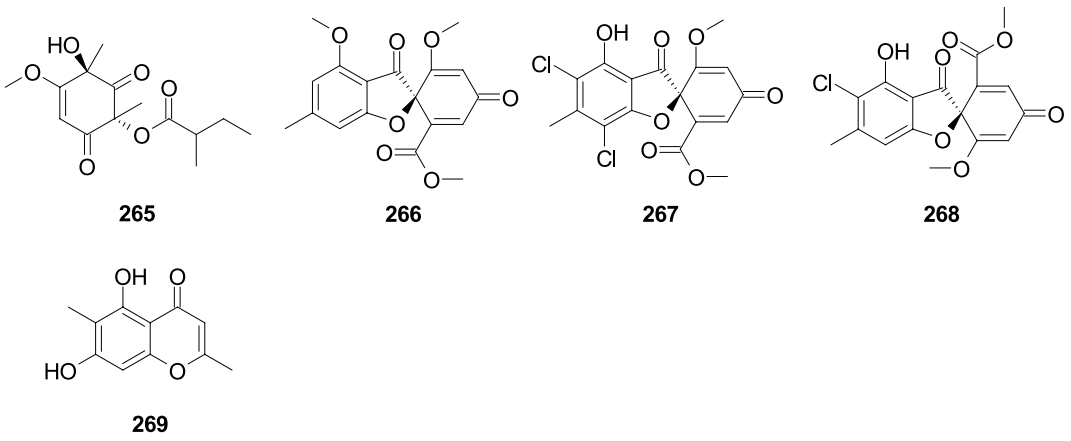

FIGURE 12
Chemical structures of other antibacterial polyketide metabolites **241**–**269** from *Aspergillus* spp.

(Ren et al., 2020). Compound **281** showed significant inhibitory activities against *Micrococcus lysodeikticus*, *B. cereus*, *Bacillus megaterium*, *Bacillus Anthracis*, and *Salmonella typhi*, with the MIC values of 0.07, 0.07, 0.07, 0.30, and 0.60 μM, respectively. Compound **282** showed effective inhibitory activity against *M. lysodeikticus* with an MIC value of 1.30 μM. A new C-23 steroid with bicyclo[4.4.1]A/B ring aspergillsteroid A (**283**) and a known analog neocyclocitrinol B (**284**) exhibited antibacterial activity against *V. harveyi* KP635244 with the MIC values of 16.0 and 128.0 μg/mL, respectively, which were separated from marine-derived fungus *Aspergillus* sp. LS116 (Xu P. et al., 2020). Demethylincisterol A_2 (**285**) was separated from the coral-derived fungus *A. hiratsukae* SCSIO $5Bn_1003$ (Zeng et al., 2022a). Compound **285** displayed strong activity against *B. subtilis* with the MIC value of 10.26 μg/mL. Two new polyhydroxylated mycoecdysteroids, punicesterones B (**286**) and C (**287**), were separated from the deep-sea-derived fungus *A. puniceus* SCSIO z021 (Huang et al., 2023). Compounds **286** and **287** could show significantly inhibitory activity against *S. iniae*, *S. agalactiae*, *E. coli*, *B. subtilis*, and *S. aureus* at a concentration of 0.132 mM (Figure 13).

2.5 Other classes

Additionally, there were also some other classes of antibacterial secondary metabolites isolated from *Aspergillus* spp., including fatty acids, glycosides, and benzene derivatives. A total of 50 antibacterial compounds (including 14 new compounds) were isolated from the *Aspergillus* spp. The structures, like three undescribed compounds, carnemycins H−I and stromemycin B, were elucidated by comprehensive spectroscopic data and *J*-based configurational analysis.

A new phenyl ether derivative, 3-hydroxy-5-(3-hydroxy-5-methylphenoxy)-4-methoxybenzoic acid (**288**), together with two known analogs 3,4-dihydroxy-5-(3-hydroxy-5-methylphenoxy)benzoic acid (**289**) and 3-hydroxy-5-(3-hydroxy-5-methylphenoxy)-benzoic acid (**290**), were separated from the marine-derived fungus *A. carneus* (Xu et al., 2017). Compounds **288**–**290** had weak activity against *S. aureus*, *V. anguillarum*, and *E. coli* with the same MIC value of 25 μM. A new compound aspergetherin C (**291**) and two known analogs, methyl 3,5-dichloroasterric acid (**292**) and methyl chloroasterrate (**293**), were isolated from the fungus *A. terreus* 164,018 (Li J. X. et al., 2023). Compounds **291** and **293** showed weak antibacterial activity against MRSA 05–72 and MRSA USA300 (MIC, 64.0 μg/mL). Compound **292** had strong inhibitory activity against MRSA 05–72 with the MIC value of 1.0 μg/mL. Dimethyl 2,3′-dimethylosoate (**294**) was isolated from *A. fumigatus* H22 (Zhang R. et al., 2022). Compound **294** showed strong inhibitory activity against MRSA with the same MIC value of 5.0 μM. 4-Methoxycarbonyldiorcinol (**295**), showed strong inhibitory activity against *P. aeruginosa* with the MIC value of 13.9 μM, which was separated from the marine algae-derived fungus *A. versicolor* OUCMDZ-2738 (Liu et al., 2019). One new diphenyl ether, diorcinol K (**296**), along with two known analog diorcinols D (**297**) and I (**298**), were isolated from a fungus *Aspergillus* sp. CUGB-F046 (Xu et al., 2018). Compounds **296**–**298** displayed significant antibacterial activity against *S. aureus* and MRSA with the MIC values from 3.13 to 6.25 μg/mL. Diorcinol (**299**) was isolated from the deep-sea-derived *A. versicolor* 170,217 (Lin S. H. et al., 2023). Compound **299** exhibited weak inhibitory activity against *V. parahemolyticus* with an MIC value of 128.0 μg/mL. Violaceol-I (**300**), violaceol-II (**301**), 4-carbethoxydiorcinal (**302**), and 1,9-dimethyl-3,7-dibenzofurandiol (**303**) were isolated from the fungus *Aspergillus* sp. ZZ1861 (Ha et al., 2024). Compounds **300**–**303** showed inhibitory activity against MRSA and *E. coli* with the MIC values from 6.25 to 50.0 μg/mL. Two new diphenyl ethers, aspergillusethers E (**304**) and *F* (**309**), together with three known compounds aspergillusethers C (**305**) and D (**306**) and pilobolusate (**307**), were isolated from sponge-derived fungus *Aspergillus* sp. PSU-MF16 (Saetang et al., 2021). Compound **304** demonstrated moderate inhibitory activity against *S. aureus* and MRSA with the same MIC value of 16.0 μg/mL. Compounds **305**–**307** had weak antibacterial activity against *S. aureus* and MRSA with MIC values from 64.0 to 128.0 μg/mL. Aspergillusethers J (**308**) and F (**309**) showed inhibitory activity against MRSA, *M. variabilis*, and *M. jannaschii* with MIC values ranging 2.0–64.0 μg/mL, which were separated from coral-derived fungus *A. unguis* GXIMD 02505 (Zhang Y. T. et al., 2022). Two new cerebroside derivatives, flavusides A (**310**) and B (**311**), were isolated from the marine-derived fungus *A. flavus* MFA500 (Yang et al., 2011). Compounds **310** and **311** showed moderate inhibitory activity against *S. aureus* with the same MIC value of 15.6 μg/mL. One new phenol

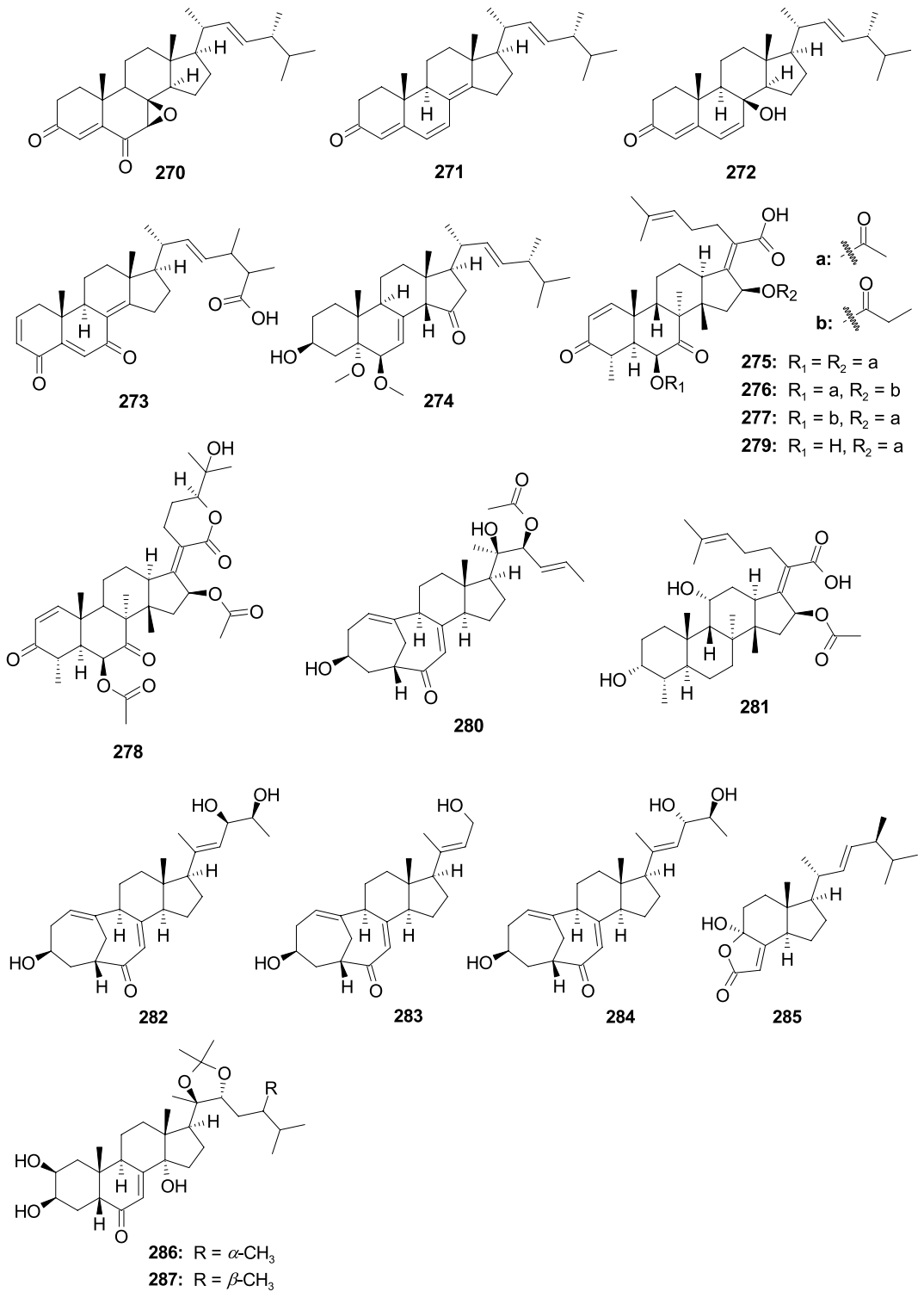

FIGURE 13
Chemical structures of antibacterial steroids **270**–**287** from *Aspergillus* spp.

derivative, acetylpeniciphenol (**312**), showed activity against *E. tarda*, *V. alginolyticus*, and *V. vulnificus* with the MIC values of 4.0, 8.0, and 8.0 μg/mL, respectively, which was separated from the cold-seep-derived fungus *A. insuetus* SD-512 (Chi et al., 2021a). Fumagiringillin (**313**) and fumagillin (**314**) were isolated from the marine-derived fungus *A. fumigatus* H22 (Zhang R. et al., 2022). Compounds **313** and **314** showed inhibitory activity against MRSA with MIC values of 25.0 and 2.50 μg/mL, respectively. 8-*O*-4-dehydrodiferulic acid (**315**) was isolated from the sponge-derived fungus *Aspergillus* sp. (Zhou et al., 2014). Compound **315** displayed activity against *R. litoralis* with an MIC value of 1.0 μg/mL. A new citrinin monomer penicitrinol L (**316**) and a known compound penicitrinol A (**317**) were separated from the

marine algal-derived fungus *A. sydowii* EN-534 (Yang et al., 2018b). Compound **316** displayed weak inhibitory activity against *E. coli*, *E. ictaluri* and *V. alginolyticus* with the same MIC value of 64.0 μg/mL. Compound **317** showed inhibitory activity against *E. coli*, *M. luteus*, *E. ictaluri*, *V. alginolyticus*, and *V. parahaemolyticus* with the MIC values from 4.0 to 32.0 μg/mL. 2-(Hydroxymethyl)-3-propylphenol (**318**) and (−)-brassicadiol (**319**) were separated from the mangrove-derived fungus *Aspergillus* sp. ZJ-68 (Cai et al., 2019). Compounds **318** and **319** showed strong activity against *S. aureus*, *E. coli* and *B. subtilis* (MIC, 4.15–12.5 μg/mL). 4,6-Dichloro-5-methylbenzene-1,3-diol (**320**) was isolated from deep-sea derived fungus *A. terreus* CC-S06-18 (Huang et al., 2024). Compound **320** showed inhibitory activity against *V. parahaemolyticus* ATCC 17802, exhibiting an MIC value of 7.8 μg/mL. 1-(2,6-Dihydroxy-4-methoxy-3,5-dimethylphenyl)-2-methylbutan-1-one (**321**) was isolated from *A. unguis* GXIMD 02505 (Zhang Y. T. et al., 2022). Compound **321** showed inhibitory activities against *M. variabilis* and *M. jannaschii* with MIC values of 8.0 and 32.0 μg/mL, respectively. Two novel compounds, asperporonins A (**322**) and B (**323**), were separated from a marine fungus *A. terreus* SCSIO 41202 (Zhang et al., 2024). Compounds **322** and **323** showed antibacterial effects against *X. citri* subsp. *citri* with the same MIC value of 0.3125 mg/mL. Terrusnolide A (**324**) was separated from the deep-sea-derived fungus *Aspergillus* sp. SCSIO 41029 (Chen et al., 2021). Compound **324** displayed inhibitory activity against *S. aureus* with an MIC value of 6.25 μg/mL. Candidusin A (**325**), terphenyllin (**326**), and 4″-deoxyterphenyllin (**327**) were separated from a coral-derived fungus *Aspergillus* sp. SCSIO40435 (Ye et al., 2022). Compound **325** showed antibacterial activities against *E. coli*, *A. baumannii*, *S. aureus*, and MRSA with the MIC values of 1.0, 64.0, 32.0, and 16.0 μg/mL, respectively. Compound **326** had strong antibacterial activity against *E. coli* with an MIC value of 0.5 μg/mL. Compound **327** exhibited weak inhibitory activity against *B. subtilis* and *M. luteus* with MIC values of 64.0 and 32.0 μg/mL, respectively. 5[(3*E*,5*E*)-nona-3,5-dien-1-yl] benzene (**328**) was separated from the sponge-associated fungus *A. stellatus* KUFA2017 (Machado et al., 2022). Compound **328** showed antibacterial activity against *E. faecalis* ATCC 29212, *E. faecalis* B3/101 (VRE), *S. aureus*, and MRSA with the MIC values of 16.0, 16.0, 32.0, and 16.0 μg/mL, respectively (9*R*,10*E*,12*E*)-9-methoxyoctadecadienoic acid (**329**) was separated from a marine fungus *A. terreus* SCSIO41202 (Zhang et al., 2024). Compound **329** showed an antibacterial effect against *X. citri* subsp. *citri* with an MIC value of 0.078 mg/mL. Three undescribed compounds, carnemycins H–I (**330**–**331**) and stromemycin B (**332**), together with six phenolic compounds carnemycin E (**333**), carnemycin B (**334**), carnemycin A (**335**), 2,4-dihydroxy-6-[(3*E*,5*E*)-nona-3,5-dien-1-yl]-benzoic acid (**336**), and stromemycin (**337**), were separated from marine-derived fungus *A. ustus* (Xue et al., 2024). Compounds **330**–**337** showed different inhibitory activity against *R. solanacearum* with MIC values from 3 to 35 μg/mL (Figure 14).

3 Comprehensive overview and conclusions

In recent years, marine fungi have become a research hotspot because they can produce bioactive compounds. In conjunction with a series of previous literature, we conducted a comprehensive study focusing on antimicrobial compounds produced by *Aspergillus* fungi from different marine origins between January 2010 and June 2024 in Table 1.

The structural diversities of the antibacterial secondary metabolites isolated from *Aspergillus* spp. are shown in Figure 15. The reported numbers of *Aspergillus* were based on structural classification, including 32 terpenoids, 98 nitrogen-containing compounds, 139 polyketides, 18 steroids, and 50 other derivatives discovered. The number and types of compounds with broad-spectrum antibacterial activity, activity against resistant bacteria, and activity against non-human pathogenic bacteria are shown in Figure 16.

Interesting, the conjugated double bonds at C-16 and C-18 are essential for the antibacterial activities of the ophiobolin sesterterpenes when having $-CH_2OH$ (**2**) or −CHO (**3**) groups positioned at C-7 (Chi et al., 2020). Notoamides (**69**–**71**, **118,** and **119**) are featured by the conserved moieties of a pyranoindole ring and a proline-bearing bicyclo[2.2.2]diazaoctane core. Sclerotiamide L (**65**) with a 6,6,5,7,6,5-ring system inhibited pathogenic bacteria including methicillin-resistant *S. aureus* (Meng et al., 2022). Nevertheless, this study provides indole diketopiperazine alkaloids as the undescribed natural scaffolds for the development of antibacterial agents. A large number of depsidone derivatives (**203**–**221**) had antibacterial activity against *S. aureus* and MRSA has been reported in the literature (Handayani et al., 2020; Zhang Y. T. et al., 2022; Thi et al., 2023; Saetang et al., 2021). The possible and preliminary structure–activity relationship was discussed; the phenolic hydroxyl group can improve the activity. Natural polyphenol compounds have significant antimicrobial activity (Chen et al., 2024). The chlorine-substituted group can be beneficial for the activity.

We sorted out the different marine sources of these *Aspergillus* spp., such as marine algae, corals, sponges, other animals, mangroves, seawater, and marine sediments, are shown in Figure 17. The most *Aspergillus* spp. were derived from marine sediment, accounting for 33.33%, and from marine sponges ranked second, comprising 23.42% of the total.

The number of antibacterial secondary metabolites from the genus of *Aspergillus* annually from 2010 to 2023 is shown in Figure 18. The progress of research in antimicrobial compounds from the genus *Aspergillus* was relatively slow from 2010 to 2017. However, there has been rapid development in antimicrobial research since 2018. These data indicated that research related to antibacterial compounds from *Aspergillus* spp. is increasingly receiving attention. Many of these compounds show inhibitory effects against *S. aureus*, while some showed activity against *E. coli* and *B. subtilis*. These active compounds hold promise for treating bacterial infections, offering valuable insights for the development of new anti-infective drugs.

Notably, some antimicrobial compounds produced by *Aspergillus* fungi also showed activities against agriculture and fish pathogenic bacteria and so on. For example, asperalin E (**115**), with a rare 4-amino-2-butanone moiety, exhibited the strongest inhibitory effects against fish pathogenic bacterium *S. iniae*, with potential for development as a new bactericide, and asperalin *F* (**116**) showed moderate-to-potent inhibitory activity against three fish pathogenic bacterium among *E. ictalurid*, *S. iniae*, and *S. parauberis*, with potential for development as a new bactericide. (9*R*,10*E*,12*E*)-9-methoxyoctadecadienoic acid (**329**) exhibited an excellent anti-*Xanthomonas citri* subsp. *citri* effect with the MIC value of 0.078 mg/mL, which was significantly more potent than the positive control $CuSO_4$ (MIC, 0.3125 mg/mL). Compound **329** inhibited cell growth

10.3389/fmicb.2024.1464135

by disrupting biofilm formation, destroying the cell membrane, and inducing the accumulation of reactive oxygen species. Compound **6** is highly effective in controlling citrus canker disease *in vivo* tests, indicating **6** has the potential to lead compound for the development of new environmentally friendly and efficient anti-Xcc pesticides (Zhang et al., 2024). Stromemycin B (**332**) could effectively control the development of wilting symptoms and considerably minimize the occurrence of bacterial wilt in tomato plants. At 14 days after inoculation, compound **332** exerted a controlled efficacy of over 80% at a concentration of 100 μg/mL, which was better than that of streptomycin sulfate (100 μg/mL), indicating that compound **332** was a significant candidate as an antibacterial agent against *Ralstonia*

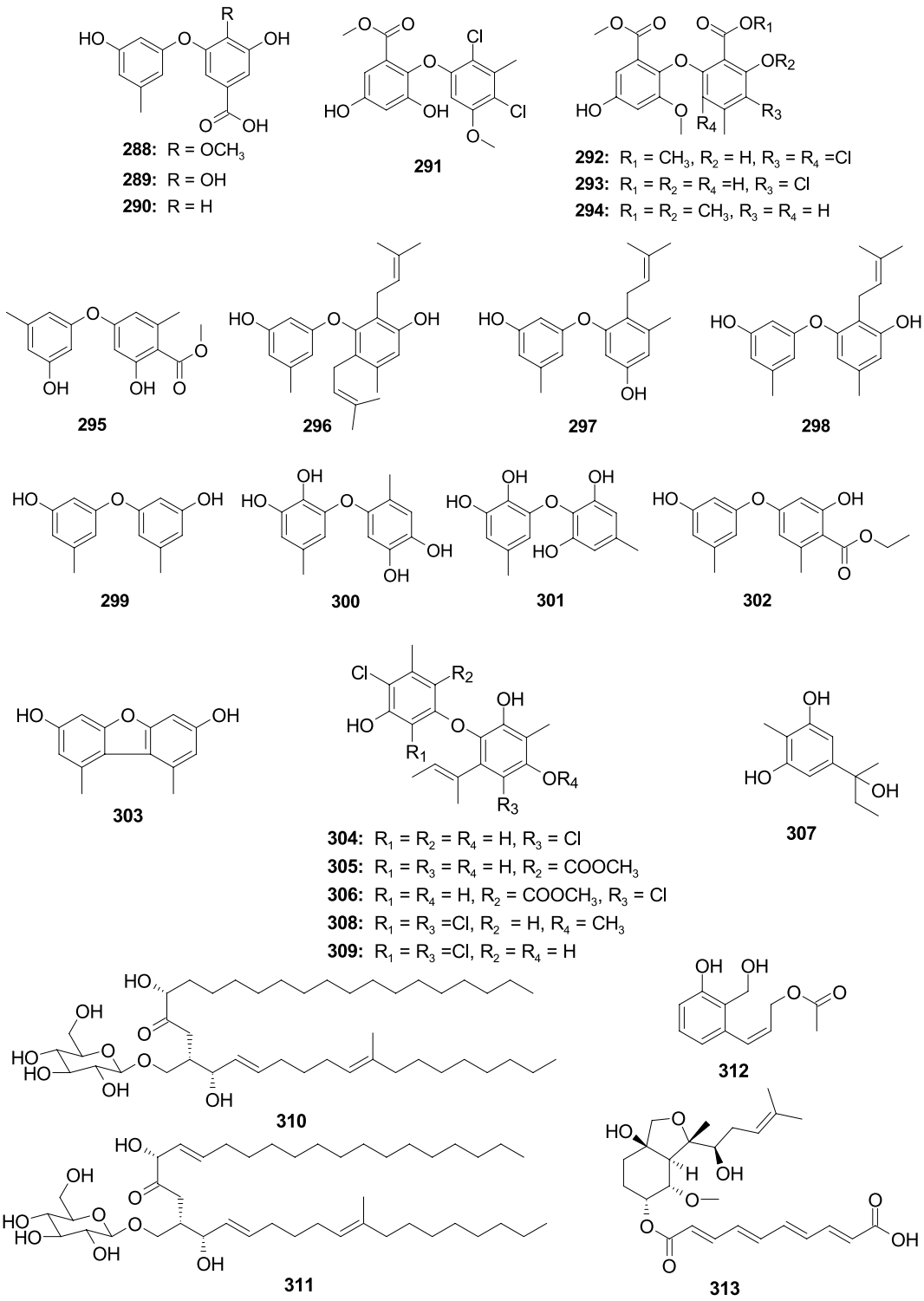

FIGURE 14 (Continued)

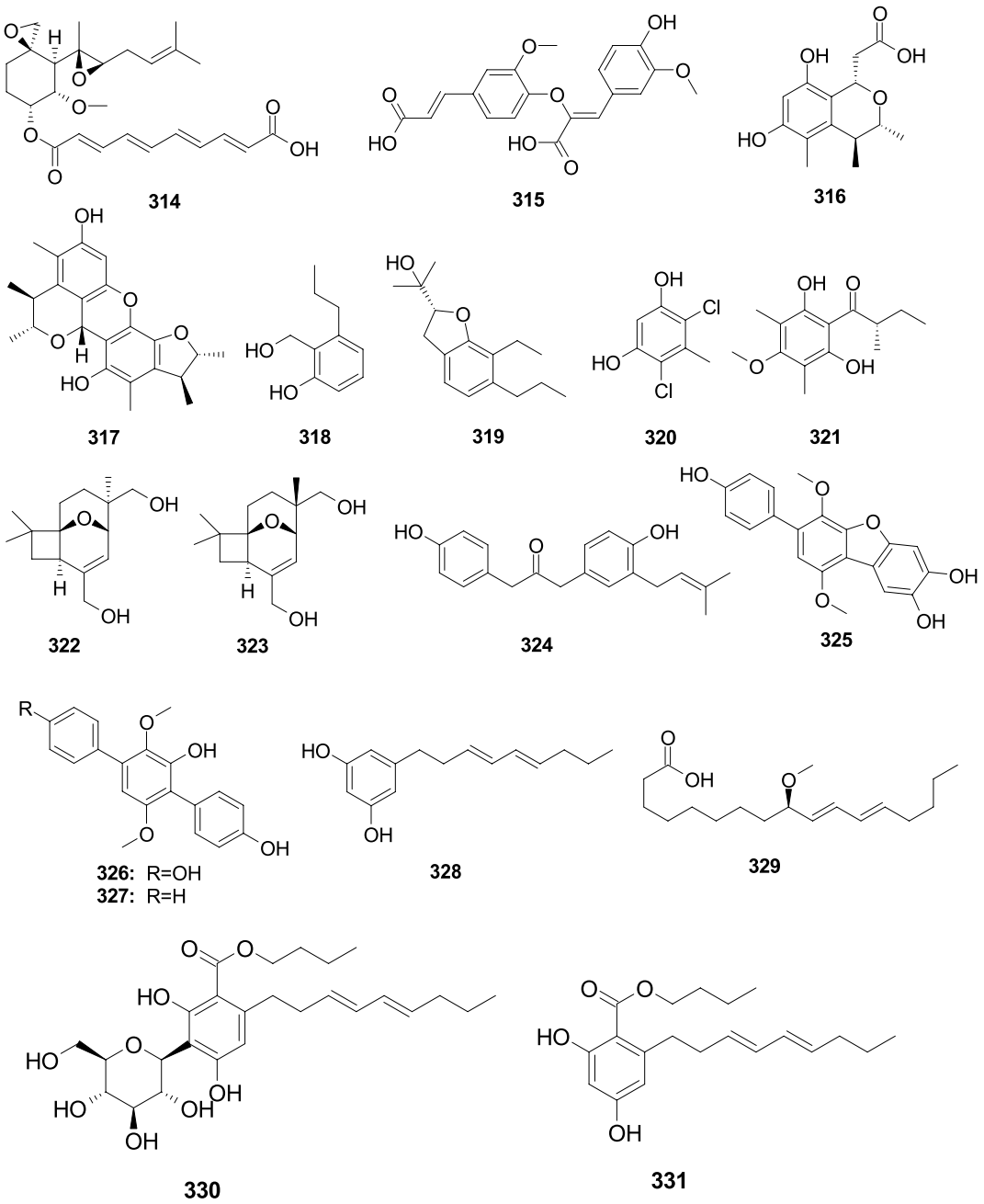

FIGURE 14 (Continued)

solanacearum (Xue et al., 2024). These results suggested that the antibacterial lead compounds might be used as one of the probable candidates' drugs for "One Health" in the utilization in healthcare, agriculture, and fishery.

4 Conclusion

337 secondary metabolites (including 145 new compounds) were isolated from marine-derived *Aspergillus* fungi; the compounds were classified into five chemical types: 32 terpenoids, 98 nitrogen-containing compounds, 139 polyketides, 18 steroids, and 50 other derivatives (Figure 15). The distribution of these compounds is as follows: terpenoids (9.50%), nitrogen-containing compounds (29.08%), polyketides (41.25%), steroids (5.34%), and other compounds (14.84%). Polyketides displayed the most substantial proportion of the observed antibacterial compounds, alongside notable contributions from terpenoids and nitrogen-containing compounds. This comprehensive analysis highlights the potential for developing antimicrobial agents from these natural products.

Additionally, the samples were obtained from various environments: 7.21% from algae, 12.61% from corals, 23.42% from sponges, 5.41% from other animals, 11.71% from mangroves, and 6.31% from seawater. Most significantly, 33.33% originated from sediment samples (Figure 18). This extensive environmental sampling underscores the compounds' efficacy and potential applications in

10.3389/fmicb.2024.1464135

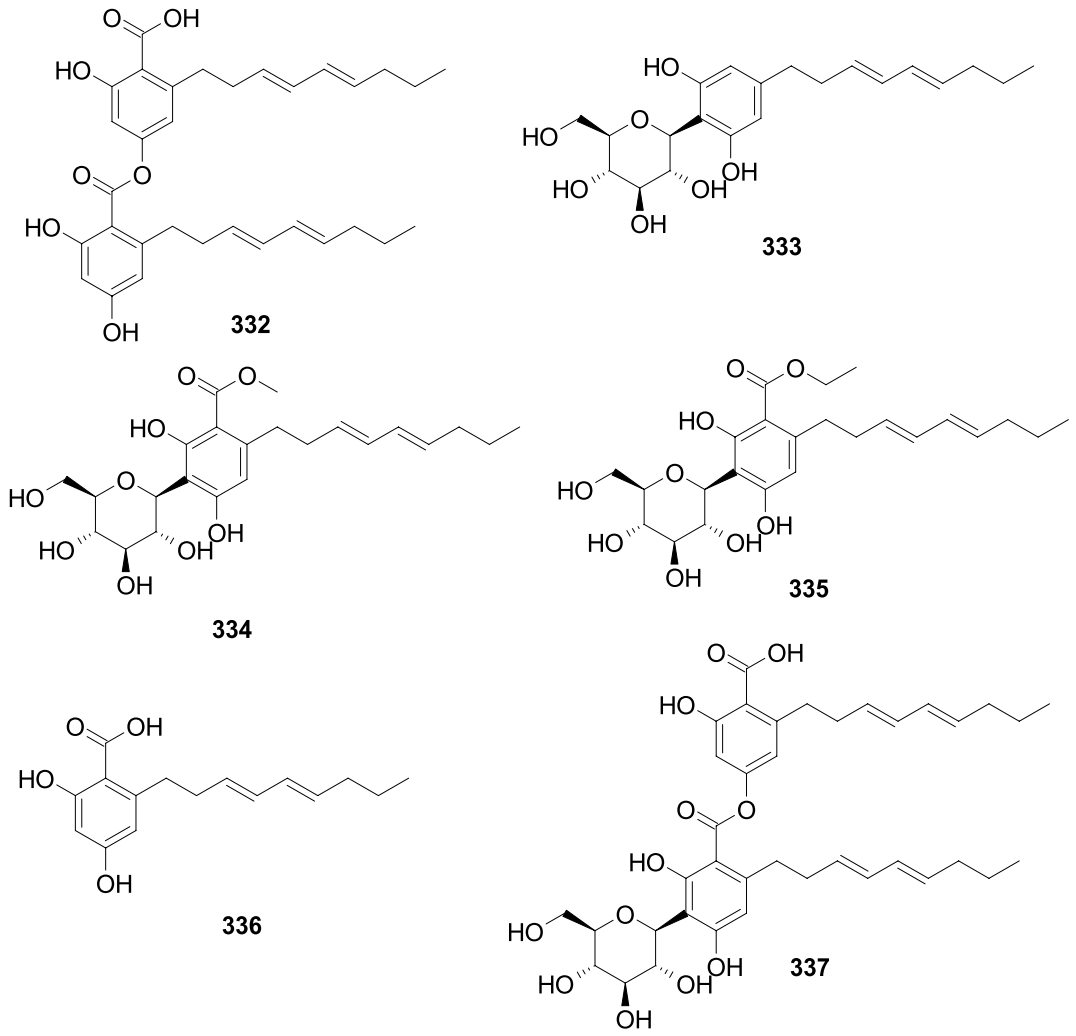

FIGURE 14
Chemical structures of other antibacterial classes **288**–**337** from *Aspergillus* spp.

combating antibiotic-resistant bacteria. Specifically, terpenoid compounds were classified as 18 sesquiterpenes, four diterpenes, and 10 meroterpenoids. Nitrogen-containing compounds included 39 indole alkaloids, 11 quinazolinone alkaloids, four cytochalasan alkaloids, 13 peptides, and 31 other nitrogen-containing compounds. Polyketide compounds were identified as 20 anthraquinones, 31 xanthones, 59 lactones, and 29 other polyketide metabolites. 18 steriods and 50 other classes are shown in Figure 15. We observed that research progress in antimicrobial compounds from the genus of *Aspergillus* was relatively slow from 2010 to 2017. However, there has been rapid development in antimicrobial research since 2018. These data indicated that research related to antibacterial compounds from *Aspergillus* spp. are increasingly receiving attention. By classifying multiple antibacterial compounds, a foundation is laid for predicting which types may exert more potent pharmacological effects on specific biological targets, guiding drug design and validation through simulation or experimentation.

Among all antibacterial active compounds, some were found to have activity levels approaching or reaching the nanomolar range, such as fumigatoside *F* (**65**), cytochalasin Z17 (**75**), dihydroisoflavipucine (**90**), emeguisin A (**204**), and fusidic acid (**265**). As a first-in-class BCG-selective diketopiperazine dimer antibiotic, brevianamide S (**34**) was indicative of a possible new mechanism of action that could, if translated to *M. tuberculosis*, represent a valuable new lead in the search for next-generation antitubercular drugs. These compounds could become promising lead compounds for use as antimicrobial agents in the future. Notably, some antimicrobial compounds produced by *Aspergillus* fungi also showed activities against agriculture and fish pathogenic bacteria, and so on.

In summary, the chemical diversity and potent antibacterial activities ofsecondary metabolites from marine-derived *Aspergillus* species indicated their potential in antibiotic drug discovery. The identified metabolites demonstrate a wide range of antimicrobial activities, showing potent effects against various pathogens. Future research aims to elucidate their mechanisms of action and optimize production methods to fully harness their therapeutic potential in fighting infectious diseases. Marine-derived *Aspergillus* species present a promising frontier for developing novel natural products with applications in medical treatments and agricultural antimicrobial agents.

TABLE 1 The antibacterial activity of secondary metabolites 1–331 from *Aspergillus* sp.

Compounds	Producing strains	Habitats	Genbank accession number	Antibacterial activity the MIC values	References
(5*S*,6*S*)-16,17-Dihydroophiobolin H (**1**)	*A. insuetus* SD-512	Cold-seep sediment, the northeast of the South China Sea	MN650839	Anti-A. hydrophilia, *E. coli*, *E. tarda*, *P. aeruginosa*, *V. alginolyticus*, V anguillarum, V. parahemolyticus, and *V. vulnificus*; 4, 4, 4, 8, 4, 32, 4, and 8 μg/mL	Chi et al. (2020)
(6*α*)-21,21-*O*-dihydroophiobolin G (**2**)	*A. insuetus* SD-512	Cold-seep sediment, the northeast of the South China Sea	MN650839	Anti-A. hydrophilia, *E. coli*, *E. tarda*, *P. aeruginosa*, *V. alginolyticus*, V anguillarum, V. parahemolyticus, and *V. vulnificus*; 8, 16, 8, 8, 4, 32, 8, and 8 μg/mL	Chi et al. (2020)
6-epi-Ophiobolin G (**3**)	*A. insuetus* SD-512	Cold-seep sediment, the northeast of the South China Sea	MN650839	Anti-A. hydrophilia, *E. coli*, *E. tarda*, *P. aeruginosa*, *V. alginolyticus*, V anguillarum, V. parahemolyticus, and *V. vulnificus*; 8, 16, 8, 8, 4, 32, 8, and 8 μg/mL	Chi et al. (2020)
Ophiobolin U (**4**)	*A. ustus* cf-42	Marine green alga, the Zhoushan Island, Zhejiang province, China	JX036023	Weak (anti-*E. coli* and *S. aureus*); Inhibitory diameters of 15 and 10 mm at 30 μg/disk	Liu et al. (2013)
(5*α*,6*α*)-Ophiobolin H (**5**)	*A. ustus* cf-42	Marine green alga, the Zhoushan Island, Zhejiang province, China	JX036023	Weak (anti-*E. coli*); Inhibitory diameter of 10 mm at 30 μg/disk	Liu et al. (2013)
Asperophiobolin E (**6**)	*A. hiratsukae* SCSIO 5Bn$_1$003	Marine coral, the South China Sea	KY806121.1	Anti-*B. subtilis* and *S. aureus*; 17.0 and 102.86 μg/mL	Zeng et al. (2022a)
Asperbrunneo acid (**7**)	A. brunneoviolaceus MF180246	Mangrove mud sample, the Xinglin Bay, Xiamen, China	–	Anti-*S. aureus*; 200 μg/mL	Xu et al. (2024)
Aspergilol C (**8**)	*Aspergillus* sp. ZZ1861	Sea mud sample, the Zhoushan Island, Zhejiang province, China	OR985107	Anti-*E. coli*; 3.12 μg/mL	Ha et al. (2024)
Punctaporonin B (**9**)	*A. terreus* SCSIO 41202	Deep-sea sediment, the coast of the South China Sea	MN613535	Anti-*X. citri* subsp. *citri*; 0.625 mg/mL	Zhang et al. (2024)
Punctaporonin D (**10**)	*A. terreus* SCSIO 41202	Deep-sea sediment, the coast of the South China Sea	MN613535	Anti-*X. citri* subsp. *citri*; 0.625 mg/mL	Zhang et al. (2024)
Punctaporonin G (**11**)	*A. terreus* SCSIO 41202	Deep-sea sediment, the coast of the South China Sea	MN613535	Anti-*X. citri* subsp. *citri*; 0.3125 mg/mL	Zhang et al. (2024)
Sesquiterpenoid (**12**)	*A. versicolor* SD-330	Marine sediment, the South China Sea	MN176407	Anti-*E. coli*, A. hydrophilia, *E. tarda*, *P. aeruginosa*, *V. harveyi*, and *V. parahaemolyticus*; 8, 8, 8, 8, 4, and 16 μg/mL	Li et al. (2021)
Aspergoterpenin C (**13**)	*A. versicolor* SD-330	Marine sediment, the South China Sea	MN176407	Anti-*E. coli*, A. hydrophilia, *E. tarda*, *P. aeruginosa*, *V. harveyi*, and *V. parahaemolyticus*; 2, 8, 4, 16, 8, and 8 μg/mL	Li et al. (2021)
Engyodontiumone I (**14**)	*A. versicolor* SD-330	Marine sediment, the South China Sea	MN176407	Anti-*E. coli*, A. hydrophilia, *E. tarda*, *P. aeruginosa*, *V. harveyi*, and *V. parahaemolyticus*; 1, 4, 4, 16, 4, and 8 μg/mL	Li et al. (2021)

(Continued)

10.3389/fmicb.2024.1464135

TABLE 1 (Continued)

Compounds	Producing strains	Habitats	Genbank accession number	Antibacterial activity the MIC values	References
Aspergillusene B (**15**)	A. sydowii LW09	Deep-sea sediment, the Southwest Indian Ridge	OP584347	Anti-*R. solanacarum*; 32 μg/mL	Yang et al. (2023)
(7*S*,11*S*)-(+)-12-Hydroxysydonic acid (**16**)	A. sydowii LW09	Deep-sea sediment, the Southwest Indian Ridge	OP584347	Anti-*P. syringae*; 32 μg/mL	Yang et al. (2023)
Expansol G (**17**)	A. sydowii LW09	Deep-sea sediment, the Southwest Indian Ridge	OP584347	Anti-*R. solanacarum*; 32 μg/mL	Yang et al. (2023)
(*S*)-Sydonic acid (**18**)	A. sydowii LW09	Deep-sea sediment, the Southwest Indian Ridge	OP584347	Anti-*R. solanacarum*; 32 μg/mL	Yang et al. (2023)
Asperolide D (**19**)	A. wentii SD-310	Deep-sea sediment, the South China Sea	KM409566	Anti-*E. tarda*; 16 μg/mL	Li et al. (2016)
Asperolide A (**20**)	A. wentii SD-310	Deep-sea sediment, the South China Sea	KM409566	Anti-*E. tarda*; 16 μg/mL	Li et al. (2016)
Sphaeropsidin A (**21**)	*A. porosus* G23	Marine alga, the marine environment by BioViotica Naturstoffe GmbH	LT671130.1	Anti-*S. aureus* ATCC 25923 and ATCC BAA-41; 32.6 and 35.3 μM	Neuhaus et al. (2019)
Aspergiloid E (**22**)	*A. porosus* G23	Marine alga, the marine environment by BioViotica Naturstoffe GmbH	LT671130.1	Anti-*S. aureus* ATCC 25923 and ATCC BAA-41; 71.6 and 77.8 μM	Neuhaus et al. (2019)
Aspergillactone (**23**)	*Aspergillus* sp. CSYZ-1	Sediment, the Zhoushan Island, the East China Sea	–	Aanti-*H. pylori* ATCC 43504, G27, Hp159, BY583 and *S. aureus* ATCC 25923, USA300, BKS231, BKS233; 2, 1, 1, 4, 16, 2, 4, and 8 μg/mL	Cen et al. (2021)
Chevalone B (**24**)	Aspergillus sp. H30	*Cucumaria japonica*, the South China Sea	–	Weak (anti-*S. aureus*)	Hu et al. (2019)
Chevalone H (**25**)	*A. hiratsukae* SCSIO 7S2001	Marine gorgonian coral, the South China Sea	MN347034	Anti-*M. lutea*, *K. pneumoniae*, MRSA, and *S. faecalis*; 6.25, 50, 6.25, and 6.25 μg/mL	Chen X. Y. et al. (2022)
Chevalone I (**26**)	*A. hiratsukae* SCSIO 7S2001	Marine gorgonian coral, the South China Sea	MN347034	Anti-*M. lutea*, MRSA, and *S. faecalis*; 25, 6.25, and 25 μg/mL	Chen X. Y. et al., 2022
Chevalone J (**27**)	*A. hiratsukae* SCSIO 7S2001	Marine gorgonian coral, the South China Sea	MN347034	Anti-*M. lutea*, *K. pneumoniae*, and MRSA; 25, 25, and 12.5 μg/mL	Chen X. Y. et al., 2022
Chevalone K (**28**)	*A. hiratsukae* SCSIO 7S2001	Marine gorgonian coral, the South China Sea	MN347034	Anti-*K. pneumoniae*, MRSA, and *S. faecalis*; 6.25, 25, and 50 μg/mL	Chen X. Y. et al., 2022
Chevalone L (**29**)	*A. hiratsukae* SCSIO 7S2001	Marine gorgonian coral, the South China Sea	MN347034	Anti-*M. lutea*, MRSA, and *S. faecalis*; 12.5, 12.5, and 12.5 μg/mL	Chen X. Y. et al., 2022
Austalide R (**30**)	Aspergillus sp.	Marine sponge, the Adriatic Sea	–	Anti-*H. aquamarina*, *P. irgensii*, *P. elyakovii*, *S. putrefaciens*, and *V. harveyi*; 0.1 μg/mL	Zhou et al. (2014)
Austalide M (**31**)	Aspergillus sp.	Marine sponge, the Adriatic Sea	–	Anti-*H. aquamarina*, *P. irgensii*, *P. elyakovii*, *R. litoralis*, *S. putrefaciens*, and *V. harveyi*; 0.001, 0.01, 0.001, 0.001, 0.001, and 0.001 μg/mL	Zhou et al. (2014)

(Continued)

10.3389/fmicb.2024.1464135

TABLE 1 (Continued)

Compounds	Producing strains	Habitats	Genbank accession number	Antibacterial activity the MIC values	References
Austalide N (**32**)	Aspergillus sp.	Marine sponge, the Adriatic Sea	–	Anti-V. natrieegens and R. litorails; 0.01 μg/mL	Zhou et al. (2014)
Griseofamine A (**33**)	*Aspergillus* sp. SCSIO 41024	Deep-sea sediment, the South China Sea	MH608347.1	Anti-*E. coli*; 64.0 μg/mL	Chen et al. (2020)
Brevianamide S (**34**)	*A. versicolor* MF030	Deep-sea sediment, the Bohai Sea, China	–	Anti-BCG; 6.25 μg/mL	Song et al. (2012)
Brevianamide T (**35**)	*A. versicolor* MF030	Deep-sea sediment, the Bohai Sea, China	–	Anti-BCG; 50 μg/mL	Song et al. (2012)
Brevianamide U (**36**)	*A. versicolor* MF030	Deep-sea sediment, the Bohai Sea, China	–	Anti-BCG; 25 μg/mL	Song et al. (2012)
Brevianamide V (**37**)	*A. versicolor* MF030	Deep-sea sediment, the Bohai Sea, China	–	Anti-BCG; 100 μg/mL	Song et al. (2012)
Brevianamide K (**38**)	*A. versicolor* MF030	Deep-sea sediment, the Bohai Sea, China	–	Anti-BCG; 50 μg/mL	Song et al. (2012)
Deoxybrevianamide E (**39**)	*A. versicolor* MF030	Deep-sea sediment, the Bohai Sea, China	–	Anti-BCG, *S. aureus* ATCC 6538, and *B. subtilis* ATCC 6633; 100, 100, and 50 μg/mL	Song et al. (2012)
9ξ-*O*-2(2,3-dimethylbut-3-enyl)-brevianamide Q (**40**)	*A. versicolor* pt20	Marine brown alga, the Pingtan Island, Fujian province, China	–	Weak (anti-*E. coli* and *S. aureus*); Inhibitory diameters of 7 and 7 mm at 30 μg/disk	Miao et al. (2012)
12,13-Dihydroxy-fumitremorgin C (**41**)	*Aspergillus* sp. SCSIO Ind09F01	Deep-sea sediment, the Indian Ocean	AY373869	Anti-*M. tuberculosis*; 2.41 μM	Luo et al. (2017)
	A. fumigatus H22	Seawater, the Western Pacific	–	Anti-MRSA and *M. bovis*; 2.50 and 25 μM	Zhang R. et al. (2022)
(−)-Stephacidin A (**42**)	*Aspergillus* sp. XS-20090066	Marine gorgonian coral, the South China Sea	HM535361	Anti-*S. epidermidis*; 14.5 μM	Chen et al. (2013)
Notoamide *F* (**43**)	*A. sclerotiorum* GDST-2013-0501	Marine sponge, the South China Sea	MT534582	Anti-*S. epidermidis*; 12.5 μM	Wang C. Y. et al. (2022)
Asperthrin A (**44**)	*Aspergillus* sp. YJ191021	The intertidal zone soil, the ZhouShan Island, Zhejiang province, China	–	Anti-*X. oryzae* pv., *E. tarda*, *V. anguillarum*, A. hydrophilia, and *V. parahaemolyticus*; 12.5, 16, 8, 32, and 16 μg/mL	Yang et al. (2021)
Asperthrin E (**45**)	*Aspergillus* sp. YJ191021	The intertidal zone soil, the ZhouShan Island, Zhejiang province, China	–	Weak (anti-*X. oryzae* pv.)	Yang et al. (2021)
24,25-Dihydroxyvariecolorin G (**46**)	*A. chevalieri* CS-122	Deep-sea cold-seep sediment, the northeast of the South China Sea	KU872171.1	Anti-*V. harveyi* and *E. coli*; 16 and 4 μg/mL	Yan et al. (2023)
25-Hydroxyrubrumazine B (**47**)	*A. chevalieri* CS-122	Deep-sea cold-seep sediment, the northeast of the South China Sea	KU872171.1	Anti-*V. harveyi*, *E. tarda*, *A. hydrophila*, *E. coli*, and *M. luteus*; 32, 16, 32, 16, and 32 μg/mL	Yan et al. (2023)
22-Chloro-25-hydroxyrubrumazine B (**48**)	*A. chevalieri* CS-122	Deep-sea cold-seep sediment, the northeast of the South China Sea	KU872171.1	Anti-*V. harveyi* and *E. coli*; 8 and 32 μg/mL	Yan et al. (2023)
25-Hydroxyvariecolorin *F* (**49**)	*A. chevalieri* CS-122	Deep-sea cold-seep sediment, the northeast of the South China Sea	KU872171.1	Anti-*V. harveyi* and *E. coli*; 32 μg/mL	Yan et al. (2023)
27-Epi-aspechinulin D (**50**)	*A. chevalieri* CS-122	Deep-sea cold-seep sediment, the northeast of the South China Sea	KU872171.1	Anti-*V. harveyi*, *E. tarda*, *A. hydrophila*, *E. coli*, and *M. luteus*; 16, 32, 32, 32, and 16 μg/mL	Yan et al. (2023)
Neoechinulin B (**51**)	*A. chevalieri* CS-122	Deep-sea cold-seep sediment, the northeast of the South China Sea	KU872171.1	Anti-*A. hydrophila* and *E. coli*; 4 and 8 μg/mL	Yan et al. (2023)

(Continued)

10.3389/fmicb.2024.1464135

TABLE 1 (Continued)

Compounds	Producing strains	Habitats	Genbank accession number	Antibacterial activity the MIC values	References
Neoechinulin A (**52**)	*Aspergillus* sp. WHUF0343	The root soil of mangroves, the Yalong Bay, Sanya, Hainan province, China	–	Anti-*H. pylori* Hp159; 16 μg/mL	Yu et al. (2022)
	A. hiratsukae SCSIO 7S2001	Marine gorgonian coral, the South China Sea	MN347034	Anti-*K. pneumoniae* and MRSA; 50 and 12.5 μg/mL	Chen X. Y. et al., 2022
Asperfumigatin (**53**)	*A. fumigatus* H22	Seawater, the Western Pacific	–	Anti-MRSA; 5 μM	Zhang R. et al. (2022)
Fumitremorgin B (**54**)	*A. fumigatus* H22	Seawater, the Western Pacific	–	Anti-MRSA; 20 μM	Zhang R. et al. (2022)
13-Oxofumitremorgin B (**55**)	*A. fumigatus* H22	Seawater, the Western Pacific	–	Anti-MRSA; 1.25 μM	Zhang R. et al. (2022)
Spirotryprostatin C (**56**)	*A. fumigatus* H22	Seawater, the Western Pacific	–	Anti-MRSA; 10 μM	Zhang R. et al. (2022)
(−)-Chaetominine (**57**)	*A. fumigatus* H22	Seawater, the Western Pacific	–	Anti-MRSA; 25 μM	Zhang R. et al. (2022)
Fumigaclavine C (**58**)	*A. fumigatus* H22	Seawater, the Western Pacific	–	Anti-MRSA; 12.5 μM	Zhang R. et al. (2022)
Epi-aszonalenin A (**59**)	*A. fumigatus* SCSIO 41012	Deep-sea sediment, the Indian Ocean	KM924435	Anti-*A. baumanii* ATCC 15122; 6.25 μg/mL	Limbadri et al. (2018)
3-((1-Hydroxy-3-(2-methylbut-3-en-2-yl)-2-oxoindolin-3-yl)methyl)-1-methyl-3,4-dih-ydrobenzo[e] [1,4]diazepine-2,5-dione (**60**)	Aspergillus sp.	Marine sponge, the Adriatic Sea	–	Anti-*V. harveyi* and *V. natriegens*; 1.0 μg/mL	Zhou et al. (2014)
Gliotoxin (**61**)	*Aspergillus* sp. SCSIO Ind09F01	Deep-sea sediment, the Indian Ocean	AY373869	Anti-*M. tuberculosis*; 0.030 μM	Luo et al. (2017)
β-Cyclopiazonic acid (**62**)	*A. felis* FM324	Beach soil, the Big Island, Hawaii	MZ227547	Anti-*S. aureus*, MRSA, and *B. subtilis*; 59.2 μM	Wang et al. (2021)
(2*R*,4b*R*,6a*S*,12b*S*,12c*S*,14a*S*)-4b-Deoxy-*β*-aflatrem (**63**)	*A. flavus* OUCMDZ-2205	Marine prawn, the Lianyungang Sea, Jiangsu province, China	KC120773	Anti-*S. aureus*; 20.5 μM	Sun et al. (2014)
Sclerotiamide K (**64**)	A. sclerotiorum LZDX-33-4	Marine gorgonian coral, the South China Sea	OK012383.1	Anti-*S. aureus* ATCC29213; 64 μM	Meng et al. (2022)
Sclerotiamide L (**65**)	A. sclerotiorum LZDX-33-4	Marine gorgonian coral, the South China Sea	OK012383.1	Anti-*S. aureus* ATCC29213; 4 μM	Meng et al. (2022)
Sclerotiamide M (**66**)	A. sclerotiorum LZDX-33-4	Marine gorgonian coral, the South China Sea	OK012383.1	Anti-*S. aureus* ATCC29213; 64 μM	Meng et al. (2022)
Sclerotiamide N (**67**)	A. sclerotiorum LZDX-33-4	Marine gorgonian coral, the South China Sea	OK012383.1	Anti-*S. aureus* ATCC29213; 64 μM	Meng et al. (2022)
Sclerotiamide O (**68**)	A. sclerotiorum LZDX-33-4	Marine gorgonian coral, the South China Sea	OK012383.1	Anti-*S. aureus* ATCC29213; 64 μM	Meng et al. (2022)
Sclerotiamide *p* (**69**)	A. sclerotiorum LZDX-33-4	Marine gorgonian coral, the South China Sea	OK012383.1	Anti-*S. aureus* ATCC29213; 32 μM	Meng et al. (2022)
Sclerotiamide Q (**70**)	A. sclerotiorum LZDX-33-4	Marine gorgonian coral, the South China Sea	OK012383.1	Anti-*S. aureus* ATCC29213; 64 μM	Meng et al. (2022)
Sclerotiamide R (**71**)	A. sclerotiorum LZDX-33-4	Marine gorgonian coral, the South China Sea	OK012383.1	Anti-*S. aureus* ATCC29213; 32 μM	Meng et al. (2022)
Fumigatoside E (**72**)	*A. fumigatus* SCSIO 41012	Deep-sea sediment, the Indian Ocean	KM924435	Anti-*A. baumanii* ATCC 19606, ATCC 15122, *S. aureus* ATCC 16339, and *K. pneumonia* ATCC 14578; 12.5, 6.25, 6.25, and 12.5 μg/mL	Limbadri et al. (2018)
Fumigatoside *F* (**73**)	*A. fumigatus* SCSIO 41012	Deep-sea sediment, the Indian Ocean	KM924435	Anti-*A. baumanii* ATCC 19606; 6.25 μg/mL	Limbadri et al. (2018)

(Continued)

10.3389/fmicb.2024.1464135

TABLE 1 (Continued)

Compounds	Producing strains	Habitats	Genbank accession number	Antibacterial activity the MIC values	References
Fumiquinazoline G (**74**)	*A. fumigatus* SCSIO 41012	Deep-sea sediment, the Indian Ocean	KM924435	Anti-*A. baumanii* ATCC 15122, *S. aureus* ATCC 16339, ATCC 29213, and *K. pneumonia* ATCC 14578; 6.25, 12.5, 12.5, and 25 μg/mL	Limbadri et al. (2018)
Cottoquinazoline H (**75**)	*A. versicolor* AS-212	Deep-sea coral, the Magellan Seamounts	OP009765.1	Anti-*E. coli*, *M. luteus*, *V. harveyi*, *V. parahaemolyticus*, *V. vulnificus*, Curvularia spicifera, and Colletotrichum gloeosporioides; 72.2, 36.1, 18.1, 9.0, 72.2, 72.2, and 72.2 μg/mL	Dong et al. (2023a)
Cottoquinazoline A (**76**)	*A. versicolor* AS-212	Deep-sea coral, the Magellan Seamounts	OP009765.1	Anti-*A. hydrophila*, *M. luteus*, *V. harveyi*, *V. parahaemolyticus*, *V. vulnificus*, C. spicifera, and C. gloeosporioides; 18.6, 74.6, 37.3, 37.3, 74.6, 74.6, and 74.6 μg/mL	Dong et al. (2023a)
	A. versicolor CF-09-9	Seawater, the Bohai Sea	–	Anti-*E. coli*; 5.0 μM	Zhang L. et al. (2020); Zhang Y. H. et al. (2020)
Aspergicin (**77**)	Aspergillus sp.	mangrove plant *Avicennia marina*, Zhangjiang, Guangdong province, China	–	Anti-*B. subtilis* and *B. dysenteriae*; 15.6 and 15.6 μg/mL	Zhu et al. (2011)
Brevianamide M (**78**)	*A. versicolor* pt20	Marine brown alga, the Pingtan Island, Fujian province, China	–	Weak (anti-*E. coli* and *S. aureus*); inhibitory diameters of 11 and 10 mm at 30 μg/disk	Miao et al. (2012)
Fumiquinazoline D (**79**)	*A. fumigatus* M580	Sea cucumber, the Co To-Thanh Island, Vietnam	MW015802	Anti-*E. faecalis* and *S. enterica*; 32 and 256 μg/mL	Tuan et al. (2022)
Fumiquinazoline C (**80**)	*A. fumigatus* M580	Sea cucumber, the Co To-Thanh Island, Vietnam	MW015802	Anti-*B. subtilis* and *B. dysenteriae*; 32 and 64 μg/mL	Tuan et al. (2022)
	A. fumigatus SCSIO 41012	Deep-sea sediment, the Indian Ocean	KM924435	Anti-*S. aureus* ATCC16339 and ATCC 29213; 1.56 and 0.78 μg/mL	Limbadri et al. (2018)
3-Hydroxy-6-methoxy-4-phenylquinolin-2(1*H*)-one (**81**)	*A. versicolor* AS-212	Deep-sea coral, the Magellan Seamounts	OP009765.1	Anti-*V. harveyi* and *V. alginolyticus*; 8.0 μg/mL	Dong et al. (2023b)
3-Methoxy-6-hydroxy-4-phenylquinolin-2(1*H*)-one (**82**)	*A. versicolor* AS-212	Deep-sea coral, the Magellan Seamounts	OP009765.1	Anti-*V. harveyi* and *V. alginolyticus*; 32 μg/mL	Dong et al. (2023b)
Cytochalasin Z17 (**83**)	Aspergillus sp.	Marine sponge, the Adriatic Sea	–	Anti-*R. litoralis*; 0.0001 μg/mL	Zhou et al. (2014)
Aspochalasin I (**84**)	*A. elegans* ZJ-2008010	Soft coral, the South China Sea	–	Anti-*S. epidermidis* and *S. aureus*; 20 and 10 μg/mL	Zheng et al. (2013)
Aspochalasin D (**85**)	*A. elegans* ZJ-2008010	Soft coral, the South China Sea	–	Anti-*S. epidermidis*, *S. aureus*, *E. coli*, and *B. cereus*; 10 μg/mL	Zheng et al. (2013)
Aspochalasin PZ (**86**)	*A. elegans* ZJ-2008010	Soft coral, the South China Sea	–	Anti-*S. epidermidis*; 20 μg/mL	Zheng et al. (2013)

(Continued)

10.3389/fmicb.2024.1464135

TABLE 1 (Continued)

Compounds	Producing strains	Habitats	Genbank accession number	Antibacterial activity the MIC values	References
Emestrins M (**87**)	*A. terreus* RA2905	Sea hare, the South China Sea	MK611650	Anti-*P. aeruginosa* ATCC 27853; 64 μg/mL	Wu et al. (2020a)
Emethacin C (**88**)	*A. terreus* RA2905	Sea hare, the South China Sea	MK611650	Anti-*P. aeruginosa* ATCC 27853; 32 μg/mL	Wu et al. (2020a)
4′-OMe-asperphenamate (**89**)	*A. elegans* ZJ-2008010	Soft coral, the South China Sea	–	Anti-*S. epidermidis*; 10 μg/mL	Zheng et al. (2013)
Asperphenamate (**90**)	*A. elegans* ZJ-2008010	Soft coral, the South China Sea	–	Anti-*S. epidermidis*; 10 μg/mL	Zheng et al. (2013)
Sclerotiotide M (**91**)	*A. insulicola* HDN151418	Marine sponge, the Prydz Bay, Antarctica	MT898544	Anti-*B. cereus*, *P. species*, *M. phlei*, *E. tarda*, *B. subtilis*, MRCNS, MRSA, and *V. parahemolyticus*; 3.13, 3.13, 3.13, 1.56, 6.25, 12.5, 25, and 3.13 μM	Sun et al. (2020)
Sclerotiotide N (**92**)	*A. insulicola* HDN151418	Marine sponge, the Prydz Bay, Antarctica	MT898544	Anti-*B. cereus*, *P. species*, *M. phlei*, *E. tarda*, *B. subtilis*, MRCNS, MRSA, and *V. parahemolyticus*; 6.25, 6.25, 12.5, 1.56, 12.5, 25, 25, and 6.25 μM	Sun et al. (2020)
Sclerotiotide O (**93**)	*A. insulicola* HDN151418	Marine sponge, the Prydz Bay, Antarctica	MT898544	Anti-*E. tarda*; 25.0 μM	Sun et al. (2020)
Sclerotiotide L (**94**)	*A. insulicola* HDN151418	Marine sponge, the Prydz Bay, Antarctica	MT898544	Anti-*B. cereus*, P. species, *E. tarda*, and V. parahemolyticus; 25.0 μM	Sun et al. (2020)
Sclerotiotide *F* (**95**)	*A. insulicola* HDN151418	Marine sponge, the Prydz Bay, Antarctica	MT898544	Anti-*B. cereus*, P. species, *E. tarda*, and V. parahemolyticus; 25.0 μM	Sun et al. (2020)
Aspertides D (**96**)	A. tamarii MA-21 and *A. insuetus* SD-512	Mangrove plant *Sonneratia paracaseolaris*, Wenchang, Hainan province, China and deep-sea sediment, the South China Sea	HQ891663 MN696202	Anti-*E. tarda*, *V. alginolyticus*, *V. anguillarum*, and *V. vulnificus*; 8.0, 16, 32, and 8.0 μg/mL	Chi et al. (2023)
Aspertides E (**97**)	A. tamarii MA-21 and *A. insuetus* SD-512	Mangrove plant *S. paracaseolaris*, Wenchang, Hainan province, China and deep-sea sediment, the South China Sea	HQ891663 MN696202	Anti-*E. tarda* and *S. aureus*; 16 and 8.0 μg/mL	Chi et al. (2023)
Unguisins A (**98**)	*A. nidulans* M256	Marine sponge *Echinodictyum conulosum*, the Bai Tu Long Sea, Quang Ninh province, Vietnam	OR166104.1	Anti-*E. faecalis*; 32 μg/mL	Thi et al. (2023)
Unguisins B (**99**)	*A. nidulans* M256	Marine sponge *E. conulosum*, the Bai Tu Long Sea, Quang Ninh province, Vietnam	OR166104.1	Anti-*E. faecalis*; 128 μg/mL	Thi et al. (2023)
Ochratoxin A methyl ester (**100**)	*A. elegans* KUFA0015	Marine sponge *Monanchora unguiculata*, the Kram Island, Thailand	KX431209	Anti-*E. faecalis* ATCC 29212, B3/101, and *S. aureus* ATCC29213; 16, 16, and 8 μg/mL	Kumla et al. (2021)
Aspergamide A (**101**)	Aspergillus sp. LS53	Marine sponge, Sanya, Hainan province, China	–	Anti-*V. harveyi*; 16 μg/mL	Zhang L. et al. (2020); Zhang Y. H. et al. (2020)
11-*O*-methylpseurotin A (**102**)	*A. fumigatus* H22	Seawater, the Western Pacific	–	Anti-MRSA; 10 μM	Zhang R. et al. (2022)
Azaspirofuran B (**103**)	*A. fumigatus* H22	Seawater, the Western Pacific	–	Anti-MRSA; 5 μM	Zhang R. et al. (2022)

(Continued)

10.3389/fmicb.2024.1464135

TABLE 1 (Continued)

Compounds	Producing strains	Habitats	Genbank accession number	Antibacterial activity the MIC values	References
Azaspirofuran A (**104**)	*A. fumigatus* H22	Seawater, the Western Pacific	–	Anti-MRSA; 5 μM	Zhang R. et al. (2022)
Dibetanide (**105**)	Aspergillus sp. LS57	Marine sponge, the Xisha islands, China	–	Anti-*B. cinerea*; 256 μg/mL	Li W. H. et al. (2023)
Ochratoxin B (**106**)	*A. elegans* KUFA0015	Marine sponge *Monanchora unguiculata* the Kram Island, Thailand		Anti-*S. aureus* 272,123; 50 μg/mL	Duraes et al. (2021)
Dihydroisoflavipucine (**107**)	Aspergillus sp.	Marine sponge *Tethya aurantium*, the Adriatic Sea	–	Anti-*S. aureus*, *S. putrefaciens*, and *V. natriegens*; 0.001 μg/mL	Zhou et al. (2014)
(+)-Asperfuranone (**108**)	*A. terreus* RA2905	Sea hare *Aplysia pulmonica*, the South China Sea	MK611650	Weak (anti-*P. aeruginosa*)	Wu et al. (2020b)
(−)-Asperfuranone (**109**)	*A. terreus* RA2905	Sea hare *A. pulmonica*, the South China Sea	MK611650	Anti-*P. aeruginosa*; 128 μg/mL	Wu et al. (2020b)
Carneusin B (**110**)	*A. carneus* GXIMD00519	Marine coral, the Weizhou Islands, Guangxi province, China	MT672623	Anti-*V. rotiferianus* and *A. macleodii*; 64 μg/mL	Lu et al. (2023)
Asperalin A (**111**)	*A. alabamensis* SYSU-6778	Mangrove plant *Enhalus acoroides*, the Dongzhai Port, Hainan province, China	MH863631.1	Anti-*S. aureus*, *S. iniae*, and *S. parauberis*; 21.8, 21.8, and 43.6 μM	Hu et al. (2023)
Asperalin B (**112**)	*A. alabamensis* SYSU-6778	Mangrove plant *E. acoroides*, the Dongzhai Port, Hainan province, China	MH863631.1	Anti-*S. aureus*, *S. iniae*, and *S. parauberis*; 21.8, 21.8, and 43.6 μM	Hu et al. (2023)
Asperalin C (**113**)	*A. alabamensis* SYSU-6778	Mangrove plant *E. acoroides*, the Dongzhai Port, Hainan province, China	MH863631.1	Anti-*S. aureus*, *S. iniae*, and *S. parauberis*; 10.1, 5.0, and 10.1 μM	Hu et al. (2023)
Asperalin D (**114**)	*A. alabamensis* SYSU-6778	Mangrove plant *E. acoroides*, the Dongzhai Port, Hainan province, China	MH863631.1	Anti-*S. aureus*, *S. iniae*, and *S. parauberis*; 10.1, 5.0, and 10.1 μM	Hu et al. (2023)
Asperalin E (**115**)	*A. alabamensis* SYSU-6778	Mangrove plant *E. acoroides*, the Dongzhai Port, Hainan province, China	MH863631.1	Anti-*S. iniae* and *S. parauberis*; 2.2 and 71.1 μM	Hu et al. (2023)
Asperalin *F* (**116**)	*A. alabamensis* SYSU-6778	Mangrove plant *E. acoroides*, the Dongzhai Port, Hainan province, China	MH863631.1	Anti-*S. aureus*, *S. iniae*, *S. parauberis*, *B. subtilis*, and *E. ictalurid*; 21.8, 43.6, 87.3, 21.8, and 10.9 μM	Hu et al. (2023)
N-(3-acetamidopropyl)-3,4-dihydroxybenzamide (**117**)	*A. alabamensis* SYSU-6778	Mangrove plant *E. acoroides*, the Dongzhai Port, Hainan province, China	MH863631.1	Anti-*E. ictalurid*; 79.3 μM	Hu et al. (2023)
Sclerotiamide I (**118**)	A. sclerotiorum LZDX-33-4.	Marine gorgonian coral, the South China Sea	OK012383.1	Anti-*S. aureus* ATCC29213; 16 μM	Meng et al. (2022)
Sclerotiamide J (**119**)	A. sclerotiorum LZDX-33-4.	Marine gorgonian coral, the South China Sea	OK012383.1	Anti-*S. aureus* ATCC29213; 16 μM	Meng et al. (2022)
Kipukasin H (**120**)	*A. versicolor*	Marine gorgonian *Dichotella* gemmacea, the Xisha Islands, the South China Sea	AY373880	Anti-*S. epidermidis*; 12.5 μg/mL	Chen et al. (2014)
Kipukasin I (**121**)	*A. versicolor*	Marine gorgonian *D.* gemmacea, the Xisha Islands, the South China Sea	AY373880	Anti-*S. epidermidis*; 12.5 μg/mL	Chen et al. (2014)
Kipukasin E (**122**)	*A. versicolor*	Marine gorgonian *D.* gemmacea, the Xisha Islands, the South China Sea	AY373880	Anti-*S. epidermidis*; 50.0 μg/mL	Chen et al. (2014)

(Continued)

10.3389/fmicb.2024.1464135

TABLE 1 (Continued)

Compounds	Producing strains	Habitats	Genbank accession number	Antibacterial activity the MIC values	References
Kipukasin D (**123**)	*A. versicolor*	Marine gorgonian *D.* gemmacea, the Xisha Islands, the South China Sea	AY373880	Anti-*S. epidermidis*; 50.0 μg/mL	Chen et al. (2014)
Perinadine B (**124**)	Aspergillus sp. LS116	Marine sponge, Linshui, Hainan province, China	FJ864703	Anti-*B. subtilis*; 32.0 μg/mL	Liu Y. et al. (2022)
Perinadine C (**125**)	Aspergillus sp. LS116	Marine sponge, Linshui, Hainan province, China	FJ864703	Anti-*B. subtilis*; 64.0 μg/mL	Liu Y. et al. (2022)
Neoaspergillic (**126**)	*Aspergillus* sp. CF07002	Marine sediment, the eastern Pacific Ocean off Panama	KM819008	Anti-*B. cereus*, *K. pneumoniae*, and *E. coli*; 30.0–40.0 μg/mL	Cardoso-Martinez et al. (2015)
Hydroxyneoaspergillic acid (**127**)	A. ochraceopetaliformis SCSIO 41018	Marine sponge	MH109740.1	Anti-MRSA, *S. aureus*, *E. faecalis*, *A. baumannii*, *E. coli*, and *K. pneumonia*; 7.8, 7.8, 0.9, 0.45, 62.5, and 7.8 μg/mL	Guo et al. (2021)
Dizinchydroxyneoaspergillin (**128**)	A. ochraceopetaliformis SCSIO 41018	Marine sponge	MH109740.1	Anti-MRSA, *S. aureus*, *E. faecalis*, *A. baumannii*, *E. coli*, and *K. pneumonia*; 3.9, 3.9, 0.9, 0.45, 125, and 3.9 μg/mL	Guo et al. (2021)
Puniceusine N (**129**)	*A. puniceus* SCSIO z021	Deep-sea sediment, Okinawa Trough	GU456970	Anti-*S. aureus*, MRSA and *E. coli*; 100 μg/mL	Liu C. M. et al. (2022)
Preussin (**130**)	*A. candidus* KUFA0062	Marine sponge, the coral reef at Similan Island National Park, Thailand	KX431210	Anti-*S. aureus* ATCC 29213, *E. faecalis* ATCC 29212, B3/101, and MRSA; 32, 32, 64, and 32 μg/mL	Buttachon et al. (2018)
6,6′-Oxybis(1,3,8-trihydroxy-2-((*S*)-1-methoxyhexyl) anthracene-9,10-dione) (**131**)	*A. versicolor* INF16-17	Marine clam, the East China Sea	–	Anti-*S. aureus*; 30 μg/mL	Li et al. (2019)
6,6′-Oxybis(1,3,8-trihydroxy-2-((*S*)-1-hydroxyhexyl) anthracene-9,10-dione) (**132**)	*A. versicolor* INF16-17	Marine clam, the East China Sea	–	Anti-*S. aureus*; 30 μg/mL	Li et al. (2019)
Xanthomegnin (**133**)	*A. elegans* KUFA0015	Marine sponge *Monanchora unguiculata* the Kram Island, Thailand	KX431209	Anti-*E. faecalis* ATCC 29212, *S. aureus* ATCC 29213, and MRSA; 32, 32, and 16 μg/mL	Kumla et al. (2021)
Viomellein (**134**)	*A. elegans* KUFA0015	Marine sponge *Monanchora unguiculata* the Kram Island, Thailand	KX431209	Anti-*E. faecalis* ATCC 29212, *S. aureus* ATCC 29213, and MRSA; 8, 8 and 2 μg/mL	Kumla et al. (2021)
Versiconol B (**135**)	Aspergillus sp. F40	Marine sponge, the sea area near Xuwen County, Guangdong province, China	KT164776	Anti-*S. aureus* and *V. parahaemolyticus*; 48 and 24 μg/mL	Tian et al. (2018)
Versiconol (**136**)	Aspergillus sp. F40	Marine sponge, the sea area near Xuwen County, Guangdong province, China	KT164776	Anti-*V. parahaemolyticus*; 12 μg/mL	Tian et al. (2018)
2-(Dimethoxymethyl)-1-hydro xyanthracene-9,10-dione (**137**)	*A. versicolor* 3A00029	Deep-sea sediment, the West Pacific Ocean	–	Anti-MRSA, *V. vulnificus*, *V. rotiferianus*, and *V. campbellii*; 3.9, 31.3, 62.5, and 15.6 μg/mL	Wang et al. (2018)

(Continued)

10.3389/fmicb.2024.1464135

TABLE 1 (Continued)

Compounds	Producing strains	Habitats	Genbank accession number	Antibacterial activity the MIC values	References
Damnacanthal (**138**)	*A. versicolor* 3A00029	Deep-sea sediment, the West Pacific Ocean	–	Anti-MRSA, *V. vulnificus*, *V. rotiferianus*, and *V. campbellii*; 62.5, 62.5, 62.5, and 125 μg/mL	Wang et al. (2018)
Xanthopurpurin (**139**)	*A. versicolor* 3A00029	Deep-sea sediment, the West Pacific Ocean	–	Anti-MRSA, *V. vulnificus*, *V. rotiferianus*, and *V. campbellii*; 62.5, 62.5, 125, and 62.5 μg/mL	Wang et al. (2018)
Isoversicolorin C (**140**)	*A. nidulans* MA-143	Mangrove plant Rhizophora stylosa	JQ839285	Anti-*E. coli*, *M. luteus*, *V. vulnificus*, *V. alginolyticus*, *E. ictaluri*, and *V. parahaemolyticus*; 32, 16, 64, 1, 4, and 32 μg/mL	Yang et al. (2018a)
Versicolorin C (**141**)	*A. nidulans* MA-143	Mangrove plant *R. stylosa*	JQ839285	Anti-*E. coli*, *M. luteus*, *V. anguillarum*, *V. alginolyticus*, *E. ictaluri*, and *V. parahaemolyticus*; 1, 32, 4, 16, 8, and 1 μg/mL	Yang et al. (2018a)
Emodin (**142**)	*A. fumigatus* MF029	Marine sponge *Hymeniacidon perleve*, the Bohai Sea	MH974808	Anti-MRSA, *S. aureus*, and BCG; 50, 50, and 1.25 μg/mL	Song Z. J. et al. (2021)
6,8-Di-*O*-methylaverufin (**143**)	*A. versicolor* pt20	Marine brown alga *Spiraea thunbergii*, the Pingtan Island, Fujian province, China	–	Anti-*E. coli* and *S. aureus*; Inhibitory diameters of 10 and 10 mm at 30 μg/disk	Miao et al. (2012)
6-*O*-methylaverufin (**144**)	*A. versicolor* pt20	Marine brown alga *S. thunbergii*, the Pingtan Island, Fujian province, China	–	Anti-*E. coli* and *S. aureus*; Inhibitory diameters of 10 and 10 mm at 30 μg/disk	Miao et al. (2012)
6,8-Di-*O*-methylaverantin (**145**)	*A. versicolor* EN-7	Marine brown alga *S. thunbergia*, the Qingdao coastline, Shandong province, China	EU042148	Weak (anti-*E. coli*); Inhibitory diameter of 7.0 mm at 20 μg/disk	Zhang et al. (2012)
6,8-Di-*O*-methylversiconol (**146**)	*A. versicolor* EN-7	Marine brown alga *S. thunbergia*, the Qingdao coastline, Shandong province, China	EU042148	Weak (anti-*E. coli*); Inhibitory diameter of 6.5 mm at 20 μg/disk	Zhang et al. (2012)
Averantin (**147**)	*A. versicolor* PF10M	Marine sponge, the Jeju Island, Korea	–	Anti-*S. pyogenes* 308A, 77A, and *S. aureus* SG511, 285, 503; 0.78, 3.13, 3.13, 3.13, and 1.56 μg/mL	Lee et al. (2010)
Averufin (**148**)	*A. versicolor* PF10M	Marine sponge, the Jeju Island, Korea	–	Anti-*S. pyogenes* 308A and *S. aureus* SG511, 285, 503; 6.25, 12.50, 12.50, and 6.25 μg/mL	Lee et al. (2010)
Nidurufin (**149**)	*A. versicolor* PF10M	Marine sponge, the Jeju Island, Korea	–	Anti-*S. pyogenes* 308A, 77A, and *S. aureus* SG511, 285, 503; 3.13, 6.25, 6.25, 3.13, 3.13, and 3.13 μg/mL	Lee et al. (2010)
6,8-Di-*O*-methylversicolorin A (**150**)	*Aspergillus* sp. WHUF05236	Deep-sea sediment	OM638737	Anti-*H. pylori* 26,695 and G27; 43.47 μM	Lv et al. (2022)
Asperpyrone A (**151**)	Aspergillus sp. DM94	The rhizosphere soil of mangrove plant *Bruguiera gymnorrhiza*	–	Anti-*H. pylori* G27 and Hp159; 4 μg/mL	Gou et al. (2020)
Aurasperone A (**152**)	Aspergillus sp. DM94	The rhizosphere soil of mangrove plant *B. gymnorrhiza*	–	Anti-*H. pylori* G27 and Hp159; 8 and 16 μg/mL	Gou et al. (2020)
Aurasperone *F* (**153**)	Aspergillus sp. DM94	The rhizosphere soil of mangrove plant *B. gymnorrhiza*	–	Anti-*H. pylori* G27 and Hp159; 4 μg/mL	Gou et al. (2020)

(Continued)

10.3389/fmicb.2024.1464135

TABLE 1 (Continued)

Compounds	Producing strains	Habitats	Genbank accession number	Antibacterial activity the MIC values	References
Aurasperone B (**154**)	Aspergillus sp. DM94	The rhizosphere soil of mangrove plant *B. gymnorrhiza*	–	Anti-*H. pylori* G27 and Hp159; 8 and 16 μg/mL	Gou et al. (2020)
Fonsecinone A (**155**)	Aspergillus sp. DM94	the rhizosphere soil of mangrove plant *B. gymnorrhiza*	–	Anti-*H. pylori*; 16 μg/mL	Gou et al. (2020)
Asperpyrones C (**156**)	Aspergillus sp. DM94	the rhizosphere soil of mangrove plant *B. gymnorrhiza*	–	Anti-*H. pylori*; 16 μg/mL	Gou et al. (2020)
	A. welwitschiae CUGBMF180262	mud sample, the Xinglin Bay, XiaMen, China	MT120310	Anti-*H. pylori* G27 and Hp159; 4 μg/mL	Han et al. (2022)
Aspergixanthone I (**157**)	Aspergillus sp. ZA-01	Sediment, the Bohai Sea	–	Anti-V. parahemolyticus, *V. anguillarum*, and *V. alginolyticus*; 1.56, 1.56, and 3.12 μM	Zhu et al. (2018)
Aspergixanthone J (**158**)	Aspergillus sp. ZA-01	Sediment, the Bohai Sea	–	Anti-V. parahemolyticus, *V. anguillarum*, and *V. alginolyticus*; 6.25, 25.0, and 25.0 μM	Zhu et al. (2018)
Aspergixanthone K (**159**)	Aspergillus sp. ZA-01	Sediment, the Bohai Sea	–	Anti-V. parahemolyticus, *V. anguillarum*, and *V. alginolyticus*; 3.12, 25.0, and 12.5 μM	Zhu et al. (2018)
Aspergixanthone A (**160**)	Aspergillus sp. ZA-01	Sediment, the Bohai Sea	–	Anti-V. parahemolyticus, *V. anguillarum*, and *V. alginolyticus*; 25.0 μM	Zhu et al. (2018)
15-Acetyl tajixanthone hydrate (**161**)	Aspergillus sp. ZA-01	Sediment, the Bohai Sea	–	Anti-V. parahemolyticus, *V. anguillarum*, and *V. alginolyticus*; 12.5, 25.0, and 12.5 μM	Zhu et al. (2018)
Tajixanthone hydrate (**162**)	Aspergillus sp. ZA-01	Sediment, the Bohai Sea	–	Anti-V. parahemolyticus, *V. anguillarum*, and *V. alginolyticus*; 6.25, 6.25, and 12.5 μM	Zhu et al. (2018)
16-Chlorotajixanthone (**163**)	Aspergillus sp. ZA-01	Sediment, the Bohai Sea	–	Anti-V. parahemolyticus, *V. anguillarum*, and *V. alginolyticus*; 25.0, 6.25, and 25.0 μM	Zhu et al. (2018)
Secalonic acid D (**164**)	A. aculeatinus WHUF0198	Deep-sea sediment, the South China Sea	–	*H. pylori* G27, 26,695, 129, 159, *S. aureus* USA300, and *B. subtilis* 168; 4.0, 4.0, 2.0, 2.0, 2.0, and 1.0 μg/mL	Wu et al. (2023)
5-Epi-asperdichrome (**165**)	*A. versicolor* HDN1009	Mangrove soil, Guangzhou, China	KP765236	Anti-V. parahemolyticus, *B. subtilis*, *M. phlei*, and *P. aeruginosa*; 100, 200, 200, and 100 μg/mL	Yu et al. (2018)
Aflaxanthone A (**166**)	*A. flavus* QQYZ	Mangrove plant *Kandelia candel*, Huizhou, Guangdong province, China	JQ776536.1	Anti-MRSA and *B. subtilis*; 12.5 and 25 μg/mL	Zang et al. (2022)
Aflaxanthone B (**167**)	*A. flavus* QQYZ	Mangrove plant *K. candel*, Huizhou, Guangdong province, China	JQ776536.1	Anti-*B. subtilis*; 25 μg/mL	Zang et al. (2022)
5-Methoxydihydrosterigmatocystin (**168**)	*A. versicolor* MF359	Marine sponge *H. perleve*, the Bohai Sea	HQ000003	Anti-*B. subtilis* and *S. aureus*; 3.125 and 12.5 μg/mL	Song et al. (2014)
Oxisterigmatocystin C (**169**)	Aspergillus sp. F40	Marine sponge, the sea area near Xuwen County, Guangdong province, China	KT164776	Anti-*S. aureus*; 48 μg/mL	Tian et al. (2018)

(Continued)

10.3389/fmicb.2024.1464135

TABLE 1 (Continued)

Compounds	Producing strains	Habitats	Genbank accession number	Antibacterial activity the MIC values	References
Sterigmatocystin (**170**)	A. sydowii DC08	Marine sponge, the Mandeh, South Coast, West Sumatra, Indonesia island	–	Anti-MRSA, MDPRA, *P. aeruginosa* ATCC 27853, *S. aureus* ATCC 25923, and *E. coli* ATCC 25922; 64, 128, 32, 32, and 16 μg/mL	Handayani et al. (2022)
2-Hydroxy-6-formyl-vertixanthone (**171**)	*A. sydowii* C1-S01-A7	Seawater, the West Pacific Ocean	MH571963	Anti-MRSA and CGMCC 1.12409; 16.3 and 16.1 μg/mL	Wang et al. (2019)
12-*O*-acetyl-sydowinin A (**172**)	*A. sydowii* C1-S01-A7	Seawater, the West Pacific Ocean	MH571963	Anti-MRSA and CGMCC 1.12409; 32.6 and 31.8 μg/mL	Wang et al. (2019)
Aspergillusone A (**173**)	*A. sydowii* C1-S01-A7	Seawater, the West Pacific Ocean	MH571963	Anti-MRSA and CGMCC 1.12409; 32.2 and 32.4 μg/mL	Wang et al. (2019)
AGI-B4 (**174**)	A. sydowii C1-S01-A7	Seawater, the West Pacific Ocean	MH571963	Anti-*V. vulnificus* MCCC E1758, MRSA, and CGMCC 1.12409; 32.5, 32.9 and 16.3 μg/mL	Wang et al. (2019)
Isosecosterigmatocystin (**175**)	*A. nidulans* MA-143	Mangrove plant *R. stylosa*	JQ839285	Anti-*E. ictaluri*; 16 μg/mL	Yang et al. (2018a)
Seco-penicitrinol A (**176**)	A. sydowii EN-534 and P. citrinum EN-535	Marine red alga *Laurencia okamurai*, Qingdao, Shandong province, China	MG242135 MG242136	Anti-*E. ictaluri* and *V. alginolyticus*; 64 and 32 μg/mL	Yang et al. (2018b)
Secalonic acid F1 (**177**)	A. brunneoviolaceus MF180246	Mangrove mud sample, the Xinglin Bay, Xiamen, China	–	Anti-*S. aureus*; 25 μg/mL	Xu et al. (2024)
Secalonic acid H (**178**)	A. brunneoviolaceus MF180246	Mangrove mud sample, the Xinglin Bay, Xiamen, China	–	Anti-*S. aureus*; 50 μg/mL	Xu et al. (2024)
Penicillixanthone A (**179**)	A. brunneoviolaceus MF180246	Mangrove mud sample, the Xinglin Bay, Xiamen, China	–	Anti-*S. aureus*; 6.25 μg/mL	Xu et al. (2024)
Chrysoxanthone C (**180**)	A. brunneoviolaceus MF180246	Mangrove mud sample, the Xinglin Bay, Xiamen, China	–	Anti-*S. aureus*; 50 μg/mL	Xu et al. (2024)
Aspergetherin A (**181**)	*A. terreus* 164,018	Marine sponge, the South China Sea	–	Anti-MRSA 05–72 and USA300; 128 μg/mL	Li J. X. et al. (2023)
Vioxanthin (**182**)	*A. elegans* KUFA0015	Marine sponge *Monanchora unguiculata* the Kram Island, Thailand	KX431209	Anti-*E. faecalis* ATCC29212, VRE, *S. aureus* ATCC 29213, and MRSA; 2, 1, 2, and 0.5 μg/mL	Kumla et al. (2021)
Aspulvinone B′ (**183**)	*A. flavipes* KUFA1152	Marine sponge *Mycale* sp., the Samaesan Island, Thailand	MT814286	Anti-*E. faecalis* ATCC29212, VRE, *S. aureus* ATCC 29213, and MRSA;32, 32, 16, and 16 μg/mL	Machado et al. (2021)
Aspulvinone H (**184**)	*A. flavipes* KUFA1152	Marine sponge *Mycale* sp., the Samaesan Island, Thailand	MT814286	Anti-*E. faecalis* ATCC29212, VRE, *S. aureus* ATCC 29213, and MRSA; 32, 64, 16 and 16 μg/mL	Machado et al. (2021)
Aspulvinone R (**185**)	*A. flavipes* KUFA1152	Marine sponge *Mycale* sp., the Samaesan Island, Thailand	MT814286	Anti-*E. faecalis* ATCC29212, VRE, *S. aureus* ATCC 29213, and MRSA; 8, 16, 8 and 16 μg/mL	Machado et al. (2021)
Aspulvinone S (**186**)	*A. flavipes* KUFA1152	Marine sponge *Mycale* sp., the Samaesan Island, Thailand	MT814286	Anti-*E. faecalis* ATCC29212, VRE, *S. aureus* ATCC 29213, and MRSA; 8, 8, 4, and 16 μg/mL	Machado et al. (2021)

(Continued)

10.3389/fmicb.2024.1464135

TABLE 1 (Continued)

Compounds	Producing strains	Habitats	Genbank accession number	Antibacterial activity the MIC values	References
Asperteretal E (**187**)	*A. terreus* SCSIO FZQ028	Deep-sea sediment, the South China	KX792117	Weak (anti-*S. aureus*, *B. thuringiensis*, *B. subtilis*, and *E. coli*); Inhibitory diameters of 8.94, 9.77, 7.98, and 7.53 mm at 30 μg/disk	Zeng et al. (2020b)
Aspernolide A (**188**)	*A. terreus* SCSIO FZQ028	Deep-sea sediment, the South China	KX792117	Weak (anti-*S. aureus*, *B. thuringiensis*, *B. subtilis*, and *E. coli*); Inhibitory diameters of 8.16, 9.13, 7.49, and 7.64 mm at 30 μg/disk	Zeng et al. (2020b)
Butyrolactone I (**189**)	*Aspergillus* sp. SCSIO 41029	Deep-sea sediment, the South China	MH591418.1	Anti-*S. aureus*; 0.78 μg/mL	Chen et al. (2021)
Asperbutenolide D (**190**)	*A. terreus* SCAU011	The rhizosphere sediment of a mangrove plant *R. stylosa*, the Techeng Isle, China	KY827341	Anti-*S. aureus*; 21.3 μM	Bao et al. (2021)
(+)-3′,3′-Di-(dimethylallyl)-butyrolactone II (**191**)	*A. terreus* SCAU011	The rhizosphere sediment of a mangrove plant *R. stylosa*, the Techeng Isle, China	KY827341	Anti-*S. aureus*; 17.4 μM	Bao et al. (2021)
Aspernolide E (**192**)	*A. terreus* SCAU011	The rhizosphere sediment of a mangrove plant *R. stylosa*, the Techeng Isle, China	KY827341	Anti-*S. aureus*; 26.1 μM	Bao et al. (2021)
Flavipesin A (**193**)	*A. flavipes* AIL8	Mangrove plant Acanthus ilicifolius, the Daya Bay, Shenzhen, China	–	Anti-*S. aureus* and *B. subtillis*; 8.0 and 0.25 μg/mL	Bai et al. (2014)
Versicolactone B (**194**)	*A. terreus* SCSIO41404	Marine soft coral *Sinularia* sp., the Sanya Bay, the South China Sea	KU866665.1	Anti-*E. faecalis*; 25 μg/mL	Peng et al. (2022)
Butyrolactone VI (**195**)	*A. terreus* SCSIO41404	Marine soft coral *Sinularia* sp., the Sanya Bay, the South China Sea	KU866665.1	Anti-*K. pneumoniae*; 50 μg/mL	Peng et al. (2022)
Asperbutenolide A (**196**)	*A. terreus* SCAU011	the rhizosphere soil of mangrove plant R. stylosa, the Techeng Isle, China	–	Anti-*S. aureus* and *V. splendidus*; 1.30 and 3.70 μg/mL	Bao et al. (2020)
5*R*-(+)-9-Hydroxy-microperfuranone (**197**)	Aspergillus sp. ZZ1861	Sea mud, the coastal area of Putuo, Zhoushan, China	OR985107	Anti-*E. coli*; 50 μg/mL	Ha et al. (2024)
5*R*-(+)-Microperfuranone (**198**)	*Aspergillus* sp. ZZ1861	Sea mud, the coastal area of Putuo, Zhoushan, China	OR985107	Anti-*E. coli*; 25 μg/mL	Ha et al. (2024)
Asperpyranone A (**199**)	*A. terreus* RA2905	Sea hare *A. pulmonica*, the South China Sea	MK611650	Anti-*P. aeruginosa*; 32 μg/mL	Wu et al. (2020b)
Asperpyranone B (**200**)	*A. terreus* RA2905	Sea hare *A. pulmonica*, the South China Sea	MK611650	Anti-*P. aeruginosa*; 128 μg/mL	Wu et al. (2020b)
Nectriapyrone (**201**)	Aspergillus sp. LS53	Marine sponge *Haliclona* sp., Sanya, Hainan province, China	–	Anti-*V. harveyi*; 64 μg/mL	Zhang L. et al. (2020); Zhang Y. H. et al. (2020)
Asperisocoumarin A (**202**)	Aspergillus sp. LS53	Marine sponge *Haliclona* sp., Sanya, Hainan province, China	–	Anti-*V. harveyi*; 32 μg/mL	Zhang L. et al. (2020); Zhang Y. H. et al. (2020)

(Continued)

10.3389/fmicb.2024.1464135

TABLE 1 (Continued)

Compounds	Producing strains	Habitats	Genbank accession number	Antibacterial activity the MIC values	References
Unguinol (**203**)	A. unguis WR8	Marine sponge *Haliclona fascigera*, the Mandeh Island, South Coast of West Sumatera, Indonesia	MN273740	Anti-*E. coli*, *P. aeruginosa*, *S. aureus*, *E. faecalis*, *B. subtilis*, MRSA, *S. typosa*, *V. cholerae*, and *M. luteus*; 1.56, 3.12, 3.12, 3.12, 0.78, 3.12, 3.12, 0.78, and 0.78 μg/disk	Handayani et al. (2020)
	A. unguis PSU-MF16	Marine sponge *Dysidea* sp., the Koh Bulon Mai Pai, Satun Province, Thailand	KY397987	Anti-*S. aureus*; 128 μg/mL	Saetang et al. (2021)
2-Chlorounguinol (**204**)	A. unguis WR8	Marine sponge *H. fascigera*, the Mandeh Island, South Coast of West Sumatera, Indonesia	MN273740	Anti-*E. coli*, *P. aeruginosa*, *S. aureus*, *E. faecalis*, *B. subtilis*, MRSA, *S. typosa*, *V. cholerae*, and *M. luteus*; 1.56, 1.56,1.56, 0.78, 0.78, 0.78, 1.56, 0.78, and 0.78 μg/dis	Handayani et al. (2020)
	A. unguis PSU-MF16	Marine sponge *Dysidea* sp., the Koh Bulon Mai Pai, Satun Province, Thailand	KY397987	Anti-*S. aureus* and MRSA; 8 μg/mL	Saetang et al. (2021)
Nidulin (**205**)	A. unguis WR8	Marine sponge *H. fascigera*, the Mandeh Island, South Coast of West Sumatera, Indonesia	MN273740	Anti-*E. coli*, *P. aeruginosa*, *S. aureus*, *E. faecalis*, *B. subtilis*, MRSA, *S. typosa*, *V. cholerae*, and *M. luteus*; 0.78, 1.56, 0.78, 0.78, 0.78, 0.78, 1.56, 0.78, and 0.78 μg/disk	Handayani et al. (2020)
Aspergillusidone H (**206**)	*A. unguis* GXIMD 02505	Marine coral *Pocillopora damicornis*, the Weizhou Islands, Guangxi, China	OL989238	Weak (anti-MRSA)	Zhang Y. T. et al. (2022)
Nornidulin (**207**)	*A. unguis* GXIMD 02505	Marine coral *P. damicornis*, the Weizhou Islands, Guangxi, China	OL989238	Anti-MRSA, *M. variabilis*, and *M. jannaschii*; 2, 8, and 16 μg/mL	Zhang Y. T. et al. (2022)
	A. unguis PSU-MF16	Marine sponge *Dysidea* sp., the Koh Bulon Mai Pai, Satun Province, Thailand	KY397987	Anti-*S. aureus* and MRSA; 2 μg/mL	Saetang et al. (2021)
Aspergillusidone B (**208**)	*A. unguis* GXIMD 02505	Marine coral *P. damicornis*, the Weizhou Islands, Guangxi, China	OL989238	*M. variabilis*; 128 μg/mL	Zhang Y. T. et al. (2022)
Aspergillusidone C (**209**)	*A. unguis* GXIMD 02505	Marine coral *P. damicornis*, the Weizhou Islands, Guangxi, China	OL989238	Anti-MRSA, *M. variabilis*, and *M. jannaschii*; 32, 8 and 32 μg/mL	Zhang Y. T. et al. (2022)
	A. unguis PSU-MF16	Marine sponge *Dysidea* sp., the Koh Bulon Mai Pai, Satun Province, Thailand	KY397987	Anti-*S. aureus* and MRSA; 2 and 1 μg/mL	Saetang et al. (2021)
7-Dechloronidulin (**210**)	*A. nidulans* M256	Marine sponge *E. conulosum*, the Bai Tu Long Sea, Quang Ninh province, Vietnam	OR166104.1	Anti-*B. cereus*, *E. faecalis*, and *S. aureus*; 2, 4 and 4 μg/mL	Thi et al. (2023)
2,4-Dichlorounguinol (**211**)	*A. nidulans* M256	Marine sponge *E. conulosum*, the Bai Tu Long Sea, Quang Ninh province, Vietnam	OR166104.1	Anti-*B. cereus*, *E. faecalis*, *S. aureus*, *E. coli*, *P. aeruginosa*, and *S. enterica*; 16, 32, 32, 16, 64 and 32 μg/mL	Thi et al. (2023)

(Continued)

10.3389/fmicb.2024.1464135

TABLE 1 (Continued)

Compounds	Producing strains	Habitats	Genbank accession number	Antibacterial activity the MIC values	References
Emeguisin B (**212**)	*A. nidulans* M256	Marine sponge *E. conulosum*, the Bai Tu Long Sea, Quang Ninh province, Vietnam	OR166104.1	Anti-*E. faecalis* and *S. aureus*; 256 and 128 μg/mL	Thi et al. (2023)
Asperunguissidone A (**213**)	*A. unguis* PSU-MF16	Marine sponge *Dysidea* sp., the Koh Bulon Mai Pai, Satun Province, Thailand	KY397987	Anti-*S. aureus* and MRSA; 64 μg/mL	Saetang et al. (2021)
Asperunguislide A (**214**)	*A. unguis* PSU-MF16	Marine sponge *Dysidea* sp., the Koh Bulon Mai Pai, Satun Province, Thailand	KY397987	Anti-*M. gypseum*; 200 μg/mL	Saetang et al. (2021)
Asperlide (**215**)	*A. unguis* PSU-MF16	Marine sponge *Dysidea* sp., the Koh Bulon Mai Pai, Satun Province, Thailand	KY397987	Anti-*S. aureus* and MRSA; 200 μg/mL	Saetang et al. (2021)
Aspergiside C (**216**)	*A. unguis* PSU-MF16	Marine sponge *Dysidea* sp., the Koh Bulon Mai Pai, Satun Province, Thailand	KY397987	Anti-*S. aureus* and MRSA; 200 μg/mL	Saetang et al. (2021)
(3*S*)-3-Ethyl-5,7-dihydroxy-3,6-Dimethyl-phthalide (**217**)	*A. unguis* PSU-MF16	Marine sponge *Dysidea* sp., the Koh Bulon Mai Pai, Satun Province, Thailand	KY397987	Anti-*S. aureus* and MRSA; 2 and 4 μg/mL	Saetang et al. (2021)
Aspergisidone (**218**)	*A. unguis* PSU-MF16	Marine sponge *Dysidea* sp., the Koh Bulon Mai Pai, Satun Province, Thailand	KY397987	Anti-*S. aureus* and MRSA; 32 and 64 μg/mL	Saetang et al. (2021)
Folipastatin (**219**)	*A. unguis* PSU-MF16	Marine sponge *Dysidea* sp., the Koh Bulon Mai Pai, Satun Province, Thailand	KY397987	Anti-*S. aureus* and MRSA; 2 and 1 μg/mL	Saetang et al. (2021)
Emeguisins A (**220**)	*A. unguis* PSU-MF16	Marine sponge *Dysidea* sp., the Koh Bulon Mai Pai, Satun Province, Thailand	KY397987	Anti-*S. aureus* and MRSA; 0.5 μg/mL	Saetang et al. (2021)
8-Demethoxy-10-methoxy-wentiquinone C (**221**)	A. sydowii C1-S01-A7	Seawater, the West Pacific Ocean	MH571963	Anti-MRSA; 32.4 μg/mL	Wang et al. (2019)
Farnesylemefuranone D (**222**)	*A. insuetus* SD-512	Cold-seep sediment, the northeast of the South China Sea	MN650839	Anti-A. hydrophilia, *E. coli*, *E. tarda*, *P. aeruginosa*, *V. alginolyticus*, V. parahemolyticus, and *V. vulnificus*; 8.0, 32, 8.0, 16, 4.0, 16, and 4.0 μg/mL	Chi et al. (2020)
Farnesylemefuranone E (**223**)	*A. insuetus* SD-512	Cold-seep sediment, the northeast of the South China Sea	MN650839	Anti-A. hydrophilia, *E. coli*, *E. tarda*, *P. aeruginosa*, *V. alginolyticus*, V. parahemolyticus, and *V. vulnificus*; 16, 32, 8.0, 16, 8.0, 16, and 4.0 μg/mL	Chi et al. (2020)
Farnesylemefuranone *F* (**224**)	*A. insuetus* SD-512	Cold-seep sediment, the northeast of the South China Sea	MN650839	Anti-A. hydrophilia, *E. coli*, *E. tarda*, *P. aeruginosa*, *V. alginolyticus*, V. parahemolyticus, and *V. vulnificus*; 8.0, 32, 4.0, 8.0, 4.0, 8.0, and 4.0 μg/mL	Chi et al. (2020)
Silvaticol (**225**)	*Aspergillus* sp. ZZ1861	Sea mud sample, the Zhoushan Island, Zhejiang province, China	OR985107	Anti-*E. coli*; 12.5 μg/mL	Ha et al. (2024)
Aspergillumarin A (**226**)	Aspergillus sp.	Mangrove plant *B. gymnorrhiza*, the South China Sea coast	–	Anti-*S. aureus* and *B. subtilis*; 50 μg/mL	Li et al. (2012)

(Continued)

10.3389/fmicb.2024.1464135

TABLE 1 (Continued)

Compounds	Producing strains	Habitats	Genbank accession number	Antibacterial activity the MIC values	References
Aspergillumarin B (**227**)	Aspergillus sp.	Mangrove plant *B. gymnorrhiza*, the South China Sea coast	–	Anti-*S. aureus* and *B. subtilis*; 50 μg/mL	Li et al. (2012)
Aspergimarin G (**228**)	Aspergillus sp. NBUF87.	Marine sponge *Hymeniacidon* sp., the Xisha Islands, the South China Sea	–	Anti-*S. aureus* and *S. enteritidis*; 16 and 64 μg/mL	Lin S. X. et al. (2023)
(*R*)-3-Hydroxymellein (**229**)	*Aspergillus* sp. SCSIO41405	Marine coral, Sanya Bay, the South China Sea	–	Anti-MRSA; 100 μg/mL	Peng et al. (2021)
(3*R*,4*S*)-Trans-4-hydroxymellein (**230**)	*Aspergillus* sp. SCSIO41405	Marine coral, Sanya Bay, the South China Sea	–	Anti-*E. faecalis*; 100 μg/mL	Peng et al. (2021)
Nipyrone A (**231**)	*A. niger* LS24	Marine sponge *Haliclona* sp., Linshui, Hainan province, China	KX290301	Anti-*S. aureus*, *E. coli*, *B. subtilis*, MRSA, and *M. tuberculosis*; 64, 32, 64, 128 and 128 μg/mL	Ding et al. (2019)
Nipyrone B (**232**)	*A. niger* LS24	Marine sponge *Haliclona* sp., Linshui, Hainan province, China	KX290301	Anti-*S. aureus*, *E. coli*, *B. subtilis*, MRSA, and *M. tuberculosis*; 64, 64, 64, 128, and 128 μg/mL	Ding et al. (2019)
Nipyrone C (**233**)	*A. niger* LS24	Marine sponge *Haliclona* sp., Linshui, Hainan province, China	KX290301	Anti-*S. aureus*, *E. coli*, *B. subtilis*, MRSA, and *M. tuberculosis*; 8, 64, 16, 128, and 64 μg/mL	Ding et al. (2019)
Germicidin C (**234**)	*A. niger* LS24	Marine sponge *Haliclona* sp., Linshui, Hainan province, China	KX290301	Anti-*S. aureus*, *E. coli*, *B. subtilis*, MRSA, and *M. tuberculosis*; 64, 64, 32, 128, and 128 μg/mL	Ding et al. (2019)
Sartorypyrone A (**235**)	*Aspergillus* sp. WHUF03110	Mangrove soil sample, the Yalong Bay, Sanya, Hainan province, China	MZ661122	Anti-*B. subtilis*, *S. aureus*, and *H. pylori*; 1–8 μg/mL	Lv et al. (2021)
Asperochrin A (**236**)	*A. ochraceus* MA-15	The rhizospheric soil of mangrove plant *B. gymnorrhiza*, Hainan province, China	KP279929	Anti-A. hydrophilia, *V. anguillarum*, and V. harvevi; 8, 16 and 8 μg/mL	Liu et al. (2015)
Chlorohydroaspyrone A (**237**)	*A. ochraceus* MA-15	The rhizospheric soil of mangrove plant *B. gymnorrhiza*, Hainan province, China	KP279929	Anti-A. hydrophilia, *V. anguillarum*, and V. harvevi; 16, 32 and 16 μg/mL	Liu et al. (2015)
Chlorohydroaspyrone B (**238**)	*A. ochraceus* MA-15	The rhizospheric soil of mangrove plant *B. gymnorrhiza*, Hainan province, China	KP279929	Anti-A. hydrophilia, *V. anguillarum*, and V. harvevi;16, 32 and 32 μg/mL	Liu et al. (2015)
$\Delta^{2'}$-1'-Dehydropenicillide (**239**)	*Aspergillus* sp. IMCASMF180035	A mud sample, the intertidal zones of the Yellow Sea, Qingdao, Shandong province, China	MW015145	Anti-*H. pylori*; 21.73 μM	Song F. H. et al. (2021)
Dehydropenicillide (**240**)	*Aspergillus* sp. IMCASMF180035	A mud sample, the intertidal zones of the Yellow Sea, Shandong province, China	MW015145	Anti-*H. pylori*; 21.61 μM	Song F. H. et al. (2021)
Aspergiloxathene A (**241**)	*Aspergillus* sp. IMCASMF180035	A mud sample, the intertidal zones of the Yellow Sea, Qingdao, Shandong province, China	MW015145	Anti-*S. aureus* and MRSA; 5.60 and 22.40 μM	Song F. H. et al. (2021)
Cowabenzophenone A (**242**)	*A. terreus*	Mangrove plant *B. gymnorrhyza*, Jaffna lagoon, Northern Province, Sri Lanka	–	Anti-*B. subtilis* and *S. aureus*; 1.0 and 2.0 μg/mL	Ukwatta et al. (2020)

(Continued)

10.3389/fmicb.2024.1464135

TABLE 1 (Continued)

Compounds	Producing strains	Habitats	Genbank accession number	Antibacterial activity the MIC values	References
Penicitrinone A (**243**)	A. sydowii EN-534 and P. citrinum EN-535	Marine red alga *L. okamurai*, Qingdao, Shandong province, China	MG242135 MG242136	Anti-*E. coli*, *V. parahaemolyticus*, *V. alginolyticus*, *M. luteus*, and *E. ictaluri*; 64, 16, 32, 16, and 32 μg/mL	Yang et al. (2018b)
Penicitrinone *F* (**244**)	A. sydowii EN-534 and P. citrinum EN-535	Marine red alga *L. okamurai*, Qingdao, Shandong province, China	MG242135 MG242136	Anti-*E. ictaluri*, *V. alginolyticus*, and *V. parahaemolyticus*; 64, 64, and 32 μg/mL	Yang et al. (2018b)
Citrinin (**245**)	A. sydowii EN-534 and P. citrinum EN-535	Marine red alga *L. okamurai*, Qingdao, Shandong province, China	MG242135 MG242136	Anti-*E. coli*, *V. alginolyticus*, *V. parahaemolyticus*, *M. luteus*, and *E. ictaluri*; 8, 16, 8, 16, and 32 μg/mL	Yang et al. (2018b)
25*S*-*O*-methylarugosin A (**246**)	*Aspergillus* sp. ZZ1861	Sea mud sample, the Zhoushan Island, Zhejiang province, China	OR985107	Weak (anti-MRSA)	Ha et al. (2024)
25*R*-*O*-methylarugosin A (**247**)	*Aspergillus* sp. ZZ1861	Sea mud sample, the Zhoushan Island, Zhejiang province, China	OR985107	Anti-MRSA; 50 μg/mL	Ha et al. (2024)
12*S*-Aspertetranone D (**248**)	*Aspergillus* sp. SY2601	Marine sediment, the Mariana Trench	OR646740	Anti-MRSA and *E. coli*; 3.75 and 5 μg/mL	Sun et al. (2024)
(10*S*,12*S*)-Chevalierone (**249**)	*A. chevalieri* HP-5	Mud sample, the coast of Shenzhen Bay, China	–	Anti-*P. aeruginosa* Inhibition rate 38.2% at the concentration of 200 μM	Wang Q. Y. et al. (2022)
(10*S*,12*R*)-Chevalierone (**250**)	*A. chevalieri* HP-5	Mud sample, the coast of Shenzhen Bay, China	–	Anti-*P. aeruginosa* and MRSA; Inhibition rate 81.9 and 74.1% at the concentration of 200 μM	Wang Q. Y. et al. (2022)
(10*R*,12*S*)-Chevalierone (**251**)	*A. chevalieri* HP-5	Mud sample, the coast of Shenzhen Bay, China	–	Anti-*P. aeruginosa* and MRSA; Inhibition rate 81.0 and 85.0% at the concentration of 200 μM	Wang Q. Y. et al. (2022)
(10*R*,12*R*)-Chevalierone (**252**)	*A. chevalieri* HP-5	Mud sample, the coast of Shenzhen Bay, China	–	Anti-*P. aeruginosa* and MRSA; Inhibition rate 91.5 and 88.5% at the concentration of 200 μM	Wang Q. Y. et al. (2022)
Asperphenone A (**253**)	Aspergillus sp. YHZ-1	Unidentified mangrove plant, Hainan province, China	–	Anti-*S. aureus*, *B. subtilis*, *S. pyogenes*, and *M. luteus*; 64.0, 64.0, 64.0, and 32.0 μg/mL	Guo et al. (2018)
Asperphenone B (**254**)	Aspergillus sp. YHZ-1	Unidentified mangrove plant, Hainan province, China	–	Anti-*S. aureus*, *B. subtilis*, *S. pyogenes*, and *M. luteus*; 32.0, 64.0, 32.0, and 32.0 μg/mL	Guo et al. (2018)
Penibenzophenone E (**255**)	*A. fumigatus* H22	Seawater, the Western Pacific	–	Anti-MRSA; 1.25 μM	Zhang R. et al. (2022)
Sulochrin (**256**)	*A. fumigatus* H22	Seawater, the Western Pacific	–	Anti-MRSA; 1.25 μM	Zhang R. et al. (2022)
Aspergiside A (**257**)	*A. unguis* PSU-MF16	Marine sponge *Dysidea* sp., the Koh Bulon Mai Pai, Satun Province, Thailand	KY397987	Anti-*S. aureus* and MRSA; 8 μg/mL	Saetang et al. (2021)
Aspergiside B (**258**)	*A. unguis* PSU-MF16	Marine sponge *Dysidea* sp., the Koh Bulon Mai Pai, Satun Province, Thailand	KY397987	Anti-*S. aureus* and MRSA; 128 μg/mL	Saetang et al. (2021)
Agonodepside A (**259**)	*A. unguis* PSU-MF16	Marine sponge *Dysidea* sp., the Koh Bulon Mai Pai, Satun Province, Thailand	KY397987	Anti-*S. aureus* and MRSA; 2 μg/mL	Saetang et al. (2021)
Agonodepside B (**260**)	*A. unguis* PSU-MF16	Marine sponge *Dysidea* sp., the Koh Bulon Mai Pai, Satun Province, Thailand	KY397987	Anti-*S. aureus* and MRSA; 8 and 16 μg/mL	Saetang et al. (2021)

(Continued)

10.3389/fmicb.2024.1464135

TABLE 1 (Continued)

Compounds	Producing strains	Habitats	Genbank accession number	Antibacterial activity the MIC values	References
Guisinol (**261**)	*A. unguis* GXIMD 02505	Marine coral *P. damicornis*, the Weizhou Islands, Guangxi, China	OL989238	Anti-MRSA and *M. variabilis*; 16 and 64 μg/mL	Zhang Y. T. et al. (2022)
Unguidepside C (**262**)	*A. unguis* 158SC-067	A seawater sample, Korea	MZ489151	Anti-*B. subtilis*, *M. luteus*, and *S. aureus*; 22.1 μM	Anh et al. (2022)
Agonodepside C (**263**)	*A. unguis* 158SC-067	A seawater sample, Korea	MZ489151	Anti-*B. subtilis*, *M. luteus*, and *S. aureus*; 8.0, 16.0, and 16.0 μM	Anh et al. (2022)
Aspergilluone A (**264**)	Aspergillus sp. LS57	Marine sponge *Haliclona* sp., Linshui, Hainan province, China	MH862766	Anti-*M. tuberculosis*, *S. aureus*, *B. subtilis*, and *E. coli*; 32, 64, 128 and 128 μg/mL	Liu et al. (2021)
Phomaligol A (**265**)	*A. flavus* MFA500	Marine green algae *Codium fragile*, the GeoMun Island, Yeosu, Korea	–	Anti-*S. aureus* and MRSA; 31.2 μg/mL	Yang et al. (2011)
Trypacidin (**266**)	*A. fumigatus* MF029	Marine sponge *H. perleve*, the Bohai Sea	MH974808	Anti-BCG, *B. subtilis* ATCC 6633, MRSA, and *S. aureus*; 1.25, 12.5, 50, and 50 μg/mL	Song Z. J. et al. (2021)
(+)-Geodin (**267**)	*A. versicolor* TA01-14	Marine gorgonian *Carijoa* sp., the South China Sea	KP759286	Anti-*S. albus*, *S. aureus*, and *V. anguillarum*; 25 μM	Zhang et al. (2019)
Chlorotrypacidin (**268**)	*A. versicolor* TA01-14	Marine gorgonian *Carijoa* sp., the South China Sea	KP759286	Anti-*S. albus*, *S. aureus*, and *V. anguillarum*; 25 μM	Zhang et al. (2019)
Eugenitol (**269**)	*Aspergillus* sp. SCSIO41407	Mangrove sediment sample, Sanya, Hainan province, China	–	Anti-MRSA; 485.4 μM	Cai et al. (2021)
7*β*,8*β*-Epoxy-(22*E*,24*R*)-24-methy-Lcholesta-4,22-diene-3,6-dione (**270**)	A. penicillioides SD-311	Deep-sea sediment, the South China Sea	MH779840	Anti-*V. anguillarum*; 32 μg/mL	Chi et al. (2021b)
Ergosta-4,6,8(14),22-tetraene-3-one (**271**)	A. penicillioides SD-311	Deep-sea sediment, the South China Sea	MH779840	Anti-*E. itarda* and *M. luteus*; 16 μg/mL	Chi et al. (2021b)
Isocyathisterol (**272**)	*A. ustus* cf-42	Marine green alga *C. fragile*, the Zhoushan Island, Zhejiang, China	JX036023	Weak (anti-*E. coli* and *S. aureus*); Inhibitory diameters 6.7 and 5.7 mm at 30 μg/disk	Liu et al. (2014)
Aspersteroid A (**273**)	*A. flavus* YJ07-1	the Bohai sea	–	Anti-*V. anguillarum*, V. parahemolyticus, and *V. alginolyticus*; 12.5 μg/mL	Yang M. Y. et al. (2018)
3*β*-Hydroxy-5*α*,6*β*-methox-yergosta-7,22-dien-15-one (**274**)	*Aspergillus* sp. NR151817	Marine sponge *Coelocarteria* sp., Hainan province, China	NR151817	Anti-*S. aureus*; 64.0 μg/mL	Wen et al. (2024)
Helvolic acid (**275**)	*Aspergillus* sp. SCS-KFD66	A bivalve mollusk *Schisandra chinensis*, the Haikou Bay, Hainan province, China	MK085984	Anti-*S. aureus* and *L. monocytogenes*; 2 and 128 μg/mL	An et al. (2018)
16-*O*-propionyl-16-*O*-deacetylhelvolic acid (**276**)	*A. fumigatus* HNMF0047	Marine sponge, the beach of Wenchang, Hainan province, China	MH101462	Anti-*S. agalactiae* and *S. aureus*; 16.0 μg/mL	Kong et al. (2018)
6-*O*-propionyl-6-*O*-deacetylhelvolic acid (**277**)	*A. fumigatus* HNMF0047	Marine sponge, the beach of Wenchang, Hainan province, China	MH101462	Anti-*S. agalactiae* and *S. aureus*; 2 and 8 μg/mL	Kong et al. (2018)

(Continued)

10.3389/fmicb.2024.1464135

TABLE 1 (Continued)

Compounds	Producing strains	Habitats	Genbank accession number	Antibacterial activity the MIC values	References
24-Epi-6β,16β-diacetoxy-25-hydroxy-3,7-dioxo-29-nordammara-1,17(20)-diene-21,24-lactone (**278**)	*A. fumigatus* HNMF0047	Marine sponge, the beach of Wenchang, Hainan province, China	MH101462	Anti-*S. agalactiae*; 64 μg/mL	Kong et al. (2018)
3,7-Diketo-cephalosporin P_1 (**279**)	*A. fumigatus* SCSIO 41012	Deep-sea sediment, the Indian Ocean	KM924435	Anti-*A. baumanii* ATCC 19606; 50 μg/mL	Limbadri et al. (2018)
22-*O*-acetylisocyclocitrinol A (**280**)	*A. fumigatus* SCSIO 41012	Deep-sea sediment, the Indian Ocean	KM924435	Anti-*A. baumanii* ATCC 15122 and *K. pneumonia* ATCC 14578; 12.5 and 3.125 μg/mL	Limbadri et al. (2018)
Fusidic acid (**281**)	*A. flavus* JK07-1	Marine sediment, the Huanghua, the Bohai Sea	–	Anti-M. lysodeikticus, *B. cereus*, *B. megaterium*, *B. anthracis*, and *S. typhi*; 0.07, 0.07, 0.07, 0.30, and 0.60 μM	Ren et al. (2020)
Neocyclocitrinol D (**282**)	*A. flavus* JK07-1	Marine sediment, the Huanghua, the Bohai Sea	–	Anti-M. lysodeikticus; 1.30 μM	Ren et al. (2020)
Aspergillsteroid A (**283**)	Aspergillus sp. LS116	Marine sponge *Haliclona* sp., Linshui, Hainan province, China	–	Anti-*V. harveyi*; 16 μg/mL	Xu P. et al. (2020)
Neocyclocitrinol B (**284**)	Aspergillus sp. LS116	Marine sponge *Haliclona* sp., Linshui, Hainan province, China	–	Anti-*V. harveyi*; 128 μg/mL	Xu P. et al. (2020)
Demethylincisterol A_2 (**285**)	*A. hiratsukae* SCSIO 5Bn1003	Marine coral, the South China Sea	KY806121.1	Anti-*B. subtilis*; 10.26 μg/mL	Zeng et al. (2022a)
Punicesterone B (**286**)	*A. puniceus* SCSIO z021	Deep-sea sediment, the Okinawa Trough	KX258801	Anti-*S. iniae*, *S. agalactiae*, *E. coli*, *B. subtilis*, and *S. aureus*; 65.8, 65.8, 65.8, 32.9, and 32.9 μM	Huang et al. (2023)
Punicesterone C (**287**)	*A. puniceus* SCSIO z021	Deep-sea sediment, the Okinawa Trough	KX258801	Anti-*S. iniae*, *S. agalactiae*, *E. coli*, *B. subtilis*, and *S. aureus*; 65.8, 65.8, 65.8, 32.9, and 32.9 μM	Huang et al. (2023)
3-Hydroxy-5-(3-hydroxy-5-methylphenoxy)-4-methoxybenzoic acid (**288**)	*A. carneus*	Seawater sample, Sanya, Hainan Province, China	KX437770	Anti-*S. aureus*, *V. anguillarum*, and *E. coli*; 25.0 μM	Xu et al. (2017)
3,4-Dihydroxy-5-(3-hydroxy-5-methylphenoxy)benzoic acid (**289**)	*A. carneus*	Seawater sample, Sanya, Hainan Province, China	KX437770	Anti-*S. aureus*, *V. anguillarum*, and *E. coli*; 25.0 μM	Xu et al. (2017)
3-Hydroxy-5-(3-hydroxy-5-methylphenoxy)benzoic acid (**290**)	*A. carneus*	Seawater sample, Sanya, Hainan Province, China	KX437770	Anti-*S. aureus*, *V. anguillarum*, and *E. coli*; 25.0 μM	Xu et al. (2017)
Aspergetherin C (**291**)	*A. terreus* 164,018	Marine sponge *Dysidea* sp., the South China Sea	–	Anti-MRSA; 64 μg/mL	Li J. X. et al. (2023)
Methyl 3,5-dichloroasterric acid (**292**)	*A. terreus* 164,018	Marine sponge *Dysidea* sp., the South China Sea	–	Anti-MRSA 05–72 and USA300; 1.0 and 16 μg/mL	Li J. X. et al. (2023)
Methyl chloroasterrate (**293**)	*A. terreus* 164,018	Marine sponge *Dysidea* sp., the South China Sea	–	Anti-MRSA; 64 μg/mL	Li J. X. et al. (2023)

(Continued)

10.3389/fmicb.2024.1464135

TABLE 1 (Continued)

Compounds	Producing strains	Habitats	Genbank accession number	Antibacterial activity the MIC values	References
Dimethyl 2,3′-dimethylosoate (**294**)	*A. fumigatus* H22	Middle seawater, the Western Pacific	–	Anti-MRSA; 5 μM	Zhang R. et al. (2022)
4-Methylcarbonyldiorcinol (**295**)	*A. versicolor* OUCMDZ-2738	Marine alga *Epiactis prolifera*, the Shilaoren beach, Qingdao, Shandong province, China	MH150818	Anti-*P. aeruginosa*, *C. perfringens*, and *S. aureus*; 13.9, 55.6, and 55.6 μM	Liu et al. (2019)
Diorcinol K (**296**)	*Aspergillus* sp. CUGB-F046	Sediment sample, the Bohai Sea	–	Anti-*S. aureus* and MRSA; 3.125 μg/mL	Xu et al. (2018)
Diorcinol D (**297**)	*Aspergillus* sp. CUGB-F046	Sediment sample, the Bohai Sea	–	Anti-*S. aureus* and MRSA; 6.25 μg/mL	Xu et al. (2018)
Diorcinol I (**298**)	*Aspergillus* sp. CUGB-F046	Sediment sample, the Bohai Sea	–	Anti-*S. aureus* and MRSA; 6.25 μg/mL	Xu et al. (2018)
Diorcinol (**299**)	*A. versicolor* 170,217	the intestinal contents of a whale *Mesoplodon densirostris*, the East China Sea	SUB13826338	Anti-V. parahemolyticus; 128 μM	Lin S. H. et al. (2023)
Violaceol-I (**300**)	*Aspergillus* sp. ZZ1861	Sea mud sample, the Zhoushan Island, Zhejiang province, China	OR985107	Anti-MRSA and *E. coli*; 50 and 6.25 μg/mL	Ha et al. (2024)
Violaceol-II (**301**)	*Aspergillus* sp. ZZ1861	Sea mud sample, the Zhoushan Island, Zhejiang province, China	OR985107	Anti-MRSA and *E. coli*; 50 and 6.25 μg/mL	Ha et al. (2024)
4-Carbethoxydiorcinal (**302**)	*Aspergillus* sp. ZZ1861	Sea mud sample, the Zhoushan Island, Zhejiang province, China	OR985107	Anti-MRSA; 25 μg/mL	Ha et al. (2024)
1,9-Dimethyl-3,7-dibenzofurandiol (**303**)	*Aspergillus* sp. ZZ1861	Sea mud sample, the Zhoushan Island, Zhejiang province, China	OR985107	Anti-*E. coli*; 12.5 μg/mL	Ha et al. (2024)
Aspergillusether E (**304**)	*A. unguis* PSU-MF16	Marine sponge *Dysidea* sp., the Koh Bulon Mai Pai, Satun Province, Thailand	KY397987	Anti-*S. aureus* and MRSA; 16 μg/mL	Saetang et al. (2021)
Aspergillusether C (**305**)	*A. unguis* PSU-MF16	Marine sponge *Dysidea* sp., the Koh Bulon Mai Pai, Satun Province, Thailand	KY397987	Anti-*S. aureus* and MRSA; 64 μg/mL	Saetang et al. (2021)
Aspergillusether D (**306**)	*A. unguis* PSU-MF16	Marine sponge *Dysidea* sp., the Koh Bulon Mai Pai, Satun Province, Thailand	KY397987	Anti-*S. aureus* and MRSA; 64 and 128 μg/mL	Saetang et al. (2021)
Pilobolusate (**307**)	*A. unguis* PSU-MF16	Marine sponge *Dysidea* sp., the Koh Bulon Mai Pai, Satun Province, Thailand	KY397987	Anti-*S. aureus* and MRSA; 64 μg/mL	Saetang et al. (2021)
Aspergillusether J (**308**)	*A. unguis* GXIMD 02505	Marine coral *P. damicornis*, the Weizhou Islands, Guangxi, China	OL989238	Anti-MRSA, *M. variabilis*, and *M. jannaschii*; 16, 32 and 64 μg/mL	Zhang Y. T. et al. (2022)
Aspergillusether *F* (**309**)	*A. unguis* GXIMD 02505	Marine coral *P. damicornis*, the Weizhou Islands, Guangxi, China	OL989238	Anti-MRSA, *M. variabilis*, and *M. jannaschii*; 2, 16, and 32 μg/mL	Zhang Y. T. et al. (2022)
Flavuside A (**310**)	*A. flavus* MFA500	Marine green algae *C. fragile*, the GeoMun Island, Yeosu, Korea	–	Anti-MRSA; 15.6 μg/mL	Yang et al. (2011)
Flavuside B (**311**)	*A. flavus* MFA500	Marine green algae *C. fragile*, the GeoMun Island, Yeosu, Korea	–	Anti-MRSA; 15.6 μg/mL	Yang et al. (2011)

(Continued)

10.3389/fmicb.2024.1464135

TABLE 1 (Continued)

Compounds	Producing strains	Habitats	Genbank accession number	Antibacterial activity the MIC values	References
Acetylpeniciphenol (**312**)	*A. insuetus* SD-512	Deep-sea sediment, the South China Sea	MN696202	Anti-E. itarda, *V. alginolyticus*, and *V. vulnificus*; 4, 8, and 8 μg/mL	Chi et al. (2021a)
Fumagiringillin (**313**)	*A. fumigatus* H22	middle seawater, the Western Pacific	–	Anti-MRSA; 25.0 μM	Zhang R. et al. (2022)
Fumagillin (**314**)	*A. fumigatus* H22	middle seawater, the Western Pacific	–	Anti-MRSA; 2.50 μM	Zhang R. et al. (2022)
8-*O*-4-dehydrodiferulic acid (**315**)	Aspergillus sp.	Marine sponge *T. aurantium*, the Adriatic Sea	–	Anti-*R. litoralis*; 1 μg/mL	Zhou et al. (2014)
Penicitrinol L (**316**)	A. sydowii EN-534 and P. citrinum EN-535	Marine red alga *L. okamurai*, Qingdao, Shandong province, China	MG242135 MG242136	Anti-*E. coli*, *E. ictaluri*, and *V. alginolyticus*; 64 μg/mL	Yang et al. (2018b)
penicitrinol A (**317**)	A. sydowii EN-534 and P. citrinum EN-535	Marine red alga *L. okamurai*, Qingdao, Shandong province, China	MG242135 MG242136	Anti-*V. alginolyticus*, *E. coli*, *V. parahaemolyticus*, *M. luteus*, and *E. ictaluri*; 32, 8, 8, 4, and 16 μg/mL	Yang et al. (2018b)
	A. versicolor 170,217	the intestinal contents of a whale *M. densirostris*, the East China Sea	SUB13826338	Anti-V. parahemolyticus; 256 μg/mL	Lin S. H. et al. (2023)
2-(Hydroxymethyl)-3-propylphenol (**318**)	Aspergillus sp. ZJ-68	Mangrove plant *K. candel*, the Zhanjiang Mangrove Nature Reserve, Guangdong Province, China	MK629267	Anti-*S. aureus*, *E. coli*, and *B. subtilis*; 4.15, 8.3, and 8.3 μg/mL	Cai et al. (2019)
(−)-Brassicadiol (**319**)	Aspergillus sp. ZJ-68	Mangrove plant *K. candel*, the Zhanjiang Mangrove Nature Reserve, Guangdong Province, China	MK629267	Anti-*S. aureus*, *E. coli*, and *B. subtilis*; 12.5 μg/mL	Cai et al. (2019)
4,6-Dichloro-5-methyl-benzene-1,3-diol (**320**)	*A. terreus* CC-S06-18	A seawater sample, the Pacific Ocean	MN463005	Anti-*V. parahaemolyticus*; 7.8 μg/mL	Huang et al. (2024)
1-(2,6-Dihydroxy-4-methoxy-3,5-dimethylphenyl)-2-methylbutan-1-one (**321**)	*A. unguis* GXIMD 02505	Marine coral *P. damicornis*, the Weizhou Islands, Guangxi, China	OL989238	Anti-*M. variabilis* and *M. jannaschii*; 8 and 32 μg/mL	Zhang Y. T. et al. (2022)
Asperporonin A (**322**)	*A. terreus* SCSIO 41202	Deep-sea sediment, the coast of the South China Sea	MN613535	Anti-*X. citri* subsp. *citri*; 0.3125 mg/mL	Zhang et al. (2024)
Asperporonin B (**323**)	*A. terreus* SCSIO 41202	Deep-sea sediment, the coast of the South China Sea	MN613535	Anti-*X. citri* subsp. *citri*; 0.3125 mg/mL	Zhang et al. (2024)
Terrusnolide A (**324**)	*Aspergillus* sp. SCSIO 41029	Deep-sea sediment, the South China	MH591418.1	Anti-*S. aureus*; 6.25 μg/mL	Chen et al. (2021)
Candidusin A (**325**)	*Aspergillus* sp. SCSIO 40435	Marine coral, the South China sea	–	Anti-*E. coli*, *A. baumannii*, and *S. aureus*; 1, 64, and 32 μg/mL	Ye et al. (2022)
Terphenyllin (**326**)	*Aspergillus* sp. SCSIO 40435	Marine coral, the South China sea	–	Anti-*E. coli*; 0.5 μg/mL	Ye et al. (2022)
4″-Deoxyterphenyllin (**327**)	*Aspergillus* sp. SCSIO 40435	Marine coral, the South China sea	–	Anti-*B. subtilis* and *M. luteus*; 64 and 32 μg/mL	Ye et al. (2022)
5[(3*E*,5*E*)-Nona-3,5-dien-1-yl]benzene (**328**)	*A. stellatus* KUFA 2017	Marine sponge *Mycale* sp., the Samaesan Island, Chonburi province, Thailand	MZ331807	Anti-*E. faecalis* ATCC 29212, VRE, *S. aureus* ATCC 29213, and MRSA; 16. 16, 32, and 16 μg/mL	Machado et al. (2022)

(Continued)

10.3389/fmicb.2024.1464135

TABLE 1 (Continued)

Compounds	Producing strains	Habitats	Genbank accession number	Antibacterial activity the MIC values	References
(9*R*,10*E*,12*E*)-9-Methoxyoc Tadecadienoic acid (**329**)	*A. terreus* SCSIO 41202	Deep-sea sediment, the coast of the South China Sea	MN613535	Anti-*X. citri* subsp. *citri*; 0.078 mg/mL	Zhang et al. (2024)
Carnemycin H (**330**)	*A. ustus*	Mangrove sediments, the Zhangjiangkou Mangrove National Nature Reserve, Fujian province, China	MN650842	Anti-*R. solanacearum*; 25 μg/mL	Xue et al. (2024)
Carnemycin I (**331**)	*A. ustus*	Mangrove sediments, the Zhangjiangkou Mangrove National Nature Reserve, Fujian province, China	MN650842	Anti-*R. solanacearum*; 15 μg/mL	Xue et al. (2024)
Stromemycin B (**332**)	*A. ustus*	Mangrove sediments, the Zhangjiangkou Mangrove National Nature Reserve, Fujian province, China	MN650842	Aanti-*R. solanacearum*; 3 μg/mL	Xue et al. (2024)
Carnemycin E (**333**)	*A. ustus*	Mangrove sediments, the Zhangjiangkou Mangrove National Nature Reserve, Fujian province, China	MN650842	Anti-*R. solanacearum*; 35 μg/mL	Xue et al. (2024)
Carnemycin B (**334**)	*A. ustus*	Mangrove sediments, the Zhangjiangkou Mangrove National Nature Reserve, Fujian province, China	MN650842	Anti-*R. solanacearum*; 30 μg/mL	Xue et al. (2024)
Carnemycin A (**335**)	*A. ustus*	Mangrove sediments, the Zhangjiangkou Mangrove National Nature Reserve, Fujian province, China	MN650842	Anti-*R. solanacearum*; 25 μg/mL	Xue et al. (2024)
2,4-Dihydroxy-6-[(3*E*,5*E*)-nona-3,5-dien-1-yl]-benzoic acid (**336**)	*A. ustus*	Mangrove sediments, the Zhangjiangkou Mangrove National Nature Reserve, Fujian province, China	MN650842	Anti-*R. solanacearum*; 5 μg/mL	Xue et al. (2024)
Stromemycin (**337**)	*A. ustus*	Mangrove sediments, the Zhangjiangkou Mangrove National Nature Reserve, Fujian province, China	MN65084	Anti-*R. solanacearum*; 8 μg/mL	Xue et al. (2024)

10.3389/fmicb.2024.1464135

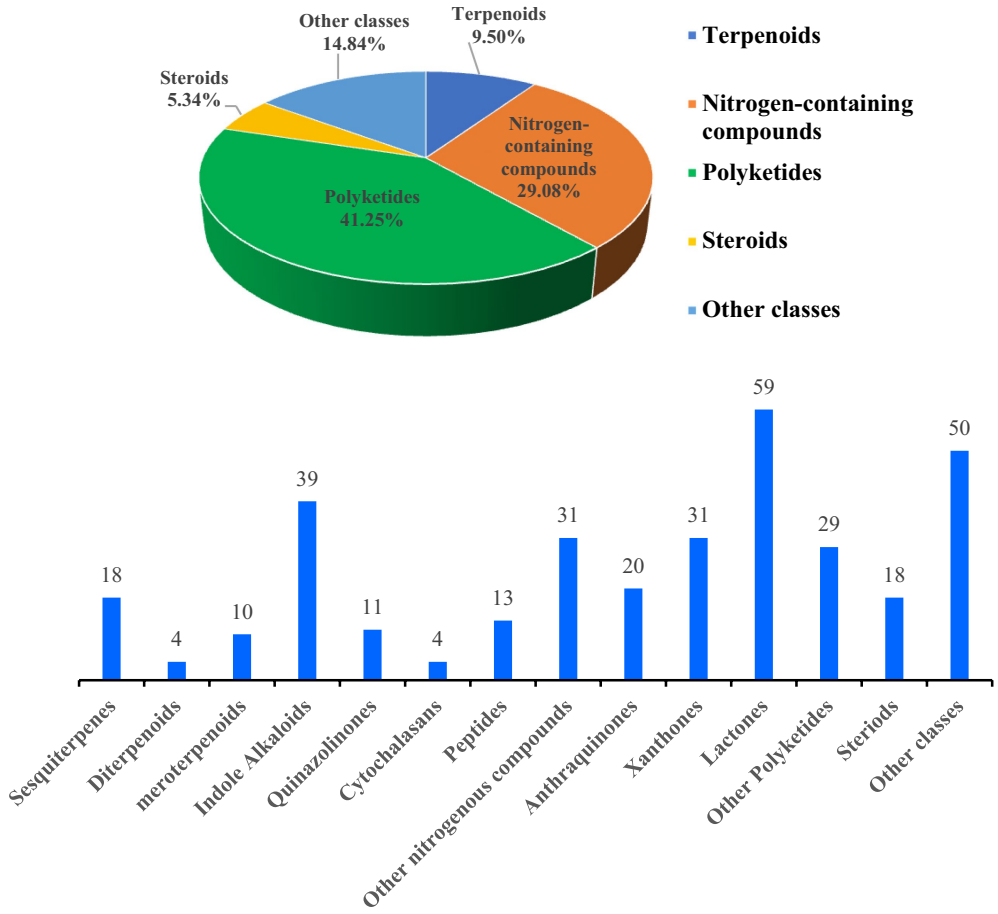

FIGURE 15
Structural diversity of the antibacterial secondary metabolites from the genus of *Aspergillus* (January 2010 to June 2024).

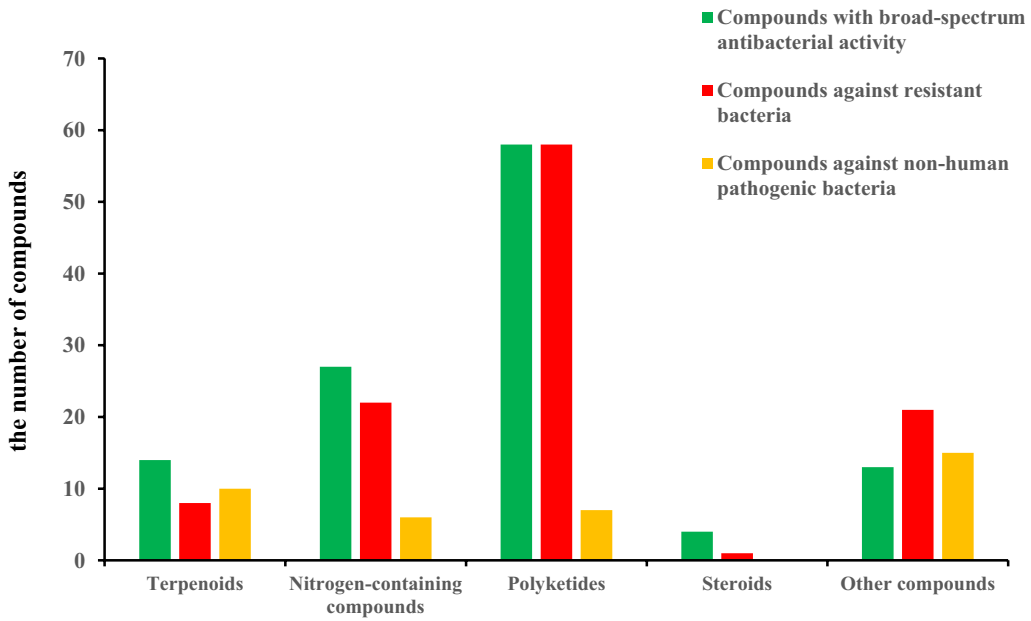

FIGURE 16
The number and types of compounds with broad-spectrum antibacterial activity, activity against resistant bacteria, and activity against non-human pathogenic bacteria.

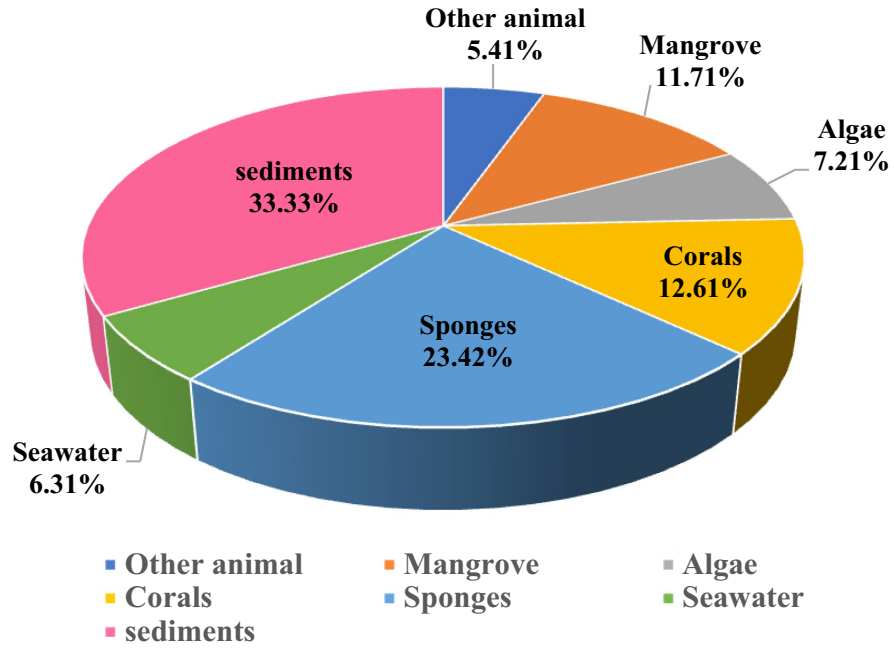

FIGURE 17
The proportion of *Aspergillus* from different marine sources.

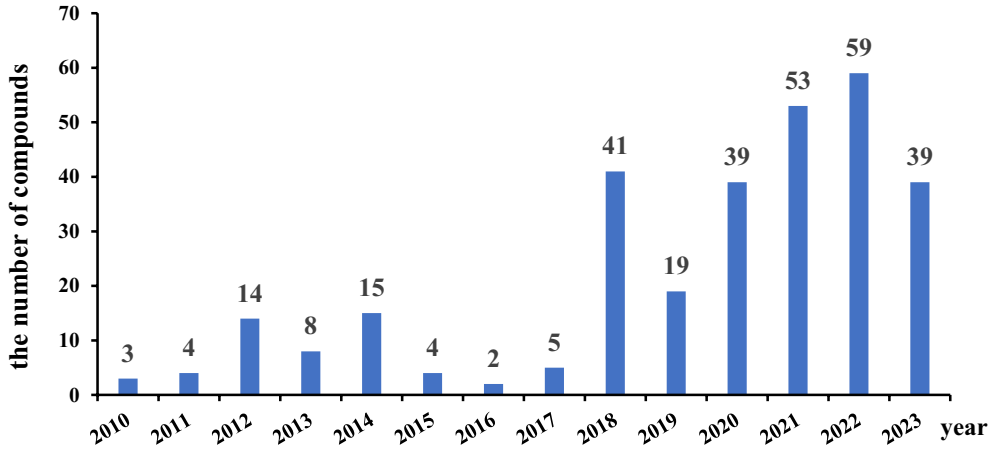

FIGURE 18
Each year of the antibacterial secondary metabolites from the genus of *Aspergillus* (2010–2023) (the data for 2024 is not accurate, so it will not be included).

Author contributions

BW: Writing – original draft, Data curation. JC: Writing – original draft, Data curation. LH: Writing – review & editing. YC: Writing – review & editing. RW: Writing – review & editing. ML: Writing – review & editing. MY: Writing – review & editing. MZ: Writing – review & editing. Nasihat: Writing – review & editing. GC: Project administration, Supervision, Writing – review & editing. GH: Project administration, Supervision, Writing – review & editing, Data curation, Software, Writing – original draft. CZ: Methodology, Project administration, Supervision, Writing – review & editing, Data curation, Software, Writing – original draft.

Funding

The author(s) declare that financial support was received for the research, authorship, and/or publication of this article. This study was supported by the National Natural Science Foundation of China (Nos. 32160108 and 2217702), the Key Research and Development Program of Hainan Province (No. ZDYF2024SHFZ116 and ZDYF2021SHFZ270), the Team Innovation Center for Academicians of Hainan Province, the Specific Research Fund for the Innovation Center of Hainan Province Academicians (No. YSPTZX202309), and the Key Science and Technology Program of Hainan Province (No. ZDKJ202008).

Conflict of interest

The authors declare that the research was conducted in the absence of any commercial or financial relationships that could be construed as a potential conflict of interest.

The reviewer FC declared a past co-authorship with the author CZ to the handling editor.

Publisher's note

References

Alahmari, A. N., Hassoubah, S. A., and Alaidaroos, B. A. (2022). Sponges-associated marine bacteria as sources of antimicrobial compounds. *Novel. Res. Microbiol. J.* 6, 1742–1767. doi: 10.21608/nrmj.2022.267424

An, C. L., Kong, F. D., Ma, Q. Y., Xie, Q. Y., Yuan, J. Z., Zhou, L. M., et al. (2018). Chemical constituents of the marine-derived fungus *Aspergillus* sp. SCS-KFD66. *Mar. Drugs* 16:468. doi: 10.3390/md16120468

Anh, C. V., Kwon, J. H., Kang, J. S., Lee, H. S., Heo, C. S., and Shin, H. J. (2022). Antibacterial and cytotoxic phenolic polyketides from two marine-derived fungal strains of *Aspergillus unguis*. *Pharmaceuticals* 15:74. doi: 10.3390/ph15010074

Bai, Z. Q., Lin, X. P., Wang, Y. Z., Wang, J. F., Zhou, X. F., Yang, B., et al. (2014). New phenyl derivatives from endophytic fungus *Aspergillus flavipes* AIL8 derived of mangrove plant *Acanthus ilicifolius*. *Fitoterapia* 95, 194–202. doi: 10.1016/j.fitote.2014.03.021

Bao, J., Li, X. X., He, F., Zhang, X. Y., Zhu, K. K., Tao, H. R., et al. (2020). Asperbutenolide a, an unusual aromatic butenolide dimer with diverse bioactivities from a marine-derived fungus *Aspergillus terreus* SCAU011. *Tetrahedron Lett.* 61:152193. doi: 10.1016/j.tetlet.2020.152193

Bao, J., Li, X. X., Zhu, K. K., He, F., Wang, Y. Y., Yu, J. H., et al. (2021). Bioactive aromatic butenolides from a mangrove sediment originated fungal species, *Aspergillus terreus* SCAU011. *Fitoterapia* 150:104856. doi: 10.1016/j.fitote.2021.104856

Buttachon, S., Ramos, A. A., Inacio, A., Dethoup, T., Gales, L., Lee, M., et al. (2018). Bis-indolyl benzenoids, hydroxypyrrolidine derivatives and other constituents from cultures of the marine sponge-associated fungus *Aspergillus candidus* KUFA0062. *Mar. Drugs* 16:119. doi: 10.3390/md16040119

Cai, J., Chen, C. M., Tan, Y. H., Chen, W. H., Luo, X. W., Luo, L. X., et al. (2021). Bioactive polyketide and diketopiperazine derivatives from the mangrove-sediment-derived fungus *Aspergillus* sp. SCSIO41407. *Molecules* 26:4851. doi: 10.3390/molecules26164851

Cai, R. L., Jiang, H. M., Zang, Z. M., Li, C. Y., and She, Z. G. (2019). New benzofuranoids and phenylpropanoids from the mangrove endophytic fungus, *Aspergillus* sp. ZJ-68. *Mar. Drugs* 17:478. doi: 10.3390/md17080478

Cai, J., Wang, X. N., Gan, X., Zhou, Q., Luo, X. W., Yang, B., et al. (2023). New chlorinated metabolites and antiproliferative polyketone from the mangrove sediments-derived fungus *Mollisia* sp. SCSIO41409. *Mar. Drugs* 21:32. doi: 10.3390/md21010032

Cardoso-Martinez, F., De la Rosa, J. M., Diaz-Marrero, A. R., Darias, J., D'Croz, L., Cerella, C., et al. (2015). Oximoaspergillimide, a fungal derivative from a marine isolate of *Aspergillus* sp. *Eur. J. Org. Chem.* 2015, 2256–2261. doi: 10.1002/ejoc.201403668

Carroll, A. R., Copp, B. R., Davis, R. A., Keyzers, R. A., and Prinsep, M. R. (2024). Marine natural products. *Nat. Prod. Rep.* 41, 162–207. doi: 10.1039/D3NP00061C

Cen, S. Y., Jia, J., Ge, Y. C., Ma, Y. H., Li, X. Y., Wei, J. H., et al. (2021). A new antibacterial 3,5-dimethylorsellinic acid-based meroterpene from the marine fungus *Aspergillus* sp. CSYZ-1. *Fitoterapia* 152:104908. doi: 10.1016/j.fitote.2021.104908

Charani, E., Mendelson, M., Pallett, S. J. C., Ahmad, R., Mpundu, M., Mbamalu, O., et al. (2023). An analysis of existing national action plans for antimicrobial resistance-gaps and opportunities in strategies optimising antibiotic use in human populations. *Lancet Glob. Health* 11, e466–e474. doi: 10.1016/S2214-109X(23)00019-0

Chen, W. H., Chen, C. M., Long, J. Y., Lan, S. J., Lin, X. P., Liao, S. R., et al. (2021). Bioactive secondary metabolites from the deep-sea derived fungus *Aspergillus* sp. SCSIO 41029. *J. Antibiot.* 74, 156–159. doi: 10.1038/s41429-020-00378-y

Chen, M., Fu, X. M., Kong, C. J., and Wang, C. Y. (2014). Nucleoside derivatives from the marine-derived fungus *Aspergillus versicolor*. *Nat. Prod. Res.* 28, 895–900. doi: 10.1080/14786419.2014.891114

Chen, X. N., Lan, W. Q., and Xie, J. (2024). Natural phenolic compounds: antimicrobial properties, antimicrobial mechanisms, and potential utilization in the preservation of aquatic products. *Food Chem.* 440:138198. doi: 10.1016/j.foodchem.2023.138198

Chen, W. H., Liu, H. Y., Long, J. Y., Tao, H. M., Lin, X. P., Liao, S. R., et al. (2020). Asperpentenone a, a novel polyketide isolated from the deep-sea derived fungus *Aspergillus* sp. SCSIO 41024. *Phytochem. Lett.* 35, 99–102. doi: 10.1016/j.phytol.2019.11.009

Chen, B., Qiu, P. J., Xu, B. F., Zhao, Q. M., Gu, Y. C., Fu, L., et al. (2022). Cytotoxic and antibacterial isomalabaricane terpenoids from the sponge *Rhabdastrella globostellata*. *J. Nat. Prod.* 85, 1799–1807. doi: 10.1021/acs.jnatprod.2c00348

Chen, M., Shao, C. L., Fu, X. M., Xu, R. F., Zheng, J. J., Zhao, D. L., et al. (2013). Bioactive indole alkaloids and phenyl ether derivatives from a marine-derived *Aspergillus* sp. fungus. *J. Nat. Prod.* 76:1229. doi: 10.1021/np400465r

Chen, X. Y., Zeng, Q., Chen, Y. C., Zhong, W. M., Xiang, Y., Wang, J. F., et al. (2022). Chevalones H-M: six new α-pyrone meroterpenoids from the gorgonian coral-drived fungus *Aspergillus hiratsukae* SCSIO 7S2001. *Mar. Drugs* 20:71. doi: 10.3390/md20010071

Chi, L. P., Li, X. M., Wan, Y. P., Li, Y. H., Li, X., and Wang, B. G. (2021a). Two new phenol derivatives from the cold seep-derived fungus *Aspergillus insuetus* SD-512. *Chem. Biodivers.* 18:e2100512. doi: 10.1002/cbdv.202100512

Chi, L. P., Li, X. M., Wan, Y. P., Li, X., and Wang, B. G. (2020). Ophiobolin sesterterpenoids and farnesylated phthalide derivatives from the deep sea cold-seep-derived fungus *Aspergillus insuetus* SD-512. *J. Nat. Prod.* 83, 3652–3660. doi: 10.1021/acs.jnatprod.0c00860

Chi, L. P., Liu, D., Li, X. M., Wan, Y. P., Wang, B. G., and Li, X. (2023). Aspertides A-E: antimicrobial pentadepsipeptides with a unique p-methoxycinnamoyl amide group from the marine isolates *Aspergillus tamarii* MA-21 and *Aspergillus insuetus* SD-512. *J. Agr. Food. Chem.* 71, 13316–13324. doi: 10.1021/acs.jafc.3c02610

Chi, L. P., Yang, S. Q., Li, X. M., Li, X. D., Wang, B. G., and Li, X. (2021b). A new steroid with 7β,8β-epoxidation from the deep sea-derived fungus *Aspergillus penicillioides* SD-311. *J. Asian Nat. Prod. Res.* 23, 884–891. doi: 10.1080/10286020.2020.1791096

de Alcântara Rodrigues, I., Ferrari, R. G., Panzenhagen, P. H. N., Mano, S. B., and Conte, C. A. J. (2020). Antimicrobial resistance genes in bacteria from animal-based foods. *Adv. Appl. Microbiol.* 112, 143–183. doi: 10.1016/bs.aambs.2020.03.001

Ding, L. J., Ren, L., Li, S., Song, J. J., Han, Z. W., He, S., et al. (2019). Production of new antibacterial 4-hydroxy-α-pyrones by a marine fungus *Aspergillus niger* cultivated in solid medium. *Mar. Drugs* 17:344. doi: 10.3390/md17060344

Dong, Y. L., Li, X. M., Shi, X. S., Wang, Y. R., Wang, B. G., and Meng, L. H. (2023a). Diketopiperazine alkaloids and bisabolene sesquiterpenoids from *Aspergillus versicolor* AS-212, an endozoic fungus associated with deep-sea coral of magellan seamounts. *Mar. Drugs* 21:293. doi: 10.3390/md21050293

Dong, Y. L., Li, X. M., Wang, Y. R., Shi, X. S., Wang, B. G., and Meng, L. H. (2023b). Oxepine-containing pyrazinopyrimidine alkaloids and quinolinone derivatives produced by *Aspergillus versicolor* AS-212, a deep-sea-derived endozoic fungus. *Fitoterapia* 168:105559. doi: 10.1016/j.fitote.2023.105559

Duraes, F., Szemeredi, N., Kumla, D., Pinto, M., Kijjoa, A., and Spengler, G. (2021). Metabolites from marine-derived fungi as potential antimicrobial adjuvants. *Mar. Drugs* 19:475. doi: 10.3390/md19090475

Gou, X. S., Jia, J., Xue, Y. X., Ding, W. J., Dong, Z. T., Tian, D. M., et al. (2020). New pyrones and their analogs from the marine mangrove-derived *Aspergillus* sp. DM94 with antibacterial activity against *Helicobacter pylori*. *Appl. Microbiol. Biotechnol.* 104, 7971–7978. doi: 10.1007/s00253-020-10792-9

Gow, N. A. R., Johnson, C., Berman, J., Coste, A. T., Cuomo, C. A., Perlin, D. S., et al. (2022). The importance of antimicrobial resistance in medical mycology. *Nat. Commun.* 13:5352. doi: 10.1038/s41467-022-32249-5

Graziano, T. S., Cuzzullin, M. C., Franco, G. C., Schwartz-Filho, O., Dias, D. A. E., Groppo, F. C., et al. (2015). Statins and antimicrobial effects: simvastatin as a potential drug against *Staphylococcus aureus* biofilm. *PLoS One* 10:e0128098. doi: 10.1371/journal.pone.0128098

Guo, C., Wang, P., Pang, X. Y., Lin, X. P., Liao, S. R., Yang, B., et al. (2021). Discovery of a dimeric zinc complex and five cyclopentenone derivatives from the sponge-associated fungus *Aspergillus ochraceopetaliformis*. *ACS Omega* 6, 8942–8949. doi: 10.1021/acsomega.0c06218

Guo, Z. K., Zhou, Y. Q., Han, H., Wang, W., Xiang, L., Deng, X. Z., et al. (2018). New antibacterial phenone derivatives asperphenone A-C from mangrove-derived fungus *Aspergillus* sp. YHZ-1. *Mar. Drugs* 16:45. doi: 10.3390/md16020045

Ha, Y. R., Zhou, Y. F., Ma, M. Z., Wang, N., Wang, P. B., and Zhang, Z. Z. (2024). Antimicrobial metabolites from the marine-derived fungus *Aspergillus* sp. ZZ1861. *Phytochemistry* 224:114164. doi: 10.1016/j.phytochem.2024.114164

Haenni, M., Dagot, C., Chesneau, O., Bibbal, D., Labanowski, J., Vialette, M., et al. (2022). Environmental contamination in a high-income country (France) by antibiotics,

antibiotic-resistant bacteria, and antibiotic resistance genes: status and possible causes. *Environ. Int.* 159:107047. doi: 10.1016/j.envint.2021.107047

Hai, Y., Wei, M. Y., Wang, C. Y., Gu, Y. C., and Shao, C. L. (2021). The intriguing chemistry and biology of sulfur-containing natural products from marine microorganisms (1987-2020). *Mar. Life Sci. Tech.* 3, 488–518. doi: 10.1007/s42995-021-00101-2

Han, J. H., Yang, N., Wei, S. Z., Jia, J., Lin, R., Li, J. P., et al. (2022). Dimeric hexylitaconic acids from the marine-derived fungus *Aspergillus welwitschiae* CUGBMF180262. *Nat. Prod. Res.* 36, 578–585. doi: 10.1080/14786419.2020.1793152

Han, Y. Q., Zhang, Q., Xu, W. F., Hai, Y., Chao, R., Wang, C. F., et al. (2023). Targeted isolation of antitubercular cycloheptapeptides and an unusual pyrroloindoline-containing new analog, asperpyrroindotide a, using LC-MS/MS-based molecular networking. *Mar. Life Sci. Tech.* 5, 85–93. doi: 10.1007/s42995-022-00157-8

Handayani, D., Dwinatrana, K., and Rustini, R. (2022). Antibacterial compound from marine sponge derived fungus *Aspergillus sydowii* DC08. *Rasayan J. Chem.* 15, 2485–2492. doi: 10.31788/RJC.2022.1546971

Handayani, D., Rendowati, A., Aminah, I., Ariantari, N. P., and Proksch, P. (2020). Bioactive compounds from marine sponge derived fungus *Aspergillus unguis* WR8. *Rasayan. J. Chem.* 13, 2633–2638. doi: 10.31788/RJC.2020.1345781

Holland, D. C., Prebble, D. W., Er, S., Hayton, J. B., Robertson, L. P., Avery, V. M., et al. (2022). α-Synuclein aggregation inhibitory prunolides and a dibrominated β-carboline sulfamate from the ascidian *Synoicum prunum*. *J. Nat. Prod.* 85, 441–452. doi: 10.1021/acs.jnatprod.1c01172

Howden, B. P., Giulier, S. G., Lung, T. W. F., Baines, S. L., Sharkey, L. K., Lee, J. Y. H., et al. (2023). *Staphylococcus aureus* host interactions and adaptation. *Nat. Rev. Microbiol.* 21, 380–395. doi: 10.1038/s41579-023-00852-y

Hu, Y. Y., Yang, M., Zhao, J., Liao, Z. X., Qi, J., Wang, X. Z., et al. (2019). A meroterpenoid isolated from the fungus *Aspergillus* sp. *Nat. Prod. Commun.* 14:1934578X1987893. doi: 10.1177/1934578X19878933

Hu, Z. B., Zhu, Y. J., Chen, J. J., Chen, J., Li, C. Y., Gao, Z. Z., et al. (2023). Discovery of novel bactericides from *Aspergillus alabamensis* and their antibacterial activity against fish pathogens. *J. Agric. Food. Chem.* 71, 4298–4305. doi: 10.1021/acs.jafc.2c09141

Huang, Z. H., Liang, X., Gu, Q., Ma, X., and Qi, S. H. (2023). Punicesterones A-G, polyhydroxylated mycoecdysteroids from the deep-sea-derived fungus *Aspergillus puniceus* SCSIO z021. *Phytochemistry* 205:113511. doi: 10.1016/j.phytochem.2022.113511

Huang, X. M., Wang, Y. C., Li, G. Y., Shao, Z. Z., Xia, J. M., Qin, J. J., et al. (2024). Secondary metabolites from the deep-sea derived fungus *Aspergillus terreus* MCCC M28183. *Front. Microbiol.* 15:1361550. doi: 10.3389/fmicb.2024.1361550

Ibrahim, S. R. M., Mohamed, S. G. A., Alsaadi, B. H., Althubyani, M. M., Awari, Z. I., Hussein, H. G. A., et al. (2023). Secondary metabolites, biological activities, and industrial and biotechnological importance of *Aspergillus sydowii*. *Mar. Drugs* 21:441. doi: 10.3390/md21080441

Ikuta, K. S., Swetschinski, L. R., Aguilar, G. R., Sharara, F., Mestrovic, T., Gray, A. P., et al. (2022). Global mortality associated with 33 bacterial pathogens in 2019: a systematic analysis for the global burden of disease study 2019. *Lancet* 400, 2221–2248. doi: 10.1016/S0140-6736(22)02185-7

Jeewon, R., Aullybux, A. A., Puchooa, D., Nazurally, N., Alrefaei, A. F., and Zhang, Y. (2023). Marine microbial polysaccharides: an untapped resource for biotechnological applications. *Mar. Drugs* 21:420. doi: 10.3390/md21070420

Jin, M., Osman, M., Green, B. A., Yang, Y. F., Ahuja, A., Lu, Z. Y., et al. (2023). Evidence for the transmission of antimicrobial resistant bacteria between humans and companion animals: a scoping review. *One Health* 17:100593. doi: 10.1016/j.onehlt.2023.100593

King, A. M., Reid-Yu, S. A., Wang, W., King, D. T., Pascale, G. D., Strynadka, N. C., et al. (2014). Aspergillomarasmine A overcomes metallo-β-lactamase antibiotic resistance. *Nature* 510, 503–506. doi: 10.1038/nature13445

Kong, F. D., Huang, X. L., Ma, Q. Y., Xie, Q. Y., Wang, P., Chen, P. W., et al. (2018). Helvolic acid derivatives with antibacterial activities against *Streptococcus agalactiae* from the marine-derived fungus *Aspergillus fumigatus* HNMF0047. *J. Nat. Prod.* 81, 1869–1876. doi: 10.1021/acs.jnatprod.8b00382

Kumla, D., Sousa, E., Marengo, A., Dethoup, T., Pereira, J. A., Gales, L., et al. (2021). 1,3-dioxepine and spiropyran derivatives of viomellein and other dimeric naphthopyranones from cultures of *Aspergillus elegans* KUFA0015 and their antibacterial activity. *Phytochemistry* 181:112575. doi: 10.1016/j.phytochem.2020.112575

Lee, Y. M., Kim, M. J., Li, H. Y., Zhang, P., Bao, B. Q., Lee, K. J., et al. (2013). Marine-derived *Aspergillus* species as a source of bioactive secondary metabolites. *Mar. Biotechnol.* 15, 499–519. doi: 10.1007/s10126-013-9506-3

Lee, Y. M., Li, H. Y., Hong, J. K., Cho, H. Y., Bae, K. S., Kim, M. A., et al. (2010). Bioactive metabolites from the sponge-derived fungus *Aspergillus versicolor*. *Arch. Pharm. Res.* 33, 231–235. doi: 10.1007/s12272-010-0207-4

Li, H. H., Fu, Y. Q., and Song, F. H. (2023). Marine *Aspergillus*: a treasure trove of antimicrobial compounds. *Mar. Drugs* 21:277. doi: 10.3390/md21050277

Li, W. H., Gao, Q., Hu, Y. J., Shi, Y. T., Yan, X. J., Ding, L. J., et al. (2023). Dibetanide, a new benzofuran derivative with the rare conjugated triene side chain from a sponge-associated fungus *Aspergillus* species. *J. Mol. Struct.* 1271:134082. doi: 10.1016/j.molstruc.2022.134082

Li, J. L., Jiang, X., Liu, X. P., He, C. W., Di, Y. X., Lu, S. J., et al. (2019). Antibacterial anthraquinone dimers from marine derived fungus *Aspergillus* sp. *Fitoterapia* 133, 1–4. doi: 10.1016/j.fitote.2018.11.015

Li, X. D., Li, X., Li, X. M., Xu, G. M., Zhang, P., Meng, L. H., et al. (2016). Tetranorlabdane diterpenoids from the deep sea sediment-derived fungus *Aspergillus wentii* SD-310. *Planta Med.* 82, 877–881. doi: 10.1055/s-0042-102965

Li, X. D., Li, X., Li, X. M., Yin, X. L., and Wang, B. G. (2021). Antimicrobial bisabolane-type sesquiterpenoids from the deep-sea sediment-derived fungus *Aspergillus versicolor* SD-330. *Nat. Prod. Res.* 35, 4265–4271. doi: 10.1080/14786419.2019.1696792

Li, S. D., Wei, M. Y., Chen, G. Y., and Lin, Y. C. (2012). Two new dihydroisocoumarins from the endophytic fungus *Aspergillus* sp. collected from the South China Sea. *Chem. Nat. Compd.* 48, 371–373. doi: 10.1007/s10600-012-0254-9

Li, J. X., Xu, Q. H., Shang, R. Y., Liu, Q., Luo, X. C., Lin, H. W., et al. (2023). Aspergetherins A-D, new chlorinated biphenyls with anti-MRSA activity from the marine sponge symbiotic fungus *Aspergillus terreus* 164018. *Chem. Biodivers.* 20:e202300010. doi: 10.1002/cbdv.202300010

Limbadri, S., Luo, X. W., Lin, X. P., Liao, S. R., Wang, J. F., Zhou, X. F., et al. (2018). Bioactive novel indole alkaloids and steroids from deep sea-derived fungus *Aspergillus fumigatus* SCSIO 41012. *Molecules* 23:2379. doi: 10.3390/molecules23092379

Lin, S. X., Li, J., Chen, W. Z., He, J. X., Shi, Y. T., Jin, H. X., et al. (2023). A new antibacterial dihydroisocoumarin from the marine sponge-associated fungus *Aspergillus* sp. *Chem. Nat. Compd.* 59, 246–248. doi: 10.1007/s10600-023-03967-z

Lin, S. H., Yan, Q. X., Zhang, Y., Wu, T. Z., Zou, Z. B., Liu, Q. M., et al. (2023). Citriquinolinones a and B: rare isoquinolinone-embedded citrinin analogues and related metabolites from the deep-sea-derived *Aspergillus versicolor* 170217. *Mar. Drugs* 21:504. doi: 10.3390/md21100504

Liu, Y., Ding, L. J., He, J. X., Zhang, Z. M., Deng, Y. T., He, S., et al. (2021). A new antibacterial chromone from a marine sponge-associated fungus *Aspergillus* sp. LS57. *Fitoterapia* 154:105004. doi: 10.1016/j.fitote.2021.105004

Liu, Y., Ding, L. J., Shi, Y. T., Yan, X. J., Wu, B., and He, S. (2022). Molecular networking-driven discovery of antibacterial perinadines, new tetracyclic alkaloids from the marine sponge-derived fungus *Aspergillus* sp. *ACS Omega* 7, 9909–9916. doi: 10.1021/acsomega.2c00402

Liu, Y., Li, X. M., Meng, L. H., and Wang, B. G. (2015). Polyketides from the marine mangrove-derived fungus *Aspergillus ochraceus* MA-15 and their activity against aquatic pathogenic bacteria. *Phytochem. Lett.* 12, 232–236. doi: 10.1016/j.phytol.2015.04.009

Liu, X. H., Miao, F. P., Liang, X. R., and Ji, N. Y. (2014). Ergosteroid derivatives from an algicolous strain of *Aspergillus ustus*. *Nat. Prod. Res.* 28, 1182–1186. doi: 10.1080/14786419.2014.923996

Liu, X. H., Miao, F. P., Qiao, M. F., Cichewicz, R. H., and Ji, N. Y. (2013). Terretonin, ophiobolin, and drimane terpenes with absolute configurations from an algicolous *Aspergillus ustus*. *RSC Adv.* 3, 588–595. doi: 10.1039/C2RA22701K

Liu, W., Wang, L. P., Wang, B., Xu, Y. C., Zhu, G. L., Lan, M. M., et al. (2019). Diketopiperazine and diphenylether derivatives from marine algae-derived *Aspergillus versicolor* OUCMDZ-2738 by epigenetic activation. *Mar. Drugs* 17:6. doi: 10.3390/md17010006

Liu, C. M., Yao, F. H., Lu, X. H., Zhang, X. X., Luo, L. X., Liang, X., et al. (2022). Isoquinoline alkaloids as protein tyrosine phosphatase inhibitors from a deep-sea-derived fungus *Aspergillus puniceus*. *Mar. Drugs* 20:78. doi: 10.3390/md20010078

Lu, C. J., Tang, Z. Z., Su, Z. W., Li, H. Y., Zhang, G. S., Gao, C. H., et al. (2023). Secondary metabolites from marine-derived fungus *Aspergillus carneus* GXIMD00519. *Rec. Nat. Prod.* 17, 343–351. doi: 10.25135/rnp.355.2207.2518

Luo, X. W., Zhou, X. F., Lin, X. P., Qin, X. C., Zhang, T. Y., Wang, J. F., et al. (2017). Antituberculosis compounds from a deep-sea-derived fungus *Aspergillus* sp. SCSIO Ind09F01. *Nat. Prod. Res.* 31, 1958–1962. doi: 10.1080/14786419.2016.1266353

Lv, H. W., Wang, K. B., Xue, Y. X., Chen, J., Su, H. B., Zhang, J. K., et al. (2021). Three new metabolites from the marine-derived fungus *Aspergillus* sp. WHUF03110. *Nat. Prod. Commun.* 16:1934578X2110550. doi: 10.1177/1934578X211055009

Lv, H. W., Zhang, J. K., Xue, Y. X., Li, S. W., Sun, X. Y., Jia, J., et al. (2022). Two new austocystin analogs from the marine-derived fungus *Aspergillus* sp. WHUF05236. *Chem. Biodivers.* 19:e202200207. doi: 10.1002/cbdv.202200207

Machado, F. P., Kumla, D., Pereira, J. A., Sousa, E., Dethoup, T., Freitas-Silva, J., et al. (2021). Prenylated phenylbutyrolactones from cultures of a marine sponge-associated fungus *Aspergillus flavipes* KUFA1152. *Phytochemistry* 185:112709. doi: 10.1016/j.phytochem.2021.112709

Machado, F. P., Rodrigues, I. C., Gales, L., Pereira, J. A., Costa, P. M., Dethoup, T., et al. (2022). New alkylpyridinium anthraquinone, isocoumarin, c-glucosyl resorcinol derivative and prenylated pyranoxanthones from the culture of a marine sponge-associated fungus, *Aspergillus stellatus* KUFA 2017. *Mar. Drugs* 20:672. doi: 10.3390/md20110672

Meng, Q. Y., Guo, X., Wu, J. S., Liu, D., Gu, Y. C., Huang, J., et al. (2022). Prenylated notoamide-type alkaloids isolated from the fungus *Aspergillus sclerotiorum* and their inhibition of NLRP3 inflammasome activation and antibacterial activities. *Phytochemistry* 203:113424. doi: 10.1016/j.phytochem.2022.113424

Miao, F. P., Li, X. D., Liu, X. H., Cichewicz, R. H., and Ji, N. Y. (2012). Secondary metabolites from an algicolous *Aspergillus versicolor* strain. *Mar. Drugs* 10, 131–139. doi: 10.3390/md10010131

Neuhaus, G. F., Adpressa, D. A., Bruhn, T., and Loesgen, S. (2019). Polyketides from marine-derived *Aspergillus porosus*: challenges and opportunities for determining absolute configuration. *J. Nat. Prod.* 82, 2780–2789. doi: 10.1021/acs.jnatprod.9b00416

Okeke, I. N., de Kraker, M. E. A., Van Boeckel, T. P., Kumar, C. K., Schmitt, H., Gales, A. C., et al. (2024). The scope of the antimicrobial resistance challenge. *Lancet* 403, 2426–2438. doi: 10.1016/S0140-6736(24)00876-6

Orfali, R., Aboseada, M. A., Abdel-Wahab, N. M., Hassan, H. M., Perveen, S., Ameen, F., et al. (2021). Recent updates on the bioactive compounds of the marine-derived genus *Aspergillus*. *RSC Adv.* 11, 17116–17150. doi: 10.1039/D1RA01359A

Peng, Q. Y., Cai, J., Long, J. Y., Yang, B., Lin, X. P., Wang, J. F., et al. (2021). New azaphthalide and phthalide derivatives from the marine coral-derived fungus *Aspergillus* sp. SCSIO41405. *Phytochem. Lett.* 43, 94–97. doi: 10.1016/J.PHYTOL.2021.03.019

Peng, Q. Y., Chen, W. H., Lin, X. P., Xiao, J., Liu, Y. H., and Zhou, X. F. (2022). Butenolides from the coral-derived fungus *Aspergillius terreus* SCSIO41404. *Mar. Drugs* 20:212. doi: 10.3390/md20030212

Pinedo-Rivilla, C., Aleu, J., and Duran-Patron, R. (2022). Cryptic metabolites from marine-derived microorganisms using OSMAC and epigenetic approaches. *Mar. Drugs* 20:84. doi: 10.3390/md20020084

Prestinaci, F., Pezzotti, P., and Pantosti, A. (2015). Antimicrobial resistance: a global multifaceted phenomenon. *Pathog. Glob. Health* 109, 309–318. doi: 10.1179/2047773215Y.0000000030

Ren, J. M., Yang, J. K., Zhu, H. J., and Cao, F. (2020). Bioactive steroids from the marine-derived fungus *Aspergillus flavus* JK07-1. *Chem. Nat. Compd.* 56, 945–947. doi: 10.1007/s10600-020-03195-9

Saetang, P., Rukachaisirikul, V., Phongpaichit, S., Preedanon, S., Sakayaroj, J., Hadsadee, S., et al. (2021). Antibacterial and antifungal polyketides from the fungus *Aspergillus unguis* PSU-MF16. *J. Nat. Prod.* 84, 1498–1506. doi: 10.1021/acs.jnatprod.0c01308

Song, F. H., Lin, R., Yang, N., Jia, J., Wei, S. Z., Han, J. H., et al. (2021). Antibacterial secondary metabolites from marine-derived fungus *Aspergillus* sp. IMCASMF180035. *Antibiotics* 10:377. doi: 10.3390/antibiotics10040377

Song, Z. J., Liu, Y., Gao, J. Y., Hu, J. S., He, H. T., Dai, S. W., et al. (2021). Antitubercular metabolites from the marine-derived fungus strain *Aspergillus fumigatus* MF029. *Nat. Prod. Res.* 35, 2647–2654. doi: 10.1080/14786419.2019.1660331

Song, F. H., Liu, X. R., Guo, H., Ren, B., Chen, C. X., and Piggott, A. M. (2012). Brevianamides with antitubercular potential from a marine-derived isolate of *Aspergillus versicolor*. *Org. Lett.* 14, 4770–4773. doi: 10.1021/ol302051x

Song, F. H., Ren, B., Chen, C. X., Yu, K., Liu, X. R., Zhang, Y. H., et al. (2014). Three new sterigmatocystin analogues from marine-derived fungus *Aspergillus versicolor* MF359. *Appl. Microbiol. Biotechnol.* 98, 3753–3758. doi: 10.1007/s00253-013-5409-5

Sun, C. Z., Ha, Y. R., Liu, X., Wang, N., Lian, X. Y., and Zhang, Z. Z. (2024). Isolation and structure elucidation of new metabolites from the mariana-trench-associated fungus *Aspergillus* sp. SY2601. *Molecules* 29:459. doi: 10.3390/molecules29020459

Sun, K. L., Li, Y., Guo, L., Wang, L., Liu, P. P., and Zhu, W. M. (2014). Indole diterpenoids and isocoumarin from the fungus, *Aspergillus flavus*, isolated from the prawn, *Penaeus vannamei*. *Mar. Drugs* 12, 3970–3981. doi: 10.3390/md12073970

Sun, L. X., Wang, H. N., Yan, M. C., Sai, C. M., and Zhang, Z. (2022). Research advances of bioactive sesquiterpenoids isolated from marine-derived *Aspergillus* sp. *Molecules* 27:7376. doi: 10.3390/molecules27217376

Sun, C. X., Zhang, Z. P., Ren, Z. L., Yu, L., Zhou, H., Han, Y. X., et al. (2020). Antibacterial cyclic tripeptides from Antarctica-sponge-derived fungus *Aspergillus insulicola* HDN151418. *Mar. Drugs* 18:532. doi: 10.3390/md18110532

Thi, H. A. N., Mai, A. N., Thi, T. H. V., Thi, M. H. D., Van, C. P., Thanh, X. D., et al. (2023). Antimicrobial activity of depsidones and macrocyclic peptides isolated from marine sponge-derived fungus *Aspergillus nidulans* M256. *Chem. Biodivers.* 20:e202301660. doi: 10.1002/cbdv.202301660

Tian, Y. Q., Lin, S. T., Kumaravel, K., Zhou, H., Wang, S. Y., and Liu, Y. H. (2018). Polyketide-derived metabolites from the sponge-derived fungus *Aspergillus* sp. F40. *Phytochem. Lett.* 27, 74–77. doi: 10.1016/j.phytol.2018.06.009

Tuan, C. D., Van Hung, N., Minh, L. T. H., Lien, H. T. H., Chae, J. W., Yun, H. Y., et al. (2022). A new indole glucoside and other constituents from the sea cucumber-derived *Aspergillus fumigatus* M580 and their biological activities. *Rec. Nat. Prod.* 16, 633–638. doi: 10.25135/rnp.310.2110.2248

Ukwatta, K. M., Lawrence, J. L., and Wijayarathne, C. D. (2020). Antimicrobial, anti-cancer, anti-filarial and anti-inflammatory activities of cowabenzophenone a extracted from the endophytic fungus *Aspergillus terreus* isolated from a mangrove plant *Bruguiera gymnorrhyza*. *Mycology* 11, 297–305. doi: 10.1080/21501203.2019.1707722

Wallis, R. S., O'Garra, A., Sher, A., and Wack, A. (2023). Host-directed immunotherapy of viral and bacterial infections: past, present and future. *Nat. Rev. Immunol.* 23, 121–133. doi: 10.1038/s41577-022-00734-z

Wang, W. Y., Chen, R. X., Luo, Z. H., Wang, W., and Chen, J. M. (2018). Antimicrobial activity and molecular docking studies of a novel anthraquinone from a marine-derived fungus *Aspergillus versicolor*. *Nat. Prod. Res.* 32, 558–563. doi: 10.1080/14786419.2017.1329732

Wang, Q. Y., Chen, H. P., Wu, K. Y., Li, X. Y., and Liu, J. K. (2022). Antibacterial and *β*-amyloid precursor protein-cleaving enzyme 1 inhibitory polyketides from the fungus *Aspergillus chevalieri*. *Front. Microbiol.* 13:1051281. doi: 10.3389/fmicb.2022.1051281

Wang, K. W., and Ding, P. (2018). New bioactive metabolites from the marine-derived fungi *Aspergillus*. *Mini-Rev. Med. Chem.* 18, 1072–1094. doi: 10.2174/1389557518666180305160856

Wang, W. Y., Gao, M. L., Luo, Z. H., Liao, Y. Y., Zhang, B. B., Ke, W. Q., et al. (2019). Secondary metabolites isolated from the deep sea-derived fungus *Aspergillus sydowii* C1-S01-A7. *Nat. Prod. Res.* 33, 3077–3082. doi: 10.1080/14786419.2018.1519561

Wang, C. Y., Liu, X. H., Zheng, Y. Y., Ning, X. Y., Zhang, Y. H., Fu, X. M., et al. (2022). 2,5-diketopiperazines from a sponge-derived fungus *Aspergillus sclerotiorum*. *Front. Microbiol.* 13:808532. doi: 10.3389/fmicb.2022.808532

Wang, C., Sarotti, A. M., Zaman, K. H., Ahammad, U., Wu, X. H., and Cao, S. G. (2021). New alkaloids from a Hawaiian fungal strain *Aspergillus felis* FM324. *Front. Chem.* 9:724617. doi: 10.3389/fchem.2021.724617

Wen, H. M., Zhang, Y. W., Feng, F. J., Huang, G. B., Lv, Y. H., Zhang, Z. Y., et al. (2024). Antibacterial oxygenated ergostane-type steroids produced by the marine sponge-derived fungus *Aspergillus* sp. *J. Asian Nat. Prod. Res.* 26, 548–554. doi: 10.1080/10286020.2023.2259317

Wu, J. S., Shi, X. H., Yao, G. S., Shao, C. L., Fu, X. M., Zhang, X. L., et al. (2020a). New thiodiketopiperazine and 3,4-dihydroisocoumarin derivatives from the marine-derived fungus *Aspergillus terreus*. *Mar. Drugs* 18:132. doi: 10.3390/md18030132

Wu, J. S., Shi, X. H., Zhang, Y. H., Shao, C. L., Fu, X. M., Li, X., et al. (2020b). Benzyl furanones and pyrones from the marine-derived fungus *Aspergillus terreus* induced by chemical epigenetic modification. *Molecules* 25:3927. doi: 10.3390/molecules25173927

Wu, J., Shui, H., Zhang, M. K., Zeng, Y. D., Zheng, M. X., Zhu, K. K., et al. (2023). Aculeaxanthones A-E, new xanthones from the marine-derived fungus *Aspergillus aculeatinus* WHUF0198. *Front. Microbiol.* 14:1138830. doi: 10.3389/fmicb.2023.1138830

Xu, P., Ding, L. J., Wei, J. X., Li, Q., Gui, M. J., He, X. P., et al. (2020). A new aquatic pathogen inhibitor produced by the marine fungus *Aspergillus* sp. LS116. *Aquaculture* 520:734670. doi: 10.1016/j.aquaculture.2019.734670

Xu, X. L., Han, J. H., Zhang, X. W., Xu, W., Yang, J. P., and Song, F. H. (2024). Investigation on the chemical constituents of the marine-derived fungus strain *Aspergillus brunneoviolaceus* MF180246. *Nat. Prod. Res.* 38, 1369–1374. doi: 10.1080/14786419.2022.2144300

Xu, W. F., Wu, N. N., Wu, Y. W., Qi, Y. X., Wei, M. Y., Pineda, L. M., et al. (2022). Structure modification, antialgal, antiplasmodial, and toxic evaluations of a series of new marine-derived 14-membered resorcylic acid lactone derivatives. *Mar. Life Sci. Tech.* 4, 88–97. doi: 10.1007/s42995-021-00103-0

Xu, X. L., Yang, H. J., Xu, H. T., Yin, L. Y., Chen, Z. K., and Shen, H. H. (2018). Diphenyl ethers from a marine-derived isolate of *Aspergillus* sp. CUGB-F046. *Nat. Prod. Res.* 32, 821–825. doi: 10.1080/14786419.2017.1363754

Xu, K., Yuan, X. L., Li, C., and Li, A. X. (2020). Recent discovery of heterocyclic alkaloids from marine-derived *Aspergillus* species. *Mar. Drugs* 18:54. doi: 10.3390/md18010054

Xu, L. L., Zhang, C. C., Zhu, X. Y., Cao, F., and Zhu, H. J. (2017). Bioactive phenyl ether derivatives from the marine-derived fungus *Aspergillus carneus*. *Nat. Prod. Res.* 31, 1875–1879. doi: 10.1080/14786419.2016.1263848

Xuan, J. Q., Feng, W. G., Wang, J. Y., Wang, R. C., Zhang, B. W., Bo, L. T., et al. (2023). Antimicrobial peptides for combating drug-resistant bacterial infections. *Drug Resist. Update* 68:100954. doi: 10.1016/j.drup.2023.100954

Xue, J. J., Guo, X. P., Xu, G. X., Chen, X., Jiao, L. H., and Tang, X. X. (2024). Discovery, identification, and mode of action of phenolics from marine-derived fungus *Aspergillus ustus* as antibacterial wilt agents. *J. Agr. Food. Chem.* 72, 2989–2996. doi: 10.1021/acs.jafc.3c07826

Yan, L. H., Du, F. Y., Li, X. M., Yang, S. Q., Wang, B. G., and Li, X. (2023). Antibacterial indole diketopiperazine alkaloids from the deep-sea cold seep-derived fungus *Aspergillus chevalieri*. *Mar. Drugs* 21:195. doi: 10.3390/md21030195

Yang, J., Gong, L. Z., Guo, M. M., Jiang, Y., Ding, Y., Wang, Z. J., et al. (2021). Bioactive indole diketopiperazine alkaloids from the marine endophytic fungus *Aspergillus* sp. YJ191021. *Mar. Drugs* 19:157. doi: 10.3390/md19030157

Yang, S. Q., Li, X. M., Li, X., Li, H. L., Meng, L. H., and Wang, B. G. (2018b). New citrinin analogues produced by coculture of the marine algal-derived endophytic fungal strains *Aspergillus sydowii* EN-534 and *Penicillium citrinum* EN-535. *Phytochem. Lett.* 25, 191–195. doi: 10.1016/j.phytol.2018.04.023

Yang, S. Q., Li, X. M., Xu, G. M., Li, X., An, C. Y., and Wang, B. G. (2018a). Antibacterial anthraquinone derivatives isolated from a mangrove-derived endophytic fungus *Aspergillus nidulans* by ethanol stress strategy. *J. Antibiot.* 71, 778–784. doi: 10.1038/s41429-018-0063-x

Yang, G. H., Sandjo, L., Yun, K., Leutou, A. S., Kim, G. D., Choi, H. D., et al. (2011). Flavusides a and B, antibacterial cerebrosides from the marine-derived fungus *Aspergillus flavus*. *Chem. Pharm. Bull.* 59, 1174–1177. doi: 10.1248/cpb.59.1174

Yang, M. Y., Yang, J. K., Yang, J. K., Hu, L. D., Zhu, H. J., and Cao, F. (2018). New oxygenated steroid from the marine-derived fungus *Aspergillus flavus*. *Nat. Prod. Commun.* 13:1934578X1801300. doi: 10.1177/1934578X1801300807

Yang, X., Yu, H. J., Ren, J. W., Cai, L., Xu, L. J., and Liu, L. (2023). Sulfoxide-containing bisabolane sesquiterpenoids with antimicrobial and nematicidal activities from the marine-derived fungus *Aspergillus sydowii* LW09. *J. Fungi* 9:347. doi: 10.3390/jof9030347

Ye, W. X., Zhao, M. R., Wang, L., Jiang, X. D., Zhang, W. J., Zhang, C. S., et al. (2022). Isolation, identification, and bioactive metabolites of coral-derived fungus *Aspergillus* sp. SCSIO 40435 from the South China Sea. *Weishengwu Xuebao* 62, 1819–1831. doi: 10.13343/j.cnki.wsxb.20210568

Yu, G. H., Wu, G. W., Sun, Z. C., Zhang, X. M., Che, Q., Gu, Q. Q., et al. (2018). Cytotoxic tetrahydroxanthone dimers from the mangrove-associated fungus *Aspergillus versicolor* HDN1009. *Mar. Drugs* 16:335. doi: 10.3390/md16090335

Yu, H. J., Xue, Y. X., Hong, K., Jia, J., Bi, H. K., Xu, L. J., et al. (2022). Secondary metabolites from a mangrove-derived fungus *Aspergillus* sp. WHUF0343. *Weishengwu Xuebao* 62, 2658–2670. doi: 10.13343/j.cnki.wsxb.20210655

Yurchenko, A. N., Girich, E. V., and Yurchenko, E. A. (2021). Metabolites of marine sediment-derived fungi: actual trends of biological activity studies. *Mar. Drugs* 19:88. doi: 10.3390/md19020088

Zang, Z. M., Yang, W. C., Cui, H., Cai, R. L., Li, C. Y., Zou, G., et al. (2022). Two antimicrobial heterodimeric tetrahydroxanthones with a 7,7′-linkage from mangrove endophytic fungus *Aspergillus flavus* QQYZ. *Molecules* 27:2691. doi: 10.3390/molecules27092691

Zeng, Q., Chen, Y. C., Wang, J. F., Shi, X. F., Che, Y. H., Chen, X. Y., et al. (2022a). Diverse secondary metabolites from the coral-derived fungus *Aspergillus hiratsukae* SCSIO $5Bn_1003$. *Mar. Drugs* 20:150. doi: 10.3390/md20020150

Zeng, Q., Zhong, W. M., Chen, Y. C., Xiang, Y., Chen, X. Y., Tian, X. P., et al. (2020b). A new butenolide derivative from the deep-sea fungus *Aspergillus terreus* SCSIO FZQ028. *Nat. Prod. Res.* 34, 1984–1991. doi: 10.1080/14786419.2019.1569658

Zhang, J., Gao, L. L., Lin, H. T., Liang, Y., You, M. N., Ding, L. J., et al. (2024). Discovery of antibacterial compounds against *Xanthomonas citri* subsp. citri from a marine fungus *Aspergillus terreus* SCSIO 41202 and the mode of action. *J. Agric. Food. Chem.* 72, 12596–12606. doi: 10.1021/acs.jafc.4c02769

Zhang, Y. H., Hou, X. M., Yu, M. L., and Wang, C. Y. (2019). Secondary metabolites and their bioactivities from the gorgonian-derived fungus *Aspergillus versicolor*. *Chem. Nat. Compd.* 55, 327–330. doi: 10.1007/s10600-019-02680-0

Zhang, Y. T., Li, Z. C., Huang, B. Y., Liu, K., Peng, S., Liu, X. M., et al. (2022). Anti-osteoclastogenic and antibacterial effects of chlorinated polyketides from the beibu gulf coral-derived fungus *Aspergillus unguis* GXIMD02505. *Mar. Drugs* 20:178. doi: 10.3390/md20030178

Zhang, Y., Li, X. M., and Wang, B. G. (2012). Anthraquinone derivatives produced by marine-derived fungus *Aspergillus versicolor* EN-7. *Biosci. Biotechnol. Biochem.* 76, 1774–1776. doi: 10.1271/bbb.120047

Zhang, L., Qiu, P. P., Ding, L. J., Li, Q., Song, J. J., Han, Z. W., et al. (2020). A new antibacterial chlorinated amino acid derivative from the sponge-derived fungus *Aspergillus* sp. LS53. *Chem. Nat. Compd.* 56, 109–111. doi: 10.1007/s10600-020-02955-x

Zhang, R., Wang, H. F., Chen, B. S., Dai, H. Q., Sun, J. Z., Han, J. J., et al. (2022). Discovery of anti-MRSA secondary metabolites from a marine-derived fungus *Aspergillus fumigatus*. *Mar. Drugs* 20:302. doi: 10.3390/md20050302

Zhang, Y. H., Xu, Y., Wang, C. Y., and Cao, F. (2020). Alkaloids and sesquiterpenoids from the marine-derived fungus *Aspergillus versicolor*. *Chem. Nat. Compd.* 56, 971–973. doi: 10.1007/s10600-020-03205-w

Zheng, C. J., Shao, C. L., Wu, L. Y., Chen, M., Wang, K. L., Zhao, D. L., et al. (2013). Bioactive phenylalanine derivatives and cytochalasins from the soft coral-derived fungus, *Aspergillus elegans*. *Mar. Drugs* 11, 2054–2068. doi: 10.3390/md11062054

Zhou, Y. M., Debbab, A., Wray, V., Lin, W. H., Schulz, B., Trepos, R., et al. (2014). Marine bacterial inhibitors from the sponge-derived fungus *Aspergillus* sp. *Tetrahedron Lett.* 55, 2789–2792. doi: 10.1016/j.tetlet.2014.02.062

Zhu, S. H., Chang, Y. M., Su, M. Z., Yao, L. G., Li, S. W., Wang, H., et al. (2024). Nine new antibacterial diterpenes and steroids from the South China Sea soft coral *Lobophytum catalai Tixier-Durivault*. *Mar. Drugs* 22:50. doi: 10.3390/md22010050

Zhu, F., Chen, G. Y., Chen, X., Huang, M. Z., and Wan, X. Q. (2011). Aspergicin, a new antibacterial alkaloid produced by mixed fermentation of two marine-derived mangrove epiphytic fungi. *Chem. Nat. Compd.* 47, 767–769. doi: 10.1007/s10600-011-0053-8

Zhu, A., Zhang, X. W., Zhang, M., Li, W., Ma, Z. Y., Zhu, H. J., et al. (2018). Aspergixanthones I-K, new anti-vibrio prenylxanthones from the marine-derived fungus *Aspergillus* sp. ZA-01. *Mar. Drugs* 16:312. doi: 10.3390/md16090312

frontiers | Frontiers in Microbiology

TYPE Original Research
PUBLISHED 30 October 2024
DOI 10.3389/fmicb.2024.1416844

OPEN ACCESS

EDITED BY
Octavio Luiz Franco,
Catholic University of Brasilia (UCB), Brazil

REVIEWED BY
Muneeswaran Thillaichidambaram,
University of Chile, Chile
Huma Qureshi,
University of Chakwal, Pakistan

*CORRESPONDENCE
Wenjie Jian
✉ 201300010176@xmmc.edu.cn

†These authors have contributed equally to this work

RECEIVED 13 April 2024
ACCEPTED 17 October 2024
PUBLISHED 30 October 2024

CITATION
He P, Wang W and Jian W (2024) Antibacterial activity against pathogenic *Vibrio* and cytotoxicity on human hepatocyte of nano-silver prepared by polysaccharide-protein complexes. *Front. Microbiol.* 15:1416844. doi: 10.3389/fmicb.2024.1416844

Antibacterial activity against pathogenic *Vibrio* and cytotoxicity on human hepatocyte of nano-silver prepared by polysaccharide-protein complexes

Peirong He[1,2†], Wenying Wang[2†] and Wenjie Jian[2*]

[1]College of Public Health, Fujian Medical University, Fuzhou, China, [2]Department of Public Health and Medical Technology, Xiamen Medical College, Xiamen, China

Silver nanoparticles (AgNPs) are potential antibacterial agents against pathogenic *Vibrio* bacteria in the field of public health, yet their widespread use is limited by dispersibility and biocompatibility. In a previous study, highly dispersible AgNPs were fabricated using a polysaccharide–protein complex (PSP) obtained from the viscera *of Haliotis discus*. In this study, the antibacterial activity of PSP-AgNPs against pathogenic *Vibrio* and its cytotoxicity for human hepatocytes (LO2) was evaluated. At dosages of 3.125–25.0 μg/mL, PSP-AgNPs demonstrated excellent antibacterial activity against several pathogenic *Vibrio* strains (such as *V. fluvialis*, *V. mimicus*, *V. hollisae, V. vulnificus*, and *V. furnissii*), and no cytotoxicity on LO2 cells. This was evidenced by cellular viability, reactive oxygen species, and antioxidase activities. However, severe cytotoxicity was observed at a PSP-AgNPs concentration of 50.0 μg/mL. Furthermore, intracellular oxidative stress was the predominant mechanism of toxicity induced by PSP-AgNPs. Overall, PSP-AgNPs are highly biocompatible in the range of effective antibacterial dosages, identifying them as promising bactericide candidates in the field of public health.

KEYWORDS

pathogenic *Vibrio*, silver nanoparticles, cytotoxicity, antibacterial activity, polysaccharide-protein complexes, human hepatocyte

1 Introduction

Diseases caused by infection with pathogenic bacteria of the genus *Vibrio* are common in the field of public health and aquaculture (Brumfield et al., 2021; Fleischmann et al., 2022). These diseases can cause large-scale mortality in all stages of aquatic animal culture and infectious diseases in humans (Brumfield et al., 2021; Neetoo et al., 2022).

To control pathogenic *Vibrio* strains, various approaches including antibiotics, probiotics, and plant-based products have been employed in aquaculture (Chandrakala and Parameswari, 2021; Abioye and Okoh, 2018). However, these approaches cannot fully meet practical demand, and have several negative side effects. For example, the overuse of antibiotics leads to the emergence of drug-resistant bacterial strains (Sony et al., 2021; RathnaKumari et al., 2018). Thus, the search for safe and effective antimicrobial agents against pathogenic *Vibrio* strains has become a major research goal worldwide.

Recent developments in silver nanoparticles (AgNPs) have identified these as good alternatives to overcome the above problems, because of their broad-spectrum and efficient efficacy against bacteria, fungi, and antibiotic-resistant pathogens (Serrano-Díaz et al., 2023). Despite their excellent bactericidal effect, the widespread use of AgNPs is commonly limited by their dispersion stability and biological safety resulting from preparation methods (Yang and Wu, 2022). Traditionally, AgNPs are prepared by chemical vapor deposition irradiation or chemical reduction of metal salts with sodium borohydride. These processes result in unsuitable dispensability, harmful by-products, and toxic residues.

To overcome these defects, a suitable polysaccharide-protein (PSP) complex was obtained from the viscera of *Haliotis discus*. PSP has been used for the preparation of AgNPs in a previous study by our team (Sony et al., 2021). The PSP complex plays the role of a reducing and capping agent under a simple redox system of silver nitrate without the addition of a reducing agent. The prepared PSP-AgNPs demonstrated excellent antibacterial activity against *Staphylococcus aureus* (Gram-positive) and *Escherichia coli* (Gram-negative). Additionally, PSP-AgNPs achieved highly stable dispersion even in seawater (Jian et al., 2020).

Overall, to explore the potential application of PSP-AgNPs as an antibacterial agent against pathogenic *Vibrio* strains, it is necessary to measure the antibacterial activity against the main pathogenic *Vibrio* strains and gauge its cytotoxicity. So far, numerous studies demonstrated that one predominant mechanism of toxicity is the intracellular oxidative stress, which is induced by AgNPs in a dose and time-dependent manner (Xue et al., 2018; Komazec et al., 2023). This intracellular oxidative stress leads to cell membrane leakage, mitochondria injury, and subsequent apoptotic cell death (Xue et al., 2016; Salama et al., 2023). Therefore, measuring the oxidative stress is an effective method to determine the toxicity of AgNPs. Oxidative stress can be represented by depletion of glutathione (GSH) as well as induction of reactive oxygen species (ROS), lipid peroxidation, superoxide dismutase (SOD), and catalase (Suliman et al., 2015; Lu et al., 2022). Limited by research capacity, the human hepatocyte cell line (LO2) was chosen as the model system in this study, as an *in vivo* biodistribution study indicated that AgNPs are mainly accumulated in the liver (Xue et al., 2018).

In short, the objective of this study was to evaluate the antibacterial activity against the main pathogenic members of the genus *Vibrio* (*V. fluvialis*, *V. mimicus*, *V. hollisae*, *V. vulnificus*, and *V. furnissii*). Based on the result of antibacterial tests, cytotoxicity and oxidative stress of PSP-AgNPs on LO2 cells was further examined by determining cellular viability, as well as the content of malondialdehyde (MDA), and the activity of lactate dehydrogenase (LDH), glutathione peroxidase (GSH-Px), and SOD.

TABLE 1 Antibacterial activities [minimum inhibitory concentration (MIC) and minimum bactericidal concentration (MBC)] of polysaccharide–protein complex silver nanoparticles (PSP-AgNPs) against various pathogenic *Vibrio* strains.

Bacteria of interest	MIC (μ g/mL)	MBC (μ g/mL)
Vibrio fluvialis	12.5	12.5
Vibrio mimicus	6.25	25.0
Vibrio hollisae	6.25	12.5
Vibrio vulnificus	12.5	25.0
Vibrio furnissii	3.125	12.5

2 Results

2.1 Antibacterial activities against pathogenic *Vibrio* strains

The antibacterial activities of PSP-AgNPs against several pathogenic *Vibrio* strains are listed in Table 1. The minimum inhibitory concentration (MIC) and minimum bactericidal concentration (MBC) of PSP-AgNPs against *V. fluvialis* were both 12.5 μg/mL. The corresponding values for PSP-AgNPs against *V. mimicus* were 6.25 and 25.0 μg/mL, respectively. The smallest MIC of 3.125 μg/mL was found in *V. furnissii*, and the smallest MBC value of 12.5 μg/mL was found in *V. fluvialis*, *V. hollisae*, and *V. furnissii*. Thus, it can be concluded that the effective concentration range of PSP-AgNPs against pathogenic *Vibrio* was 3.125–25.0 μg/mL.

2.2 Cytotoxicity on LO2 cells

As shown in Figure 1, PSP-AgNPs showed no cytotoxicity on LO2 cells within the effective dosages of PSP-AgNPs against bacteria (6.25–25.0 μg/mL). However, significantly decreased cellular viability was observed at dosages of 50.0 and 100.0 μg/mL ($p < 0.01$). Compared to control, the cellular viabilities at dosages of 50.0 and 100.0 μg/mL were 43.4 ± 8.59% and 11.38 ± 2.01%, respectively. The dose-response curve of LO2 cells is displayed in Figure 1. The exact concentration of LC_{50} was 49.0 μg/mL.

2.3 Intracellular ROS levels and MDA content

Excessive production of ROS induces cellular apoptosis; therefore, the ROS formation after 24 h of PSP-AgNPs exposure was assessed using the 2-7-dichlorodiacetate (DCFH-DA) assay. As shown in Figure 2, the ROS levels increased significantly at concentrations of 50.0 or 100.0 μg/mL compared to Control, and no significant changes were found at other concentration levels (6.25–25.0 μg/mL). As shown in Figure 2, a significant increase of the intracellular MDA ($p < 0.01$) was observed in groups treated with PSP-AgNPs at concentrations of 50.0 and 100.0 μg/mL. Simultaneously, compared to Control, the MDA content did not increase in groups treated with PSP-AgNPs at concentrations of 6.25, 12.5, or 25.0 μg/mL.

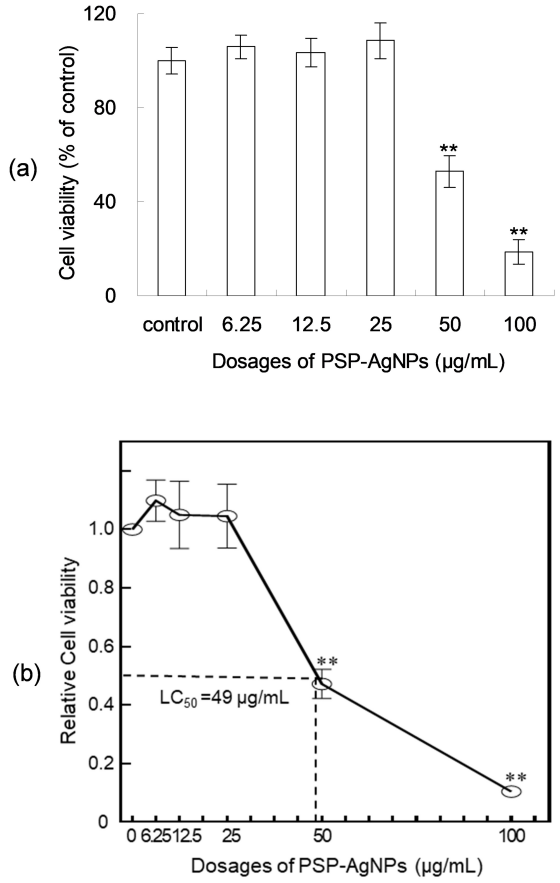

FIGURE 1
Viability **(a)** and dose-response curve **(b)** of LO2 cells treated with polysaccharide-protein complex silver nanoparticles (PSP-AgNPs) (6.25–100.0 μg/mL) for 24 h. Data are mean ± SD, $^{**}P < 0.01$ vs. Control.

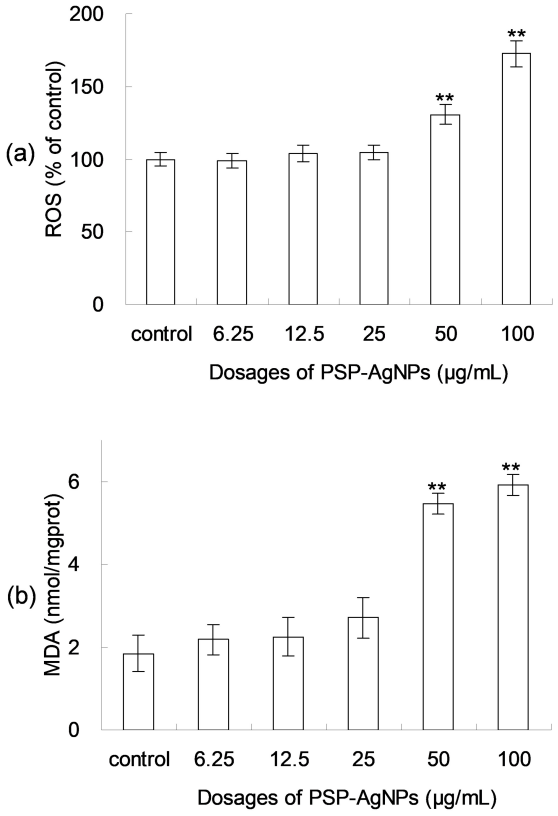

FIGURE 2
Levels of reactive oxygen species (ROS) **(a)** and malondialdehyde (MDA) content **(b)** in LO2 cells treated with PSP-AgNPs (6.25–100.0 μg/mL) for 24 h. Data are mean ± SD, $^{**}P < 0.01$ vs. Control.

2.4 Level of intracellular LDH

Based on the above results of cellular viability and MDA content, the level of intracellular LDH in LO2 was further evaluated. As shown in Figure 3, the level of intracellular LDH significantly decreased ($p < 0.01$) in groups exposed to PSP-AgNPs at concentrations of 50.0 and 100.0 μg/mL. However, compared to Control, no significant difference was found in groups treated with PSP-AgNPs at concentrations of 6.25, 12.5, and 25.0 μg/mL.

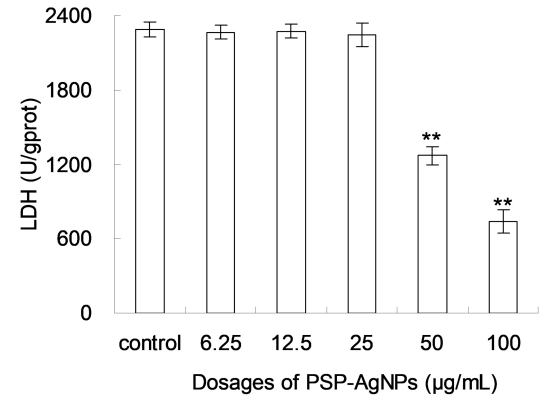

FIGURE 3
Levels of intracellular lactate dehydrogenase (LDH) in LO2 cells treated with PSP-AgNPs (6.25–100.0 μg/mL) for 24 h. Data are mean ± SD, $^{**}P < 0.01$ vs. Control.

2.5 Activities of antioxidases

As shown in Figure 4, dose-dependent decreases of SOD and GSH-Px activity were found in LO2 cells exposed to PSP-AgNPs. In the treatment of PSP-AgNPs at concentrations of 50.0 and 100.0 μg/mL, SOD and GSH-Px activity were significantly lower than those in the Control. However, significant differences were not found in other treatments compared to Control. These observations show that the activity of antioxidant enzymes within LO2 were markedly inhibited by PSP-AgNPs exposure at concentrations up to 50.0 μg/mL.

3 Discussion

The antibacterial activity of PSP-AgNPs against *V. vulnificus* was superior to that in literature in which a higher dosage of AgNPs, stabilized by carboxy methyl cellulose, was needed (Prema et al., 2017). MIC values and MBC values of AgNPs against *V. vulnificus* were 60.0 and 70.0 μg/mL, respectively. However,

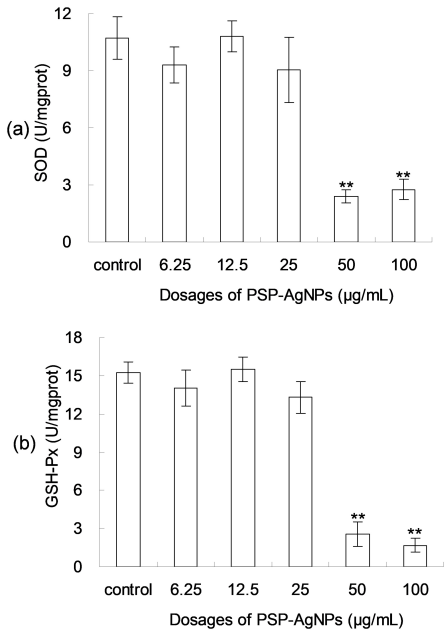

FIGURE 4
The levels of intracellular superoxide dismutase (SOD) **(a)** and glutathione peroxidase (GSH-Px) **(b)** in LO2 cells treated with PSP-AgNPs (6.25–100.0 μg/mL) for 24 h. Data are mean ± SD, $^{**}P < 0.01$ vs. Control.

the corresponding values of PSP-AgNPs against *V. vulnificus* were 12.50 and 25.0 μg/mL, respectively. A similar phenomenon was also found in AgNPs prepared by the Red alga *Portieria hornemannii*, for which the MIC value against *V. vulnificus* was 15.62 μg/mL (Fatima et al., 2020).

In addition to *V. vulnificus*, PSP-AgNPs also demonstrated superior antibacterial activity against *V. fluvialis* compared to the literature (Meneses-Márquez et al., 2019). Previously, a dosage of 22.5 μg/mL was needed to completely inhibit the growth of *V. fluvialis* by AgNPs, which was prepared by sodium citrate (Meneses-Márquez et al., 2019). However, in the present study, the MIC of PSP-AgNPs against *V. fluvialis* was 12.5 μg/mL. So far, no antibacterial activity of AgNPs against *V. mimicus*, *V. hollisae*, or *V. furnissii* had been reported in the literature. In conclusion, PSP-AgNPs displayed effective antibacterial activity against pathogenic *Vibrio* strains within a concentration range of 3.125–25.0 μg/mL. Additionally, the excellent antibacterial activities demonstrated by PSP-AgNPs should be ascribed to its small average particle size (5 nm) and highly stable dispersion (Jian et al., 2019).

The observations of cellular viability of LO2 cells were in accordance with the results of a previous study, in which PSP-AgNPs were freshly prepared (Jian et al., 2019). This result further confirmed the excellent dispersion stability of PSP-AgNPs as previously reported (Jian et al., 2020). Further, the above findings also showed that PSP-AgNPs injured LO2 cells at dosages exceeding 50.0 μg/mL ($p < 0.01$). This critical toxic concentration of LO2 cells found in PSP-AgNPs approximated to the value reported in the literature, in which LO2 cells maintained normal viability at an exposure level below 80 μg/mL of AgNPs coated with polyvinylpyrrolidone (Jian et al., 2020). Overall, the results of this study confirmed that high dosages of AgNPs exerted cellular damage on LO2 cells, which was also reported in the literature (Piao et al., 2011). Thus, the following determination of oxidative stress were conducted to elucidate the mechanism.

The findings found in our study was partly consistent with the report in the literature, in which AgNPs caused the generation of ROS in a dose-dependent manner in many cell types (Rezvani et al., 2019). However, previous research demonstrated that AgNPs coated by polyvinylpyrrolidone did not induce increased ROS levels in LO2 cells over a concentration range of 20.0–160.0 μg/mL (Xue et al., 2018). This inconsistency between the present study and the literature may be caused by the different physiochemical properties of AgNPs used. This further indicates that the physiochemical properties of AgNPs play an important part in its toxicity and biological effect (Rezvani et al., 2019). The detailed mechanism should be fully examined in the future.

In addition to cell viability and ROS, the content of MDA is also an important index for cellular injuries caused by oxidative stress. Being a byproduct of lipid peroxidation, MDA is a common marker for the quantification of lipid peroxide (Ale et al., 2019). These observations of ROS levels and MDA contents were fully consistent with cellular viability findings. Further, oxidative damage only occurred in LO2 cells when the concentration of PSP-AgNPs exceeded 50.0 μg/mL. In addition, the dose dependent effects of AgNPs on MDA accumulation were also reported before (El Mahdy et al., 2015), in which the tests were done in other cell lines, tissues (El-Samad et al., 2022), or animals (Alwan et al., 2021).

LDH is a soluble yet stable cytoplasmic enzyme that is released into the cell culture medium once the cell membrane is damaged (Alhajjar et al., 2022). Thus, the level of intracellular LDH can be used to assess the integrity of the cell membrane. A decreased level of intracellular LDH indicates an injured cell membrane (Xue et al., 2018). Thus, the observed levels of intracellular LDH demonstrated that the cell membrane was damaged at concentrations of PSP-AgNPs up to 50.0 μg/mL. Cell membranes showed no injury at concentrations of PSP-AgNPs below 25.0 μg/mL. This finding of LDH levels was in accordance with observations of cell viability and MDA content.

Additionally, this toxicity of PSP-AgNPs on cell membrane integrity was lower than that reported in the literature, in which 20.0 μg/mL of AgNPs significantly disrupted the cell membrane integrity of LO2 (Xue et al., 2018). This showed that PSP-AgNPs had lower toxicity compared to other AgNPs. This difference in toxicity may be ascribed to the coating, particle sizes, or preparation methods (Rezvani et al., 2019), and the detailed mechanism should be fully analyzed in the future.

It has been reported that treatment with AgNPs generates elevated intracellular ROS levels and disrupts the activities of antioxidant enzymes (Suliman et al., 2015). SOD and GSH-Px are essential intracellular antioxidant enzymes that help cells to resist oxidative damage. Their ability to remove free radicals is directly proportional to their enzyme activity. Excessive free radicals within cells can trigger cellular toxicity, leading to a reduction in intracellular antioxidant enzyme levels (Nguyen et al., 2020). SOD converts superoxide radical to hydrogen peroxide and oxygen, and thus eliminates cellular damage caused by superoxide radical. Similarly, GSH-Px works on peroxides to prevent cell injury (Fouda et al., 2021).

These findings of antioxidant enzyme activity were contrary to previous research in which AgNPs were found to induce increased

level of ROS and SOD, when their concentrations were elevated to a critical value (Suliman et al., 2015; Jiang et al., 2014). The elevated activities of SOD reported in the literature were ascribed to the need to scavenge ROS after exposure to AgNPs (Jiang et al., 2014). An opposing phenomenon in SOD activity was observed between this research and the literature, which may be ascribed to various factor, such as physical-chemical properties of AgNPs, treated subjects, and observation time (Lin et al., 2022). The detailed mechanism should be further studies in the future.

4 Materials and methods

4.1 Cell culture and materials

The LO2 cell line was obtained from iCell Bioscience Inc. (Shanghai, China). Dulbecco's modified Eagle medium (DMEM), which is a low glucose liquid medium (cat. no. D6046) was purchased from Merck & Co., Inc. (Rahway, NJ, USA). Fetal bovine serum (cat. no. 10437) was purchased from Invitrogen (Thermo Fisher Scientific, Waltham, MA, USA). Penicillin (cat. no. 87-08-1) and streptomycin (cat. no. 3810-74-0) with purities of up to 99.9% were obtained from Sigma Aldrich (Milwaukee, Missouri,USA). DCFH-DA (cat. no. D6883) was purchased from Merck & Co., Inc.

Vibrio fluvialis (ATCC 33809), *Vibrio mimicus* (ATCC 33653), *Vibrio hollisae* (ATCC 35084), *Vibrio vulnificus* (ATCC 27562) and *Vibrio furnissii* (ATCC 35016) were purchased from China General Microbiological Culture Collection Center.

Ultrapure water (18 MΩ, Millipore) was used in all experiments. The assay kits for the determination of MDA (cat. no. A003-4-1), LDH (cat. no. A020-2-2), SOD (cat. no. A001-3-2), and GSH-Px (cat. no. A005-1-2) were supplied by the Nanjing Jian-cheng Bioengineering Institute (Nanjing, China).

4.2 PSP and PSP-AgNPs

PSP was obtained in our previous research, via hydrolysis of viscera *of Haliotis discus* upon further purification of membrane filtration and gel permeation chromatography (Jian et al., 2019). The weight-averaged molecular weight (Mw) of PSP was 25.38 ± 0.75 kDa with a polydispersity index of 1.181 ± 1.32. A random coil conformation was found in PSP, with a root-mean-square radius (Rz) of 32.23 ± 2.76 nm. The contents of sugar and protein of PSP were 55.51 ± 0.43% and 27.01 ± 0.54%, respectively. Seven types of monosaccharide were found in the polysaccharides of PSP, and the protein of PSP was composed of 18 types of amino acids. Detailed information about PSP can be found in our previous study (Jian et al., 2019).

Based on the obtained PSP, PSP-AgNPs was prepared using a simple redox system of silver nitrate, using PSP as both a reducing and capping agent. AgNPs were firmly capped by PSP through the formation of Ag-O, Ag-N, and Ag-S bonds. An average particle size of 6.3 ± 2.4 nm, a spherical morphology, and cubic face-centered silver were found in AgNPs. The hydrodynamic diameter, polydispersity index, and zeta potential of PSP-AgNPs were 79.5 ± 10.4 nm, 0.39 ± 0.024, and −33.9 ± 3.6 mV, respectively, when it was dispersed in de-ionized water at pH 7.0. The silver content in PSP-AgNPs was approximately 10.10 ± 0.54% (w/w), as detected by inductively coupled plasma optical emission spectroscopy. Other physiochemical properties and preparation of PSP-AgNPs are fully described in our previous studies (Jian et al., 2020; Jian et al., 2019).

4.3 Preparation of PSP-AgNPs dispersion

The dispersion of PSP-AgNPs was prepared by dispersing the lyophilized powder of PSP-AgNPs into ultrapure water at a concentration of 1.0 mg/mL. The lyophilized powder of PSP-AgNPs had been stored for 6 months in a desiccator at room temperature. Then, the dispersion of PSP-AgNPs was stored at 4°C for further use.

4.4 Antibacterial assays against pathogenic *Vibrio* strains

Antibacterial assays on the cultures of pathogenic *Vibrio* strains (*V. fluvialis*, *V. mimicus*, *V. hollisae*, *V. vulnificus*, and *V. furnissii*) were conducted using the procedure of broth micro-dilution (Jian et al., 2020). Mueller-Hinton broth medium was purchased from Guangdong Huankai Bio-Technology Co., Ltd., Guangzhou, China. This medium was composed of 5 g/l glucose, 10 g/l beef extract, 10 g/l peptone, 3 g/l yeast extract, 1 g/l soluble starch, 0.5 g/l cysteine HCl, 5 g/l sodium chloride, 3 g/l sodium acetate, and 0.5 g/l agar.

Vibrio inoculum was prepared in advance, adjusted to a concentration of 1×10^8 CFU/mL using a Densimat, and then diluted to 1×10^6 CFU/mL using Mueller-Hinton broth medium. After dilution, 1 mL of bacterial suspensions and 1 mL of serial dilutions of PSP-AgNPs (200.0, 100.0, 50.0, 25.0, 12.5, 6.25, 3.125, or 1.56 μg/mL) dispersed in Mueller-Hinton broth were blended in treatment tubes with a capacity of 10 mL. The total volume of fermentation broth in each treated tube was 2 mL. The treatment tubes were incubated at 37°C for 24 h under aerobic conditions. After cultivation, MIC was defined through treatment tubes without bacterial growth in the highest dilution of PSP-AgNPs. Based on the results of MIC, MBC was determined by measurements of bacterial colonies on agar plates after incubation at 37°C for 48 h, using aliquots from treatment tubes without bacterial growth. Briefly, 100.0 μl of these aliquots were withdrawn from treatment tubes showing no visible growth and were spread on agar plates containing Mueller-Hinton broth medium. These plates were then incubated at 37°C for 48 h under aerobic conditions. After this incubation period, the highest dilution which inhibited colony formation on agar was noted as MBC. Each assay was done in quintuples.

4.5 Cell culture and assay on cytotoxicity

Dispersions of PSP-AgNPs (1.0 mg/mL) were prepared in DMEM without fetal bovine serum, and further diluted to the required concentration using DMEM before cell cultivation. To

ensure homogeneity, the final dispersion of PSP-AgNPs was vortexed vigorously for 1 min and sonicated for 3 min.

Freshly prepared DMEM containing 10% fetal bovine serum, penicillin (100.0 U/mL), and streptomycin (100.0 μg/mL) was used to culture LO2 cells. The cultivation utilized 96-well plates under a humidified atmosphere of 95% air and 5% CO_2 at 37°C (Jian et al., 2017). After cultivation for three passages, LO2 cells (5×10^4 mL^{-1}) were grown in medium containing PSP-AgNPs, the concentration of which was set to 0 (blank control), 6.25, 12.5, 25.0, 50.0, or 100.0 μg/mL. After cultivation for 24 h in 96-well plates under a humidified atmosphere of 95% air and 5% CO_2 at 37°C, the supernatant was discarded, and cells were washed twice with phosphate buffer solution. Then, 200 μl MTT (0.5 mg/ml) was added, and the mixture was further incubated for 4 h. Thereafter, the supernatant was removed. Finally, 20 ul of dimethyl sulfoxide was added and the mixture was shaken for 2 min using a vortex mixer, followed by measuring the optical density at 490 nm using a microplate reader (Bio-Rad Laboratories, Hercules, CA, USA). Viability was calculated as the ratio of the mean of optical density obtained for each condition to that of the control (Jian et al., 2019).

4.6 Determination of the oxidative stress response of LO2 cells

After incubation and treatment with PSP-AgNPs as mentioned in Section 4.5, the medium was discarded, and cells were collected for the measurement of intracellular LDH, MDA, SOD, and GSH-Px by the following protocols. The cells were homogenized via sonication at 300 W for 1 min after scraping into ice-cold phosphate buffer solution. Then, the homogenate was centrifuged (12000 × g, 30 min, 4°C) and the supernatant was collected for determination via LDH assay kit (cat. no. A020-2-2), MDA assay kit (cat. no. A003-4-1), SOD assay kit (cat. no. A001-3-2), or GSH-Px assay kit (cat. no. A005-1-2), respectively.

4.7 Measurement of ROS

Based on the literature, the intracellular ROS levels were measured by the DCFH-DA method (Huang et al., 2021). After separation as mentioned in Section 4.5, LO2 cells were further incubated for 30 min in the dark with DMEM containing DCFH-DA (10 mM) under a humidified atmosphere of 95% air and 5% CO_2 at 37°C in 96-well plates. Thereafter, the medium was discarded. Cells were washed three times with 200 μL of PBS and fixed with 4% paraformaldehyde for 10 min. Afterwards, the treated cells were used to measure the fluorescence intensity using a safire fluorescence plate reader, at an excitation wavelength of 488 nm and an emission wavelength of 525 nm. Finally, values are expressed as percentages of fluorescence intensity relative to control.

4.8 Statistical analysis

All experiments were performed in quintuple. SPSS 16.0 software was used to conduct analyses of variance with Student's t test ($P < 0.01$). The results are expressed as means ± standard deviations. The significance level of $P < 0.01$ is labeled with double asterisks in all figures.

5 Conclusion

PSP-AgNPs showed no cytotoxicity on LO2 cells within effective dosage ranges against pathogenic *Vibrio* bacteria (3.125–25.0 μg/mL), and serious cytotoxicity was observed when the concentration was increased up to 50.0 μg/mL. Intracellular oxidative stress was the predominant mechanism of toxicity PSP-AgNPs induced in LO2 cells. Overall, this study showed that PSP-AgNPs are highly biocompatible in the range of effective antibacterial dosages; therefore, PSP-AgNPs can be used as a potential bactericide against pathogenic *Vibrio* strains, because of their suitable dispersion behavior, antibacterial activity, and biosafety.

Data availability statement

The original contributions presented in the study are included in the article/supplementary material, further inquiries can be directed to the corresponding author.

Ethics statement

Ethical approval was not required for the studies on humans in accordance with the local legislation and institutional requirements because only commercially available established cell lines were used. Ethical approval was not required for the studies on animals in accordance with the local legislation and institutional requirements because only commercially available established cell lines were used. All protocols on LO2 cells used in this study were approved by the Ethics Committee of Xiamen Medical College (Xiamen, China; No. XMMC2020040213), and were performed in accordance with the institutional ethical guidelines for human cells.

Author contributions

PH: Investigation, Writing – original draft. WW: Data curation, Methodology, Writing – original draft. WJ: Conceptualization, Writing – review and editing.

Funding

The author(s) declare financial support was received for the research, authorship, and/or publication of this article.

This work was supported by the Natural Science Foundation of Xiamen (Grant Nos.: 3502Z202373128 and 3502Z202373129), the Disinfection Program of the Chinese Preventive Medicine Association (Grant No.: 2023083), the Program for Young Teachers in Higher College from Fujian Province (Grant No.: JAT220414), and the Natural Science Foundation of Fujian Province (Grant No.: 2023J011654).

Acknowledgments

This research received technical support from Lin Lin (Brain Hospital of Hunan Province, China), Ni Zhang (Zhongshan Hospital Affiliated to Xiamen University, China), Xiaopei Zhu (Jimei University, China), and Ying Ma (Jimei University, China).

Conflict of interest

The authors declare that they do not have any commercial or associative interests that represent a conflict of interest in connection with the work presented.

Publisher's note

All claims expressed in this article are solely those of the authors and do not necessarily represent those of their affiliated organizations, or those of the publisher, the editors and the reviewers. Any product that may be evaluated in this article, or claim that may be made by its manufacturer, is not guaranteed or endorsed by the publisher.

References

Abioye, O., and Okoh, A. (2018). Limpet (Scutellastra cochlear) recovered from some estuaries in the Eastern Cape Province, South Africa act as reservoirs of pathogenic Vibrio species. *Front. Public Health* 6:381997. doi: 10.3389/fpubh.2018.00237

Ale, A., Liberatori, G., Vannuccini, M., Bergami, E., Ancora, S., Mariotti, G., et al. (2019). Exposure to a nanosilver-enabled consumer product results in similar accumulation and toxicity of silver nanoparticles in the marine mussel Mytilus galloprovincialis. *Aquat. Toxicol.* 211, 46–56. doi: 10.1016/j.aquatox.2019.03.018

Alhajjar, R., Roche, K., and Techtmann, S. (2022). Comparative Analysis of the Mechanism of Resistance to Silver Nanoparticles and the Biocide 2, 2-Dibromo-3-Nitrilopropionamide. *Antimicrob. Agents Chemother.* 66, e2031–e2021. doi: 10.1128/aac.02031-21

Alwan, S., Al-Saeed, M., and Abid, H. (2021). Safety assessment and biochemical evaluation of the effect of biogenic silver nanoparticles (using bark extract of C. zeylanicum) on Rattus norvegicus rats. *Baghdad J. Biochem. Appl. Biol. Sci.* 2, 133–145. doi: 10.47419/bjbabs.v2i03.67

Brumfield, K., Usmani, M., Chen, K., Gangwar, M., Jutla, A., Huq, A., et al. (2021). Environmental parameters associated with incidence and transmission of pathogenic Vibrio spp. *Environ. Microbiol.* 23, 7314–7340. doi: 10.1111/1462-2920.15716

Chandrakala, N., and Parameswari, P. (2021). Comparative study on the in vitro antibacterial activity of selected medicinal plants against pathogenic vibrio species from diseased penaeus monodon (fab). *J. Adv. Sci. Res.* 12(04 Suppl. 1), 288–291. doi: 10.55218/JASR.s1202112433

El Mahdy, M., Eldin, T., Aly, H., Mohammed, F., and Shaalan, M. (2015). Evaluation of hepatotoxic and genotoxic potential of silver nanoparticles in albino rats. *Exp. Toxicol. Pathol.* 67, 21–29. doi: 10.1016/j.etp.2014.09.005

El-Samad, L., Bakr, N., El-Ashram, S., Radwan, E., Aziz, K., Hussein, H., et al. (2022). Silver nanoparticles instigate physiological, genotoxicity, and ultrastructural anomalies in midgut tissues of beetles. *Chemico-Biol. Interact.* 367, 110166. doi: 10.1016/j.cbi.2022.110166

Fatima, R., Priya, M., Indurthi, L., Radhakrishnan, V., and Sudhakaran, R. (2020). Biosynthesis of silver nanoparticles using red algae Portieria hornemannii and its antibacterial activity against fish pathogens. *Microb. Pathog.* 138, 103780. doi: 10.1016/j.micpath.2019.103780

Fleischmann, S., Herrig, I., Wesp, J., Stiedl, J., Reifferscheid, G., Strauch, E., et al. (2022). Prevalence and distribution of potentially human pathogenic Vibrio spp. on German North and Baltic Sea coasts. *Front. Cell. Infect. Microbiol.* 12:846819. doi: 10.3389/fcimb.2022.846819

Fouda, M., Dosoky, W., Radwan, N., Abdelsalam, N., Taha, A., and Khafaga, A. (2021). Oral administration of silver nanoparticles–adorned starch as a growth promotor in poultry: Immunological and histopathological study. *Int. J. Biol. Macromol.* 187, 830–839. doi: 10.1016/j.ijbiomac.2021.07.157

Huang, M., Ye, K., Hu, T., Liu, K., You, M., Wang, L., et al. (2021). Silver nanoparticles attenuate the antimicrobial activity of the innate immune system by inhibiting neutrophil-mediated phagocytosis and reactive oxygen species production. *Int. J. Nanomed.* 2021, 1345–1360. doi: 10.2147/IJN.S292482

Jian, W., Ma, Y., Wu, H., Zhu, X., Wang, J., Xiong, H., et al. (2019). Fabrication of highly stable silver nanoparticles using polysaccharide-protein complexes from abalone viscera and antibacterial activity evaluation. *Int. J. Biol. Macromol.* 128, 839–847. doi: 10.1016/j.ijbiomac.2019.01.197

Jian, W., Ma, Y., Zhu, X., Zhang, N., Lin, L., Jia, B., et al. (2020). Quantitative insight into dispersity and antibactericidal capability of silver nanoparticles noncovalently conjugated by polysaccharide-protein complexes. *Int. J. Biol. Macromol.* 150, 459–467. doi: 10.1016/j.ijbiomac.2020.02.098

Jian, W., Tu, L., Wu, L., Xiong, H., Pang, J., and Sun, Y. (2017). Physicochemical properties and cellular protection against oxidation of degraded Konjac Glucomannan prepared by γ-irradiation. *Food Chem.* 231, 42–50. doi: 10.1016/j.foodchem.2017.03.121

Jiang, H., Qiu, X., Li, G., Li, W., and Yin, L. (2014). Silver nanoparticles induced accumulation of reactive oxygen species and alteration of antioxidant systems in the aquatic plant Spirodela polyrhiza. *Environ. Toxicol. Chem.* 33, 1398–1405. doi: 10.1002/etc.2577

Komazec, B., Cvjetko, P., Balen, B., Letofsky-Papst, I., Lyons, D., and Peharec Stefaniæ, P. (2023). The occurrence of oxidative stress Induced by Silver nanoparticles in Chlorella vulgaris depends on the surface-stabilizing Agent. *Nanomaterials* 13, 1967. doi: 10.3390/nano13131967

Lin, X., Lin, Y., Liao, Z., Niu, X., Wu, Y., Shao, D., et al. (2022). Preservation of Litchi Fruit with Nanosilver Composite Particles (Ag-NP) and Resistance against Peronophythora litchi. *Foods* 11, 2934. doi: 10.3390/foods11192934

Lu, C., Lv, Y., Kou, G., Liu, Y., Liu, Y., Chen, Y., et al. (2022). Silver nanoparticles induce developmental toxicity via oxidative stress and mitochondrial dysfunction in zebrafish (Danio rerio). *Ecotoxicol. Environ. Saf.* 243, 113993. doi: 10.1016/j.ecoenv.2022.113993

Meneses-Márquez, J., Hamdan-Partida, A., Del Carmen Monroy-Dosta, M., Castro-Mejía, J., Faustino-Vega, A., Soria-Castro, E., et al. (2019). Use of silver nanoparticles to control Vibrio fluvialis in cultured angelfish Pterophyllum scalare. *Dis. Aquatic Organ.* 137, 65–72. doi: 10.3354/dao03423

Neetoo, H., Reega, K., Manoga, Z., Nazurally, N., Bhoyroo, V., Allam, M., et al. (2022). Prevalence, genomic characterization, and risk assessment of human pathogenic Vibrio Species in Seafood. *J. Food Prot.* 85, 1553–1565. doi: 10.4315/JFP-22-064

Nguyen, N., Tran, G., and Nguyen, C. (2020). Anti-oxidative effects of superoxide dismutase 3 on inflammatory diseases. *J. Mol. Med.* 98, 59–69. doi: 10.1007/s00109-019-01845-2

Piao, M., Kang, K., Lee, I., Kim, H., Kim, S., Choi, J., et al. (2011). Silver nanoparticles induce oxidative cell damage in human liver cells through inhibition of reduced glutathione and induction of mitochondria-involved apoptosis. *Toxicol. Lett.* 201, 92–100. doi: 10.1016/j.toxlet.2010.12.010

Prema, P., Thangapandiyan, S., and Immanuel, G. (2017). CMC stabilized nano silver synthesis, characterization and its antibacterial and synergistic effect with broad spectrum antibiotics. *Carbohydrate Polym.* 158, 141–148. doi: 10.1016/j.carbpol.2016.11.083

RathnaKumari, P., Kolanchinathan, P., Siva, D., Abirami, B., Masilamani, V., John, G., et al. (2018). Antibacterial efficacy of seagrass Cymodocea serrulata-engineered silver nanoparticles against prawn pathogen Vibrio parahaemolyticus and its combative effect on the marine shrimp Penaeus monodon. *Aquaculture* 493, 158–164. doi: 10.1016/j.aquaculture.2018.04.061

Rezvani, E., Rafferty, A., McGuinness, C., and Kennedy, J. (2019). Adverse effects of nanosilver on human health and the environment. *Acta Biomater.* 94, 145–159. doi: 10.1016/j.actbio.2019.05.042

Salama, B., Alzahrani, K., Alghamdi, K., Al-Amer, O., Hassan, K., Elhefny, M., et al. (2023). Silver nanoparticles enhance oxidative stress, inflammation, and apoptosis in liver and kidney tissues: Potential protective role of thymoquinone. *Biol. Trace Element Res.* 201, 2942–2954. doi: 10.1007/s12011-022-03399-w

Serrano-Díaz, P., Williams, D., Vega-Arreguin, J., Manisekaran, R., Twigg, J., Morse, D., et al. (2023). Geranium leaf-mediated synthesis of silver nanoparticles and their transcriptomic effects on Candida albicans. *Green Process. Synth.* 12, 20228105. doi: 10.1515/gps-2022-8105

Sony, M., Sumithra, T., Anusree, V., Amala, P., Reshma, K., Alex, S., et al. (2021). Antimicrobial resistance and virulence characteristics of Vibrio vulnificus, Vibrio parahaemolyticus and Vibrio harveyi from natural disease outbreaks of marine/estuarine fishes. *Aquaculture* 539, 736608. doi: 10.1016/j.aquaculture.2021.736608

Suliman, Y. A., Ali, D., Alarifi, S., Harrath, A., Mansour, L., and Alwasel, S. (2015). Evaluation of cytotoxic, oxidative stress, proinflammatory and genotoxic effect of silver nanoparticles in human lung epithelial cells. *Environ. Toxicol.* 30, 149–160. doi: 10.1002/tox.21880

Xue, Y., Wang, J., Huang, Y., Gao, X., Kong, L., Zhang, T., et al. (2018). Comparative cytotoxicity and apoptotic pathways induced by nanosilver in human liver HepG2 and L02 cells. *Hum. Exper. Toxicol.* 37, 1293–1309. doi: 10.1177/0960327118769718

Xue, Y., Zhang, T., Zhang, B., Gong, F., Huang, Y., and Tang, M. (2016). Cytotoxicity and apoptosis induced by silver nanoparticles in human liver HepG2 cells in different dispersion media. *J. Appl. Toxicol.* 36, 352–360. doi: 10.1002/jat.3199

Yang, X., and Wu, J. (2022). Synthetic Conditions, Physical Properties, and Antibacterial Activities of Silver Nanoparticles with Exopolysaccharides of a Medicinal Fungus. *Materials* 15, 5620. doi: 10.3390/ma15165620

frontiers | Frontiers in Microbiology

TYPE Original Research
PUBLISHED 06 January 2025
DOI 10.3389/fmicb.2024.1501951

OPEN ACCESS

EDITED BY
Dany Domínguez Pérez,
Zoological Station Anton Dohrn, Italy

REVIEWED BY
Ton That Huu Dat,
Vietnam Academy of Science and Technology, Vietnam
Sonia Ilaria Maffioli,
Naicons Srl, Italy

*CORRESPONDENCE
Luisa Villamil
✉ luisa.villamil@unisabana.edu.co
Luis Díaz
✉ luis.diaz1@unisabana.edu.co

RECEIVED 25 September 2024
ACCEPTED 26 November 2024
PUBLISHED 06 January 2025

CITATION
De La Hoz-Romo MC, Díaz L, Gómez-León J, Quintero M and Villamil L (2025) Marine actinobacteria metabolites: unlocking new treatments for acne vulgaris.
Front. Microbiol. 15:1501951.
doi: 10.3389/fmicb.2024.1501951

Marine actinobacteria metabolites: unlocking new treatments for acne vulgaris

María Clara De La Hoz-Romo[1,2], Luis Díaz[1,2]*, Javier Gómez-León[3], Marynes Quintero[3] and Luisa Villamil[1]*

[1]Doctoral Program of Biosciences, School of Engineering, Universidad de La Sabana, Chía, Cundinamarca, Colombia, [2]Bioprospecting Research Group, School of Engineering, Universidad de La Sabana, Chía, Colombia, [3]Marine Bioprospecting Line, Marine and Coastal Research Institute "José Benito Vives de Andréis" INVEMAR, Santa Marta, Colombia

Marine-derived actinobacteria isolated from sponge *Cliona varians* and soft coral *Eunicea fusca* were screened for antibacterial activity against acne-related bacteria, specifically *Staphylococcus epidermidis* ATCC 14990, methicillin-resistant *Staphylococcus aureus* ATCC BAA44, and *Cutibacterium acnes* ATCC 6919. Cytotoxicity assays were performed on human dermal fibroblast (HDFa) and keratinocyte (HaCaT) cell lines to assess the safety profile of the extracts. Chemical characterization was conducted using high-performance liquid chromatography coupled with tandem mass spectrometry (HPLC–MS/MS). Among the extracts, six derived from *Kocuria* sp., *Rhodococcus* sp., *Nocardia* sp., *Micrococcus* sp., and *Streptomyces* sp. demonstrated significant antibacterial activity. Notably, extract Z9.216 from *Kocuria* sp. exhibited the highest efficacy, inhibiting *S. epidermidis* by 68%, *S. aureus* by 93%, and *C. acnes* by 98.7% at a concentration of 0.003 mg/mL, which was comparable to the standard antibiotics erythromycin and vancomycin, while maintaining over 90% cell viability in both HDFa and HaCaT cell lines. Untargeted metabolomic analysis suggested that antibacterial activity might be associated with compounds from the chemical families of alkaloids, terpenoids, and fatty acids, among others. These findings highlight the therapeutic potential of marine actinobacteria in underexplored environments as a promising strategy for treating acne vulgaris, a chronic inflammatory skin condition.

KEYWORDS

marine actinobacteria, acne vulgaris, antibacterial activity, secondary metabolites, *Cutibacterium acnes*

1 Introduction

Acne vulgaris is a multifactorial chronic inflammatory disease of the pilosebaceous follicle, which includes the hair shafts and sebaceous glands. It is the most common dermatological condition worldwide, with an estimated 650 million people (Moradi Tuchayi et al., 2015). Young people constitute the most compromised population (85%) (Melnik, 2018; Bernhardt and Myntti, 2016).

Disease severity is closely associated with the inflammatory response, mainly to *Cutibacterium acnes*, a prominent member of the skin microbiota. The skin microbiota is largely composed of Actinobacteria (Corynebacterineae and Propionibacterineae), Proteobacteria, Firmicutes (Staphylococcaceae), and Bacteroidetes (Mayslich et al., 2021). Certain phylotypes of *C. acnes* have been identified as opportunistic pathogens capable of causing invasive infections and forming biofilms (Mayslich et al., 2021; Achermann et al., 2014; Keshari et al., 2019). Additionally, bacterial interactions, such as those between *Staphylococcus*

epidermidis and *C. acnes*, may be influenced by changes in host characteristics. These alterations can lead to the selection of pathogenic *C. acnes* strains that produce virulence factors, thereby increasing their inflammatory potential (Mayslich et al., 2021). Furthermore, shifts in the populations of *C. acnes* and *S. epidermidis* on the skin could promote colonization by *Staphylococcus aureus*, which is associated with acne vulgaris as well as other dermatological conditions, such as atopic dermatitis (Fournière et al., 2020).

Given the complexity of microbial interactions in acne, antibiotics are commonly used for its management. Nevertheless, they do not neutralize secretory toxins but instead exert selection pressure on non-target bacteria at a systematic level (Keshari et al., 2019). This has led to the emergence of resistance to erythromycin, clindamycin, and tetracycline in *C. acnes* and *S. aureus* strains, increasing the likelihood of treatment failure (Alkhawaja et al., 2020; Sermswan et al., 2023). This dynamic is particularly concerning in the context of bacterial resistance, as seen in *Staphylococcus aureus*. In 2019, methicillin-resistant *S. aureus* (MRSA) was responsible for an estimated 4.95 million deaths globally (Dadgostar, 2019). In addition, other treatment options for acne, such as isotretinoin, also produce side effects, including psychiatric events and inflammatory bowel disease (Costa et al., 2018).

Historically, natural products extracted from plants, animals, and microorganisms have been a prolific source of bioactive compounds. Nonetheless, these treatment options have been applied specifically to help stop the skin aging processes and pigmentation or improve the general appearance (Duarte et al., 2022; Bungau et al., 2023). Actinobacteria, in particular, are responsible for producing about 70% of currently used antibiotics (Dholakiya et al., 2017). Of the approximately 500.000 natural compounds are derived from biological sources, and 70.000 are of microbial origin, of which 29% are obtained from actinomycetes (Siro et al., 2022). Marine microbial communities have been reported as the most diverse source of biologically active compounds (Siddharth, 2019), and unique bioactive natural products have been reported from marine actinobacterial strains, such as marinopyrroles, heronapyrroles, ansalactam ammosamides, salinosporamide A6, and flavonoids, which were initially reported only in plants (Panche et al., 2016; Cheng et al., 2013). Furthermore, marine actinobacteria have been less explored than their terrestrial counterparts, providing an interesting field of study and a source of new bioactive compounds.

Three-quarters of all newly discovered bioactive microbial products in marine environments are produced by bacteria associated with marine invertebrates, and approximately 30% of these compounds originate from marine sponges (Rajasabapathy et al., 2020). Corals rank second after sponges in terms of productivity, with 5,800 compounds derived from corals accounting for nearly 20% of all natural marine products (Siro et al., 2022).

In this study, we explored extracts obtained from marine actinobacteria isolated from sponges and octocorals in the Colombian Caribbean. These extracts were obtained from 13 strains and were subjected to antibacterial analysis against *S. epidermidis*, *S. aureus,* and *C. acnes*. The promising extracts were further evaluated for cytotoxicity against human keratinocytes and fibroblast cell lines. Chemical analysis of the extracts was performed using a metabolomic approach. This analysis indicated that the compounds probably related to antibacterial activity belonged to the alkaloid, terpenoid, naphthalene, and stilbene families, among others, which have previously been reported to have significant antimicrobial potential. Furthermore, molecular identification of the strains producing these promising extracts revealed that most belong to a genera classified as rare actinobacteria, such as *Nocardia* sp., *Micrococcus* sp., *Rhodococcus* sp., and *Kocuria* sp.

These findings highlight the potential of marine actinobacteria as a promising source of bioactive compounds with significant antimicrobial properties, creating opportunities for the development of new therapeutic alternatives for treating acne vulgaris.

2 Materials and methods

2.1 Actinobacteria strains

Marine actinobacteria were obtained from the Microbial Collection of the Bioprospecting Research Group at Universidad de La Sabana, Colombia. These isolates were originally obtained from sponge and octocorals collected by scuba diving from the Colombian Caribbean, Bahía de Taganga, Punta Venado (11°16′23.9″ N, 74°12′24.9″ W), Bahía de Santa Marta, Punta Betín (11°15′02.1″ N, 74°13′16.0″ W), Magdalena, Colombia, at depths of 13 and 9 m, respectively (Sánchez-Suárez et al., 2021). The bacteria used in the present study were of Colombian origin and were obtained according to Amendment No. 5 to ARG Master Agreement No. 117 of May 26, 2015, granted by the Ministry of Environment and Sustainable Development, Colombia. Supplementary Table S1 describes the actinobacterial strains and their isolation sources.

Staphylococcus epidermidis (ATCC 14990), *C. acnes* (ATCC 6919), and methicillin-resistant *S. aureus* (ATCC BAA44) were acquired from the American Type Culture Collection (ATCC).

2.2 Actinobacteria culture and extracts obtention

Actinomycete isolates were inoculated in 100 mL of liquid Glucose, Yeast, and Malt extract broth (GYM) or Zobell Marine broth (Zobell), according to the original isolation medium (Sánchez-Suárez et al., 2021). Briefly, the culture started using a 55.81 mm^2 plug from a 7-day-old lawn growth plate as a seed in 3 mL of broth. Each culture was incubated at 30°C with agitation at 200 rpm for 7 days. From this culture, 1 mL was used to inoculate 9 mL of GYM or Zobell broth, which was incubated for 7 days at 30°C with agitation at 200 rpm. Finally, the previous culture product (10 mL) was used to inoculate 90 mL of GYM or Zobell broth into 250 mL flasks on a rotary shaker (200 rpm) for 7 days. Then, 25 mL of each culture were placed in 50 mL plastic tubes, then freeze-dried (FreeZone Laboratory Freeze Dryer 2.5 liters, Labconco USA, Kansas), with a pressure of 0.22 millibar and a temperature of −55°C. The freeze-dried culture was transferred to a 50 mL Erlenmeyer flask, mixed with 10 mL of ethyl acetate (EtOAc), and agitated (150 rpm) for 24 h. The extraction was repeated three times using fresh EtOAc. The organic layers were evaporated under vacuum (Heidolph evaporator). Then, a stock concentration of 50 mg/mL was prepared for each actinobacteria extract, which was then used to perform antibacterial assays at the reported concentrations.

2.3 *Cutibacterium acnes* culture conditions

Cutibacterium acnes ATCC 6919 was activated according to the manufacturer instructions. Briefly, two media were used for its activation: ATTC Medium 2107: Modified Reinforced Clostridial (MRC) and ATCC Medium 260: trypticase soy agar/broth with defibrinated sheep blood under aseptic conditions and incubated in an anaerobic atmosphere at 37°C for 48–72 h. Anaerobic conditions were achieved using test tubes with a gas cannula system connected to anaerobic gas. Loose screw caps were placed in the test tubes in an activated anaerobic gas pack jar.

2.4 Antibacterial activity assays

The antibacterial activity of the extracts was estimated from the growth curve through the optical density using a Synergy H1 Multimode Reader (BioTek, Winooski, VT, USA). The antibacterial activity was determined using a microbroth susceptibility assay in 96-well plates, each containing 100 µL of extracts at different concentrations (initially 0.3, 0.03, and 0.003 mg/mL), following protocols standardized by the Bioprospecting Group of the Universidad de La Sabana, with slight modifications to the yield of the extracts (Sarmiento-Tovar et al., 2024). Extracts that did not show activity at the initial concentrations were further assessed at the highest concentration prepared (1.25 mg/mL), based on the yield of the extracts, with 100 µL of bacterial inoculum (*S. epidermidis*, MRSA, and *C. acnes*) at a cell density of $1.5\,x\,10^{8}$ UFC/mL. The absorbance was maintained within the range of 0.08–0.1 at 600 nm (Bauermeister et al., 2019). The optical density (OD) was measured at 600 nm at 30 min intervals for up to 18–20 h for *S. epidermidis* and MRSA. For *C. acnes*, the incubation time was 72–150 h the time at which the bacteria reached a stationary phase. The bacteria in Tryptic Soy Broth (TSB) and modified reinforced clostridial broth (MRC) were used as negative controls. The commercial antibiotics vancomycin and erythromycin, which were used at the same concentrations as the extracts, were used as the positive controls. Percentage inhibition was calculated using the following formula (Equation 1) (Rajivgandhi et al., 2016):

$$\%\ of\ inhibition: \frac{\left(Untreated\ bacteria\ OD\ 600\ nm - Treated\ bacteria\ OD\ 600\ nm\right)}{Untreated\ bacteria\ OD\ 600\ nm} \times 100 \quad (1)$$

2.5 Determination of maximum specific growth rate and maximum OD

Specific growth rates were determined using ComBase[1]. This database contained statistical models that fit the nature of the data. The inhibition percentage was calculated using the following formula (Equation 2):

$$\%\ inhibition = \left(\frac{Untreated\ bacteria\ Gr^{1} - Treated\ bacteria\ Gr^{1}}{Untreated\ bacteria\ Gr^{1}}\right) \times 100 \quad (2)$$

[1]growth rate.

2.6 Minimal inhibitory concentration of bioactive extracts

The minimal inhibitory concentration (MIC) of extracts was determined using the broth microdilution method, according to the protocol described by Balagurunathan et al. (2020). Actinobacteria extracts and vancomycin and erythromycin (positive controls) were prepared by the serial 2-fold dilution method from the highest concentration observed in the antibacterial activity screening, 1.25 mg/mL (1.25–0.312 mg/mL) in TSB medium for *S. epidermidis* and *S. aureus*, and MRC broth for *C. acnes*. Freshly grown colonies of bacterial cultures were suspended in 10 mL fresh medium. The bacterial suspension was adjusted to a density of 5×10^{5} CFU/mL (Wang et al., 2017; Akhter et al., 2018) and added to 96-well plates. Each well contains 100 µL of the bacterial suspension and 100 µL of the extract. The negative controls included 100 µL of bacterial suspension and 100 µL of culture broth. As the extracts were dissolved in isopropyl alcohol (the maximum final concentration of isopropyl alcohol was 0.3%), a control with this solvent was also included. Each experiment was performed in duplicates. Plates were incubated for 20 h at 37°C for *S. aureus* and *S. epidermidis* and incubated for 150 h at 37°C under anaerobic conditions for *C. acnes* because of its naturally slower growth rate. MIC was determined by observing the lowest concentration of the extract that inhibited bacterial growth.

2.7 Cytotoxicity assay

Cell viability assays were performed to evaluate the cytotoxicity of the extracts against HDFa (Primary Dermal Fibroblast; Normal, Human, Adult ATCC® PCS-201-012™) and HACAT (spontaneously immortalized human keratinocyte cell line derived from a distant periphery of malignant melanoma) following the methodology described by van de Loosdrecht et al. (1991), with some modifications. Briefly, the cell lines were cultured in Dulbecco's modified Eagle's medium (DMEM) supplemented with 10% Fetal Bovine Serum (FBS) and 1% penicillin/streptomycin, using (3-(4,5-dimethylthiazol-2-yl)-2,5-diphenyltetrazolium bromide) (MTT) at 0.5 mg/mL an incubated 4 h. Cells (10^{4} cells/well) were seeded in triplicate in 96-well plates and cultured overnight at 37°C and 5% CO_2. Bioactive extracts were added to 96-well plates at final concentrations of 0.3, 0.03, and 0.003 mg/mL and 1.25, 0.625, and 0.3125 mg/mL in DMEM supplemented with 10% fetal bovine serum. Dimethyl sulfoxide (DMSO, between 1 and 10% *v*/*v*) was used as the negative control. After 24 h of incubation, MTT was removed, and DMSO was added to each well to dissolve the formazan crystals. The amount of formazan was determined by measuring absorbance at 570 nm (Mosmann, 1983). Cell viability was calculated using the following formula (Equation 3) (Sánchez-Suárez et al., 2021):

1 https://www.combase.cc/index.php/en/

$$\%\ viability = \left(\frac{OD_{Samples}}{OD_{Control\ group}} \right) \times 100 \quad (3)$$

2.8 Sequencing of 16S rRNA gene and phylogenetic analysis

Genomic DNA was extracted using a Quick-DNA Fungal/Bacterial Microprep kit (Zymo Research Corporation, Irvine, CA, USA) according to the manufacturer's instructions. The 16S rRNA gene was amplified using the universal primers 27F (forward primer: 5′-AGAGTTTGATCMTGGCTCAG-3′) and 1492R (reverse primer: 5′-TACGGYTACCTTGTTACGACTT-3′) under the following cycling conditions: denaturation at 94°C for 3 min, followed by 30 cycles of 94°C for 1 min, 50°C for 1 min, and 72°C for 2 min, with a final extension at 72°C for 7 min using Thermal Cycler (Bio-Rad). The amplified products were evaluated by electrophoresis of DNA samples on agarose gel. The agarose gel used in this study was 1% agarose gel in a buffer solution of Tris Acetate EDTA (TAE) (Anggelina et al., 2021).

The 16S rRNA sequences were run on the Basic Local Alignment Search Tool (BLAST) using the NCBI BLAST search tool, and the nearest neighbors were identified. MEGA version X (Molecular Evolutionary Genetics Analysis, version 10[2]), using the Tamura 3-parameter model, was used to construct a phylogenetic tree using the neighbor-joining method with a bootstrap test (1,000 replicates).

2.9 HPLC-QTOF-MS metabolomic analysis of extracts

Metabolomic analysis of the antibacterial active extracts and non-active extracts was performed using an Agilent Technologies 1,260 Liquid Chromatography system coupled with a Q-TOF 6545 time-of-flight quadrupole mass analyzer with electrospray ionization (ESI). The separation process was performed on a C18 column (InfinityLab Poroshell 120 EC-C18 100 × 3.0 mm, 2.7 µm). Two µL of the extracts were injected at 30°C and a gradient elution composed of: 0.1% (v/v) formic acid in Milli-Q water (Phase A) and 0.1% (v/v) formic acid in acetonitrile (Phase B) with a constant flow rate of 0.4 mL/min. The elution gradient program was: 0–15 min; 2–30% B, 15–17 min; 30–98% B, 17–21 min; 98% B and 21–26 min; 2%B.

Mass spectrometric detection was performed in the positive ESI mode in the full scan mode, and MS/MS was performed from 100 to 1.800 m/z. The following reference masses were used for mass correction during analysis: m/z = 121.0509 ($C_5H_4N_4$) and m/z = 922.0098 ($C_{18}H_{18}O_6N_3P_3F_{24}$). The ESI source parameters were as follows: capillary voltage (3,000 V); drying gas (8 L/min); gas temperature (325°C); nebulizer pressure (50 psi); sheath gas temperature (350°C); and sheath gas glow (11 L/min). Q-ToF parameters included fragmentor voltage (175 V), skimmer voltage (65 V), and octapole radiofrequency peak-to-peak voltage (OCT RF Vpp) (750 V). Quality control (QC) samples were prepared according to the technique by pooling equal volumes of all groups of samples. QC pool samples were injected every 10 samples to evaluate stability and reproducibility throughout the analysis.

Data processing was performed using Agilent MassHunter Profinder software (version 10.0), which carried out deconvolution, alignment, and integration. These procedures were executed using the recursive feature extraction (RFE) algorithm. Datasets were filtered to remove features with a coefficient of variation (CV) > 20% in QC samples, retaining only those present in at least 80% of each sample group.

For metabolite identification, the CEU MASS MEDIATOR (accessible at https://ceumass.eps.uspceu.es/ as of August 15, 2023) (Gil-De-La-Fuente et al., 2019) was used to identify statistically significant m/z values. This tool integrates various platforms, including Metlin, Kegg, HDMB, and LipidMaps, with a tolerance of 10 ppm to annotate more abundant molecular features. Additionally, we utilized the StreptomeDB v3.0 (Moumbock et al., 2021) and the Natural Products Atlas v2.0 (Van Santen et al., 2022) databases.

To validate the identity of the metabolites, MS/MS analyses were conducted using MS-DIAL 4.8 (http://prime.psc.riken.jp/compms/msdial/main.html, accessed on August 22, 2023). These analyses involved *in silico* mass spectral fragmentation using CFM-ID 4.0 (available at https://cfmid.wishartlab.com/ as of August 28, 2023), and manual MS/MS spectral interpretation using the Agilent MassHunter Qualitative Analysis program (version 10.0, USA) (Camargo et al., 2023). The identified metabolites were reported according to the confidence level of compound annotation described by Blaženovi (2018).

2.10 Statistical data analysis

Data are presented as mean ± standard deviation (SD), and differences were examined using two-way analysis of variance (ANOVA) with a significance level of 5%. ANOVA assumptions of normality, homogeneity of variance, and independence of the data were checked. Dunnett's test was performed to compare treatments at the 95% confidence level.

For metabolomic analysis, univariate statistical analysis (UVA) and multivariate statistical analysis (MVA) were performed to assess statistically significant differences among the metabolomic profiles of the groups using Metaboanalyst 5.0 and SIMCA 16.0 (Umetrics, Umea, Sweden), respectively. Initially, MVA based on principal component analysis (PCA) was applied to evaluate the quality of the acquired data. This ensured that the quality control (QC) samples were appropriately clustered in these models to guarantee the stability of the analytical system. Subsequently, orthogonal partial least squares discriminant analysis (OPLS-DA) models were constructed to maximize and examine the differences between the active and inactive extracts in the study groups and select the metabolites responsible for group separation.

Pareto scaling was applied for transformation before statistical analysis. In UVA, the *p-value* with a Benjamini-Hochberg false discovery rate correction (FDR) was determined (Quintero et al., 2022). Significant features were those with an adjusted *p-value* < 0.05, and variance important in projection (VIP) >1 with a jackknife confidence interval (JK). To determine the predictability and validity of the OPLS-DA model and to avoid overfitting and false positives, the models were subjected to cross-validation using K-fold and permutation tests ($n = 100$).

2 https://megasoftware.net

3 Results

3.1 Antibacterial activity of actinobacterial extracts

The antibacterial activity of ethyl acetate extracts from 13 actinomycete isolates was evaluated and established as a decrease in bacterial viability compared with that of untreated bacteria. Six extracts demonstrated activity against *Staphylococcus epidermidis*, MRSA, and *C. acnes*. The minimum inhibitory concentrations (MICs) were determined based on the concentrations tested. The Z9.216 extract exhibited MIC of 0.3 mg/mL against *S. epidermidis* and 0.003 mg/mL against both *S. aureus* and *C. acnes*. Extracts Z6.29 and Z9.11 had MIC values of 0.312 mg/mL for *S. epidermidis*, although MICs for *S. aureus* and *C. acnes* could not be determined within the tested concentration range due to the limited yield of the extracts. Table 1 shows the bacterial growth inhibition percentages of the extracts that were active against the three bacteria. These were selected for molecular identification by 16S rRNA gene sequencing. Biological profiling was carried out by metabolomic analyses of the end products using High-Performance Liquid Chromatography coupled with electrospray ionization quadrupole time-of-flight mass spectrometry (HPLC-QToF-MS) and mass spectrometry (MS/MS) analyses.

TABLE 1 Percentage of inhibition of bacterial growth by the most promising ethyl acetate extracts from marine actinobacteria against *Staphylococcus epidermidis* ATCC 14990, methicillin-resistant *Staphylococcus aureus* ATCC BA440, and *Cutibacterium acnes* ATCC 6919.

Extracts code	Extract concentration (mg/mL)	*S. epidermidis* ATCC 14990 (% of inhibition)	*S. aureus* ATCC BAA440 (% of inhibition)	*C. acnes* ATCC 6919 (% of inhibition)
Z9.216	0.003	68 ± 4.3[a]	93 ± 4.7[a]	98.7 ± 0.1[a]
G6.210	0.625	43 ± 0.0 [a]	54 ± 2.0[a]	67 ± 6.1[a]
Z9.23	1.250	48 ± 5.6[a]	50 ± 3.4[a]	68.2 ± 7.5[a]
Z6.29	0.312	98 ± 3.5[a]	42 ± 5.6[a]	76.7 ± 4.0[a]
Z9.21	0.625	20 ± 2.0[a]	19 ± 3.8[a]	71 ± 8.0[a]
Z9.11	0.312	100 ± 0.7[a]	23 ± 0.2[a]	80 ± 4.0[a]

Values are expressed as mean ± standard deviation ($n = 2$). The minimum concentration at which each extract showed activity is reported. [a] Standard deviation (±SD) of two experiments.

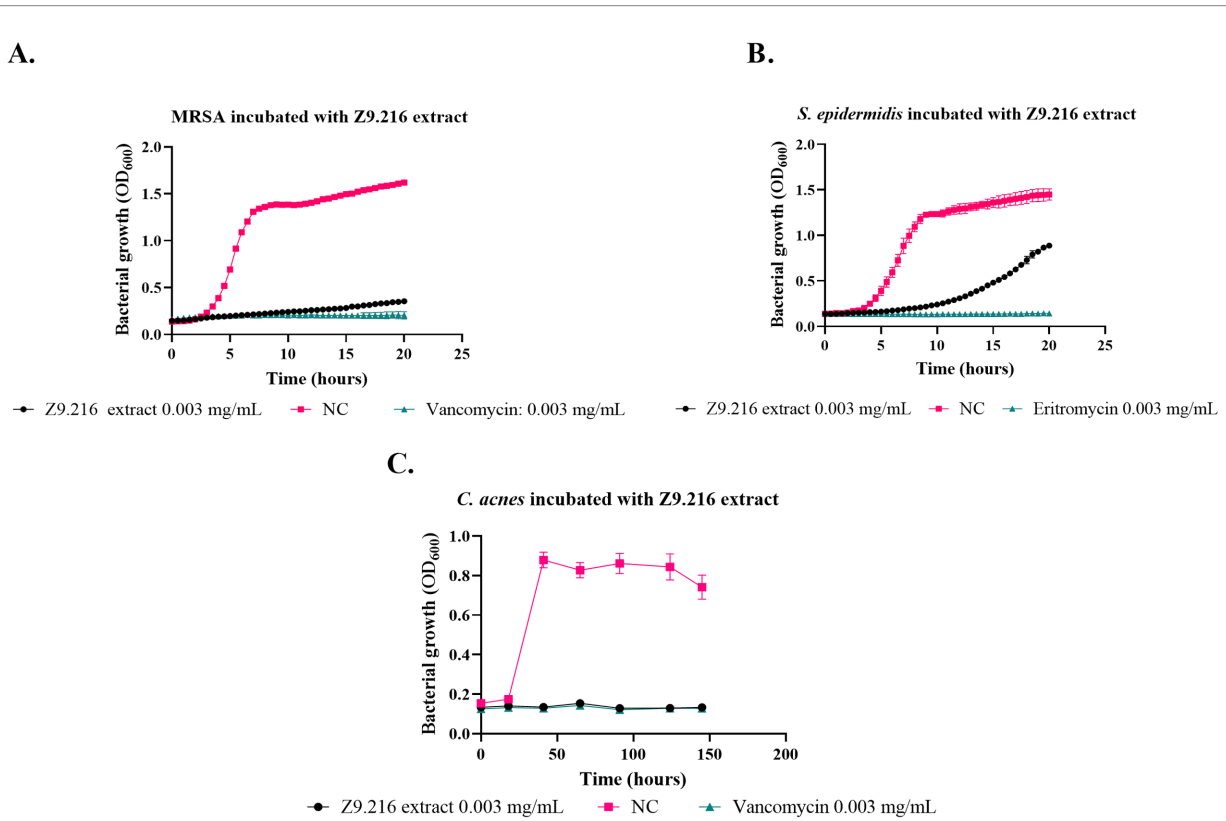

FIGURE 1
Effect of Z9.216 extract (0.003 mg/mL) on the growth of *S. epidermidis* ATCC 14990, methicillin-resistant *S. aureus* (MRSA) ATCC BA440, and *C. acnes* ATCC 6919. **(A)** Growth curve of *S. aureus* ATCC BA440; **(B)** Growth curve of *S. epidermidis* ATCC 14990; **(C)** Growth curve of *C. acnes* ATCC 6919. NC: Negative control, untreated bacteria.

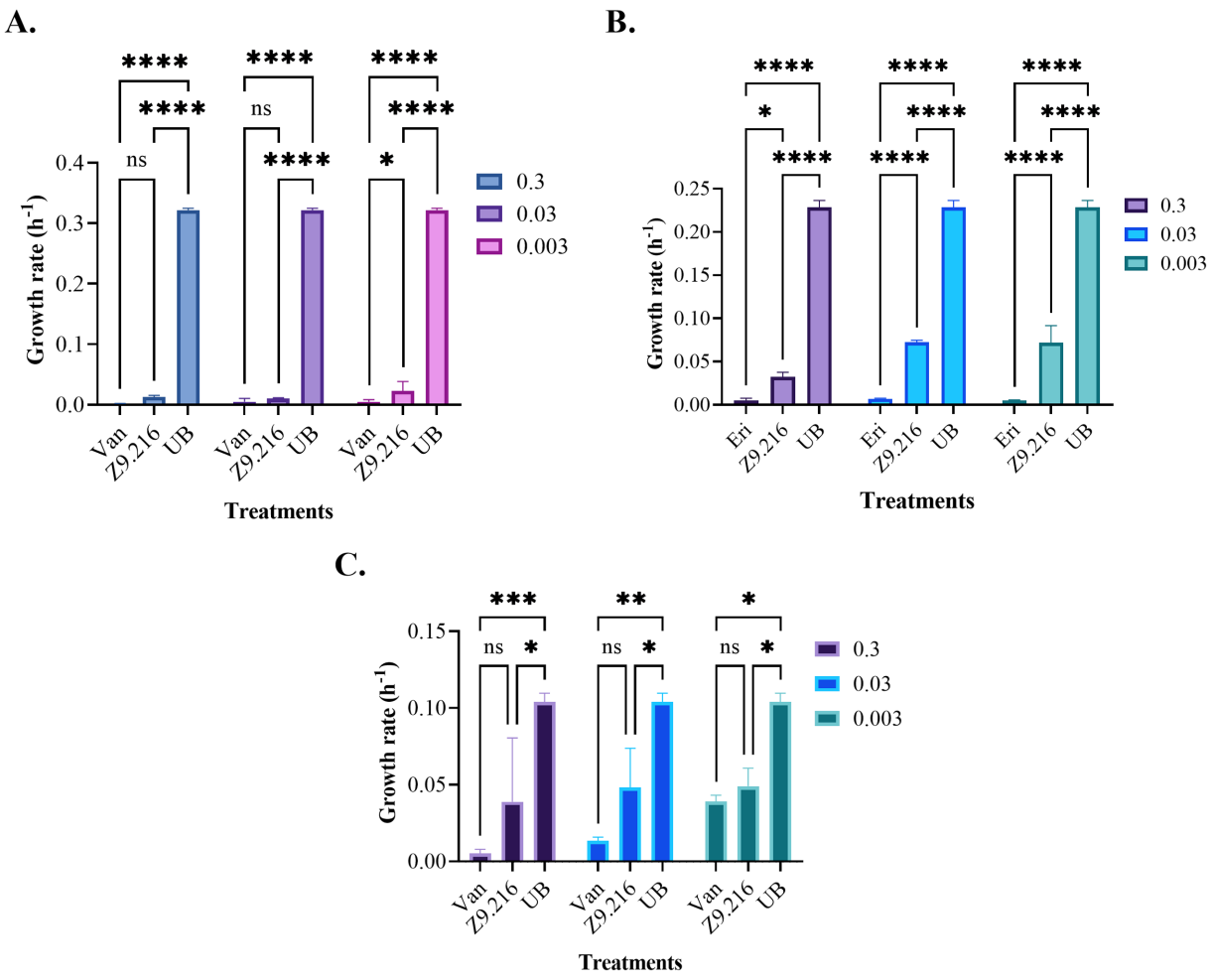

FIGURE 2
Growth rates of the bacteria studied in the presence of the Z9.216 extract (0.3–0.003 mg/mL). **(A)** Growth rate of methicillin-resistant *S. aureus* (MRSA) ATCC BA440. **(B)** Growth rate of *S. epidermidis* ATCC 14990. **(C)** Growth rate of *C. acnes* ATCC 6919. Values are expressed as mean ± standard error of the mean (SEM) and are compared with the positive control group. Significance levels are indicated as follows. ****p-value < 0.0001; ***p-value < 0.0007; **p-value < 0.0015; *p-value < 0.05.

The most promising isolates were selected because they exhibited more than 50% growth inhibition against some of the bacteria evaluated, namely Z9.216, G6.210, Z9.23, Z6.29, Z9.21, and Z9.11. The extract with the highest percentage of growth inhibition, Z9.216, was selected for further studies. Figure 1 presents the bacterial growth curves of MRSA, *S. epidermidis*, and *C. acnes* in the presence of Z9.216 extract.

3.2 Determination of maximum specific growth rate

The growth rate of bacteria treated with various extracts was assessed using the Baranyi and Roberts predictive primary model, because it had the best R^2 parameters (>97%) and the lowest squared error (<0.2). The maximum growth rate (measured in units of hours (h^{-1})), represented by the μ parameter, indicating the exponential growth phase of the bacteria (Dalgaard et al., 1994; Lindqvist and Barmark, 2014), was determined based on this model. Analysis of the data revealed that the bacterial growth rate in the presence of the most promising extract, Z9.216, at concentrations of 0.3, 0.03, and 0.003 mg/mL closely resembled that of the antibiotic vancomycin against MRSA and erythromycin against *S. epidermidis* and *C. acnes*. Interestingly, bacteria tested in the presence of extracts G6.210, Z9.23, and Z6.29 at 1.25 mg/mL exhibited growth rates surpassing those of the antibiotics but falling short of the growth rate observed in untreated bacteria. In comparison, the performances of extracts Z9.21 and Z9.11 were found to be similar. Figure 2 illustrates the growth rates of the studied bacteria in the presence of the most promising extract, Z9.216.

3.3 *In vitro* safety evaluation of the actinobacterial extracts

The most promising extract, Z9.216, maintained cell viability above 90% in both the HDFa and HACAT cell lines. In contrast, the bioactive extracts G6.210, Z9.23, and Z9.11, exhibited the highest cytotoxic activity against the HACAT cell line, reducing viability by 44, 36, and 46%, respectively, at the highest concentrations evaluated.

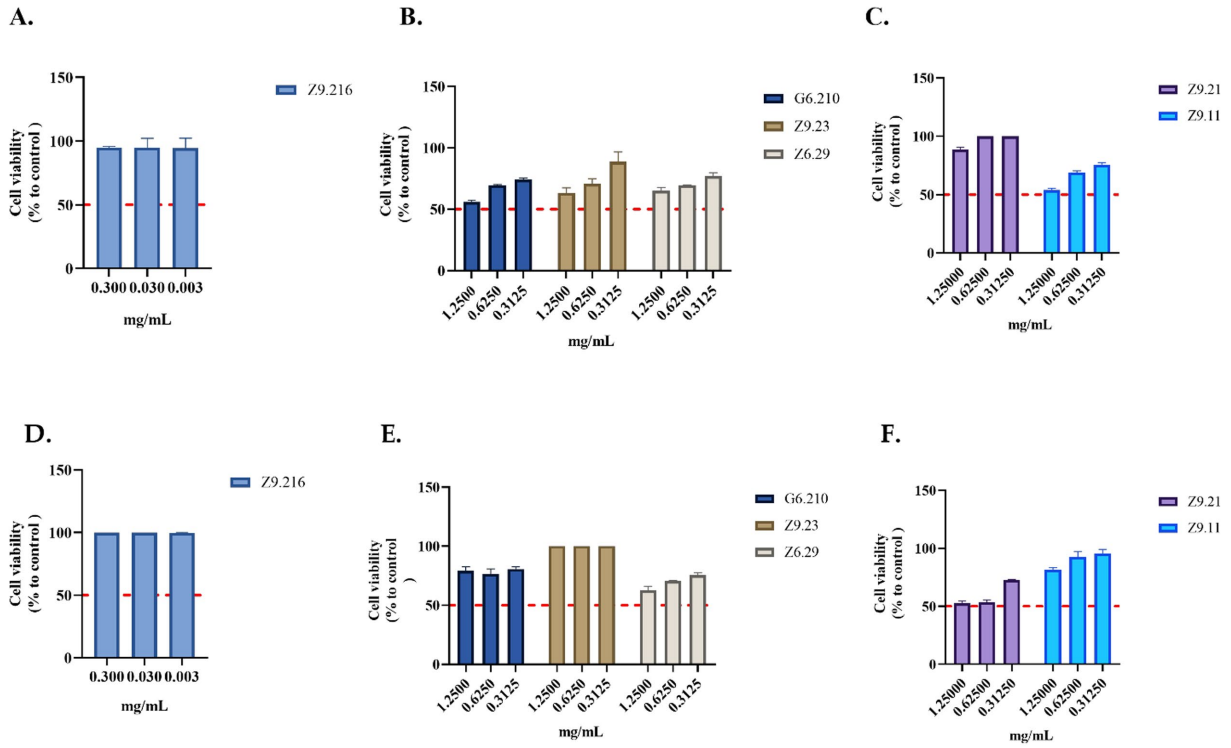

FIGURE 3
Evaluation of the viability of actinobacterial extracts. **(A–C)** Extracts evaluated in the HACAT cell line. **(D–F)** Extracts evaluated in HDFa cells. The crude extracts were evaluated at concentrations that showed activity. Each value represents the mean (n = 2) and error bars represent the standard deviation (SD). Cell viability was calculated by comparing the viability of untreated cells (control).

In the HDFa cell line, the extracts Z6.29 and Z9.21 demonstrated the highest cytotoxicity, decreasing cell viability by 37 and 47%, respectively, at the highest concentrations tested. For the remaining actinobacterial extracts, cell viability remained above 70% (Figure 3).

3.4 Identification of isolates with antibacterial activity by 16S rRNA gene sequencing

The cladogram led to the classification of bioactive isolates among actinobacterial genera, and Z9.216 was identified as a *Kocuria*, Z9.23 as *Nocardia*, Z6.29 as *Rhodococcus*, Z9.11 as *Micrococcus*, and Z9.21 as *Streptomyces* (Figure 4). The G6.210 isolate belonged to the *Streptomyces* genus, as previously reported (Sánchez-Suárez et al., 2021). Consensus sequences of the remaining extracts were deposited in GenBank under accession numbers PP389604, PP741801, PP741804, PP741802, and PP741803. The coding of the end-products and the names of the identified strains are presented in Supplementary Table S1.

3.5 Untargeted metabolomics by HPLC-QTOF-MS of promising microbial extracts

A total of 468 features were obtained from the analysis, and the comparison between the antibacterial active extracts and non-active extracts yielded 45 statistically significant features. Among these, only 16 were annotated based on the criteria described by Blaženovi (2018). Furthermore, the retention time was considered to match the nature of the compounds for all the features. To assess the quality of the analytical platform, PCA was performed for each analysis.

Clear clustering of QC samples in the unsupervised PCA models (Figure 5A) showed the stability and quality of the acquired data for ESI analysis in the positive mode. Therefore, this result supports that separation between groups is related to biological differentiation. Additionally, PCA revealed distinct clustering of antibacterial (green) and inactive (red) samples (Figure 5B).

The OPLS-DA model successfully differentiated samples into active antibacterial and inactive extracts. The OPLS-DA score plots (Figure 6A) clearly show separation, with the active group represented by green circles and the inactive group represented by red circles. The quality and robustness of the OPLS-DA model were validated using permutation tests (n = 100) (Figure 6B). The Q^2 intercept value was 0.739, indicating that the original model was statistically effective, the slope of the Q^2 values in the permutation test was negative for Y axes, and all predicted Q^2 values were lower than those calculated by the Q^2 model, indicating not over-fitted model (Triba et al., 2015; Betancur et al., 2020).

A univariate analysis (UVA) was performed to assess the significance of each metabolite for comparison. The parameters used to select statistically significant metabolites were those that met the following criteria: $p < 0.05$, VIP >1. The metabolites that met these requirements were identified as putative, confirmed, or unknown and are presented in Table 2.

Sixteen metabolites were identified as statistically significant when the antibacterial activities of the active and inactive extracts

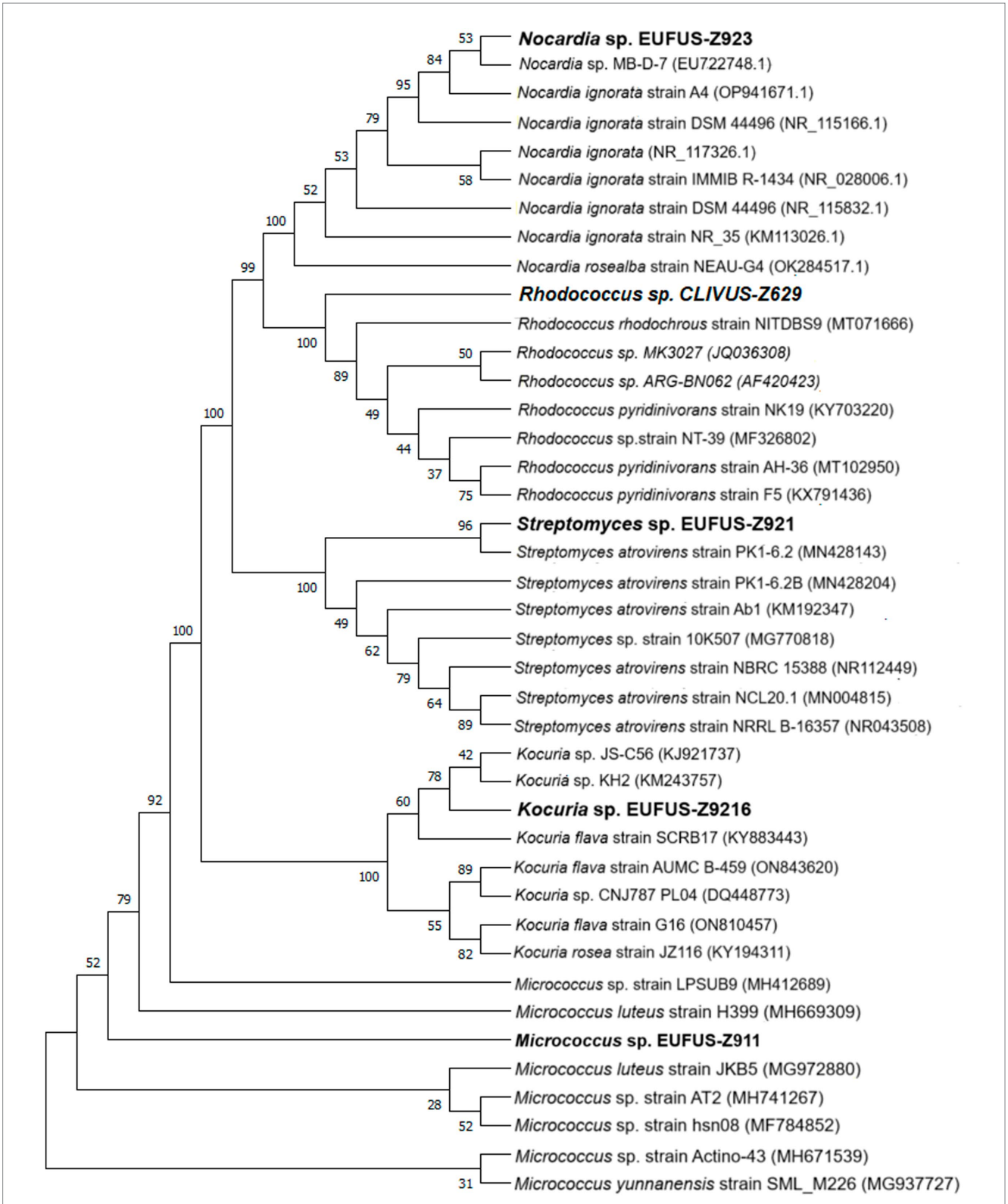

FIGURE 4
Phylogenetic tree of the bioactive isolates: cladogram for strains of genera *Kocuria* sp., *Nocardia* sp., *Rhodococcocus* sp., *Micrococcus* sp., and *Streptomyces* sp., using 16S rDNA sequences. An optimal tree is shown. The accession codes for the blasted strains are shown in parentheses. The percentage of replicate trees with associated taxa clustered together in the bootstrap test (1,000 replicates) is displayed next to the branches. All ambiguous positions were removed from each pair of sequences (i.e., pairwise deletions).

were compared. Among these compounds are alkaloids, such as indoles and their derivatives, quinolines, and other compounds, such as carboxylic acids, naphthalenes, stilbenes, and terpenoids (Figure 7). These features were characterized at different levels: level

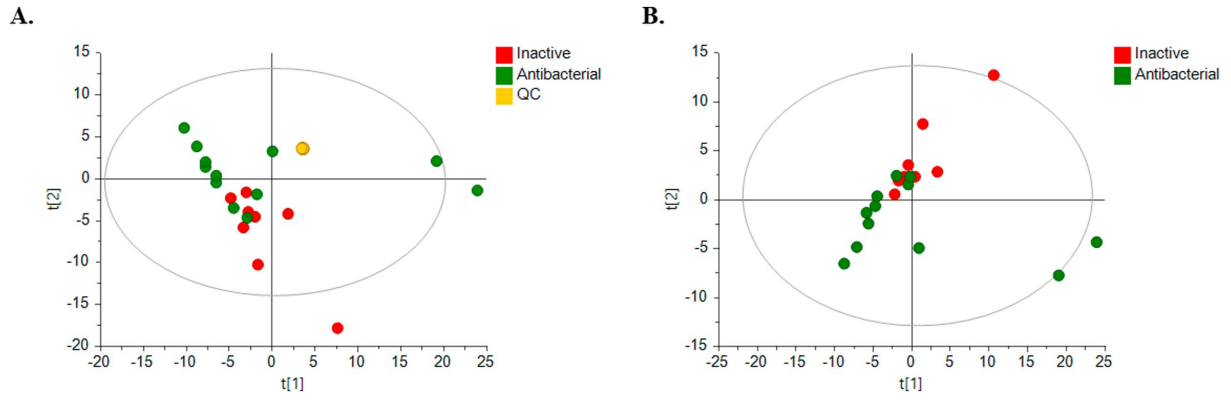

FIGURE 5
PCA score plots for untargeted metabolomics in positive ESI mode. (Green dots, bioactive samples; red dots, inactive samples; yellow dots, quality control samples, QC.) **(A)** HPLC-QTOF-MS (+) with QC samples: R^2 = 0.733, Q^2 = 0.293; **(B)** HPLC-QTOF-MS (+): R^2 = 0.619, Q^2 = 0.225.

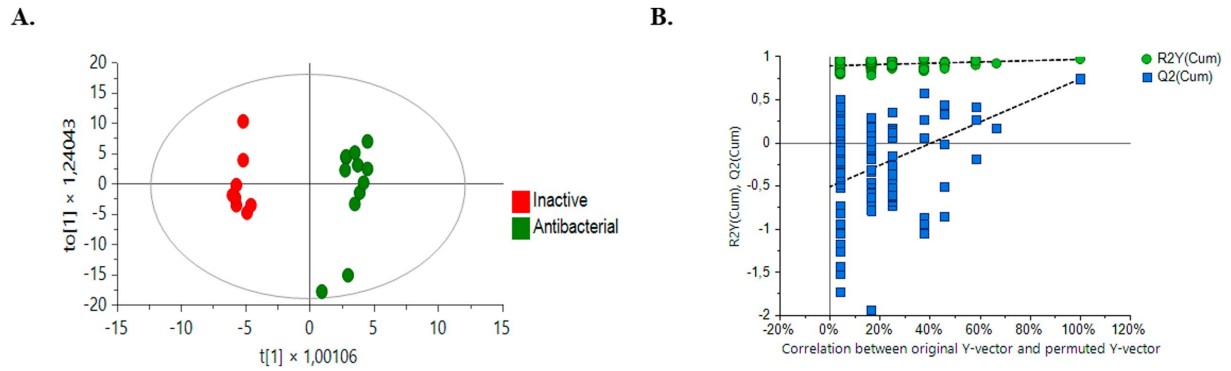

FIGURE 6
Comparison of supervised OPLS-DA models for untargeted metabolomics of inactive samples and bioactive samples (green dots, bioactive samples; red dots, inactive samples). **(A)** Positive ESI mode comparison HPLC-QTOF-MS (+): R^2Y (*cum*): 0.966, Q^2 (*cum*): 0.739, CV ANOVA: $1{,}3^{-3}$ **(B)** Permutation test (n = 100) results for the OPLS-DA model.

2 (probable structure: matched to literature data or databases by diagnostic evidence) utilizing library spectrum matching through MS2 fragmentation with the aid of MSDial software and CFM-ID; level 3 (possible structure or class: most likely structure, isomers possible, substance class, or substructure match Probable structure: matched to literature data or database); and level 4 (an unknown feature of interest) based on the confidence level of compound annotation described by Blaženovi (2018). At level 2, we annotated four compounds (Figure 8), all of which belong to the alkaloid family. Notably, these compounds exhibited a high fold change (Table 2). One such compound, indole-carbinol **(1)**, has been reported in cruciferous vegetables and fungi (Lin et al., 2019; Sung and Lee, 2007). High-resolution time-of-flight mass spectrometry (HP*LC-QTOF-MS*) data for **(1)** showed adduct molecular ions at *m/z* 147.0684 $[M + H\text{-}H2O]^{+\cdot}$ which were analyzed using the molecular formula C_9H_9NO. Moreover, at Level 2, we annotated indoline **(2)**. HP*LC-QTOF-MS* data for **(2)** showed adduct molecular ions at *m/z* 137.0841 $[M + H\text{-}H2O]^{+\cdot}$ corresponding to the molecular formula C_8H_9N. This metabolite has been previously reported in actinobacteria with antibacterial properties, specifically in Streptomyces (Katsuyama, 2019). Harman **(3)**, a *β*-carboline alkaloid, was also annotated in this level of identification. HP*LC-QTOF-MS* data for **(3)** showed adduct molecular ions at *m/z* 182.0844 $[M + H]^{+\cdot}$ which were analyzed using the molecular formula $C_{12}H_{10}N_2$. Finally, Norharman **(4),** another β-carboline alkaloid, was annotated with HP*LC-QTOF-MS* data, showing adduct molecular ions at *m/z* 168.0687 $[M + H]^{+}$, corresponding to the molecular formula $C_{11}H_8N_2$.

Furthermore, we identified other compounds that have been mostly reported in Actinobacteria. Some of these compounds were hydroxyquinoline **(5)** and caryophyllene **(6)** (Figure 8). Similarly, we also annotated compounds at level 3 (Figure 8), although they have not been previously reported in actinobacteria, showed a great abundance (Table 2), some of which have been isolated from plants, such as trimethyl-decatetraene **(7)**, a fatty acyl compound, (aminobutyl)-(hydroxy-methoxyphenyl) prop-enimidic acid **(8)**, a compound belonging to the carboxylic acid class, which is a natural product of antimicrobial activity, desmethylterbinafine **(9)**, a naphthalene compound, di-tert-butylbenzene **(10)**, benzene and substituted derivative, and Longistylin A **(11),** a compound annotated

TABLE 2 Metabolites significantly differentiated between antibacterial active extracts and non-active extracts using ESI modes by untargeted metabolomics via quadrupole time-of-flight mass spectrometry.

										Antibacterial vs. inactive samples		
Compound	Formula	Mass	RT (min)	Mass Error (ppm)	Adduct	[a]CV for QC (%)[a]	Analytical platform	DET	ID level	[b]Fold change	[c]VIP	[d]*p*-value
Alkaloids												
Norharman	$C_{11}H_8N_2$	168.0687	9.76	3	$[M + H]^+$	1.13	GM-RF-LC-QTOF-MS	ESI+	2	3.77	1.43	9.56^{-03}
Harman	$C_{12}H_{10}N_2$	182.0844	10.76	3	$[M + H]^+$	1.14	GM-RF-LC-QTOF-MS	ESI+	2	2.67	1.26	3.87^{-02}
Hydroxyquinoline	C_9H_7NO	145.0528	6.88	3	$[M + H]^+$	1.98	GM-RF-LC-QTOF-MS	ESI+	3	2.10	1.31	2.57^{-02}*
Indoles and derivates												
Indole-carbinol	C_9H_9NO	147.0684	15.36	3	$[M + H\text{-}H2O]^+$	6.60	GM-RF-LC-QTOF-MS	ESI+	2	2.54	1.38	7.30^{-03}
Indoline	C_8H_9N	137.0841	14	5	$[M + H\text{-}H2O]^+$	1.47	GM-RF-LC-QTOF-MS	ESI+	2	1.95	1.06	1.84^{-02}
Fatty acyls												
Trimethyl-decatetraene	$C_{13}H_{20}$	176.1565	10.1	2	$[M + Na]^+$	1.97	GM-RF-LC-QTOF-MS	ESI+	3	1.86	1.01	4.06^{-02}
Benzene and substituted derivatives												
Di-tert-butylbenzene	$C_{14}H_{22}$	190.1722	12.44	4	$[M + Na]^+$	1.90	GM-RF-LC-QTOF-MS	ESI+	3	1.96	1.08	4.06^{-02}
Carboxylic acid												
Proclavaminic acid	$C_8H_{14}N_2O_4$	202.0954	2.3	2	[M + H-H2O]+	2.36	GM-RF-LC-QTOF-MS	ESI+	3	0.67	1.18	3.14^{-02}
(Aminobutyl)-(hydroxy-methoxyphenyl)prop-enimidic acid	$C_{14}H_{20}N_2O_3$	264.1474	14	3	[M + H-H2O]+	1.39	GM-RF-LC-QTOF-MS	ESI+	3	2.05	1.12	2.26^{-02}
Glycoside												
Chivosazole E	$C_{46}H_{65}NO_{12}$	823.4507	18.83	5	$[M + Na]^+$	9.75	GM-RF-LC-QTOF-MS	ESI+	3	0.04	1.75	9.56^{-03}
Naphthalenes												
Desmethylterbinafine	$C_{20}H_{23}N$	277.183	15.36	3	[M + Na]+	4.63	GM-RF-LC-QTOF-MS	ESI+	3	2.26	1.13	2.02^{-02}
Sphingoid bases												
Dimethyl-Safingol	$C_{20}H_{43}NO_2$	329.3294	18.88	5	$[M + H]^+$	4.67	GM-RF-LC-QTOF-MS	ESI+	3	0.26	1.52	4.58^{-02}*

(Continued)

10.3389/fmicb.2024.1501951

TABLE 2 (Continued)

Compound	Formula	Mass	RT (min)	Mass Error (ppm)	Adduct	[a]CV for QC (%)	Analytical platform	DET	ID level	Antibacterial vs. inactive samples		
										[b]Fold change	[c]VIP	[d]p-value
Sphingolipids												
SPB 18:0;O3	$C_{18}H_{39}NO_3$	317.293	18.26	5	$[M+H]^+$	2.34	GM-RF-LC-QTOF-MS	ESI+	3	0.19	1.69	2.57^{-02*}
Stilbenes												
Longistylin A	$C_{20}H_{22}O_2$	294.162	10.58	9	$[M+H\text{-}H2O]^+$	1.28	GM-RF-LC-QTOF-MS	ESI+	4	2.31	1.30	2.02^{-02}
Terpenoid												
Caryophyllene	$C_{14}H_{22}$	190.1721	10.94	5	$[M+Na]^+$	1.57	GM-RF-LC-QTOF-MS	ESI+	3	3.85	1.55	2.01^{-02}
Unknown	$C_{15}H_{20}N_2O_2$	260.1525	16.11	2	$[M+H]+$	2.09	GM-RF-LC-QTOF-MS	ESI+	4	2.14	1.44	2.52^{-02}

[a]CV, coefficient of variation in the metabolites in the QC samples; [b]Change, percent change in the abundance of the specified comparison calculated as ((case−control)/control) × 100, where the sign indicates the direction of change in the case group; [c]VIP, variable importance in projection; [d]*p*-value * corresponding to the *p*-values calculated by the Benjamini–Hochberg false discovery rate *post hoc* correction (FDR < 0.05). GM, global metabolomics; LC, liquid chromatography; QTOF-MS, quadrupole time-of-flight mass spectrometry. RF, reverse phase.

at level 4, but this has been reported to have significant anti-MRSA activity (Wu et al., 2020) belonging to the Stilbenes class of compounds.

The remaining compounds, described in Table 2, were very low in abundance, especially in the inactive samples. Some of these compounds include clavaminic acid, carboxylic acid Chivosazole E, the glycoside compound dimethylsafingol, sphingoid base, SPB 18:0, and O3, a sphingolipid. Moreover, a considerable number of molecules were categorized as 'unknown.' However, among these, only one molecule met the criteria for statistical significance and demonstrated a biological relationship consistent with expected antibacterial activity.

4 Discussion

Actinobacteria are a relevant source of bioactive compounds primarily in terrestrial ecosystems (Kashfi et al., 2020). However, the repetitive discovery of land-based compounds (Ngamcharungchit et al., 2023; Siddharth and Rai, 2019) has allowed marine actinobacteria to emerge as promising alternative sources, leading to increased interest in marine bioprospecting. Corals, marine sponges, and their associated actinomycetes serve as repositories for novel natural products with diverse and potent biological activities and significant pharmaceutical value (Yang et al., 2015; Balasubramanian et al., 2018).

In our quest for new therapeutic options for acne vulgaris that minimize side effects and address bacterial resistance, we found that six out of 13 isolates studied could inhibit the growth of *S. epidermidis*, MRSA, and *C. acnes*. However, these extracts were characterized by a notably low yield, a challenge that has been previously described in similar studies (Lacret et al., 2019; Sujatha et al., 2005). Ethyl acetate was selected as the solvent because of its proven efficacy in isolating bioactive compounds from Actinobacteria, as documented in previous studies (Kurnianto et al., 2021; Sathish Kumar and Kokati Venkata Bhaskara, 2012). Remarkably, the Z9.216 extract displayed significant inhibition of over 95% against MRSA and *C. acnes,* and over 65% against *S. epidermidis* at a concentration of 0.003 mg/mL. The antibacterial activity of this extract was comparable to that of the standard antibiotic vancomycin, which was used as a reference, and exhibited 99% inhibition against both MRSA and *C. acnes* at the same concentration. These results align with those of previous studies, such as Paderog et al. (2020), who reported significant antibacterial activity of marine actinobacterial extracts against MRSA (Paderog et al., 2020).

Additionally, the growth rate assessment revealed no significant differences between the antibiotics and Z9.216 extract for MRSA and *C. acnes* (p-value < 0.05). Although research on the effects of actinobacterial extracts on *C. acnes* is limited, our findings are consistent with those of Kim et al. (2023) who demonstrated the antibacterial properties of a marine-derived pigment against *C. acnes*. The antibiotics currently used for *C. acnes* treatment, such as clindamycin and erythromycin, are derived from terrestrial actinobacteria, specifically from the *Streptomyces* genus, or are synthetically derived, such as tetracycline (De La Hoz-Romo et al., 2022). To the best of our knowledge, this study is among the first to demonstrate the therapeutic potential of marine actinobacterial extracts for treating acne vulgaris by targeting *C. acnes*.

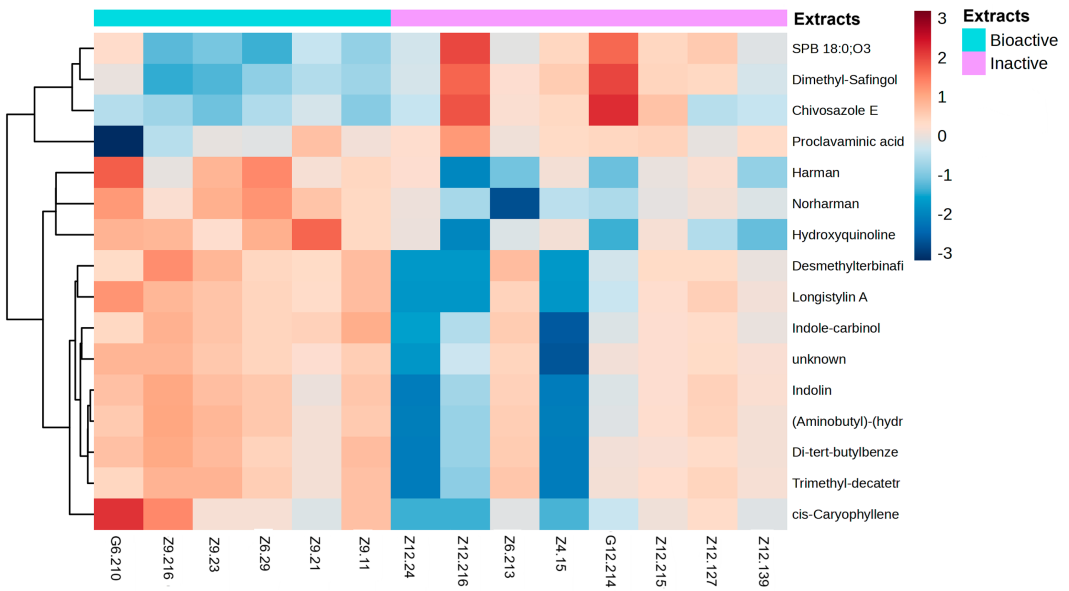

FIGURE 7
Heatmap of metabolites grouped by fold-change. The heatmap ranges from −3 to 3. Metabolites were identified by selecting the features most responsible for the antibacterial activity using discriminatory analysis (OPLS-DA), which were deemed significant by the linear model (p-value < 0.05). The antibacterial active extracts (denoted as G6.210, Z9.216, Z9.23, Z6.29, Z9.21, and Z9.11) and the non-active extracts (denoted as Z12.24, Z12.216, Z6.213, Z4.15, G12.214, Z12.215, Z12.127, and Z12.139). Hierarchical clustering of the strains was performed using Euclidean distances between the metabolites.

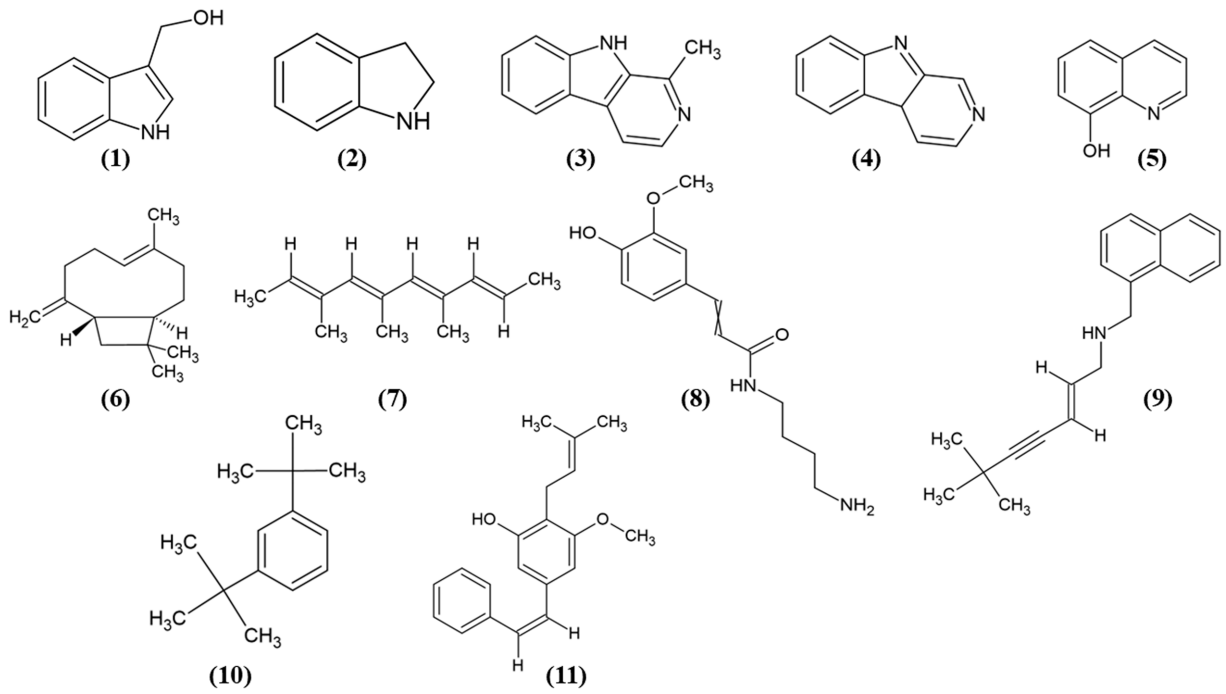

FIGURE 8
Chemical structures of the identified compounds at different confidence levels. Level 2 compounds (1–4): **(1)** Indole-3-carbinol, **(2)** Indoline, **(3)** Harman, and **(4)** Norharman. Level 3 compounds (5–11): **(5)** Hydroxyquinoline, **(6)** Caryophyllene, **(7)** Trimethyldecatetraene, **(8)** (Aminobutyl)-(hydroxy-methoxyphenyl) propenimidic acid, **(9)** Desmethylterbinafine, **(10)** Di-tert-butylbenzene, **(11)** Longistylin A.

Cytotoxic tests revealed that extract Z9.216 preserved the viability of human keratinocytes and fibroblasts at concentrations at which antibacterial activity was observed. In contrast, the Z9.23 extract caused the highest cytotoxicity at 1.25 mg/mL in HACAT cells, resulting in a viability reduction of up to 40%, a similar result also reported by Dahal et al. (2020).

Streptomyces remains the most prolific genus of actinobacteria (Newaz et al., 2022); however, bioprospecting of rare actinobacterial strains offers a promising source for identifying novel metabolites (Arasu Valan et al., 2016). In our study, four of the six bioactive strains belonged to the rare actinomycete strains *Kokuria* sp. strain EUFUS-Z9216, *Nocardia* sp. strain EUFUS-Z923, *Rhodococcus* sp. strain CLIVUS-Z629, and *Micrococcus* sp. strain EUFUS-Z911. Recent research has underscored the antibacterial potential of these less-known Actinobacteria genera. For instance, *Kocuria* species have been reported to produce antimicrobial compounds that are effective against various pathogenic bacteria, including MRSA (Jagannathan et al., 2021; Uzair et al., 2018). Similarly, *Nocardiopsis* strains have been found to synthesize novel antibiotics with potent activity against gram-positive and gram-negative bacteria (Kamarudheen et al., 2019). The diversity of rare actinobacterial strains examined in this study likely accounts for the range of compounds identified in the extracts.

Metabolomic analyses comparing antibacterial active and non-active extracts revealed diverse alkaloid derivatives as the dominant products, identified at level 2. While these compounds have predominantly been associated with the *Streptomyces* genus, as evidenced by the bulk of existing literature (Newaz et al., 2022; De Rop et al., 2022; Zhang et al., 2019; Yang et al., 2017; Zhang et al., 2017; Chen et al., 2019), their presence among extracts from other genera suggests a broader biosynthetic potential across various actinobacterial lineages.

In this study, a range of alkaloids were detected, including, hydroxyquinoline, derivatives of indole, Indole-carbinol, Indoline, and *β*-carboline compounds, such as Harman, and Norharman. These compounds were identified at the highest level and abundance, through metabolomic analysis as indicated by the fold change in Table 2. The indole nucleus, which is prevalent in many of these compounds, is a crucial structural motif in the pursuit of novel drug candidates and has been termed a "privileged structure" (Newaz et al., 2022; de Sa et al., 2009) owing to its versatile interactions with target proteins. Moreover, these compounds exhibit a spectrum of activities, including cytotoxic, antineoplastic, antibacterial, and antifungal (Newaz et al., 2022). In particular, the presence of nitrogen in their molecular architecture appears to play a crucial role in mediating these effects (Netz and Opatz, 2015).

Indole-carbinol, identified in this study, likely contributes to the antibacterial activity of bioactive extracts against MRSA, *S. epidermidis*, and *C. acnes*. This naturally occurring alkaloid, commonly found in cruciferous vegetables like broccoli and cauliflower (Netz and Opatz, 2015), is known for its anticancer, anti-inflammatory, and broad-spectrum antibacterial effects, including antibacterial activity against antibiotic-resistant strains (Sung and Lee, 2007; Wu et al., 2019; Wu et al., 2020).

Harman and Norharman, both β-carboline alkaloids, are commonly found in nature from a variety of sources, including plants, insects, and marine organisms (Netz and Opatz, 2015; Suzuki et al., 2018). Harman, known for its antibiotic potential, has previously been identified in marine invertebrates, notably within the tunicate-associated bacterium *Enterococcus faecium* (Aassila et al., 2003). This aligns with our findings as it supports the presence and potential bioactivity of similar compounds in marine actinobacterial extracts. Similarly, Norharman, an antimicrobial compound isolated from *Pseudoalteromonas piscicida* associated with the sponge *Hymeniacidon perleve*, was previously identified by Zheng et al. (2005) as a major antimicrobial agent against *Bacillus subtilis*, *S. aureus*, and *Escherichia coli* (Blockley et al., 2017). The β-carboline structure, common to both compounds, has been associated with the efficacy against certain antibiotic-resistant strains, suggesting its potential as a basis for novel antimicrobial agents (Suzuki et al., 2018). Additionally, the broad-spectrum antimicrobial activity of quaternary ammonium compounds against both gram-positive and gram-negative bacteria is noteworthy. These agents disrupt bacterial cell membranes by interacting with their negative charges, leading to the release of K+ ions and cytoplasmic content, ultimately causing bacterial cell death (Suzuki et al., 2018). Collectively, these insights help to elucidate our results and support the hypothesis that the observed antibacterial activity in actinobacterial extracts may be due to compounds with similar structures and mechanisms.

Among the identified metabolites, hydroxyquinoline (HQ), a quinoline-class alkaloid, demonstrated a statistically significant presence despite its low abundance in metabolomic analysis (Table 2). HQ is well known for its antimicrobial and anticancer activities, and has been frequently reported in actinobacteria, particularly within the *Streptomyces* genus (De Rop et al., 2022; Balthazar et al., 2022). The diverse biological properties of HQ and its derivatives, including anticancer, antibacterial, and anti-HIV activities, highlight their therapeutic relevance (Odingo et al., 2019; Song et al., 2015). HQ binds with a high affinity to various biological targets, offering the potential for new bioactive compound discovery (Song et al., 2015). The antibacterial mechanisms of HQ involve chelation with divalent ions, inhibition of RNA synthesis, and metallopeptidase activity. Structural modifications, particularly at positions 2 and 5, have been shown to enhance antibacterial efficacy, with substituted phenyl esters demonstrating potent activity against *S. aureus* and gram-negative bacteria. Notably, electron-withdrawing groups at the para position further increased this activity (Joaquim et al., 2021). The inclusion of HQ in our findings supports the hypothesis that such compounds contribute significantly to the antibacterial activity observed in marine actinobacterial extracts and underscores the potential for structural optimization to enhance bioactivity.

Additional identified compounds include caryophyllene, a sesquiterpene found widely in plants (Wu et al., 2020) and part of the terpenoid family, frequently reported in actinobacteria owing to terpene synthase genes in their genomes (Wu et al., 2020). Terpenoids exhibit various biological activities, such as antibacterial, antioxidant, anxiolytic, and anti-inflammatory effects, with caryophyllene also noted for its anti-aging and neuroprotective effects in animal studies (Rabe et al., 2013). Stilbenes and other compounds with high fold-changes, as shown in Table 2, are typical of actinobacteria and may contribute to the antibacterial activity of the extracts.

Four compounds were detected in the inactive samples, including two sphingolipids, which were significantly overproduced in these samples compared with the active ones. These sphingolipids displayed statistical significance, with adjusted *p-values* and high Variable Importance in Projection (VIP) scores, contributing to a clear separation between the groups. The excess

production of these metabolites in the inactive extracts suggests a possible blocking effect of certain compounds related to antibacterial activity. Future studies could explore the impact of sphingolipids by adding them to active samples at varying concentrations to determine the point at which the antibacterial activity decreases. This approach could clarify whether the overproduction of these two metabolites was directly responsible for the observed reduction in activity in the inactive extracts.

This inhibitory role aligns with the known biological functions of sphingolipids, which are typically produced by eukaryotes but have been recently detected in some bacterial taxa (Kunz and Kozjak-Pavlovic, 2019). These lipids support membrane regeneration and may promote bacterial growth. Recent evidence has identified *Streptomyces aurantiacus* as being capable of synthesizing ceramides, which are fundamental components of more complex sphingolipids. Furthermore, sphingolipids can act as carbon sources, supporting bacterial growth and helping counteract antibacterial compounds that target cell membranes. This role could explain the probable antagonistic effects, emphasizing the need for further research on sphingolipids in bacterial metabolism and resistance mechanisms (Stankeviciute et al., 2019; Stankeviciute et al., 2022; Peters et al., 2024).

5 Conclusion and perspectives

Marine actinobacteria isolated from the sponge *Cliona varians* and the octocoral *Eunicea fusca* demonstrate considerable potential as a source of bioactive compounds effective against acne vulgaris-associated bacteria, including *Staphylococcus epidermidis*, methicillin-resistant *Staphylococcus aureus* (MRSA), and *Cutibacterium acnes*. The extract Z9.216 from *Kocuria* sp. exhibited significant antibacterial activity, comparable to that of conventional antibiotics, without cytotoxic effects on human keratinocytes and fibroblasts at effective concentrations. The identification of these bioactive strains, many of which belong to rare Actinobacteria, highlights an underexplored group with significant potential for novel therapeutic applications. Metabolomic profiling revealed diverse bioactive compounds, particularly alkaloids and terpenoids, which likely contribute to the observed antibacterial effects. Although identified at preliminary confidence levels, further structural elucidation using advanced techniques such as 1D and 2D carbon-hydrogen nuclear magnetic resonance (NMR) is necessary to confirm and detail these findings. Future research should also focus on optimizing the production methods for these potent extracts in marine actinobacteria and exploring delivery systems, such as encapsulation, to enhance stability and efficacy. Overall, our findings underscore the therapeutic potential of marine actinobacteria, positioning them as valuable sources for developing new and effective treatments for acne vulgaris, and laying the groundwork for further exploration and application of marine-derived bioactive compounds in dermatological health.

Data availability statement

The datasets presented in this study can be found in online repositories. The names of the repository/repositories and accession number(s) can be found in the article/supplementary material.

Ethics statement

Ethical approval was not required for the studies on humans in accordance with the local legislation and institutional requirements because only commercially available established cell lines were used. Ethical approval was not required for the studies on animals in accordance with the local legislation and institutional requirements because only commercially available established cell lines were used. The actinobacteria used in this research were of Colombian origin and were obtained according to Amendment No. 5 to ARG Master Agreement No. 117 of May 26, 2015, granted by the Ministry of Environment and Sustainable Development, Colombia.

Author contributions

MC: Conceptualization, Data curation, Software, Validation, Visualization, Formal analysis, Investigation, Methodology, Writing – original draft, Writing – review & editing. LD: Conceptualization, Formal analysis, Funding acquisition, Investigation, Methodology, Project administration, Resources, Supervision, Validation, Writing – review & editing. JG-L: Formal analysis, Funding acquisition, Methodology, Project administration, Resources, Supervision, Writing – review & editing. MQ: Formal analysis, Funding acquisition, Methodology, Project administration, Resources, Supervision, Writing – review & editing. LV: Conceptualization, Formal analysis, Funding acquisition, Investigation, Methodology, Project administration, Resources, Supervision, Validation, Visualization, Writing – review & editing.

Funding

The author(s) declare that financial support was received for the research, authorship, and/or publication of this article. This research was funded by Minciencias (Ministerio de Ciencia, Tecnología e Innovación—Colombia, Fondo Francisco José De Caldas project code 2105-905-87457 contract 80740-458-2021), as well as by Universidad de La Sabana and Clínica Universidad de La Sabana through the Biomedical Campus Grant (General Research Directorate, project ING-PHD-42-2021).

Acknowledgments

We extend our heartfelt gratitude to the Minciencias (Ministerio de Ciencia, Tecnología e Innovación—Colombia, Fondo Francisco José De Caldas) for funding the project code 2105-905-87457 contract 80740-458-2021, as well as to the Marine and Coastal Research Institute "José Benito Vives de Andréis" (INVEMAR) and its Evaluation and Use of Marine and Coastal Resources Program / Marine Bioprospecting Line (Contribution No. 1385) for their unwavering support and for facilitating our activities throughout the development of this project. We are also grateful to the Universidad de La Sabana for the Carlos Jordana PhD scholarship and to the Metabolomics

Group at Universidad de los Andes (MetCore), particularly to José Leonardo Guerrero.

Conflict of interest

The authors declare that the research was conducted in the absence of any commercial or financial relationships that could be construed as a potential conflict of interest.

Generative AI statement

The authors declare that Generative AI was used in the creation of this manuscript. The author(s) verify and take full responsibility for the use of generative AI in the preparation of this manuscript. ChatGPT was used, in its GPT-4 version, for its assistance with editing this work. ChatGPT was utilized to review and enhance the grammar of the article but did not directly contribute to its conceptualization or content creation. Additionally, Grammarly was employed as a complementary tool for grammar and style refinement.

Publisher's note

All claims expressed in this article are solely those of the authors and do not necessarily represent those of their affiliated organizations, or those of the publisher, the editors and the reviewers. Any product that may be evaluated in this article, or claim that may be made by its manufacturer, is not guaranteed or endorsed by the publisher.

Supplementary material

The Supplementary material for this article can be found online at: https://www.frontiersin.org/articles/10.3389/fmicb.2024.1501951/full#supplementary-material

References

Aassila, H., Bourguet-Kondracki, M. L., Rifai, S., Fassouane, A., and Guyot, M. (2003). Identification of harman as the antibiotic compound produced by a tunicate-associated bacterium. *Mar. Biotechnol.* 5, 163–166. doi: 10.1007/s10126-002-0060-7

Achermann, Y., Goldstein, E. J. C., Coenye, T., and Shirtliffa, M. E. (2014). *Propionibacterium acnes*: from commensal to opportunistic biofilm-associated implant pathogen. *Clin. Microbiol. Rev.* 27, 419–440. doi: 10.1128/CMR.00092-13

Akhter, N., Liu, Y., Auckloo, B. N., Shi, Y., Wang, K., Chen, J., et al. (2018). Stress-driven discovery of new Angucycline-type antibiotics from a marine *Streptomyces pratensis* NA-Zhou S1. *Mar. Drugs* 16, 331–346. doi: 10.3390/md16090331

Alkhawaja, E., Hammadi, S., Abdelmalek, M., Mahasneh, N., Alkhawaja, B., and Abdelmalek, S. M. (2020). Antibiotic resistant Cutibacterium acnes among acne patients in Jordan: a cross sectional study. *BMC Dermatol.* 20, 1–9. doi: 10.1186/s12895-020-00108-9

Anggelina, A. C., Pringgenies, D., and Setyati, W. A. (2021). Presence of biosynthetic gene clusters (NRPS/PKS) in actinomycetes of mangrove sediment in Semarang and Karimunjawa, Indonesia. *Environ. Nat. Resour. J. [Internet]*. 19, 391–40. doi: 10.32526/ennrj/19/202100050

Arasu Valan, M., Esmail, G. A., and Al-Dhabi, N. A. (2016). Hypersaline Actinomycetes and their biological applications. *Intech* 11:13. doi: 10.5772/61065

Balagurunathan, R, Radhakrishnan, M, Shanmugasundaram, T, Gopikrishnan, V, and Jerrine, J. *Protocols in Actinobacterial Research [Internet]*. (2020) (Springer Protocols Handbooks). Available at: http://link.springer.com/10.1007/978-1-0716-0728-2

Balasubramanian, S., Skaf, J., Holzgrabe, U., Bharti, R., Foerstner, K. U., Ziebuhr, W., et al. (2018). A new bioactive compound from the marine sponge-derived Streptomyces sp SBT348 inhibits staphylococcal growth and biofilm formation. *Front. Microbiol.* 9:1473. doi: 10.3389/fmicb.2018.01473

Balthazar, J. D., Soosaimanickam, M. P., Emmanuel, C., Krishnaraj, T., Sheikh, A., Alghafis, S. F., et al. (2022). 8-Hydroxyquinoline a natural chelating agent from Streptomyces spp. inhibits A549 lung cancer cell lines via BCL2/STAT3 regulating pathways. *World J. Microbiol. Biotechnol.* 38, 182–112. doi: 10.1007/s11274-022-03368-4

Bauermeister, A., Pereira, F., Grilo, I. R., Godinho, C. C., Paulino, M., Almeida, V., et al. (2019). Intra-clade metabolomic profiling of MAR4 Streptomyces from the Macaronesia Atlantic region reveals a source of anti-biofilm metabolites. *Environ. Microbiol.* 21, 1099–1112. doi: 10.1111/1462-2920.14529

Bernhardt, M. J., and Myntti, M. F. (2016). Topical treatment with an agent disruptive to *P. acnes* biofilm provides positive therapeutic response: results of a randomized clinical trial. *J. Drugs Dermatol.* 15, 677–683.

Betancur, L. A., Forero, A. M., Vinchira-Villarraga, D. M., Cárdenas, J. D., Romero-Otero, A., Chagas, F. O., et al. (2020). NMR-based metabolic profiling to follow the production of anti-phytopathogenic compounds in the culture of the marine strain Streptomyces sp. PNM-9. *Microbiol. Res.* 239:126507. doi: 10.1016/j.micres.2020.126507

Blaženovi, I. (2018). Software tools and approaches for compound identification of LC-MS/MS data in metabolomics. *Metabolites [Internet]*. 8, 20–49. doi: 10.3390/metabo8020031

Blockley, A., Elliott, D. R., Roberts, A. P., and Sweet, M. (2017). Symbiotic microbes from marine invertebrates: driving a new era of natural product drug discovery. *Diversity* 9, 1–13. doi: 10.3390/d9040049

Bungau, A. F., Radu, A. F., Bungau, S. G., Vesa, C. M., Tit, D. M., Purza, A. L., et al. (2023). Emerging insights into the applicability of essential oils in the Management of Acne Vulgaris. *Molecules* 28, 1–25. doi: 10.3390/molecules28176395

Camargo, F. D. G., Santamaria-Torres, M., Cala, M. P., Guevara-Suarez, M., Restrepo, S. R., Sánchez-Camargo, A., et al. (2023). Genome-scale metabolic reconstruction, non-targeted LC-QTOF-MS based metabolomics data, and evaluation of anticancer activity of *Cannabis sativa* leaf extracts. *Meta* 13, 788–818. doi: 10.3390/metabo13070788

Chen, M.-H., Zhang, W.-L., Chen, L., Lin, R., Xie, Y., Fang, D.-S., et al. (2019). Isolation, purification and identification of two new alkaloids metabolites from marine-derived *Verrucosispora* sp. FIM06025. *Nat. Prod. Res.* 33, 2897–2903. doi: 10.1080/14786419.2018.1509333

Cheng, Y.-B., Jensen, P. R., and Fenical, W. (2013). Cytotoxic and antimicrobial Napyradiomycins from two marine-derived, MAR 4 Streptomyces strains. *Eur. J. Org. Chem.* 2013, 3751–7. doi: 10.1002/ejoc.201300349

Costa, CS, Bagatin, E Martimbianco A, Da Silva, E, Lúcio, M, Magin, P, and Riera, R. (2018).¿Cuán efectivo y seguro es el fármaco llamado "isotretinoína" en comprimidos para el acné vulgar? Available at: https://www.cochrane.org/es/CD009435/SKIN_cuan-efectivo-y-seguro-es-el-farmaco-llamado-isotretinoina-en-comprimidos-para-el-acne-vulgar (Accessed 05 September, 2024).

Dadgostar, P. (2019). Antimicrobial resistance: implications and costs. *Infect Drug Resist [Internet]*. 12:3903–10. doi: 10.2147/IDR.S234610

Dahal, RH, Nguyen, TM, Shim, DS, Kim, JY, Lee, J, and Kim, J. Development of multifunctional cosmetic cream using bioactive materials from *Streptomyces* sp. T65 with synthesized mesoporous silica particles SBA-15. *Antioxidants [Internet]*. (2020) 9:278. Available at: https://www.mdpi.com/2076-3921/9/4/278

Dalgaard, P., Ross, T., Kamperman, L., Neumeyer, K., and McMeekin, T. A. (1994). Estimation of bacterial growth rates from turbidimetric and viable count data. *Int. J. Food Microbiol.* 23, 391–404. doi: 10.1016/0168-1605(94)90165-1

De La Hoz-Romo, M. C., Díaz, L., and Villamil, L. (2022). Marine Actinobacteria a new source of antibacterial metabolites to treat acne vulgaris disease—a Systematic Literature Review. *Antibiotics* 11:965. doi: 10.3390/antibiotics11070965

De Rop, A. S., Rombaut, J., Willems, T., De Graeve, M., Vanhaecke, L., Hulpiau, P., et al. (2022). Novel alkaloids from marine actinobacteria: discovery and characterization. *Mar. Drugs* 20, 1–23. doi: 10.3390/md20010006

de Sa, A. F., Barreiro, E., and Manssour, F. C. (2009). From nature to drug discovery: the indole scaffold as a privileged structure. *Mini-Reviews Med. Chem.* 9, 782–793. doi: 10.2174/138955709788452649

Dholakiya, R. N., Kumar, R., Mishra, A., Mody, K. H., and Jha, B. (2017). Antibacterial and antioxidant activities of novel Actinobacteria strain isolated from gulf of Khambhat, Gujarat. *Front. Microbiol.* 8:8. doi: 10.3389/fmicb.2017.02420

Duarte, A. P., Proença, A. C., and Duarte, A. P. (2022). The role of herbal medicine in the treatment of acne vulgaris: A Systematic Review of Clinical Trials. *Evidence-based complementary and alternative medicine*. 2022, 1–22. doi: 10.1155/2022/2011945

Fournière, M., Latire, T., Souak, D., Feuilloley, M. G. J., and Bedoux, G. (2020). *Staphylococcus epidermidis* and cutibacterium acnes: two major sentinels of skin

microbiota and the influence of cosmetics. *Microorganisms* 8, 1–31. doi: 10.3390/microorganisms8111752

Gil-De-La-Fuente, A., Godzien, J., Saugar, S., Garcia-Carmona, R., Badran, H., Wishart, D. S., et al. (2019). CEU mass mediator 3.0: a metabolite annotation tool. *J. Proteome Res.* 18, 797–802. doi: 10.1021/acs.jproteome.8b00720

Jagannathan, S. V., Manemann, E. M., Rowe, S. E., Callender, M. C., and Soto, W. (2021). Marine actinomycetes, new sources of biotechnological products. *Mar. Drugs* 19:365. doi: 10.3390/md19070365

Joaquim, A. R., Gionbelli, M. P., Gosmann, G., Fuentefria, A. M., Lopes, M. S., and Fernandes De Andrade, S. (2021). Novel antimicrobial 8-Hydroxyquinoline-based agents: current development, structure-activity relationships, and perspectives. *J. Med. Chem.* 64, 16349–16379. doi: 10.1021/acs.jmedchem.1c01318

Kamarudheen, N., Naushad, T., and Rao, K. V. B. (2019). Biosynthesis, characterization and antagonistic applications of extracellular melanin pigment from marine Nocardiopsis sps. *Indian J. Pharm. Educ. Res.* 53, S112–S120. doi: 10.5530/ijper.53.2s.55

Kashfi, R., Kelsey, C., Gang, D. J., Call, D. R., and Gang, D. R. (2020). Metabolomic diversity and identification of antibacterial activities of Bacteria isolated from marine sediments in Hawai'i and Puerto Rico. *Front. Mol. Biosci.* 7:23. doi: 10.3389/fmolb.2020.00023

Katsuyama, Y. (2019). Mining novel biosynthetic machineries of secondary metabolites from actinobacteria. *Biosci. Biotechnol. Biochem.* 83, 1606–1615. doi: 10.1080/09168451.2019.1606700

Keshari, S., Kumar, M., Balasubramaniam, A., Chang, T. W., Tong, Y., and Huang, C. M. (2019). Prospects of acne vaccines targeting secreted virulence factors of Cutibacterium acnes. *Expert Rev. Vaccines* 18, 433–437. doi: 10.1080/14760584.2019.1593830

Kim, H. J., Lee, M. S., Jeong, S. K., and Lee, S. J. (2023). Transcriptomic analysis of the antimicrobial activity of prodigiosin against *Cutibacterium acnes*. *Sci. Rep.* 13, 17412–17419. doi: 10.1038/s41598-023-44612-7

Kunz, T. C., and Kozjak-Pavlovic, V. (2019). Diverse facets of sphingolipid involvement in bacterial infections. *Front Cell. Dev. Biol.* 7, 1–10. doi: 10.3389/fcell.2019.00203

Kurnianto, M. A., Kusumaningrum, H. D., Lioe, H. N., and Chasanah, E. (2021). Antibacterial and antioxidant potential of ethyl acetate extract from Streptomyces AIA12 and AIA17 isolated from gut of *Chanos chanos*. *Biodiversitas J. Biolog. Diver.* 22, 22, 3196–3206. doi: 10.13057/biodiv/d220813

Lacret, R., Oves-Costales, D., Perez-Victoria, I., de la Cruz, M., Diaz, C., Vicente, F., et al. (2019). MDN-0171, a new medermycin analogue from *Streptomyces albolongus* CA-186053. *Nat. Prod. Res.* 33, 66–73. doi: 10.1080/14786419.2018.1434636

Lin, L., Jiang, N., Wu, H., Mei, Y., Yang, J., and Tan, R. (2019). Cytotoxic and antibacterial polyketide-indole hybrids synthesized from indole-3-carbinol by Daldinia eschscholzii. *Acta Pharm. Sin. B* 9, 369–380. doi: 10.1016/j.apsb.2018.09.011

Lindqvist, R., and Barmark, G. (2014). Specific growth rate determines the sensitivity of escherichia coli to lactic acid stress: implications for predictive microbiology. *Biomed. Res. Int.* 2014, 1–8. doi: 10.1155/2014/471317

Mayslich, C., Grange, P. A., and Dupin, N. (2021). Cutibacterium acnes as an opportunistic pathogen: an update of its virulence-associated factors. *Microorganisms.* 9, 1–21. doi: 10.3390/microorganisms9020303

Melnik, B. C. (2018). Acne vulgaris: the metabolic syndrome of the pilosebaceous follicle. *Clin. Dermatol.* 36, 29–40. doi: 10.1016/j.clindermatol.2017.09.006

Moradi Tuchayi, S., Makrantonaki, E., Ganceviciene, R., Dessinioti, C., Feldman, S. R., and Zouboulis, C. C. (2015). Acne vulgaris. *Nat. Rev. Dis. Prim.* 1:15029. doi: 10.1038/nrdp.2015.29

Mosmann, T. (1983). Rapid colorimetric assay for cellular growth and survival: application to proliferation and cytotoxicity assays. *J. Immunol. Methods* 65, 55–63. doi: 10.1016/0022-1759(83)90303-4

Moumbock, A. F. A., Gao, M., Qaseem, A., Li, J., Kirchner, P. A., Ndingkokhar, B., et al. (2021). Streptome DB 3.0: an updated compendium of streptomycetes natural products. *Nucleic Acids Res.* 49, D600–D604. doi: 10.1093/nar/gkaa868

Netz, N., and Opatz, T. (2015). Marine indole alkaloids. *Mar. Drugs* 13, 4814–4914. doi: 10.3390/md13084814

Newaz, A. W., Yong, K., Lian, X.-Y., and Zhang, Z. (2022). Streptoindoles A–D, novel antimicrobial indole alkaloids from the marine-associated actinomycete *Streptomyces* sp. ZZ1118. *Tetrahedron*:104. doi: 10.1016/j.tet.2021.132598

Ngamcharungchit, C., Chaimusik, N., Panbangred, W., Euanorasetr, J., and Intra, B. (2023). Bioactive metabolites from terrestrial and marine Actinomycetes. *Molecules* 28, 1–33. doi: 10.3390/molecules28155915

Odingo, J. O., Early, J. V., Smith, J., Johnson, J., Bailey, M. A., Files, M., et al. (2019). 8-Hydroxyquinolines are bactericidal against *Mycobacterium tuberculosis*. *Drug Dev. Res.* 80, 566–572. doi: 10.1002/ddr.21531

Paderog, M. J. V., Suarez, A. F. L., Sabido, E. M., Low, Z. J., Saludes, J. P., and Dalisay, D. S. (2020). Anthracycline shunt metabolites from Philippine marine sediment-derived Streptomyces destroy cell membrane integrity of multidrug-resistant *Staphylococcus aureus*. *Front. Microbiol.* 11:743. doi: 10.3389/fmicb.2020.00743

Panche, A. N., Diwan, A. D., and Chandra, S. R. (2016). Flavonoids: an overview. *J. Nutr. Sci.* 5, 1–15. doi: 10.1017/jns.2016.41

Peters, L, Drechsler, M, Pees, B, Angelidou, G, Salzer, L, Moors, KA, et al. Polyketide synthase-derived sphingolipids determine microbiota-mediated protection against pathogens in *C. elegans [Internet]*. (2024). doi: 10.1101/2024.02.06.579051

Quintero, M., Santander, M. J., Velásquez, S., Zapata, J., and Cala, M. P. (2022). Exploring chemical markers related to the acceptance and sensory profiles of concentrated liquid coffees: an untargeted metabolomics approach. *Food Secur.* 11:473. doi: 10.3390/foods11030473

Rabe, P., Citron, C. A., and Dickschat, J. S. (2013). Volatile terpenes from actinomycetes: a biosynthetic study correlating chemical analyses to genome data. *Chembiochem* 14, 2345–2354. doi: 10.1002/cbic.201300329

Rajasabapathy, R., Ghadi, S. C., Manikandan, B., Mohandass, C., Surendran, A., Dastager, S. G., et al. (2020). Antimicrobial profiling of coral reef and sponge associated bacteria from southeast coast of India. *Microb. Pathog.* 141:103972. doi: 10.1016/j.micpath.2020.103972

Rajivgandhi, G., Vijayan, R., Kannan, M., Santhanakrishnan, M., and Manoharan, N. (2016). Molecular characterization and antibacterial effect of endophytic actinomycetes Nocardiopsis sp. GRG1 (KT235640) from brown algae against MDR strains of uropathogens. *Bioact Mater.* 1, 140–150. doi: 10.1016/j.bioactmat.2016.11.002

Sánchez-Suárez, J., Villamil, L., Coy-Barrera, E., and Díaz, L. (2021). *Cliona varians*-derived actinomycetes as bioresources of photoprotection-related bioactive end-products. *Mar. Drugs* 19:674. doi: 10.3390/md19120674

Sarmiento-Tovar, A. A., Prada-Rubio, S. J., Gonzalez-Ronseria, J., Coy-Barrera, E., and Diaz, L. (2024). Exploration of the bioactivity of pigmented extracts from Streptomyces strains isolated along the banks of the Guaviare and Arauca Rivers (Colombia). *Fermentation* 10:529. doi: 10.3390/fermentation10100529

Sathish Kumar, S. R., and Kokati Venkata Bhaskara, R. (2012). In-vitro antimicrobial activity of marine actinobacteria against multidrug resistance *Staphylococcus aureus*. Asian Pac. *J Trop Biomed.* 2, S1802–S1807. doi: 10.1016/S2221-1691(12)60230-5

Sermswan, P., Sriharat, R., Saithong, S., Laowansiri, M., Amornruk, N., Chiewchengchol, D., et al. (2023). A cross-sectional study examining the prevalence of antibiotic-resistant Cutibacterium acnes isolated from patients with acne in Bangkok, Thailand. *J Dermatol.* 50, 1008–1013. doi: 10.1111/1346-8138.16823

Siddharth, S. V. R. R. (2019). Isolation, characterization, and structural elucidation of 4-methoxyacetanilide from marine actinobacteria Streptomyces sp. SCA29 and evaluation of its enzyme inhibitory, antibacterial, and cytotoxic potential. *Arch Microbiol.* 201, 737–746. doi: 10.1007/s00203-019-01634-y

Siddharth, S., and Rai, V. R. (2019). Isolation and characterization of bioactive compounds with antibacterial, antioxidant and enzyme inhibitory activities from marine-derived rare actinobacteria, *Nocardiopsis* sp. SCA21. *Microb. Pathog.*:137. Available at: https://www.scopus.com/inward/record.uri?eid=2-s2.0-85073123381&doi=10.1016%2Fj.micpath.2019.103775&partnerID=40&md5=36a4dcd2f330198e29d094f6f6b40cc3

Siro, G., Pipite, A., Christi, K., Srinivasan, S., and Subramani, R. (2022). Marine Actinomycetes associated with stony corals: a potential hotspot for specialized metabolites. *Microorganisms* 10, 1–32. doi: 10.3390/microorganisms10071349

Song, Y., Xu, H., Chen, W., Zhan, P., and Liu, X. (2015). 8-Hydroxyquinoline: a privileged structure with a broad-ranging pharmacological potential. *Medchemcomm* 6, 61–74. doi: 10.1039/C4MD00284A

Stankeviciute, G., Guan, Z., Goldfine, H., and Klein, E. A. (2019). *Caulobacter crescentus* adapts to phosphate starvation by synthesizing anionic Glycoglycerolipids and a novel glycosphingolipid. *Mol. Biol. Physiol.* 10, 1–13. doi: 10.1128/mBio.00107-19

Stankeviciute, G., Tang, P., Ashley, B., Chamberlain, J. D., Hansen, M. E. B., Coleman, A., et al. (2022). Convergent evolution of bacterial ceramide synthesis. *Nat. Chem. Biol.* 18, 305–312. doi: 10.1038/s41589-021-00948-7

Sujatha, P., Bapi Raju, K. V. V. S. N., and Ramana, T. (2005). Studies on a new marine streptomycete BT-408 producing polyketide antibiotic SBR-22 effective against methicillin resistant *Staphylococcus aureus*. *Microbiol. Res.* 160, 119–126. doi: 10.1016/j.micres.2004.10.006

Sung, W. S., and Lee, D. G. (2007). In vitro antimicrobial activity and the mode of action of indole-3-carbinol against human pathogenic microorganisms. *Biol. Pharm. Bull.* 30, 1865–1869. doi: 10.1248/bpb.30.1865

Suzuki, K., Nomura, I., Ninomiya, M., Tanaka, K., and Koketsu, M. (2018). Synthesis and antimicrobial activity of β-carboline derivatives with N 2-alkyl modifications. *Bioorganic Med. Chem. Lett.* 28, 2976–2978. doi: 10.1016/j.bmcl.2018.06.050

Triba, M. N., Le Moyec, L., Amathieu, R., Goossens, C., Bouchemal, N., Nahon, P., et al. (2015). PLS/OPLS models in metabolomics: the impact of permutation of dataset rows on the K-fold cross-validation quality parameters. *Mol. BioSyst.* 11, 13–19. doi: 10.1039/C4MB00414K

Uzair, B., Menaa, F., Khan, B. A., Mohammad, F. V., Ahmad, V. U., Djeribi, R., et al. (2018). Isolation, purification, structural elucidation and antimicrobial activities of kocumarin, a novel antibiotic isolated from actinobacterium *Kocuria marina* CMG S2 associated with the brown seaweed *Pelvetia canaliculata*. *Microbiol. Res.* 206, 186–197. doi: 10.1016/j.micres.2017.10.007

van de Loosdrecht, A. A., Nennie, E., Ossenkoppele, G. J., Beelen, R. H. J., and Langenhuijsen, M. M. A. C. (1991). Cell mediated cytotoxicity against U 937 cells by

human monocytes and macrophages in a modified colorimetric MTT assay. *J. Immunol. Methods.* 141, 15–22. doi: 10.1016/0022-1759(91)90205-T

Van Santen, J. A., Poynton, E. F., Iskakova, D., Mcmann, E., Alsup, T. A., Clark, T. N., et al. (2022). The natural products atlas 2.0: a database of microbially-derived natural products. *Nucleic Acids Res.* 50, D1317–D1323. doi: 10.1093/nar/gkab941

Wang, D., Wang, C., Gui, P., Liu, H., Khalaf, S. M. H., Elsayed, E. A., et al. (2017). Identification, bioactivity, and productivity of Actinomycins from the marine-derived *Streptomyces heliomycini*. *Front. Microbiol.* 8:1147. doi: 10.3389/fmicb.2017.01147

Wu, Y., He, Q., Yu, L., Pham, Q., Cheung, L., Kim, Y. S., et al. (2020). Indole-3-carbinol inhibits *Citrobacter rodentium* infection through multiple pathways including reduction of bacterial adhesion and enhancement of cytotoxic T cell activity. *Nutrients* 12, 1–14. doi: 10.3390/nu12040917

Wu, Y., Li, R. W., Huang, H., Fletcher, A., Yu, L., Pham, Q., et al. (2019). Inhibition of tumor growth by dietary indole-3-carbinol in a prostate cancer xenograft model may be associated with disrupted gut microbial interactions. *Nutrients* 11:467. doi: 10.3390/nu11020467

Wu, J., Li, B., Xiao, W., Hu, J., Xie, J., Yuan, J., et al. (2020). Longistylin a, a natural stilbene isolated from the leaves of *Cajanus cajan*, exhibits significant anti-MRSA activity. *Int. J. Antimicrob. Agents* 55:105821. doi: 10.1016/j.ijantimicag.2019.10.002

Wu, Y., He, Q., Yu, L., Pham, Q., Cheung, L., Kim, YS., et al (2020). Indole-3-carbinol inhibits Citrobacter rodentium infection through multiple pathways including reduction of bacterial adhesion and enhancement of cytotoxic T cell activity. *Nutrients.* 12, 1–4.

Wu, J., Zhu, Y., Zhang, M., Li, H., and Sun, P. (2020). Micaryolanes a and B, two new Caryolane-type Sesquiterpenoids from marine *Streptomyces* sp AH25. *Chem. Biodivers.* 17:e2000769. doi: 10.1002/cbdv.202000769

Yang, J., Li, J., Hu, Y., Li, L., Long, L., Wang, F., et al. (2015). Characterization of a thermophilic hemoglobin-degrading protease from *Streptomyces rutgersensis* SCSIO 11720 and its application in antibacterial peptides production. *Biotechnol. Bioprocess Eng.* 20, 79–90. doi: 10.1007/s12257-013-0771-9

Yang, C. L., Wang, Y. S., Liu, C. L., Zeng, Y. J., Cheng, P., Jiao, R. H., et al. (2017). Strepchazolins a and B: two new alkaloids from a marine *Streptomyces chartreusis* NA02069. *Mar. Drugs* 15:244. doi: 10.3390/md15080244

Zhang, X., Chen, L., Chai, W., Lian, X.-Y., and Zhang, Z. (2017). A unique indolizinium alkaloid streptopertusacin a and bioactive bafilomycins from marine-derived Streptomyces sp HZP-2216E. *Phytochemistry* 144, 119–126. doi: 10.1016/j.phytochem.2017.09.010

Zhang, D., Yi, W., Ge, H., Zhang, Z., and Wu, B. (2019). Bioactive Streptoglutarimides A-J from the marine-derived Streptomyces sp. ZZ741. *J. Nat. Prod.* 82, 2800–2808. doi: 10.1021/acs.jnatprod.9b00481

Zheng, L., Chen, H., Han, X., Lin, W., and Yan, X. (2005). Antimicrobial screening and active compound isolation from marine bacterium NJ6-3-1 associated with the sponge *Hymeniacidon perleve*. *World J. Microbiol. Biotechnol.* 21, 201–206. doi: 10.1007/s11274-004-3318-6

frontiers | Frontiers in Marine Science

TYPE Mini Review
PUBLISHED 13 February 2025
DOI 10.3389/fmars.2025.1558320

OPEN ACCESS

EDITED BY
Guillermin Agüero-Chapin,
University of Porto, Portugal

REVIEWED BY
Carlos Jimenez,
University of A Coruña, Spain

*CORRESPONDENCE
Syed Shams ul Hassan
Shams1327@yahoo.com
Shikai Yan
Shkyan@126.com
Huizi Jin
Kimhz@sjtu.edu.cn

RECEIVED 10 January 2025
ACCEPTED 29 January 2025
PUBLISHED 13 February 2025

CITATION
Pan C, Hassan SSu, Ishaq M, Yan S and Jin H (2025) Marine actinomycetes: a hidden treasure trove for antibacterial discovery. *Front. Mar. Sci.* 12:1558320. doi: 10.3389/fmars.2025.1558320

Marine actinomycetes: a hidden treasure trove for antibacterial discovery

Chengqian Pan[1], Syed Shams ul Hassan[2*], Muhammad Ishaq[3], Shikai Yan[2*] and Huizi Jin[2*]

[1]School of Pharmacy, Jiangsu University, Zhenjiang, China, [2]Shanghai Key Laboratory for Molecular Engineering of Chiral Drugs, School of Pharmacy, Shanghai Jiao Tong University, Shanghai, China, [3]Guangdong Key Laboratory for Research and Development of Natural Drugs, School of Pharmacy, Guangdong Medical University, Dongguan, China

Oceans boast a substantial microbial diversity, which is widely prevalent in seawater, marine sediments, and marine organisms. In contrast to terrestrial resources explored in traditional natural product research, the habitats of marine microorganisms are distinctly unique. Actinomycetes serve as a vital source of secondary metabolites, including antibiotics and other potent natural products like streptomycin and tetracycline. They have played a pivotal role in clinical treatments for significant diseases such as pathogenic bacterial infections. Nevertheless, the extensive use of antibiotics has led to a sharp increase in the variety and number of drug-resistant bacteria, notably multidrug-resistant (MDR) and extensively drug-resistant (XDR) bacteria, in clinical settings, posing a grave threat to human survival. Consequently, there is an immediate need to discover structurally novel antibacterial natural products and develop new antibiotics. This mini review summarizes a total of 45 novel antibacterial natural products derived from marine actinomycetes, published in 2024. These products, including polyketides, alkaloids, macrolactams, and peptides, are highlighted in terms of their structures and biological activities. The objective of this article is to provide valuable insights for the research and development of novel antibiotics.

KEYWORDS

marine actinomycetes, antibacterial activity, polyketides, alkaloids, macrolactams

1 Introduction

In recent years, the emergence of multidrug-resistant (MDR) and extensively drug-resistant (XDR) bacteria has become a significant threat to global public health due to the overuse of antibiotics (Chin et al., 2018; Hu et al., 2019; Lin et al., 2019; Cui et al., 2020; Wang X. et al., 2020; Ding Q. et al., 2021; Wei et al., 2021; Zhu et al., 2021; Rasheed et al., 2024). The Lancet journal published a comprehensive analysis of the global impact of antimicrobial resistance (Murray et al., 2022). Analysis of data from 204 countries and regions revealed that antimicrobial resistance has become a major cause of death worldwide. In 2019, infections caused by antimicrobial resistance directly resulted in

1.27 million deaths and indirectly led to 4.95 million deaths, surpassing those from AIDS or malaria (Murray et al., 2022).

On the other hand, since the late 1990s, with the continuous exploitation of natural resources, discovering new bioactive natural products has become increasingly challenging (Demain, 2009; Spížek et al., 2010). Traditional strategies for the isolation and identification of natural products have led to the repeated isolation of numerous known compounds, making it increasingly difficult to discover new bioactive natural products. Over the past two decades, the number of antibiotics discovered by pharmaceutical companies has been declining (Zhang et al., 2022; Brüssow, 2024). There is an urgent need for humans to search for new natural products with novel structures, unique bioactivities, and mechanisms of action as lead compounds for new drug development (Cui et al., 2019; Ding et al., 2019; Li et al., 2019; Afrin et al., 2020; Zhang J. et al., 2020; Chen et al., 2024; Muhammad et al., 2024).

Compared to terrestrial biological resources, marine organisms inhabit vastly different environments (Liu et al., 2019; Zhong et al., 2020; Otero et al., 2023). The drastic differences in survival conditions (such as high pressure, high salinity, oligotrophic environments, lack of light, lack of oxygen, etc.) determine that marine organisms exhibit significant characteristics in metabolism, survival strategies, information transmission, and adaptation mechanisms (Surendhiran et al., 2021; Hamadou et al., 2023; Iqbal et al., 2024). Actinomycetes in marine organisms, as an important component, have always been one of the hotspots in natural product research (Jagannathan et al., 2021; Ryu et al., 2023). Eravacycline (Xerava®), a novel fluorocycline antibacterial agent, is a semisynthetic derivative of tetracycline from *Streptomyces*, which functions by inhibiting bacterial protein synthesis (Huang P. Y. et al., 2024). In 2018, it was approved by the U.S.A. FDA and exhibits potent *in vitro* activity against Gram-positive and -negative strains expressing certain common tetracycline-specific acquired resistance mechanisms. *In vitro*, eravacycline demonstrates potent activity against a broad spectrum of clinically relevant Gram-positive and -negative aerobic and anaerobic bacteria.

The actinomycetes genome typically contains a rich repertoire of biosynthetic gene clusters for secondary metabolites (Scherlach and Hertweck, 2021; Wen et al., 2024). The number of compounds we have discovered so far is far less than the number of compounds that microorganisms can produce, and a large number of potential secondary metabolites remain undiscovered (Zhang X. et al., 2020; Tianqiao et al., 2021; Zhang et al., 2021). Searching for potential novel secondary metabolites and exploring lead molecules with significant pharmacological activities, marine actinomycete secondary metabolites, as important sources of new drug precursors, are gradually demonstrating significant research value and application potential (Donald et al., 2022; Gomez-Banderas, 2022; Ngamcharungchit et al., 2023; Zhang et al., 2024).

Based on data from PubMed, Elsevier, the American Chemical Society, and Google Scholar, this review comprehensively summarizes the sources, structures, and bioactivity progress of 45 novel antibacterial active natural products isolated from marine actinomycetes in 2024. According to their structural characteristics, these natural products are classified into four major categories, including polyketides (57.8%, 26/45), alkaloids (26.7%, 12/45), macrolactams (8.9%, 4/45), and peptides (6.7%, 3/45) (Figure 1A). These secondary metabolites are primarily isolated from actinomycetes across 6 different sources, including China (60%, 9/15), Korea (13.3%, 2/15), Thailand (6.7%, 1/15), United States (6.7%, 1/15), Japan (6.7%, 1/15) and Indian Ocean (6.7%, 1/15) (Figure 1B). Among these biological samples, 12 belong to the genus *Streptomyces*, accounting for 80%, highlighting the significance of *Streptomyces* in the discovery of novel antibacterial natural products (Figure 1C). Of particular note are the remarkable findings by Professor Jongheon Shin and Kibong Oh, researchers at Seoul National University, who discovered corynetoxin U17a (32). This compound demonstrated potent antibacterial activity against *Staphylococcus aureus*, with a minimum inhibitory concentration (MIC) of 0.06 μg/mL (Lee et al., 2024). Table 1 outlines the names, sources of isolation, species, and MIC values of the antibacterial compounds identified.

2 Polyketides

Among the secondary metabolites produced by microorganisms, polyketide compounds typically constitute the majority in statistical analysis due to their large quantity and diverse types of activities (Yang et al., 2020; Li et al., 2021; Yixuan et al., 2021). They primarily originate from the condensation of short-chain fatty acids by microorganisms. Additionally, the biosynthesis of polyketides can also involve modifications of the carbon chain produced at each step through processes such as oxidation and hydroxylation, leading to the generation of numerous distinct structures and a wide range of activities.

Four unique compounds (1-4), characterized by the presence of an $_{L}$-rhodinose and spiroketal moiety, and featuring unusual continuous hydroxy groups within their macrolide structure, were isolated from a marine-derived *Micromonospora* sp. FIMYZ51 (Figure 1D) (Zhao W. et al., 2024). These compounds demonstrated strong antifungal properties against *A. niger*, with MIC values ranging from 0.5 to 2 μg/mL. Additionally, they exhibited varying levels of inhibitory activity against the pathogenic bacterium *M. luteus*, with MIC values from 0.0625 μg/mL to 1 μg/mL (Table 1). Separately, two heronamides (5 and 6) were isolated from a deep-sea *Streptomyces* sp. OUCT16-38 (Zhao Y. et al., 2024). When tested for antibacterial activity, both 5 and 6 showed significant growth inhibition against multidrug-resistant pathogens *E. faecium* and *E. faecalis*, with MIC values of 3.1 μg/mL (Table 1).

Metabolomic fingerprinting analysis, utilizing mass spectrometry (MS) and nuclear magnetic resonance (NMR), of the marine-derived actinomycete *Streptomyces* sp. FXY-T5 resulted in the identification of five novel oligomycins: 24-lumooligomycin B (7), 4-lumooligomycin B (8), 6-lumooligomycin B (9), 40-homooligomycin B (10), and 15-hydroxy-oligomycin B (11) (Figure 1D) (Feng et al., 2024). Notably, 40-homooligomycin B (10) exhibited antifungal activity that was either stronger or comparable to that of positive controls, suggesting its potential as a biocontrol agent against plant pathogens such as *C. musae* and *C. coccodes* (Table 1). In a separate study, Xiaofei Huang and

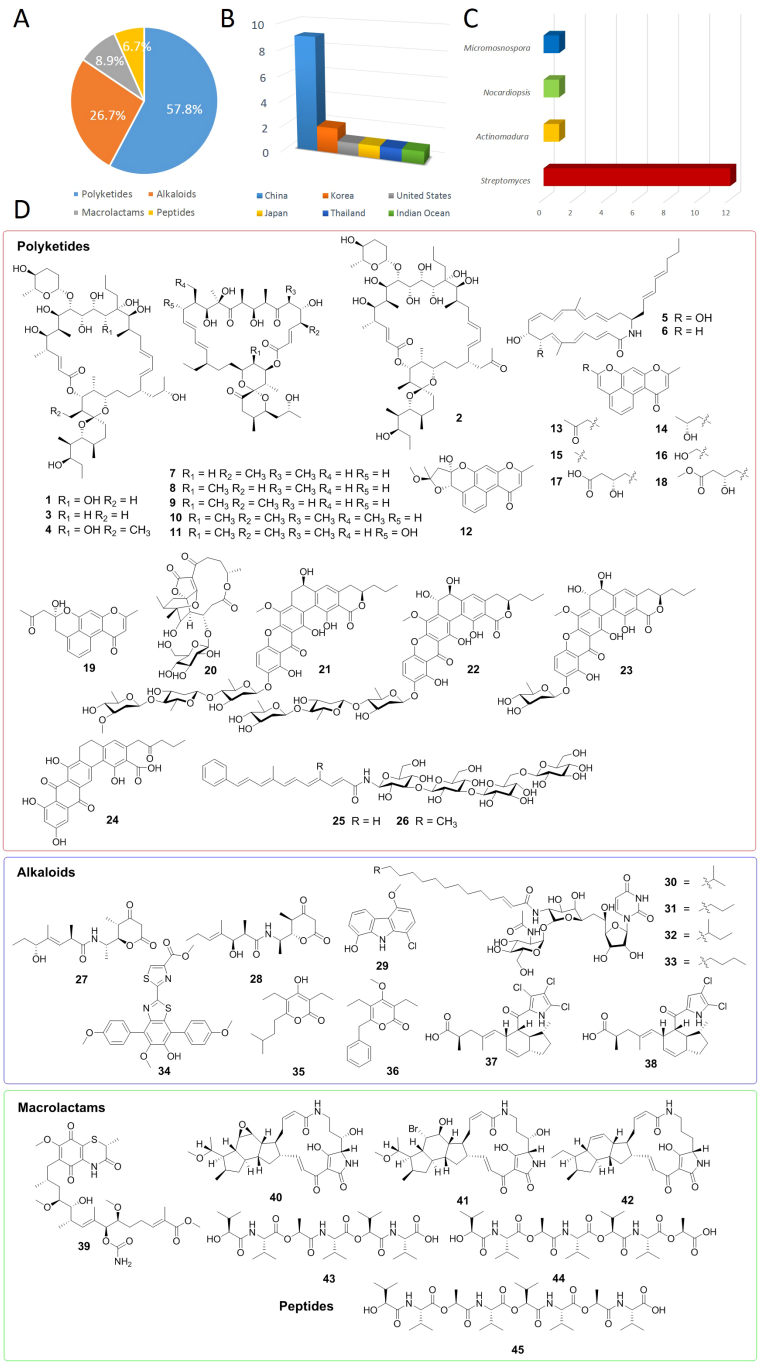

FIGURE 1
(A) Antibacterial compounds derived from marine actinomycetes according to structure types. **(B)** The different sources of marine actinomycetes. **(C)** The different genus of marine actinomycetes. **(D)** Chemical structures of compounds 1-45.

colleagues reported the discovery of eight new aromatic polyketides, naphpyrones A-H (12-19), from the heterologous expression strain *Streptomyces coelicolor* (Huang X. et al., 2024). Evaluation of their bioactivity showed that compounds 12 and 13 possessed antibacterial activity against *S. aureus*, with MIC values of 1 μg/mL and 4 μg/mL, respectively.

Glycoabyssomicin A (20), a novel abyssomicin variant incorporating a sugar moiety, was isolated from the deep-sea *Streptomyces koyangensis* SCSIO5802 through LC-MS-guided analysis (Zhu et al., 2024). When tested against a panel of Gram-positive and Gram-negative bacteria (including *M. luteus*, *S. aureus*, MRSA, and *E. coli*), it exhibited no antibacterial activity at a concentration of 10 μg per filter paper disc. During a screening of actinomycetes from mangrove rhizosphere sediment samples, a strain of *Streptomyces* sp. SCSIO 40068 demonstrated robust antibacterial activity. Further purification of its extract led to the

TABLE 1 Antibacterial compounds from marine actinomycetes.

Compounds	Source	Species	Activities (MIC, μg/mL)	Ref
Polyketides				
IB96212 (**1**)	China	*Micromonospora* sp. FIMYZ51	*M.luteus* 1; *A.niger* 1; *C.albicans* 4	(Zhao W. et al., 2024)
43-Oxy-IB96212 (**2**)			*M.luteus* 1; *A.niger* 0.5; *C.albicans* 2	
11-Dehydroxy-IB96212 (**3**)			*M.luteus* 0.0625; *A.niger* 1; *C.albicans* 4	
46-Methy-IB96212 (**4**)			*M.luteus* 0.5; *A.niger* 1-2; *C.albicans* 4	
Heronamide C (**5**)	Indian Ocean	*Streptomyces* sp. OUCT16-38	*S. aureus* 12.5; *E. faecium* 3.1; *E. faecalis* 3.1	(Zhao Y. et al., 2024)
8-Deoxyheronamide C (**6**)			*S. aureus* >50; *E. faecium* 3.1; *E. faecalis* 3.1	
24-Lumooligomycin B (**7**)	China	*Streptomyces* sp. FXY-T5	*C. musae* 0.42 mm[a]; *C. coccodes* 0.57 mm[a]	(Feng et al., 2024)
4-Lumooligomycin B (**8**)			*C. coccodes* 0.60 mm[a]	
6-Lumooligomycin B (**9**)			Inactive	
40-Homooligomycin B (**10**)			*C. musae* 0.94 mm[a]; *C. coccodes* 0.73 mm[a]	
15-Hydroxy-oligomycin B (**11**)			Inactive	
Naphpyrone A (**12**)	China	*Streptomyces coelicolor*	MRCNS[b] 64; MRSA[c] 64; *S. aureus* 1	(Huang X. et al., 2024)
Naphpyrone B (**13**)			MRCNS[b] 32; *S. aureus* 4	
Naphpyrone C (**14**)			MRCNS[b] 16; MRSA[c] 32	
Naphpyrone D (**15**)			Inactive	
Naphpyrone E (**16**)			Inactive	
Naphpyrone F (**17**)			Inactive	
Naphpyrone G (**18**)			Inactive	
Naphpyrone H (**19**)			Inactive	
Glycoabyssomicin A (**20**)	China	*Streptomyces koyangensis* SCSIO 5802	Inactive	(Zhu et al., 2024)
Kebanmycin A (**21**)	China	*Streptomyces* sp. SCSIO 40068	*S. aureus* 0.125; MRSA[c] 0.125	(Zhao M. et al., 2024)
Kebanmycin B (**22**)			*S. aureus* 2; *B. subtilis* 1	
Kebanmycin C (**23**)			*S. aureus* 0.5; *B. subtilis* 4	
Kebanmycin D (**24**)			*S. aureus* 32	
Maduraflavacin A (**25**)	China	*Actinomadura glauciflava*	*S. aureus*; 4 mm[a], 0.5 mg/mL	(Zou et al., 2024)
Maduraflavacin B (**26**)		NA03286	*M. luteus*; 3 mm[a], 0.5 mg/mL	
Alkaloids				
Alpiniamide H (**27**)	China	*Streptomyces* sp. ZS-A65	Inactive	(Pu et al., 2024)
Alpiniamide I (**28**)			*P. aeruginosa* 87.5 μM	
1-Chloro-4-methoxy-9H-carbazol-8-ol (**29**)	Thailand	*Streptomyces* sp. OUCMDZ-5511	*C. violaceum* 100	(Liu et al., 2024)
Tunicamycin VII (**30**)	Korea	*Streptomyces* sp. MBTG32	*S. aureus* 0.13; *E. faecalis* 2; *E. faecium* 2	(Lee et al., 2024)
Tunicamycin VIII (**31**)			*S. aureus* 0.13; *E. faecalis* 2; *E. faecium* 2	
Corynetoxin U17a (**32**)			*S. aureus* 0.06; *E. faecalis* 1; *E. faecium* 2	
Tunicamycin IX (**33**)			*S. aureus* 0.25; *E. faecalis* 4; *E. faecium* 8	
Nocarterphenyl I (**34**)	China	*Nocardiopsis* sp. HDN154086	*B. subtilis* 0.8; *E. coli* 0.8 μM	(Zhou et al., 2024)

(Continued)

TABLE 1 Continued

Compounds	Source	Species	Activities (MIC, μg/mL)	Ref
Alkaloids				
Nocardiopyrone D (**35**)			Inactive	
Nocardiopyrone E (**36**)			MRSA[c] 12.5; *B. subtilis* 50 μM	
Indanopyrrole A (**37**)	United States	*Streptomyces* sp. CNY-716	MRSA[c] 2; VRE[d] 2; *E. coli* 4	(Sweeney et al., 2024)
Indanopyrrole B (**38**)			Inactive	
Macrolactams				
Seco-geldanamycin B (**39**)	China	*Streptomyces* sp. ZYX-F-97	*S. aureus* 64; *B. subtilis* 64	(Yi et al., 2024)
Hydroxycapsimycin (**40**)	Japan	*Streptomyces* sp. KKMA-0239	*M. intracellulare* 50	(Shigeno et al., 2024)
Brokamycin (**41**)			*M. avium* 50; *M. intracellulare* 12.5	
Ikarugamycin (**42**)			*M. avium* 25; *M. intracellulare* 25; *B. subtilis* 3.13	
Peptides				
Homiamide A (**43**)	Korea	*Streptomyces* sp. ROA-065	*B. subtilis* 32; *S. aureus* 32; *E. coli* 64	(Ding et al., 2023)
Homiamide B (**44**)			*B. subtilis* 64; *S. aureus* 32; *E. coli* 32	
Homiamide C (**45**)			*B. subtilis* 32; *S. aureus* 64; *E. coli* 64	

[a]Zones of inhibition (mm).
[b]MRCNS, methicillin-resistant coagulase negative *Staphylococci.*
[c]MRSA, methicillin-resistant *Staphylococcus aureus.*
[d]VRE, vancomycin-resistant *Enterococcus faecium.*

identification of four new compounds, kebanmycins A-D (21-24) (Figure 1D) (Zhao M. et al., 2024). Among them, kebanmycin A (21) stood out for its potent antibacterial activity against *S. aureus* and MRSA, with an MIC value of 0.125 μg/mL, which is generally lower than that of the positive control vancomycin (MIC 1 μg/mL). Kebanmycin A's (21) notable anti-MRSA efficacy makes it a promising candidate for further drug development targeting MRSA. Additionally, two new phenyl polyene metabolites, maduraflavacins A and B (25, 26), were isolated from a rare marine-derived actinomycete strain, *Actinomadura glauciflava* NA03286 (Figure 1D) (Zou et al., 2024). These compounds displayed weak antibacterial activity against the Gram-positive bacteria *S. aureus* and *M. luteus*, respectively (Table 1).

3 Alkaloids

Alkaloids are a class of nitrogen-containing alkaline organic compounds with complex and diverse chemical structures, occupying an important position among secondary metabolites (Liu et al., 2020; Sun et al., 2020; Zhang C. et al., 2020; Wang et al., 2022; Xia et al., 2022). Alkaloids exhibit abundant physiological activities and pharmacological effects, such as antibacterial, anti-inflammatory, and antitumor activities, making them a crucial resource for drug development and possessing potential value for the research and development of new drugs (Liu et al., 2021; Bhatti et al., 2022; Waseem et al., 2022; Mei et al., 2023; Yu et al., 2023).

During an investigation of *Streptomyces* sp. ZS-A65, which was isolated from marine sediments, two novel alpiniamide-type alkaloids were discovered: alpiniamides H and I (27, 28) (Figure 1D) (Pu et al., 2024). When tested for antibacterial activity against *P. aeruginosa*, compound 28 demonstrated robust antibiofilm activity, with an MIC of 87.5 μM (Table 1). Additionally, a new 9H-carbazole derivative, compound 29, was isolated from a solid fermented medium of the mangrove-derived *Streptomyces* strain OUCMDZ-5511, collected in Thailand, which was grown under fluoride stress conditions (Figure 1D) (Liu et al., 2024). Compound 29 exhibited antiquorum sensing activity against *C. violaceum* by reducing violacein production and inhibiting biofilm formation in a concentration-dependent manner, suggesting its potential as a novel quorum sensing inhibitor (Table 1). Furthermore, four tunicamycin class compounds, tunicamycin VII (30), tunicamycin VIII (31), corynetoxin U17a (32), and tunicamycin IX (33), were isolated from the culture broth of the marine-derived *Streptomyces* sp. MBTG32 (Figure 1D) (Lee et al., 2024). These compounds displayed potent antibacterial activity against Gram-positive bacteria, particularly *S. aureus*, with MIC values ranging from 0.06 to 0.25 μg/mL (Table 1). The research also supported the notion that tunicamycins exert their antibacterial effects by inhibiting the MraY enzyme activity in *S. aureus*.

Utilizing the OSMAC strategy, researchers isolated and characterized one novel *p*-terphenyl and two new α-pyrone derivatives, specifically nocarterphenyl I (34) and nocardiopyrone D-E (35, 36), from the marine sediment-derived actinomycete *Nocardiopsis* sp. HDN154086 (Figure 1D) (Zhou et al., 2024). Notably, compound 34 features a rare 2,2'-bithiazole structure among natural products and exhibited promising antibacterial activity against *B. subtilis* and *E. coli*, with MIC values of 0.8 μM. 36 displayed notable antibacterial activity against MRSA when compared to the positive control ciprofloxacin (Table 1). In another study, Douglas Sweeney and colleagues employed

pattern-based genome mining to explore the biosynthetic potential of the marine-derived actinomycete *Streptomyces* sp. CNY-716. This led to the discovery of the first halogenated pyrroloketoindane natural products, indanopyrrole A (37) and B (38) (Figure 1D) (Sweeney et al., 2024). Indanopyrrole A (37) demonstrated potent broad-spectrum antibiotic activity against clinically relevant pathogens, including *E. coli* (MIC = 4 μg/mL), MRSA (MIC = 2 μg/mL), and VRE (MIC = 2 μg/mL) (Table 1).

4 Macrolactams

Macrolactams are a class of large molecular cyclic compounds produced by microorganisms through secondary metabolic pathways, containing amide bonds and multiple ring structures (Hong et al., 2018; Wang P. et al., 2020; Ding L. et al., 2021). Macrolactams generally exhibit pharmacological activities such as antibacterial and antitumor effects, making them an important resource for drug development.

The ansamycin derivative, seco-geldanamycin B (39), was obtained through solid fermentation of the marine-derived actinomycete *Streptomyces* sp. ZYX-F-97 (Figure 1D) (Yi et al., 2024). This compound displayed moderate inhibitory effects against *S. aureus* and *B. subtilis*, with MIC values of 64 μg/mL (Table 1). Additionally, two novel polycyclic tetramate macrolactams (PTMs), hydroxycapsimycin (40) and brokamycin (41), were isolated alongside the known PTM ikarugamycin (42) from the culture broth of marine-derived *Streptomyces* sp. KKMA-0239 (Figure 1D) (Shigeno et al., 2024). Compound 40 showed weak activity against *M. intracellulare*, with an MIC of 50μg/mL. Compound 41 exhibited moderate activity against both *M. intracellulare* and drug-resistant *M. avium*, with MICs of 12.5 and 50 μg/ml, respectively. In comparison, ikarugamycin (42) demonstrated more potent antimicrobial activity than both 40 and 41 (Table 1).

5 Peptides

Peptides are primarily synthesized by microorganisms through non-ribosomal peptide synthetase (NRPS) pathways, and these compounds typically possess complex structures and diverse biological activities (Xu et al., 2023). Peptides occupy an important position among microbial secondary metabolites, not only in terms of their large quantity but also their rich variety. They often exhibit pharmacological activities such as antibacterial, antitumor, and immunoregulatory effects, holding tremendous potential value and application prospects for new drug development (Xu et al., 2020; Liang et al., 2018; Zhang et al., 2019; Wen et al., 2020; Wong et al., 2020; Chai et al., 2021).

From a marine sediment-derived strain of *Streptomyces* sp. ROA-065 (Figure 1D), researchers isolated three novel depsipeptides named homiamides A-C (43-45) (Ding et al., 2023). These compounds displayed weak antibacterial activities against both Gram-positive (*B. subtilis*, *S. aureus*) and Gram-negative (*E. coli*) bacteria, with MIC values ranging from 32 to 64 μg/mL (Table 1).

6 Conclusion

The escalating problem of global drug resistance has spurred intensive searches for novel antibacterial agents. Marine natural products have proven pivotal in drug discovery, forming the foundation for the early stages of generic drug development (Cao et al., 2016; Hussain et al., 2021; Shams Ul Hassan et al., 2021; Hassan et al., 2022; Carroll et al., 2024; Hassan et al., 2024). This review delves into 45 compounds reported in 2024 to possess antibacterial activity, sourced from marine actinomycetes. These compounds encompass polyketides, alkaloids, macrolactams, and peptides (Figure 1D; Table 1). The review outlines the origins, chemical structures, and biological activities of these compounds. In essence, the persistent emergence of drug-resistant bacteria poses a grave risk to human health. Marine microbial secondary metabolites present a promising avenue for discovering natural antibacterial agents characterized by unique structures, robust activities, and specific modes of action. Thus, the pursuit of novel antibacterial drugs from marine actinomycetes warrants particular focus.

Author contributions

CP: Data curation, Methodology, Writing – review & editing. SH: Conceptualization, Software, Writing – review & editing. MI: Formal analysis, Resources, Writing – review & editing. SY: Validation, Writing – review & editing, Project administration. HJ: Investigation, Writing – review & editing, Project administration, Validation, Supervision.

Funding

The author(s) declare financial support was received for the research, authorship, and/or publication of this article. This work was supported by NSFC (No. 82404465), the Senior Talent Foundation of Jiangsu University (5501290012), the Chugai Foundation for Innovative Drug Discovery Science: C-FINDs (2025-CF-01). The work was supported by NSFC (81973191), project supported by the Modern Plateau Plant Medicine Research Project of Shanghai Jiao Tong University (SA1700208).

Conflict of interest

The authors declare that the research was conducted in the absence of any commercial or financial relationships that could be construed as a potential conflict of interest.

Generative AI statement

The author(s) declare that no Generative AI was used in the creation of this manuscript.

Publisher's note

References

Afrin, S., Haneefa, S. M., Fernandez-Cabezudo, M. J., Giampieri, F., Al-Ramadi, B. K., and Battino, M. (2020). Therapeutic and preventive properties of honey and its bioactive compounds in cancer: An evidence-based review. *Nutr. Res. Rev.* 33, 50–76. doi: 10.1017/S0954422419000192

Bhatti, S. A., Hussain, M. H., Mohsin, M. Z., Mohsin, A., Zaman, W. Q., Guo, M., et al. (2022). Evaluation of the antimicrobial effects of Capsicum, *Nigella sativa*, *Musa paradisiaca L.*, and *Citrus limetta*: A review. *Front. Sustain. Food Syst.* 6, 1043823. doi: 10.3389/fsufs.2022.1043823

Brüssow, H. (2024). The antibiotic resistance crisis and the development of new antibiotics. *Microbial Biotechnol.* 17, e14510. doi: 10.1111/1751-7915.14510

Cao, J., Wang, J., Wang, S., and Xu, X. (2016). Porphyra species: a mini-review of its pharmacological and nutritional properties. *J. medicinal Food* 19, 111–119. doi: 10.1089/jmf.2015.3426

Carroll, A. R., Copp, B. R., Grkovic, T., Keyzers, R. A., and Prinsep, M. R. (2024). Marine natural products. *Natural Product Rep.* 41, 162–207. doi: 10.1039/D3NP00061C

Chai, T. T., Xiao, J., Dass, S. M., Teoh, J. Y., Ee, K. Y., Ng, W. J., et al. (2021). Identification of antioxidant peptides derived from tropical jackfruit seed and investigation of the stability profiles. *Food Chem.* 340, 127876. doi: 10.1016/j.foodchem.2020.127876

Chen, M., Xiao, J., El-Seedi, H. R., Woźniak, K. S., Daglia, M., Little, P. J., et al. (2024). Kaempferol and atherosclerosis: From mechanism to medicine. *Crit. Rev. Food Sci. Nutr.* 64, 2157–2175. doi: 10.1080/10408398.2022.2121261

Chin, P. S., Ang, G. Y., Yu, C. Y., Tan, E. L., Tee, K. K., Yin, W. F., et al. (2018). Prevalence, antimicrobial resistance, and genetic diversity of Listeria spp. isolated from raw chicken meat and chicken-related products in Malaysia. *J. Food Prot.* 81, 284–289. doi: 10.4315/0362-028X.JFP-17-186

Cui, H., Zhang, C., Li, C., and Lin, L. (2019). Preparation and antibacterial activity of *Litsea cubeba* essential oil/dandelion polysaccharide nanofiber. *Ind. Crops Products* 140, 111739. doi: 10.1016/j.indcrop.2019.111739

Cui, H., Zhang, C., Li, C., and Lin, L. (2020). Inhibition mechanism of cardamom essential oil on methicillin-resistant *Staphylococcus aureus* biofilm. *Lwt* 122, 109057. doi: 10.1016/j.lwt.2020.109057

Demain, A. L. (2009). Antibiotics: natural products essential to human health. *Medicinal Res. Rev.* 29, 821–842. doi: 10.1002/med.20154

Ding, Q., Jiang, H., Chen, Y., Luo, L., He, R., Ma, H., et al. (2019). Influence of nitrogen protection on the extraction yield and antioxidant activities of polyphenols by ultrasonic-assisted extraction from rapeseed meal. *J. Food Process Eng.* 42, e13104. doi: 10.1111/jfpe.13104

Ding, Q., Sheikh, A. R., Chen, Q., Hu, Y., Sun, N., Su, X., et al. (2023). Understanding the mechanism for the structure-activity relationship of food-derived ACEI peptides. *Food Rev. Int.* 39, 1751–1769. doi: 10.1080/87559129.2021.1936005

Ding, Q., Sheikh, A. R., Gu, X., Li, J., Xia, K., Sun, N., et al. (2021). Chinese propolis: ultrasound-assisted enhanced ethanolic extraction, volatile components analysis, antioxidant and antibacterial activity comparison. *Food Sci. Nutr.* 9, 313–330. doi: 10.1002/fsn3.1997

Ding, L., Zhang, S. D., Haidar, A. K., Bajimaya, M., Guo, Y., Larsen, T. O., et al. (2021). Polycyclic tetramate macrolactams—a group of natural bioactive metallophores. *Front. Chem.* 9, 772858. doi: 10.3389/fchem.2021.772858

Donald, L., Pipite, A., Subramani, R., Owen, J., Keyzers, R. A., and Taufa, T. (2022). *Streptomyces*: Still the biggest producer of new natural secondary metabolites, a current perspective. *Microbiol. Res.* 13, 418–465. doi: 10.3390/microbiolres13030031

Feng, X. Y., Li, J. H., Li, R. J., Yuan, S. Z., Sun, Y. J., Peng, X. P., et al. (2024). Structures, biosynthesis, and bioactivity of oligomycins from the marine-derived Streptomyces sp. FXY-T5. *J. Agric. Food Chem.* 72, 1082–1095. doi: 10.1021/acs.jafc.3c06307

Gomez-Banderas, J. (2022). Marine natural products: A promising source of environmentally friendly antifouling agents for the maritime industries. *Front. Mar. Sci.* 9, 858757. doi: 10.3389/fmars.2022.858757

Hamadou, A. H., Zhang, J., Chen, C., Xu, J., and Xu, B. (2023). Vitamin C and β-carotene co-loaded in marine and egg nanoliposomes. *J. Food Eng.* 340, 111315. doi: 10.1016/j.jfoodeng.2022.111315

Hassan, S. S. U., Abdel-Daim, M. M., Behl, T., and Bungau, S. (2022). Natural products for chronic diseases: a ray of hope. *Molecules* 27, 5573. doi: 10.3390/molecules27175573

Hassan, S. S. U., Wu, J., Li, T., Ye, X., Rehman, A., Yan, S., et al. (2024). Unlocking marine microbial treasures: new PBP2a-targeted antibiotics elicited by metals and enhanced by RSM-driven transcriptomics and chemoinformatics. *Microbial Cell factories* 23, 303. doi: 10.1186/s12934-024-02573-0

Hong, Y. Q., Guo, X., Chen, G. H., Zhou, J. W., Zou, X. M., Liao, X., et al. (2018). Determination of five macrolide antibiotic residues in milk by micellar electrokinetic capillary chromatography with field amplified sample stacking. *J. Food Saf.* 38, e12382. doi: 10.1111/jfs.2018.38.issue-1

Hu, W., Li, C., Dai, J., Cui, H., and Lin, L. (2019). Antibacterial activity and mechanism of *Litsea cubeba* essential oil against methicillin-resistant *Staphylococcus aureus* (MRSA). *Ind. Crops Products* 130, 34–41. doi: 10.1016/j.indcrop.2018.12.078

Huang, P. Y., Hsu, C. K., Tang, H. J., and Lai, C. C. (2024). Eravacycline: a comprehensive review of *in vitro* activity, clinical efficacy, and real-world applications. *Expert Rev. Anti-infective Ther.* 22, 387–398. doi: 10.1080/14787210.2024.2351552

Huang, X., Xu, X., Zhou, L., Ma, C., Wang, W., Li, C., et al. (2024). Naphpyrones A–H, antibacterial aromatic polyketides isolated from the *Streptomyces coelicolor* A3 (2)/spi1 Δ spi H3. *J. Agric. Food Chem.* 73, 541–548. doi: 10.1021/acs.jafc.4c09101

Hussain, H., Mamadalieva, N. Z., Ali, I., Green, I. R., Wang, D., Zou, L., et al. (2021). Fungal glycosides: structure and biological function. *Trends Food Sci. Technol.* 110, 611–651. doi: 10.1016/j.tifs.2021.02.029

Iqbal, M. W., Riaz, T., Mahmood, S., Bilal, M., Manzoor, M. F., Qamar, S. A., et al. (2024). Fucoidan-based nanomaterial and its multifunctional role for pharmaceutical and biomedical applications. *Crit. Rev. Food Sci. Nutr.* 64, 354–380. doi: 10.1080/10408398.2022.2106182

Jagannathan, S. V., Manemann, E. M., Rowe, S. E., Callender, M. C., and Soto, W. (2021). Marine actinomycetes, new sources of biotechnological products. *Mar. Drugs* 19, 365. doi: 10.3390/md19070365

Lee, J., Hwang, J. Y., Oh, D., Oh, D. C., Park, H. G., Shin, J., et al. (2024). Tunicamycins from marine-derived *Streptomyces bacillaris* inhibit MurNAc-pentapeptide translocase in *Staphylococcus aureus*. *Mar. Drugs* 22, 293. doi: 10.3390/md22070293

Li, B. Y., Xu, X. Y., Gan, R. Y., Sun, Q. C., Meng, J. M., Shang, A., et al. (2019). Targeting gut microbiota for the prevention and management of diabetes mellitus by dietary natural products. *Foods* 8, 440. doi: 10.3390/foods8100440

Li, S., Yang, B., Tan, G. Y., Ouyang, L. M., Qiu, S., Wang, W., et al. (2021). Polyketide pesticides from actinomycetes. *Curr. Opin. Biotechnol.* 69, 299–307. doi: 10.1016/j.copbio.2021.05.006

Liang, Q., Chalamaiah, M., Ren, X., Ma, H., and Wu, J. (2018). Identification of new anti-inflammatory peptides from zein hydrolysate after simulated gastrointestinal digestion and transport in Caco-2 cells. *J. Agric. Food Chem.* 66, 1114–1120. doi: 10.1021/acs.jafc.7b04562

Lin, L., Agyemang, K., Abdel-Samie, M. A. S., and Cui, H. (2019). Antibacterial mechanism of *Tetrapleura tetraptera* extract against *Escherichia coli* and *Staphylococcus aureus* and its application in pork. *J. Food Saf.* 39, e12693. doi: 10.1111/jfs.12693

Liu, Y., Liu, J., Yan, P., Kachanuban, K., Liu, P., Jia, A., et al. (2024). Carbazole and quinazolinone derivatives from a fluoride-tolerant *Streptomyces* strain OUCMDZ-5511. *J. Agric. Food Chem.* 72, 6424–6431. doi: 10.1021/acs.jafc.4c00780

Liu, J., Wan, J., Du, W., Wang, D., Wen, C., Wei, Y., et al. (2021). *In vivo* functional verification of four related genes involved in the 1-deoxynojirimycin biosynthetic pathway in mulberry leaves. *J. Agric. Food Chem.* 69, 10989–10998. doi: 10.1021/acs.jafc.1c03932

Liu, J., Wan, J., Wang, D., Wen, C., Wei, Y., and Ouyang, Z. (2020). Comparative transcriptome analysis of key reductase genes involved in the 1-deoxynojirimycin biosynthetic pathway in mulberry leaves and cloning, prokaryotic expression, and functional analysis of MaSDR 1 and MaSDR 2. *J. Agric. Food Chem.* 68, 12345–12357. doi: 10.1021/acs.jafc.0c04832

Liu, Y., Zhang, D., Liu, G. M., Chen, Q., and Lu, Z. (2019). Ameliorative effect of dieckol-enriched extraction from *Laminaria japonica* on hepatic steatosis induced by a high-fat diet via *β*-oxidation pathway in ICR mice. *J. Funct. Foods* 58, 44–55. doi: 10.1016/j.jff.2019.04.051

Mei, S., Ding, J., and Chen, X. (2023). Identification of differential volatile and non-volatile compounds in coffee leaves prepared from different tea processing steps using HS-SPME/GC–MS and HPLC-Orbitrap-MS/MS and investigation of the binding mechanism of key phytochemicals with olfactory and taste receptors using molecular docking. *Food Res. Int.* 168, 112760. doi: 10.1016/j.foodres.2023.112760

Muhammad, N., Uddin, N., Liu, Z., Yang, M., and Liu, M. (2024). Research progress and biosynthetic mechanisms of nutritional compounds obtained from various organs during the developmental stages of a medicinal plant (*Chinese Jujube*). *Plant Foods Hum. Nutr.* 79, 744–758. doi: 10.1007/s11130-024-01225-3

Murray, C. J., Ikuta, K. S., Sharara, F., Swetschinski, L., Aguilar, G. R., Gray, A., et al. (2022). Global burden of bacterial antimicrobial resistance in 2019: a systematic analysis. *Lancet* 399, 629–655. doi: 10.1016/S0140-6736(21)02724-0

Ngamcharungchit, C., Chaimusik, N., Panbangred, W., Euanorasetr, J., and Intra, B. (2023). Bioactive metabolites from terrestrial and marine actinomycetes. *Molecules* 28, 5915. doi: 10.3390/molecules28155915

Otero, P., Carpena, M., Garcia-Oliveira, P., Echave, J., Soria-Lopez, A., García-Pérez, P., et al. (2023). Seaweed polysaccharides: Emerging extraction technologies, chemical modifications and bioactive properties. *Crit. Rev. Food Sci. Nutr.* 63, 1901–1929. doi: 10.1080/10408398.2021.1969534

Pu, F., Fang, J., Li, W., Zhang, B., Hong, X., Xu, L., et al. (2024). New alpiniamide-type polyketide with antibiofilm activities from the marine-derived Streptomyces sp. ZS-A65. *Chem. Biodiversity* 21, e202400029. doi: 10.1002/cbdv.202400029

Rasheed, H. A., Rehman, A., Karim, A., Al-Asmari, F., Cui, H., and Lin, L. (2024). A comprehensive insight into plant-derived extracts/bioactives: Exploring their antimicrobial mechanisms and potential for high-performance food applications. *Food Bioscience* 59, 104035. doi: 10.1016/j.fbio.2024.104035

Ryu, D., Hillman, P. F., Akinniyi, G., Nam, S. J., and Yang, I. (2023). Marine mudflat actinomycetes as a novel natural products source. *Front. Mar. Sci.* 10, 1297446. doi: 10.3389/fmars.2023.1297446

Scherlach, K., and Hertweck, C. (2021). Mining and unearthing hidden biosynthetic potential. *Nat. Commun.* 12, 3864. doi: 10.1038/s41467-021-24133-5

Shams Ul Hassan, S., Ishaq, M., Zhang, W. D., and Jin, H. Z. (2021). An overview of the mechanisms of marine fungi-derived anti-inflammatory and anti-tumor agents and their novel role in drug targeting. *Curr. Pharm. design* 27, 2605–2614. doi: 10.2174/1381612826666200728142244

Shigeno, S., Kadowaki, M., Nagai, K., Hosoda, K., Terahara, T., Nishimura, T., et al. (2024). New polycyclic tetramate macrolactams with antimycobacterial activity produced by marine-derived Streptomyces sp. KKMA-0239. *J. Antibiotics* 77, 265–271. doi: 10.1038/s41429-024-00710-w

Spížek, J., Novotná, J., Řezanka, T., and Demain, A. L. (2010). Do we need new antibiotics? The search for new targets and new compounds. *J. Ind. Microbiol. Biotechnol.* 37, 1241–1248. doi: 10.1007/s10295-010-0849-8

Sun, X., Zhang, D., Zhao, L., Shi, B., Xiao, J., Liu, X., et al. (2020). Antagonistic interaction of phenols and alkaloids in *Sichuan pepper* (*Zanthoxylum bungeanum*) pericarp. *Ind. Crops Products* 152, 112551. doi: 10.1016/j.indcrop.2020.112551

Surendhiran, D., Li, C., Cui, H., and Lin, L. (2021). Marine algae as efficacious bioresources housing antimicrobial compounds for preserving foods-A review. *Int. J. Food Microbiol.* 358, 109416. doi: 10.1016/j.ijfoodmicro.2021.109416

Sweeney, D., Bogdanov, A., Chase, A. B., Castro-Falcón, G., Trinidad-Javier, A., Dahesh, S., et al. (2024). Pattern-based genome mining guides discovery of the antibiotic indanopyrrole A from a marine *Streptomycete*. *J. Natural Products* 87, 2768–2778. doi: 10.1021/acs.jnatprod.4c00934

Tianqiao, S., Xiong, Z., You, Z., Dong, L., Jiaoling, Y., Junjie, Y., et al. (2021). Genome-wide identification of Zn2Cys6 class fungal-specific transcription factors (ZnFTFs) and functional analysis of UvZnFTF1 in ustilaginoidea virens. *Rice Sci.* 28, 567–578. doi: 10.1016/j.rsci.2021.03.001

Wang, F., Bao, Y., Zhang, C., Zhan, L., Khan, W., Siddiqua, S., et al. (2022). Bioactive components and anti-diabetic properties of *Moringa oleifera* Lam. *Crit. Rev. Food Sci. Nutr.* 62, 3873–3897. doi: 10.1080/10408398.2020.1870099

Wang, P., Wang, D., Zhang, R., Wang, Y., Kong, F., Fu, P., et al. (2020). Novel macrolactams from a deep-sea-derived *Streptomyces* species. *Mar. Drugs* 19, 13. doi: 10.3390/md19010013

Wang, X., Yang, Y., and Huycke, M. M. (2020). Risks associated with enterococci as probiotics. *Food Res. Int.* 129, 108788. doi: 10.1016/j.foodres.2019.108788

Waseem, M., Akhtar, S., Ahmad, N., Ismail, T., Lazarte, C. E., Hussain, M., et al. (2022). Effect of microwave heat processing on nutritional indices, antinutrients, and sensory attributes of potato powder-supplemented flatbread. *J. Food Qual.* 2022, 2103884. doi: 10.1155/2022/2103884

Wei, Z., Shan, C., Zhang, L., Wang, Y., Xia, X., Liu, X., et al. (2021). A novel subtilin-like lantibiotics subtilin JS-4 produced by *Bacillus subtilis* JS-4, and its antibacterial mechanism against *Listeria monocytogenes*. *LWT* 142, 110993. doi: 10.1016/j.lwt.2021.110993

Wen, X., Wang, L., Li, J., Chen, Y., Zhuo, D., Anjago, W. M., et al. (2024). Staurosporine-producing Streptomyces sp. strain 11× 1 cell-free culture filtrates control diseases caused by the oomycete plant pathogens *Pythium myriotylum* and *Phytophthora sojae*. *Biocontrol Sci. Technol.* 34, 123–147. doi: 10.1080/09583157.2023.2301646

Wen, C., Zhang, J., Feng, Y., Duan, Y., Ma, H., and Zhang, H. (2020). Purification and identification of novel antioxidant peptides from watermelon seed protein hydrolysates and their cytoprotective effects on H_2O_2-induced oxidative stress. *Food Chem.* 327, 127059. doi: 10.1016/j.foodchem.2020.127059

Wong, F. C., Xiao, J., Wang, S., Ee, K. Y., and Chai, T. T. (2020). Advances on the antioxidant peptides from edible plant sources. *Trends Food Sci. Technol.* 99, 44–57. doi: 10.1016/j.tifs.2020.02.012

Xia, G., Li, Y., Tao, H., Zhang, L., Zhang, J., Yang, H., et al. (2022). Inactivation mechanism of catalytic infrared against *Pseudomonas aeruginosa* and its decontamination application on dry green Sichuan pepper (*Zanthoxylum schinifolium*). *Food Control* 132, 108483. doi: 10.1016/j.foodcont.2021.108483

Xu, Z., Chen, H., Fan, F., Shi, P., Cheng, S., Tu, M., et al. (2020). Pharmacokinetics and transport of an osteogenic dodecapeptide. *J. Agric. Food Chem.* 68, 9961–9967. doi: 10.1021/acs.jafc.0c02779

Xu, D., Zhang, Z., Yao, L., Wu, L., Zhu, Y., Zhao, M., et al. (2023). Advances in the adenylation domain: discovery of diverse non-ribosomal peptides. *Appl. Microbiol. Biotechnol.* 107, 4187–4197. doi: 10.1007/s00253-023-12585-2

Yang, Q., Solairaj, D., Apaliya, M. T., Abdelhai, M., Zhu, M., Yan, Y., et al. (2020). Protein expression profile and transcriptome characterization of *Penicillium expansum* induced by *Meyerozyma guilliermondii*. *J. Food Qual.* 2020, 8056767. doi: 10.1155/2020/8056767

Yi, K. X., Xie, Q. Y., Ma, Q. Y., Yang, L., Dai, H. F., Zhao, Y. X., et al. (2024). Diverse ansamycin derivatives from the marine-derived Streptomyces sp. ZYX-F-97 and their antibacterial activities. *Fitoterapia* 173, 105814. doi: 10.1016/j.fitote.2023.105814

Yixuan, L., Qaria, M. A., Sivasamy, S., Jianzhong, S., and Daochen, Z. (2021). Curcumin production and bioavailability: a comprehensive review of curcumin extraction, synthesis, biotransformation and delivery systems. *Ind. Crops Products* 172, 114050. doi: 10.1016/j.indcrop.2021.114050

Yu, Z., Xia, M., Lan, J., Yang, L., Wang, Z., Wang, R., et al. (2023). A comprehensive review on the ethnobotany, phytochemistry, pharmacology and quality control of the genus *Lycium* in China. *Food Funct.* 14, 2998–3025. doi: 10.1039/D2FO03791B

Zhang, H., Ahima, J., Yang, Q., Zhao, L., Zhang, X., and Zheng, X. (2021). A review on citrinin: Its occurrence, risk implications, analytical techniques, biosynthesis, physiochemical properties and control. *Food Res. Int.* 141, 110075. doi: 10.1016/j.foodres.2020.110075

Zhang, Y., Hao, R., Chen, J., Li, S., Huang, K., Cao, H., et al. (2024). Health benefits of saponins and its mechanisms: perspectives from absorption, metabolism, and interaction with gut. *Crit. Rev. Food Sci. Nutr.* 64, 9311–9332. doi: 10.1080/10408398.2023.2212063

Zhang, Y., Hassan, M. M., Rong, Y., Liu, R., Li, H., Ouyang, Q., et al. (2022). A solid-phase capture probe based on upconvertion nanoparticles and inner filter effect for the determination of ampicillin in food. *Food Chem.* 386, 132739. doi: 10.1016/j.foodchem.2022.132739

Zhang, J., Wen, C., Li, C., Duan, Y., Zhang, H., and Ma, H. (2019). Antioxidant peptide fractions isolated from wheat germ protein with subcritical water extraction and its transport across Caco-2 cells. *J. Food Sci.* 84, 2139–2146. doi: 10.1111/1750-3841.14720

Zhang, J., Wen, C., Zhang, H., Duan, Y., and Ma, H. (2020). Recent advances in the extraction of bioactive compounds with subcritical water: A review. *Trends Food Sci. Technol.* 95, 183–195. doi: 10.1016/j.tifs.2019.11.018

Zhang, X., Wu, F., Gu, N., Yan, X., Wang, K., Dhanasekaran, S., et al. (2020). Postharvest biological control of Rhizopus rot and the mechanisms involved in induced disease resistance of peaches by *Pichia membranefaciens*. *Postharvest Biol. Technol.* 163, 111146. doi: 10.1016/j.postharvbio.2020.111146

Zhang, C., Yu, X., Shi, X., Han, Y., Guo, Z., and Liu, Y. (2020). Development of carbon quantum dot–labeled antibody fluorescence immunoassays for the detection of morphine in hot pot soup base. *Food Analytical Methods* 13, 1042–1049. doi: 10.1007/s12161-020-01700-y

Zhao, Y., Chen, H., Yue, L., Dong, Y., Su, D., Lyu, J., et al. (2024). Heronamides with unreported skeletons from deep-sea *Streptomyces*: discovery and biosynthesis. *Organic Chem. Front.* 11, 1175–1183. doi: 10.1039/D3QO01837G

Zhao, W., Jiang, H., Ge, Y., Zhou, C., Ma, Y., Zhou, J., et al. (2024). Antimicrobial spiroketal macrolides and dichloro-diketopiperazine from Micromonospora sp. FIMYZ51. *Fitoterapia* 175, 105946. doi: 10.1016/j.fitote.2024.105946

Zhao, M., Zhang, W., Yang, C., Zhang, L., Huang, H., Zhu, Y., et al. (2024). Discovery of kebanmycins with antibacterial and cytotoxic activities from the mangrove-derived Streptomyces sp. SCSIO 40068. *J. Natural Products* 87, 1591–1600. doi: 10.1021/acs.jnatprod.4c00232

Zhong, R., Wan, X., Wang, D., Zhao, C., Liu, D., Gao, L., et al. (2020). Polysaccharides from marine *Enteromorpha*: structure and function. *Trends Food Sci. Technol.* 99, 11–20. doi: 10.1016/j.tifs.2020.02.030

Zhou, L., Chang, Y., Yang, S., Huang, X., Wang, J., Jiang, C., et al. (2024). Antibacterial *p*-terphenyl and α–pyrone derivates isolated from the marine-derived actinomycete Nocardiopsis sp. HDN154086. *J. Antibiotics* 77, 201–205. doi: 10.1038/s41429-023-00698-9

Zhu, Y., Li, C., Cui, H., and Lin, L. (2021). Encapsulation strategies to enhance the antibacterial properties of essential oils in food system. *Food Control* 123, 107856. doi: 10.1016/j.foodcont.2020.107856

Zhu, X., Wang, S., Song, Y., Chen, T., and Yan, Y. (2024). LC-MS guided discovery of a new type of abyssomicin, glycoabyssomicin A, from a deep-sea derived *Streptomyces*. *Natural Product Res.*, 1–6. doi: 10.1080/14786419.2024.2417839

Zou, Y., Shi, J., Sun, J. L., Li, L. Y., Yan, Z. Y., Guo, Z. K., et al. (2024). Maduraflavacins A–E, unusual phenyl polyene metabolites produced by a rare marine-derived Actinomadura sp. *J. Natural Products* 87, 2530–2536. doi: 10.1021/acs.jnatprod.4c00836

Frontiers in Microbiology

Explores the habitable world and the potential of microbial life

The largest and most cited microbiology journal which advances our understanding of the role microbes play in addressing global challenges such as healthcare, food security, and climate change.

Discover the latest Research Topics

See more →

Frontiers

Avenue du Tribunal-Fédéral 34
1005 Lausanne, Switzerland
frontiersin.org

Contact us

+41 (0)21 510 17 00
frontiersin.org/about/contact